STRATEGIC MOLECULAR BIOMARKERS AND MICRORNAs IN CANCER

EDITED BY: César López-Camarillo, Ondrej Slaby and
Macrina Beatriz Silva Cázares

PUBLISHED IN: Frontiers in Oncology

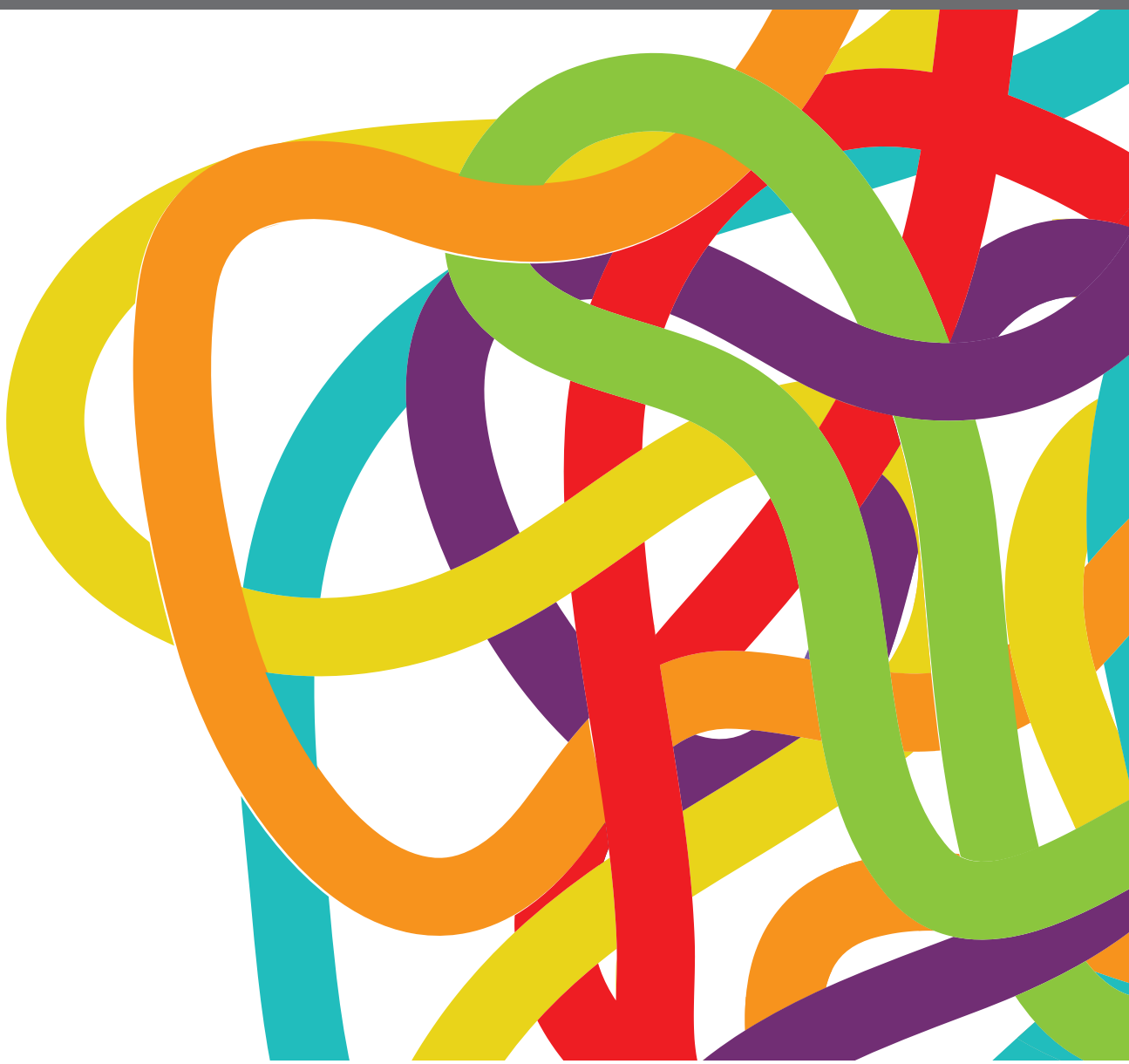

frontiers Research Topics

frontiers

ISSN 1664-8714
ISBN 978-2-83250-600-4
DOI 10.3389/978-2-83250-600-4

About Frontiers

Frontiers is more than just an open-access publisher of scholarly articles: it is a pioneering approach to the world of academia, radically improving the way scholarly research is managed. The grand vision of Frontiers is a world where all people have an equal opportunity to seek, share and generate knowledge. Frontiers provides immediate and permanent online open access to all its publications, but this alone is not enough to realize our grand goals.

Frontiers Journal Series

The Frontiers Journal Series is a multi-tier and interdisciplinary set of open-access, online journals, promising a paradigm shift from the current review, selection and dissemination processes in academic publishing. All Frontiers journals are driven by researchers for researchers; therefore, they constitute a service to the scholarly community. At the same time, the Frontiers Journal Series operates on a revolutionary invention, the tiered publishing system, initially addressing specific communities of scholars, and gradually climbing up to broader public understanding, thus serving the interests of the lay society, too.

Dedication to Quality

Each Frontiers article is a landmark of the highest quality, thanks to genuinely collaborative interactions between authors and review editors, who include some of the world's best academicians. Research must be certified by peers before entering a stream of knowledge that may eventually reach the public - and shape society; therefore, Frontiers only applies the most rigorous and unbiased reviews.
Frontiers revolutionizes research publishing by freely delivering the most outstanding research, evaluated with no bias from both the academic and social point of view. By applying the most advanced information technologies, Frontiers is catapulting scholarly publishing into a new generation.

What are Frontiers Research Topics?

Frontiers Research Topics are very popular trademarks of the Frontiers Journals Series: they are collections of at least ten articles, all centered on a particular subject. With their unique mix of varied contributions from Original Research to Review Articles, Frontiers Research Topics unify the most influential researchers, the latest key findings and historical advances in a hot research area! Find out more on how to host your own Frontiers Research Topic or contribute to one as an author by contacting the Frontiers Editorial Office: frontiersin.org/about/contact

STRATEGIC MOLECULAR BIOMARKERS AND MICRORNAs IN CANCER

Topic Editors:
César López-Camarillo, Universidad Autónoma de la Ciudad de México, Mexico
Ondrej Slaby, Central European Institute of Technology (CEITEC), Czechia
Macrina Beatriz Silva Cázares, Autonomous University of San Luis Potosí, Mexico

Citation: López-Camarillo, C., Slaby, O., Cázares, M. B. S., eds. (2022). Strategic Molecular Biomarkers and MicroRNAs in Cancer. Lausanne: Frontiers Media SA. doi: 10.3389/978-2-83250-600-4

Table of Contents

frontiers | Frontiers in Oncology

TYPE Editorial
PUBLISHED 12 October 2022
DOI 10.3389/fonc.2022.1031349

OPEN ACCESS

EDITED AND REVIEWED BY
Claudio Sette,
Catholic University of the Sacred Heart, Rome, Italy

*CORRESPONDENCE
Macrina Beatriz Silva-Cázares
macrina.silva@uaslp.mx

SPECIALTY SECTION
This article was submitted to Cancer Genetics, a section of the journal Frontiers in Oncology

RECEIVED 29 August 2022
ACCEPTED 28 September 2022
PUBLISHED 12 October 2022

CITATION
López-Camarillo C, Slaby O and Silva-Cázares MB (2022) Editorial: Strategic molecular biomarkers and microRNAs in cancer. *Front. Oncol.* 12:1031349. doi: 10.3389/fonc.2022.1031349

Editorial: Strategic molecular biomarkers and microRNAs in cancer

César López-Camarillo[1], Ondrej Slaby[2] and Macrina Beatriz Silva-Cázares[3]*

[1]Posgrado en Ciencias Genómicas, Universidad Autónoma de la Ciudad de México, Ciudad de Mexico, Mexico, [2]Molecular Oncology II-Solid Cancer Central European Institute of Technology, Brno, Czechia, [3]Coordinación Académica Región Altiplano, Universidad Autónoma de San Luis Potosí, Matehuala, Mexico

KEYWORDS

Molecular Biomarker, MicroRNAs, cancer, gene, expression

Editorial on the Research Topic
Strategic molecular biomarkers and microRNAs in cancer

Introduction

Breast cancer is a highly heterogeneous disease. Throughout the last few years, various therapies emerged in the era of cancer genomics. Advances in breast cancer have been made at the molecular and genomic levels, which facilitate us in identifying new prognostic markers and therapeutic targets. microRNAs (miRNAs) are implicated in carcinogenesis and their expression supply potential markers for cancer detection and progression. The biomarkers should predict not only prognosis, but also the response to therapies.

There are several Research Topics mentioning here. In 2001, a Research Topic titled "*Non–coding RNA genes and the modern RNA world*" was published in "Nature Review Genetics" (1). In 2009, Shi (2009) gave a review of microRNA expression and its implications for the diagnosis and therapeutic strategies of breast cancer (2). In 2019, Frontiers in Oncology published another Research Topic titled "*From "Junk DNA" to Clinically Relevant Tools for Cancer Diagnosis, Staging, and Tailored Therapies: The Incredible Case of Non-Coding RNAs*" (3) Recently, there is progress in research on molecular biomarkers and microRNAs in cancer, for example, noncoding RNA (ncRNAs) (4).

The present Research Topic "*Strategic Molecular Biomarkers and MicroRNAs in Cancer*" aimed at widening the knowledge on novel biomarkers and microRNAs in cancer biology and therapy emphasizing interdisciplinary contributions. The issue currently includes 9 manuscripts on the analysis of miRNAs expression in cancer cells, usefulness of cancer gene panel tests and miRNA analysis in histopathological diagnosis and functions emphasizing their contributions as important molecular markers for

cancer diagnosis. The studies presented in the Special Issue arise from diverse fields across biology molecular, oncogenomic, and clinical cancer.

Analysis of miRNAs expression in cancer cells

Micro-RNAs (miRNAs) are currently used as cancer biomarkers. Rajthala et al., investigated miR-138 dysregulation in cancer-associated fibroblasts (CAFs) in oral squamous cell carcinoma (OSCC) and its effects. The expression of miR-138 showed marked heterogeneity in both OSCC tissues and cultured fibroblasts. Ectopic miR-138 expression reduced fibroblasts' motility and collagen contraction ability and suppressed invasion of suprajacent OSCC cells, while its inhibition resulted in the opposite outcome. In conclusion, this study supports a tumor-suppressive role for miR-138 in OSCC while expressed in stromal fibroblasts, despite its heterogeneous expression. The miR-15b-5p is encoded by MIR15B gene which participates in the pathogenesis of several cancers as well as non-malignant conditions, such as abdominal aortic aneurysm, Alzheimer's and Parkinson's, cerebral ischemia reperfusion injury, coronary artery disease, dexamethasone induced steatosis, diabetic complications and doxorubicin-induced cardiotoxicity. Dysregulation of miR-15b-5p in clinical samples has been associated with poor outcome in different kinds of cancers. In this review, the authors discuss the role of miR-15b-5p in malignant and non-malignant conditions (Ghafouri-Fard et al., 2022).

Usefulness of cancer gene panel test and miRNAs analysis in histopathological diagnosis

MicroRNAs (miRNAs) are endogenous, noncoding, single-stranded RNAs that regulate gene expression, a characteristic that confers the potential for identifying malignancy (5). Dai et al. describe an original research article, of the fusions of receptor tyrosine kinase (RTK) involving anaplastic lymphoma kinase (ALK), c-ros oncogene 1 (ROS1), and neurotrophic receptor tyrosine kinase (NTRK) represent the potential targets of therapeutic intervention for various types of solid tumors. These results may provide genomic information for the personalized clinical management of solid tumor patients with ALK, ROS1, and NTRK fusions in the era of precision medicine. In other hand, Zhang et al., identified a prognostic signature composed of enhancer RNA-regulated genes (eRGs) for hepatocellular carcinoma (HCC). The findings of this study have significant practical implications in terms of providing a deeper insight into the investigation of pathogenesis of HCC, optimizing individualized treatment, and improving the prognosis of HCC patients.

Functions of miRNAs in relation to important molecular markers for cancer diagnosis

Salinas-Vera et al., present a review about microRNAs regulation of cancer hallmarks in 3D cell cultures from different types of cancers. The authors discuss the utilization of different types of 3D culture models including spheroids, organotypic models and patient-derived organoids in gynecologic cancers research, as well as its potential applications in oncological research mainly for screening drugs with major physiological and clinical relevance. Huang et al., present epidemiological evidence between variants in matrix metalloproteinases-2, -7, and -9 and cancer risk. Their findings support the relations between variants of MMP-2, MMP-7, and MMP-9 and various cancers risk, demonstrating the credibility of these relations and offer valuable data to design future research to assess variants in MMP factors for cancer risk.

Perspectives

In conclusion, investigations of molecular biomarkers and microRNAs continue to be essential in the development of new strategies that produce more successful treatments in human cancers. It is clear that target molecules of miRNAs are useful as molecular markers for cancer, and research to clarify the functions of miRNAs and their target molecules has an important role in the treatment of cancer. This Research Topic could contribute to the actual efforts focused in the search of novel biomarkers and microRNAs with potential applications on oncology research and therapy.

Author contributions

All authors listed have made a substantial, direct, and intellectual contribution to the work and approved it for publication.

Acknowledgments

We deeply thank all the authors and reviewers who have participated in this Research Topic. We also thank to the editorial team at Frontiers for their invaluable support.

Conflict of interest

The authors declare that the research was conducted in the absence of any commercial or financial relationships that could be construed as a potential conflict of interest.

Publisher's note

References

1. Eddy SR. Non-coding RNA genes and the modern RNA world. *Nat Rev Genet* (2001) 2(12):919–29. doi: 10.1038/35103511

2. Shi M, Guo N. MicroRNA expression and its implications for the diagnosis and therapeutic strategies of breast cancer. *Cancer Treat Rev* (2009) 35(4):328–34. doi: 10.1016/J.CTRV.2008.12.002

3. Iorio MV, Palmieri D. Editorial: From "junk DNA" to clinically relevant tools for cancer diagnosis, staging, and tailored therapies: From incredible case of non-coding RNAs. *Front Oncol* (2019) 9:389(MAY). doi: 10.3389/FONC.2019.00389

4. Zhou JG, Huang Z, Slaby O, Navarro A. Editorial: The role of ncRNAs in solid tumors prognosis: From laboratory to clinical utility. *Front Oncol* (2020) 10:631316. doi: 10.3389/FONC.2020.631316

5. Ciarletto AM, Narick C, Malchoff CD, Massoll NA, Labourier E, Haugh K, et al. Analytical and clinical validation of pairwise microRNA expression analysis to identify medullary thyroid cancer in thyroid fine-needle aspiration samples. *Cancer cytopathology* (2021) 129(3):239–49. doi: 10.1002/CNCY.22365

frontiers in Oncology

ORIGINAL RESEARCH
published: 17 March 2022
doi: 10.3389/fonc.2022.833582

MicroRNA-138 Abates Fibroblast Motility With Effect on Invasion of Adjacent Cancer Cells

*Saroj Rajthala[1,2], Himalaya Parajuli[1,2], Harsh Nitin Dongre[1,2], Borghild Ljøkjel[3], Kristin Marie Hoven[3], Arild Kvalheim[4], Stein Lybak[3], Evelyn Neppelberg[3,5], Dipak Sapkota[6], Anne Christine Johannessen[1,7] and Daniela-Elena Costea[1,2,7]**

[1] The Gade Laboratory for Pathology, Department of Clinical Medicine, Faculty of Medicine, University of Bergen, Bergen, Norway, [2] Centre for Cancer Biomarkers (CCBIO), Faculty of Medicine, University of Bergen, Bergen, Norway, [3] Head and Neck Clinic, Haukeland University Hospital, Bergen, Norway, [4] Tannteam Private Dental Practice, Bergen, Norway, [5] Department of Oral Surgery, Institute of Clinical Dentistry, University of Bergen, Bergen, Norway, [6] Department of Oral Biology, University of Oslo, Oslo, Norway, [7] Department of Pathology, Haukeland University Hospital, Bergen, Norway

OPEN ACCESS

Edited by:
Ondrej Slaby, Central European Institute of Technology (CEITEC), Czechia

Reviewed by:
Eduardo López-Urrutia, National Autonomous University of Mexico, Mexico
Luis E. Arias-Romero, National Autonomous University of Mexico, Mexico

***Correspondence:**
Daniela-Elena Costea
Daniela.costea@uib.no

Specialty section:
This article was submitted to Cancer Genetics, a section of the journal Frontiers in Oncology

Received: *11 December 2021*
Accepted: *08 February 2022*
Published: *17 March 2022*

Citation:
Rajthala S, Parajuli H, Dongre HN, Ljøkjel B, Hoven KM, Kvalheim A, Lybak S, Neppelberg E, Sapkota D, Johannessen AC and Costea D-E (2022) MicroRNA-138 Abates Fibroblast Motility With Effect on Invasion of Adjacent Cancer Cells. Front. Oncol. 12:833582. doi: 10.3389/fonc.2022.833582

Background: Recent studies have shown aberrant expression of micro-RNAs in cancer-associated fibroblasts (CAFs). This study aimed to investigate miR-138 dysregulation in CAFs in oral squamous cell carcinoma (OSCC) and its effects on their phenotype and invasion of adjacent OSCC cells.

Methods: Expression of miR-138 was first investigated in OSCC lesions (n = 53) and OSCC-derived CAFs (n = 15). MiR-138 mimics and inhibitors were used to functionally investigate the role of miR-138 on CAF phenotype and the resulting change in their ability to support OSCC invasion.

Results: Expression of miR-138 showed marked heterogeneity in both OSCC tissues and cultured fibroblasts. Ectopic miR-138 expression reduced fibroblasts' motility and collagen contraction ability and suppressed invasion of suprajacent OSCC cells, while its inhibition resulted in the opposite outcome. Transcript and protein examination after modulation of miR-138 expression showed changes in CAF phenotype-specific molecules, focal adhesion kinase axis, and TGFβ1 signaling pathway.

Conclusions: Despite its heterogeneous expression, miR-138 in OSCC-derived CAFs exhibits a tumor-suppressive function.

Keywords: cancer-associated fibroblasts, oral cancer, heterogeneity, motility, invasion

INTRODUCTION

Carcinogenesis is a multistep process that is not only dependent on the intrinsic properties of cancer cells, but also determined by the host stroma or the surrounding tumor microenvironment (1–3). Fibroblasts are one of the major cell types in the stroma that can modulate the behavior of cancer cells at all stages of carcinogenesis, including metastasis (3, 4). In oral squamous cell carcinoma (OSCC), the role of cancer-associated fibroblasts (CAFs) for tumor progression has been demonstrated in *in vitro* cell culture studies (5–7) and *in vivo* animal studies (5). In clinical

studies involving patient biopsies, CAFs have been associated to lymph node metastasis (8, 9) and poor prognosis in OSCC (8–12).

Apart from genetic alterations, epigenetic changes in cancer cells, including dysregulation of micro-RNAs (miRNAs) (13, 14) have also been widely recognized to have critical roles in cancer (15, 16). Dysfunction of miRNAs in stromal cells has been as well proven and shown to support further progression of transformed epithelial cells (17). Previous studies have shown miRNA deregulation in OSCC, their role in tumor progression, and their possible use as diagnostic and prognostic biomarkers, as well as therapeutical targets (18–20). However, few studies investigated consequences of alterations of miRNAs in tumor stroma for tumor progression in general, and for OSCC in particular.

In a recent study that involved miRNA profiling of primary cultures of OSCC-derived CAFs and normal oral fibroblasts (NOFs), we found altered expression of twelve miRNAs in CAFs (21). When coupled with the results of our previous transcriptomic study on the same strains of OSCC-derived CAFs and NOFs that found integrin α11 upregulated in CAFs of OSCC (5), miR-204 and miR-138 were identified by *in silico* prediction tools as possible upstream regulators of integrin α11. We further showed that indeed integrin α11 is a direct target of miR-204 and that miR-204 plays an anti-invasive role in OSCC (21), but we did not investigate miR-138 for its role in OSCC.

MiR-138 has been found to be downregulated in many cancer types, including OSCC, and it was therefore coined as a tumor suppressor (22). On the other hand, it has been linked to tumor progression and recurrence in glioblastoma (23). In a previous study on OSCC (42 cases), miR-138 was shown to have a decreased expression in OSCC compared to adjacent normal mucosa (24). In another study (n = 35), its expression was relatively higher in about half of OSCC when compared to normal oral mucosa (25). *In vitro* studies showed anti-proliferative and anti-invasive role for miR-138 when expressed in OSCC cells (26), and it was suggested to have a role in suppressing cancer stemness (27).

While the above-mentioned studies illustrate the role of miR-138 in several cancers when dysregulated in either whole tumor tissue or only in the epithelial compartment, studies on the consequences of altered miR-138 expression in stromal fibroblasts for tumor progression are, to our best knowledge, non-existent. This study aimed to investigate the role of miR-138 dysregulation in CAFs on OSCC progression.

MATERIALS AND METHODS

Patient Material

For miRNA *in situ* hybridization, formalin-fixed paraffin-embedded (FFPE) tissue blocks from OSCC lesions (n = 53) were used from the diagnostic archive of the Department of Pathology of Haukeland University Hospital. Clinical data were obtained from the Electronic patient journal (n = 38, **Supplementary Table S1**). Clinical–pathological correlations of the cohort were in line with a previous finding from larger cohorts of OSCC, indicating that the cohort could be used for preliminary biomarker analysis. Multi-variate Cox regression found tumor stage, age, and gender as independent predictors of survival with increased death risk for late tumor stage HR: 2.22 (1.03–4.76), age group above 65 HR: 2.28 (1.04–5.00), and male group HR: 4.29 (1.44–12.79), respectively (**Supplementary Figure S1**). Similarly, tumor stage was as independent predictor of recurrence-free survival, with increased risk for recurrence for the late stage group HR: 3.662 (1.18–11.31). Controlled for tumor stage, tumor site predicted higher risk of recurrence for OSCC lesions involving gingiva compared to tongue HR: 3.19 (1.985–10.322).

For isolation of paired cancer-associated and normal fibroblasts, fresh tissues from the tumor and healthy mucosa (more than 1 cm away from the OSCC lesion) from OSCC patients (n = 6) were collected at the time of the surgical excision. Non-matched CAFs were also isolated from additional primary OSCC lesions (n = 9) and normal oral fibroblasts (NOFs) from oral mucosa of non-cancer individuals (n = 10). Only HPV negative primary tumors without any prior therapies were included in the study. Informed consent was obtained in all cases. Ethical approval for the study was obtained from the regional ethical committee (REKVest 2010/481).

In Situ Hybridization and miRNA Semi-Quantification

ISH of OSCC tissues was performed as described earlier (28). In brief, 3-µm sections of formalin-fixed and paraffin-embedded tissues were deparaffinized in xylene, rehydrated in series of 99%, 96%, and 70% alcohol concentration, and epitope retrieved with 15 µg/ul Proteinase K (90000; Exiqon, Denmark) solution at 37°C for 10 min. At 53°C, sections were pre-hybridized with ISH buffer (90000; Exiqon; Denmark) for 30 min, and then incubated for an hour with digoxigenin (DIG) labeled miR-138-5p specific oligonucleotides (612107-360; Exiqon, Denmark). Thereafter, tissues were washed with decreasing concentrations of saline-sodium citrate buffer (S66391L; Sigma, USA), and then blocked with 2% sheep serum (013-000-121; Jackson ImmunoResearch, USA) in 1% bovine serum albumin. Subsequently, tissues were incubated with alkaline phosphatase (ALP)-linked anti-DIG Fc fragments (1:400; 11093274910; Roche, Germany) overnight at room temperature. The tissues were thoroughly washed and then incubated with ALP substrate-Nitro blue tetrazolium chloride/5-Bromo-4-chloro-3-indolyl phosphate (NBT-BCIP) (11681451001; Roche, Germany) at 30°C for 2 h. Levamisole (X3021; Dako, USA) was mixed with the substrate to block endogenous ALP activity. Finally, tissues were counterstained with nuclear fast red. A scramble oligonucleotide without target and small nuclear RNA-U6 were used as negative and positive controls, respectively.

miR-138 staining in OSCC sections were scored negative (0) or 1–4 according to increasing stain intensity by experienced pathologists.

TCGA Data Analysis

TCGA miR-138 expressions from TCGA miRNA sequence data (n = 488) and clinical data for head and neck squamous cell

carcinoma cohort (n = 528) were accessed from the Firebrowse database version 2016_01_28 (http://www.firebrowse.org). The same cohort contained miR-138 data for normal human oral mucosa (NHOM). After exclusion of HPV-positive, non-oral cancers cases and cases with history of neoadjuvant treatment, 277 oral cancer cases (alveolar ridge: 13; base of tongue: 11; buccal mucosa: 30; floor of mouth: 56; hard palate: 5; lip: 3; unspecified region in oral cavity: 62; tongue: 112; oropharynx: 7) with miR-138 data remained. Using the same exclusion criteria, out of 45 cases, only 25 NHOM cases remained. Of the 25 NHOM cases, 24 were matched to OSCC lesions (from the same patient).

Cell Culture

Isolated CAFs and NOFs from OSCC patients and healthy donors were cultured in Dulbecco's Modified Eagle's Medium (DMEM; D6429, SIGMA) supplemented with 10% heat-inactivated newborn calf serum (NBCS; 31765068, GIBCO). OSCC cell lines UK1 (29) and Luc4 (30) were grown in DMEM/Nutrient Mixture F-12 Ham medium (D8437, Sigma) supplemented with 10% NBCS, 1× Insulin-Transferrin-Selenium (41400-04, Thermofisher Scientific), 0.4 µg/ml hydrocortisone (H0888, Sigma), 50 µg/ml L-ascorbic acid (A7631, Sigma), and 10 ng/ml epidermal growth factor (E9644, Sigma). All cell lines were propagated in humidity incubator at 5% CO_2 and 37°C temperature and regularly tested for mycoplasma contamination.

miRNA Modulation in Fibroblasts and Proliferation Assay

Each of the 1×10^6 NOFs and CAFs was reverse transfected with mimics and inhibitors of miR-138-5p (C/IH-300605; Dharmacon), and the respective controls (mimic: CN-0010000-01; inhibitor: IN-001005-05; Dharmacon) at 50 nM concentration using LipofectamineTM 3000 Transfection Reagent (L3000015; Invitrogen, USA) following the manufacturer´s protocol. Forty-eight hours after the transfection, the cells were either harvested for molecular profiling or subjected to further functional studies. In order to see the effect of miR-138 on fibroblast proliferation, 1×10^4 NOFs or CAFs were reverse transfected with mimics and inhibitors of miR-138-5p and the respective controls in quadruplicates in 24-well plates. After 48 h, the cells were Trypsin EDTA detached and counted using Trypan blue in Invitrogen Countess automated cell counter.

RNA and miRNA Isolation

Total RNA was isolated using mirVana miRNA isolation kit (AM1560, mirVana). In brief, sub-confluent CAFs and NOFs in monolayer cultures were washed with phosphate buffered saline (PBS), lysed with Lysis/Binding buffer and Phenol : Chloroform extracted. Subsequently, RNA was captured in glass fiber filter column and eluted in elution solution. The purity and quantity of the RNA was measured using NanoDrop® ND-1000 Spectrophotometer (Nanodrop Technologies; USA). Total RNA and enriched small RNAs were stored at −80°C until use.

Reverse Transcription

Total RNAs were reverse transcribed to cDNAs using miRNAs specific primers using TaqMan MicroRNA Reverse Transcriptase kit (4366596, Applied Biosystem). In brief, 10 ng of total RNA was mixed with dNTPs, reverse transcription buffer, RNase inhibitor, and miRNA specific primer and reverse transcribed to a final reaction mixture of 15 µl. Thereafter, the reaction mixture was subjected to thermal cycle at 16°C for 30 min, 42°C for 30 min, and 85°C for 5 min. For mRNA quantification, total RNA was reversed transcribed using the Taqman Reverse Transcription kit (N8080234, Applied Biosystems). In brief, 100 ng of total RNA was mixed with reverse transcription buffer, $MgCl_2$, dNTPs, random hexamer, RNase inhibitor, and reverse transcriptase to a final volume of 25 µl with RNase-free water. cDNA synthesis was performed at 20°C for 10 min, 48°C for 30 min, and 90°C for 5 min.

Quantitative Real-Time Polymerase Chain Reaction

The expression of miRNAs and gene transcripts were quantified using Taqman assays in ABI Prism 7900 HT sequence detector system (Applied Biosystems). The PCR reaction volume was set to 10 µl for each well in 384-well plates. The PCR was then run at 50°C for 2 min, 95°C for 10 min, and for 40 cycles at 95°C for 15 s and 60°C for 1 min. Each sample was run in triplicate. mRNA expression was normalized to the housekeeping gene GAPDH, and miRNA expression was normalized to the expression of RNU48. Taqman assays used are listed in **Supplementary Table S2**.

Western Blot

Semi-quantitative assessment of proteins of interest was performed using Western blot technique. In brief, protein lysates of fibroblast culture, 48 h post transfection of miR-138 mimics, inhibitors, and controls, were resolved in NuPAGE Novex 10% Bis-Tris Protein Gel (NP0303, Invitrogen) in NuPAGE MOPS SDS Running Buffer (NP0001, Invitrogen) at 160 V for 90 min and were transferred to PVDF membrane (10600069, GE Healthcare) in NuPAGE transfer buffer (NP0006, Invitrogen) at 40 V for an hour. Thereafter, PVDF membrane was blocked with 5% non-fat dry milk or 3% BSA in TBS-tween buffer for half an hour and incubated with primary antibody overnight at 4°C. The following day, PVDF membrane was thoroughly washed with TBS-tween, incubated at room temperature with secondary antibody tagged with horseradish peroxidase and thoroughly washed again. Finally, bands of proteins were visualized using SuperSignal West Pico Chemiluminescent Substrate (34080, Thermofisher) using Image Reagder LAS 1000 (Fujifilm), and protein band intensity in the captured images was quantified using ImageJ using Gel commands. GAPDH was used as loading control. Antibodies used in this study are listed in **Supplementary Table S3**.

miRNA Dual Luciferase Target Reporter Assay

3'UTR sequence of ITGA11 (NM_001004439.1) was retrieved from the UCSC genome browser (http://genome.ucsc.edu) (31). A plasmid vector with luciferase upstream of 3'UTR and renilla as a control reporter was designed and purchased from Vector Builder. Position 1-1355 of ITGA11 3'UTR length harboring

miR-138 binding site (724–730: CACCAGC)→ was inserted into the vector. For a control vector, non-complimentary mutant sequence GTGGTCG was introduced to miR-138 binding site. Transfection mix of plasmid DNA (250 ng per well in 24-well plates) and miR-204 mimic (calculated at 50 nM concentration in cell culture medium) was prepared using LipofectamineTM 3000 Transfection Reagent. Required volume of transfection mix and 5×10^5 CAFs were mixed in each well, and the cells were maintained in the culture chamber for 48 h. Thereafter, the cells were harvested, and luciferase activity was measured using Dual luciferase detection system (E1910, Promega) following the manufacturer's protocol using a Tecan Infinite M200PRO luminometer.

Fibroblast Migration in Collagen Gel Assay

On the first day of the experiment, 1×10^5 UK1 cells were plated in 24-well plates. The next day, collagen type I matrices were prepared by mixing collagen type I (354236, Corning), DMEM, NBCS and reconstitution buffer (2.2 g $NAHCO_3$ + 0.6 g NAOH + 4.766 g HEPES 100 ml water) at a volume ratio of 7:1:1:1 on ice. The collagen matrix (250 µl per well) was pipetted into 0.4-µm 24-well Corning transwell inserts (CLS3413, Sigma) and allowed to gel at 37°C in an incubation chamber. Two hours later, the gels were layered on the top with 250 µl of 5×10^5/ml fibroblasts modulated with miR-138. The co-culture system was maintained at 37°C for 5 days.

Collagen Contraction Assay

Ninety-six-well plates were blocked with 2% BSA overnight at 37°C in an incubation chamber. Forty-eight hours post miRNA modulations, fibroblasts were suspended in collagen type I matrix prepared as described above at a density of 5×10^5 cells/ml. Subsequently, 100 µl of fibroblast-collagen matrix was dispensed into each well and allowed to gel for 90 min. The gels were then gently dislodged from the surface of culture plate using 100 µl of DMEM medium. The gels were maintained at an incubation chamber and the change in gel dimension was measured at different time points.

Fibroblast-OSCC Cell 3D Organotypic Co-Culture

3D co-culture models mimicking local invasion of OSCC cells into subjacent connective tissue were constructed by layering OSCC cells on top of a fibroblast-embedded collagen I matrix. In brief, either CAFs or NOFs at a density of 2.5×10^5 cells/ml were suspended in the matrix of collagen type I prepared as above, on ice. Seven hundred microliters of the CAF- or NOF-populated collagen suspensions was pipetted into each well in 24-well plates and allowed to polymerize in a humidified incubator at 37°C. After 2 h, each well was gently added with 1 ml of complete DMEM medium to allow the cells to grow until the next day. The next day, 5×10^5 cells of UK1 or Luc4 were added on the top of the fibroblast gel. A day after, the gels were transferred to a metal grid layered with a filter paper and grown on air-medium interface in DMEM : Ham´s F12 Nutrient mixture (31765068, Thermofisher) supplemented with insulin-transferrin-selenium, hydrocortisone, and L-ascorbic acid as above, but NBCS was replaced with 0.1% bovine albumin fraction (V15260-037, Thermofisher). The gels were cultured for the next 10 days. Medium was changed at each alternative day.

Quantification of Invasion of OSCC Cells in 3D-Organotypic Models

FFPE-embedded organotypic tissues were cut into 5-µm sections and stained with hematoxylin and eosin. Images of the stained tissues were captured at 20× objective using a slide scanner (Hamamatsu NaNoZoomer-XR, Shizuoka, Japan) and the invasion depth of OSCC cells was measured using NDP.view2 (Hamamatsu, Japan). Depth of invasion was defined as the vertical distance from the reconstructed basement membrane (horizontal line along the non-invading cells) to the deepest invaded OSCC cells in the respective point. Twenty measurements of invasion at 50-µm distance along the tissue were taken and averaged. The non-uniform thick or tapered 100-µm ends of the 3D organotypic tissues were excluded from measurements.

Statistical Analysis

Student´s unpaired or paired *t*-test or one-way ANOVA was used to examine significant differences in means in between two or more than two groups, respectively. Where data did not show a normal distribution (D´Agostino & Pearson test; $p > 0.05$), non-parametric comparisons (Wilcoxon for paired comparison and Mann–Whitney for unpaired comparison between two, and Kruskal–Wallis for unpaired comparison among groups) were carried out to determine significant difference in median expression. All analysis was performed using GraphPad Prism Version 7. For statistical analysis, the OSCC cohort was categorized into a negative or a positive miR-138 staining group or a low-no (0–1) and a high (2-4) miR-138 staining group. Overall survival (OS) and recurrence-free survival (RFS) analysis for clinicopathological parameters and miR-138 expression (positive and negative staining group) was carried out using log-rank test (Mantel–Cox). Clinicopathological parameters were further tested with multivariate Cox's proportional regression to identify independent predictors of OS and RFS. Pearson's chi-square test was carried out to determine the association of miR-138 status [positive ($n = 31$) versus negative ($n = 7$); low-no miR-138 ($n = 33$) versus high miR-138 ($n = 4$)] with clinicopathological parameters. Survival and association tests were carried out using IBM SPSS Statistics Version 25.

RESULTS

miR-138 Was Expressed in a Subset of OSCC Lesions Only and Showed a Marked Heterogeneity in Both Epithelial and Stromal Compartments

Epithelial expression of miR-138 was observed in 17% ($n = 9$) of OSCC cases while stromal expression was detected in 9.4% ($n = 5$) of the cases. In 7.5% ($n = 4$) of the cases, miR-138 was expressed in both tumor and stromal compartments (**Figure 1A**). Pearson chi-square test showed that miR-138 staining

positivity associated with lower depth of invasion: <4 mm (p = 0.05) and relatively higher miR-138 expression (epithelial and stromal) associated with lower OSCC recurrence (p = 0.03). Expression of miR-138 did not associate to any other clinical or pathological parameters, including tumor stages. Epithelium of NHOM controls showed miR-138 expression in 50% of cases (n = 3) while no expression was observed in subjacent normal stroma. Compared to histologically normal peritumoral epithelium, miR-138 expression in tumor epithelium was increased in 16.1% (n = 5) and decreased in 3.2% (n = 1) cases. Stromal miR-138 expression was increased in tumor stroma compared to respective stroma in normal/peritumor regions in 9.7% (n = 3) cases, while no difference was observed for the rest (**Figure 1B**). When expressed in tumor stroma, miR-138 was localized in cells with fibroblast morphology and in a sub-population of lymphocytes (**Figures 1C, D**).

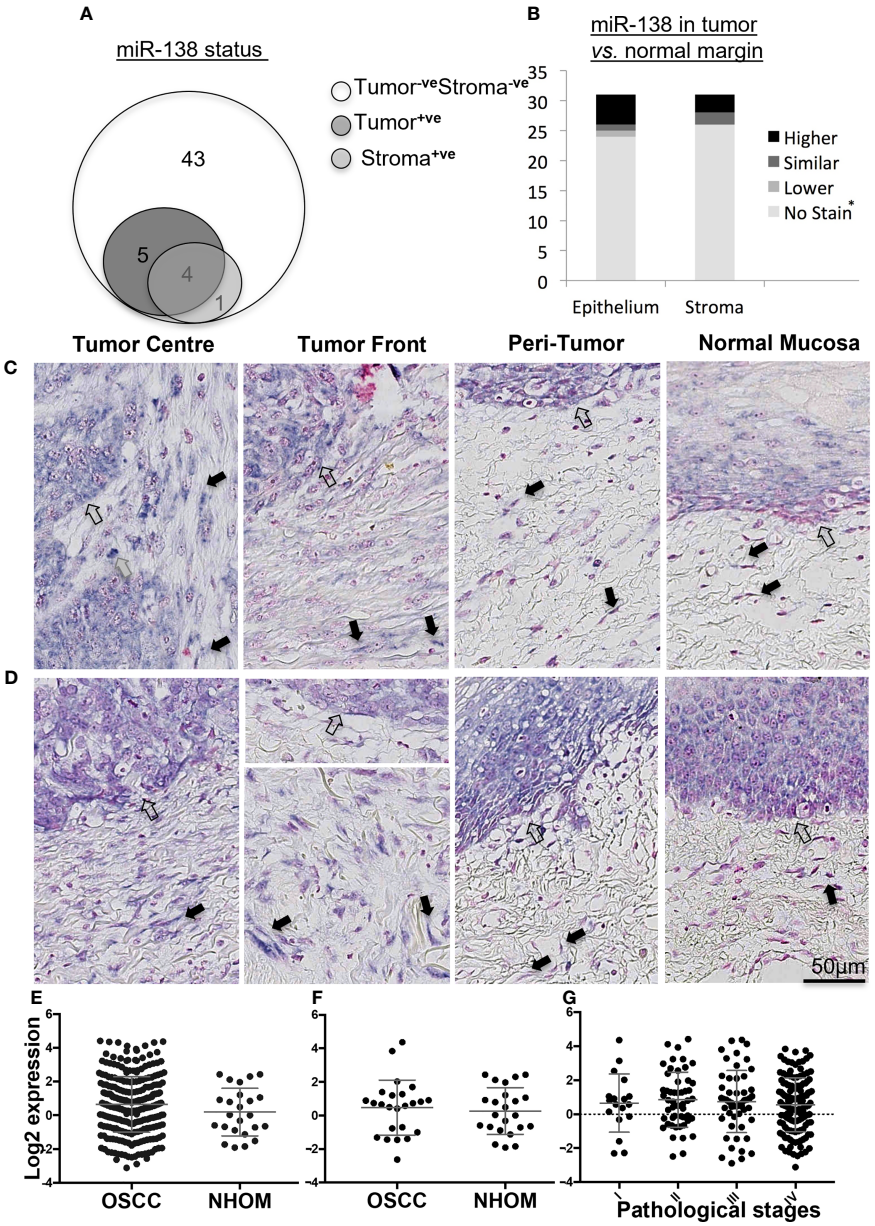

FIGURE 1 | Expression of miR-138 in OSCC. **(A)** Venn diagram showing distribution of OSCC cases according to miR-138 staining positivity in the epithelial and tumor-associated stroma regions. **(B)** Stacked bar plot comparing the miR-138 expression in epithelial and stromal compartments in the OSCC lesions compared to peritumoral/normal margins. *-veStain in both tumor and adjacent normal/peritumor area. **(C)** Higher miR-138 expression in cancer cells in tumor center (TC) and tumor front (TF) compared to adjacent peritumor (PT) and normal (TN) areas. **(D)** Higher expression in PT region compared to TC and TF. Lymphocytes, fibroblasts, and epithelial/malignant compartment in gray, black, and unfilled arrows, respectively. **(E)** TCGA miR-138 expression in between OSCC and matched NHOM, **(F)** OSCC and unmatched NHOM, and **(G)** among pathological stages in OSCC. Unpaired t-test, paired t-test, and one-way ANOVA, respectively, for **(C–E)**.

Analysis of the TCGA data showed no significant difference in miR-138 expression between whole OSCC lesions compared to NHOM (**Figure 1E**). A difference in miR-138 expression was still not observed when the subset of OSCC cases was compared to their matched NHOM (**Figure 1F**). No significant difference in miR-138 expression among overall pathological tumor stages (I–IV) was found (**Figure 1G**).

Fibroblasts From OSCC Lesions Displayed a Heterogeneous Expression of miR-138

Positive and negative miR-138-stained fibroblasts were observed to co-exist nearby the stroma of a subset of OSCC lesions (**Figures 2A, B**). qRT-PCR profiling of miR-138 expression in CAFs isolated from OSCC lesions and NOFs isolated from oral mucosa of non-related healthy, non-cancer individuals showed significantly higher expression in CAFs by 4.52-fold (**Figure 2C**). However, profiling of miR-138 in matched CAFs and NOFs showed a marked heterogeneity; out of the six matched pairs, miR-138 expression was higher in CAFs, then in NOF only in one matched pair, similar in two pairs, and lower in three pairs (**Figure 2D**).

Ectopic Expression of miR-138 Decreased Fibroblast Proliferation and Expression of Several CAF-Related Markers, but Not of ITGA11

Ectopic expression of miR-138 (modulation of miR-138 expression in fibroblasts by use of mimics and inhibitors is presented in **Supplementary Figure S2**) resulted in significantly reduced proliferation of both CAFs and NOFs compared to mimic controls in monolayer culture (**Figures 3A, B**). Reduced proliferation of fibroblasts was accompanied by significant reduction in expression of CCND1 transcript (**Figure 3C**). However, despite upregulation of CCND1 following inhibition of miR-138, a change in fibroblast proliferation was not observed between the target and control group. Modulation of miR-138 expression also induced significant changes in expression of several CAF-related molecules (TGFBR2, TGFβ1, and FAP) and EGFR (**Figures 3D–K**).

qRT-PCR profiling of miR-138 and ITGA11 transcripts in cultured fibroblasts showed an inverse correlation between their expression (**Figure 4A**). However, modulation of miR-138 expression did not result in alterations of ITGA11 expression at mRNA or protein levels (**Figures 4B–D**). Gene reporter assay showed no difference in expression of ITGA11 or mutant transcripts (**Figure 4E**), indicating that miR-138 does not target ITGA11.

Ectopic Expression of miR-138-5p Induced a Change in Fibroblasts' Morphology and Decreased Their Motility and Collagen Contraction Ability

Increasing miR-138 expression in fibroblasts (both CAFs and NOFs) changed their cellular morphology from an elongated, slender shape (**Figures 5G–H, L**) to a flattened, stellar shape and bigger size, compared to mimic controls (**Figures 5E, F, K**). Fibroblasts' motility in 3D collagen I gels towards OSCC cell line UK1 was significantly impaired following transfection with miR-138 mimics; the number of fibroblasts that migrated inside the collagen gels and the distance crossed were significantly reduced in fibroblasts transfected with mimics, compared to controls (**Figures 5M, N**). Additionally, mimicking increased miR-138 in CAFs and NOFs and significantly reduced collagen contraction ability by both CAFs and NOFs, and reversing miR-138 expression by using inhibitors resulted in the opposite effect (**Figures 5A–D** and **6**).

miR-138 Expression in Fibroblasts Decreased Invasion of Suprajacent OSCC Cells

In order to study the role of miR-138 expression in CAFs on tumor invasion or progression, miR-138 expression was altered in CAFs and NOFs prior to their co-culture with the established OSCC cell lines UK1 and Luc4 in 3D-organotypic models. Inhibition of miR-138 in both CAFs and NOFs increased invasion by OSCC cell lines UK1 and Luc4, while transfection of both fibroblasts with mimics of miR-138 significantly decreased or almost completely neutralized invasion of both UK1 and Luc4 (**Figure 7**).

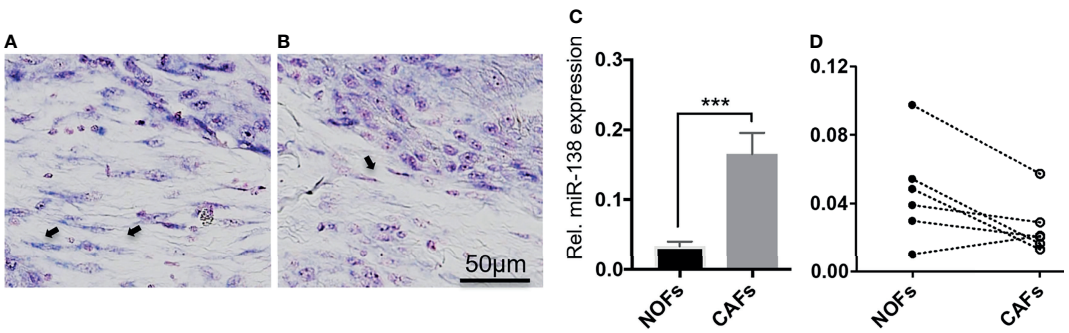

FIGURE 2 | Heterogenous expression of miR-138 in cultured fibroblasts from OSCC lesions and normal mucosa. **(A, B)** Differential miR-138 expression in CAFs from different regions of tumor center. Fibroblasts are marked with arrows. **(C)** miR-138 expression in non-matched CAFs and NOFs. **(D)** miR-138 expression in matched NOFs and CAFs. Each pair is connected by dotted lines. ***$p < 0.001$.

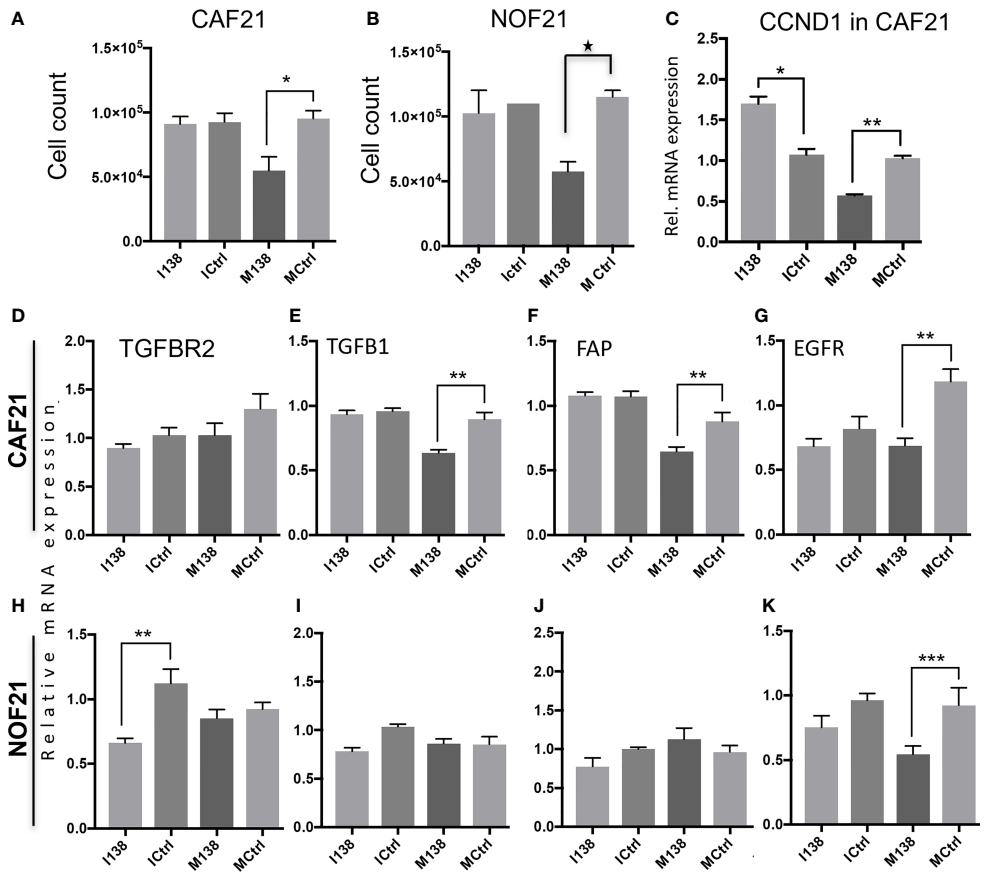

FIGURE 3 | Fibroblasts' proliferation and expression of CAF markers in monolayer culture following miR-138 modulation. Proliferation of **(A)** CAFs and **(B)** NOFs, **(C)** regulation of CCND1 transcript in CAFs, and **(D–K)** other transcripts related to the CAF-phenotype (TGFβ1, TGFBR2, and FAP) and EGFR in CAFs and NOFS 48 h post miR-138 modulation. * Significant; unpaired *t*-test $p < 0.05$. I138: inhibition of endogenous miR-138. M138: mimicking of miR-138 expression. Ictrl and MCtrl: respective controls for inhibitors and mimics. **$p < 0.01$, ***$p < 0.001$.

Pathway Focus Analysis of Molecules Targeted by miR-138 Indicates Alterations in the Focal Adhesion Pathway

Pathway analysis of genes targeted by miR-138 using miRTarBase database release 7 (32) identified several miR-138 targeted pathways, including focal adhesion and TGF-β1 pathways (**Supplementary Table S4** and **Figure S3**). Since FAK, AKT, ROCK, and CCND1 have been previously proven by luciferase gene reporter assays to be direct targets of miR-138, we decided to focus on these molecules in the focal adhesion pathway. An effect on FAK (PTK2) mRNA was observed when the cells were transfected with mimics. At the FAK, protein level seemed to be altered by both mimics and inhibitors of miR-138, in opposite directions (**Figure 8**).

DISCUSSION

This study shows that expression of miR-138 displays a marked heterogeneity, and it is detectable in a subset of OSCC lesions only. Although performed on a limited number of cases, insufficient for a definitive conclusion, this study points towards a trend for decreased miR-138 expression in tumor tissue when compared to normal oral epithelium. The absence of miR-138 staining in a relatively higher percentage (83%) of tumor samples compared to NHOM (50%) might be an indication for a tumor-suppressive role of miR-138. Inconsistent with this might be the finding that when present, in few cases, the expression of miR138 was increased in both tumor cells and CAFs compared to normal/peritumor regions. Nevertheless, increased expression was associated with lower recurrence and less depth of invasion, indicative again for a tumor-suppressive role. Of note, in our cohort, there was also no specific pattern of association of miR-138 expression with tumor stage, lymph node involvement, or later distant metastasis. This might be due to the relatively low number of cases we have studied, but analysis of the TCGA data set, which comprises many more cases, did not show either any specific association of miR-138 to clinical parameters in OSCC. Taken together, these data do not support a biomarker role for miR-138 in OSCC. However, there are indications for a tumor-suppressive function

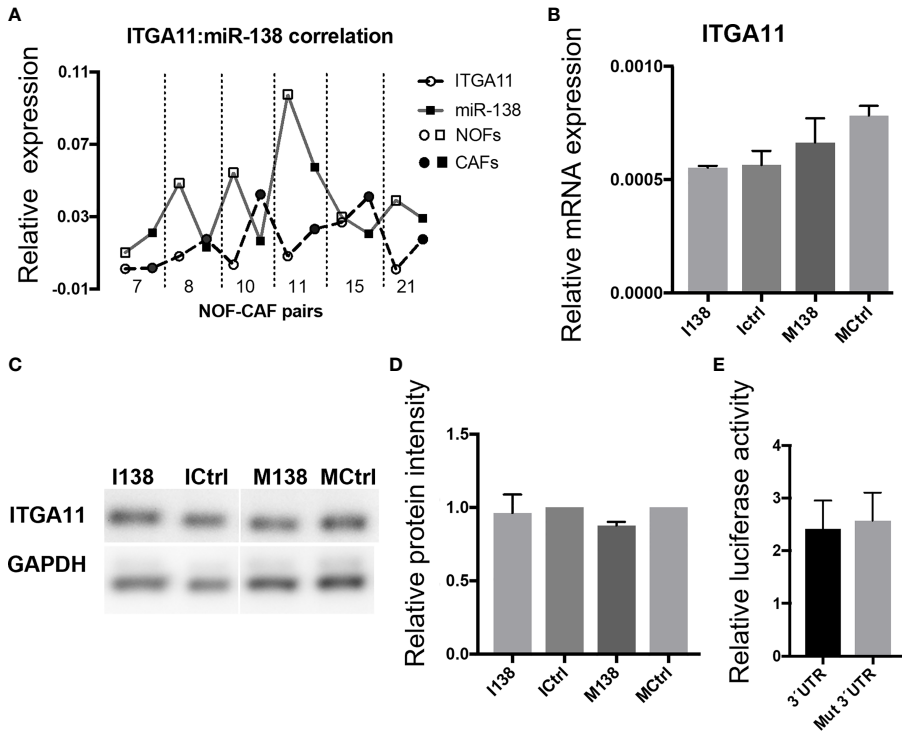

FIGURE 4 | miR-138 does not target ITGA11. **(A)** Graph showing an inverse correlation between miR-138 and ITGA11 levels in the fibroblasts. **(B)** Modulation of miR-138 expression did not result in alterations of ITGA11 expression at mRNA or **(C, D)** protein levels in CAF. **(E)**; Gene reporter assay showing no difference in the expression of ITGA11 or mutant transcripts.

for miR-138 from both previous and current studies, and thus miR-138 might be of biological importance for a subset of OSCCs.

The heterogeneity of miR-138 expression observed in stroma of OSCC tissues was paralleled by a marked heterogeneity detected in cultured fibroblasts, which might have been even more increased due to selection of different sub-populations of fibroblasts during isolation in culture. We could not identify, however, indications for selective isolation of a certain sub-population over the other. Of importance, despite its heterogenous regulation in fibroblasts, with no clear trend between CAFs and NOFs, increased expression of miR-138 using miR-138 mimics in both CAFs and NOFs had a remarkable effect on their ability to migrate in 3D, to contract collagen gels, and to induce OSCC invasion. Therefore, this study shows that regardless of type of fibroblasts used (CAFs or NOFs), ectopic expression of miR-138 in the fibroblasts results in a consistent inhibition of migration of fibroblasts themselves and of invasion of the adjacent OSCC cells. These findings are in line with the literature suggesting a tumor-suppressive function for miR-138, but while the previous studies addressed the role of miR-138 expressed in tumor cells (26, 27), here we show for the first time a tumor-suppressive effect for miR-138 expression in stromal fibroblasts. In an attempt to understand the mechanism by which alteration in miR-138 expression in the fibroblasts modulates the invasion capabilities by OSCC cells, a couple of functional assays were performed. A crucial effect of increased miR-138 expression in fibroblasts was the morphological transition from spindle-shaped CAFs and NOFs into a stellar morphology, accompanied by a decrease in their motility. The effect on motility might be the underlying mechanism by which decreased miR-138 expression in CAF decreased invasion of adjacent OSCC cells, since CAFs have been shown previously to "lead" the invasion of adjacent OSCC cells (6), and changes in their motility were reflected directly into the invasion ability of adjacent OSCC cells (5).

Similar morphological and motility changes have been previously reported to be associated to loss of FAK function, which regulates focal adhesion assembly and disassembly required for cell motility (33, 34). Our study indicates that FAK was regulated in OSCC-derived CAFs by miR-138, suggesting therefore that the changes in fibroblast morphology and motility observed to occur with increased miR-138 expression might be mediated, among other molecules, *via* FAK. However, these results need to be further confirmed by phenotype rescue experiments to prove that the motility effects we observed after modulation of miR-138 expression are mediated *via* focal adhesion kinase axis. The changes in fibroblasts' morphology and motility were accompanied by other changes in their molecular profile; ectopic expression of miR-138 significantly decreased several CAF-related markers, particularly those on the TGF-β1 pathway. A link between

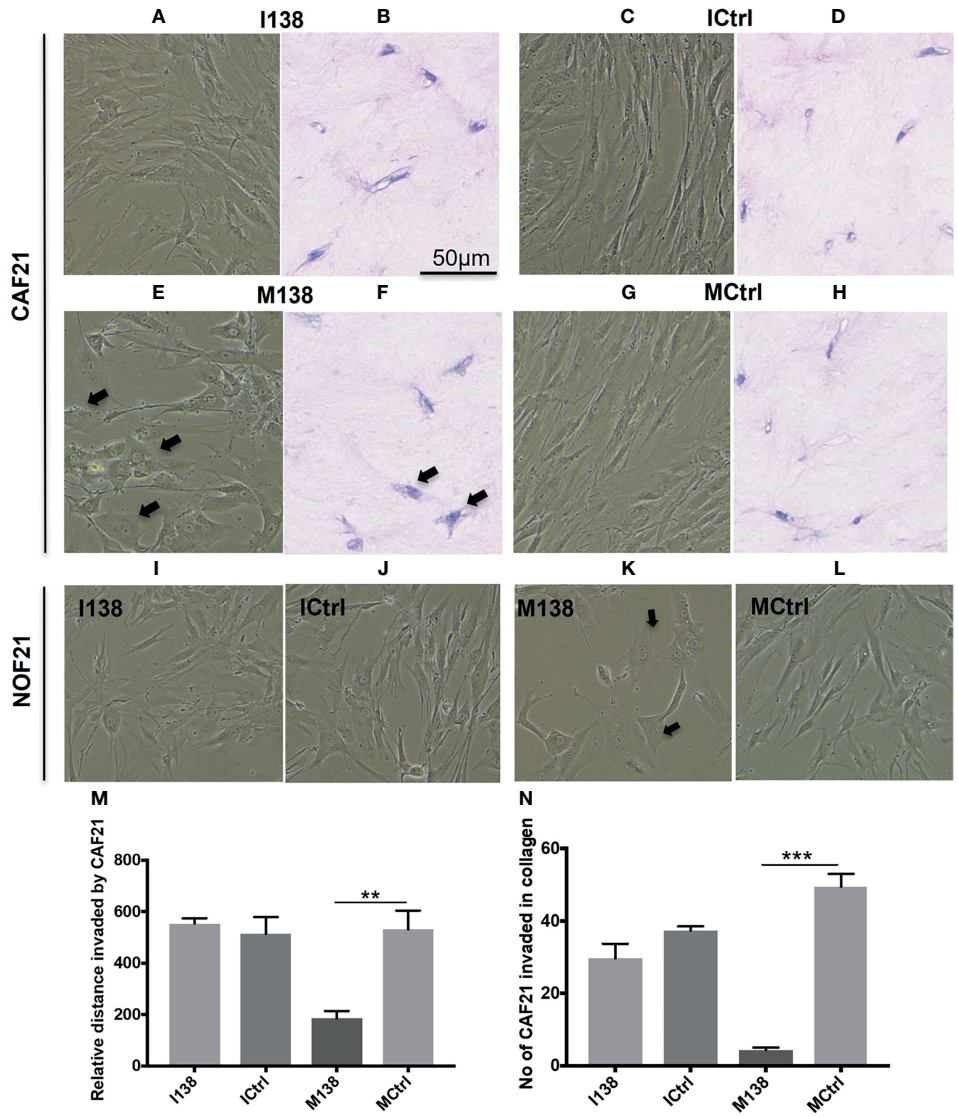

FIGURE 5 | Altered fibroblast morphology and migration following miR-138 modulation in CAF monolayer and 3D-collagen matrix. **(A, C, E, G, I–L)** Phase contrast images for cells in monolayer taken 48 h post transfection of mimic and inhibitor of miR-138, and respective mimic and inhibitor control (50 nM). **(B, D, F, H)** Images of HE-stained sections of fibroblasts in 3D-collagen matrix post miR-138 modulation **(M, N)**. Effect of miR-138 modulation in CAFs, in its migration (invasion) ability in collagen gel matrix. M138—fibroblasts treated with miR-138 mimics. (n = 4–6, unpaired t-test, $^{**}p < 0.01$, $^{***}p < 0.001$). I138—fibroblasts treated with miR-138 inhibitors of miR-13. Ictrl and MCtrl—respective controls for inhibitors and mimics.

TGFβ1 pathway and fibroblasts' motility is well established (35). Moreover, cyclin D1 (CCND1), well known to control proliferation of cells, has also been found to be decreased by ectopic expression of miR-138, and it was linked to cell motility. CCND1-deficient mouse embryonic fibroblasts were previously shown to exhibit increased cellular adhesion and decreased motility compared to the wild type (36). CCND1 deficiency was also associated with reduced migration and increased adhesion or focal adhesion substrate by mice bone marrow-derived macrophages (37). This is in line with the changes in fibroblast morphology and motility we observed in our experiments.

FAK (32, 38, 39), ROCK2 (32, 40), and CCND1 (32, 41) have all been previously shown to be direct targets of miR-138; therefore, it is not surprising that we found their expression changed in the fibroblasts that had an altered miR-138 expression. Taken together, our findings suggest that they act in cohort to control fibroblast migration, and that their expression is regulated by miR-138. ITGA11 has been previously associated with the CAF phenotype (42). Our own qRT-PCR data also showed an inverse correlation between the expression levels of miR-138 and ITGA11, which would indicate that ITGA11 is a direct target of miR-138. However, both the inhibitor/mimic experiments and the gene reporter assay could not confirm this hypothesis.

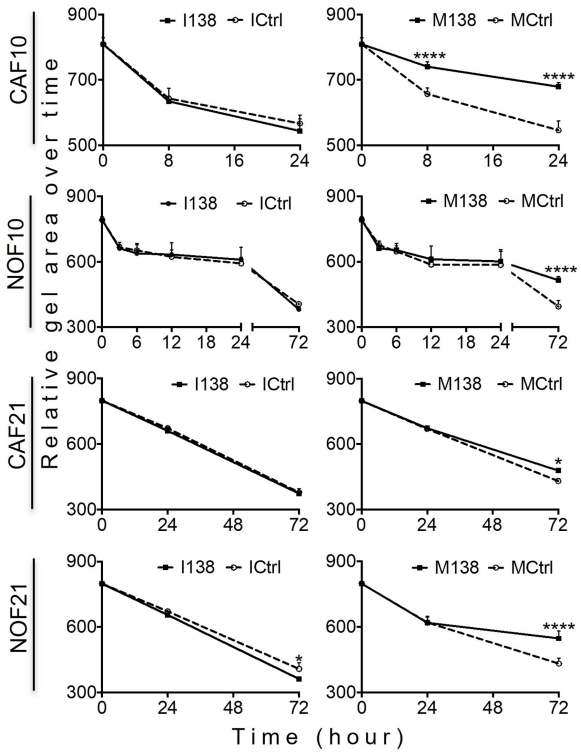

FIGURE 6 | Altered miR-138 expression modulates the ability of fibroblasts to contract collagen gels: Collagen I contraction by CAFs and NOFs over time. n = 4–6; one-way ANOVA; mean ± SD; *$p < 0.05$, ****$p < 0.0001$.

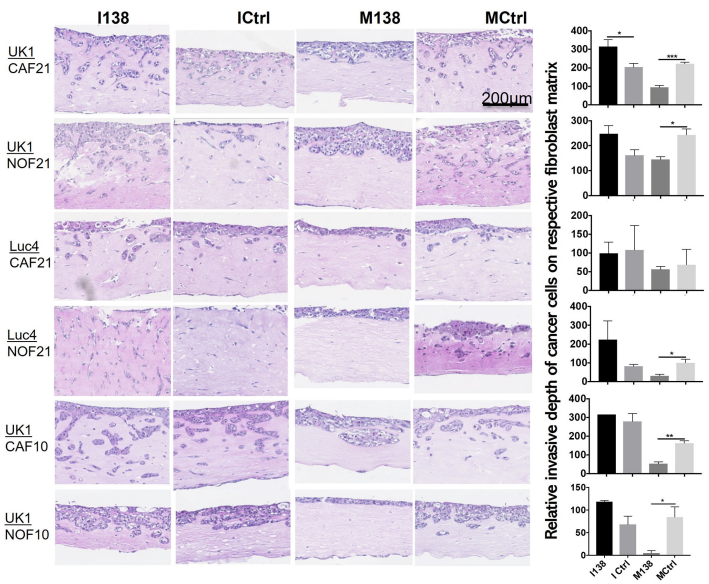

FIGURE 7 | Altered miR-138 expression in fibroblasts modulates invasion of adjacent OSCC cells. HE images of 3D organotypic co-culture depicting invasion of OSCC cells in fibroblast-collagen matrix. Measurement of corresponding invasion distance by OSCC cells on the right. *$p < 0.05$, **$p < 0.01$, ***$p < 0.001$.

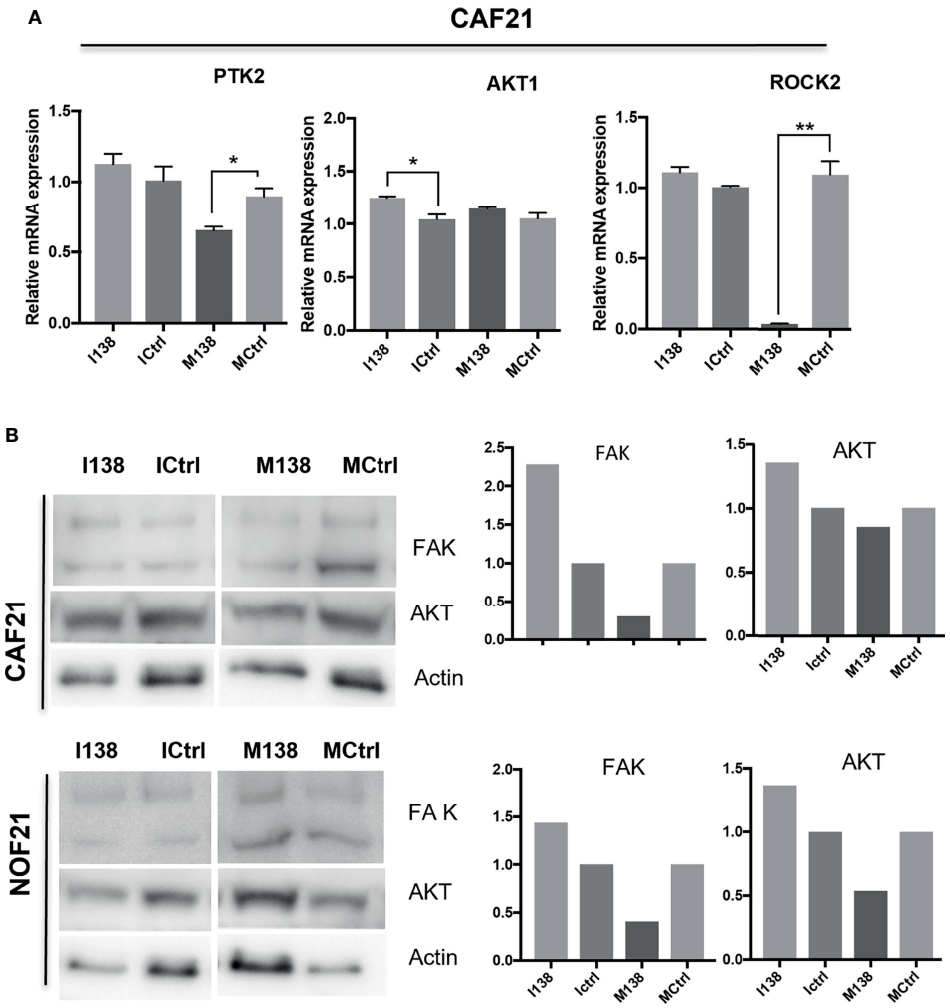

FIGURE 8 | miR-138 expression and investigation of focal adhesion kinase (FAK) axis in CAFs. Alterations in **(A)** mRNA and **(B)** protein expression of several molecules of the FAK axis following miR-204 modulation in CAFs and NOFs. **(B)** Western blot images and the semi-quantification of protein blots with ImageJ. $*p < 0.05$, $**p < 0.01$.

In conclusion, this study supports a tumor-suppressive role for miR-138 in OSCC while expressed in stromal fibroblasts, despite its heterogeneous expression.

DATA AVAILABILITY STATEMENT

The raw data supporting the conclusions of this article will be made available by the authors, without undue reservation.

ETHICS STATEMENT

Ethical approval was obtained from the regional ethical committee in Norway (West Norway; REKVest 3.2006.2620, REKVest 3.2006.1341). The patients/participants provided their written informed consent to participate in this study.

AUTHOR CONTRIBUTIONS

Conceptualization: SR, AJ, DS, and D-EC. Data curation: SR, HP, and HD. Formal analysis: SR and DS. Funding acquisition: D-EC. Investigation: SR, HP, HD, BL, KH, AK, SL, and EN. Methodology: SR, HD, HP, and DS. Project administration: AJ, DS, and D-EC. Supervision: AJ, DS, and D-EC. Validation: SR. Visualization: SR. Writing—original draft: SR. Writing—review and editing: SR, HP, HD, BL, KH, AK, SL, EN, AJ, DS, and D-EC. All authors contributed to the article and approved the submitted version.

FUNDING

This work was supported by the Research Council of Norway through its Centers of Excellence funding scheme (Grant No. 22325), the Western Norway Regional Health Authority (Helse Vest Grant Nos. 911902/2013 and 912260/2019), and the Norwegian Centre for International Cooperation in Education (project number CPEA-LT-2016/10106).

SUPPLEMENTARY MATERIAL

The Supplementary Material for this article can be found online at: https://www.frontiersin.org/articles/10.3389/fonc.2022.833582/full#supplementary-material

Supplementary Figure S1 | Diagram showing *in silico*Kaplan-Meier plot for the survival functions of the clinicopathological characteristics using Log-Rank or * Breslow test. Only significant parameters (p<0.05) are shown. Stage I and II: early stage. Stage III and V: late stage.

Supplementary Figure S2 | Diagram showing *in silico*miR-138 expression in CAF and NOF 48 hours post transfection of respective mimics and inhibitors of miRNAs, and mimics and inhibitor controls (50nM).

Supplementary Figure S3 | Diagram showing *in silico* interrogation of miR-138 targets using miRTarBase database indicating focal adhesion as one of the significantly affected pathways. All 102 miR-138 target genes were fed into DAVID KEGG pathway enrichment analysis (Threshold: Count 2, EASE 0.1, Benjamini test).

Supplementary Table S1 | Patient history and tumour characteristics of OSCC cohort.

Supplementary Table S2 | List of Taqman Assays (ThermoFisher, USA).

Supplementary Table S3 | List of antibodies used in western blot.

Supplementary Table S4 | Table showing *in silico* interrogation of miR-138 targets using miRTarBase database indicating focal adhesion as one of the significantly affected pathways. All 102 miR-138 target genes were fed into DAVID KEGG pathway enrichment analysis (Threshold: Count 2, EASE 0.1, Benjamini test).

REFERENCES

1. Fidler IJ. Timeline - The Pathogenesis of Cancer Metastasis: The 'Seed and Soil' Hypothesis Revisited. *Nat Rev Cancer* (2003) 3(6):453–8. doi: 10.1038/nrc1098
2. Hanahan D, Weinberg RA. Hallmarks of Cancer: The Next Generation. *Cell* (2011) 144(5):646–74. doi: 10.1016/j.cell.2011.02.013
3. Junttila MR, de Sauvage FJ. Influence of Tumour Micro-Environment Heterogeneity on Therapeutic Response. *Nature* (2013) 501(7467):346–54. doi: 10.1038/nature12626
4. Kalluri R. The Biology and Function of Fibroblasts in Cancer. *Nat Rev Cancer* (2016) 16(9):582–98. doi: 10.1038/nrc.2016.73
5. Costea DE, Hills A, Osman AH, Thurlow J, Kalna G, Huang X, et al. Identification of Two Distinct Carcinoma-Associated Fibroblast Subtypes With Differential Tumor-Promoting Abilities in Oral Squamous Cell Carcinoma. *Cancer Res* (2013) 73(13):3888–901. doi: 10.1158/0008-5472.CAN-12-4150
6. Gaggioli C, Hooper S, Hidalgo-Carcedo C, Grosse R, Marshall JF, Harrington K, et al. Fibroblast-Led Collective Invasion of Carcinoma Cells With Differing Roles for RhoGTPases in Leading and Following Cells. *Nat Cell Biol* (2007) 9(12):1392–400. doi: 10.1038/ncb1658
7. Daly AJ, McIlreavey L, Irwin CR. Regulation of HGF and SDF-1 Expression by Oral Fibroblasts - Implications for Invasion of Oral Cancer. *Oral Oncol* (2008) 44(7):646–51. doi: 10.1016/j.oraloncology.2007.08.012
8. Kawashiri S, Tanaka A, Noguchi N, Hase T, Nakaya H, Ohara T, et al. Significance of Stromal Desmoplasia and Myofibroblast Appearance at the Invasive Front in Squamous Cell Carcinoma of the Oral Cavity. *Head Neck-J Sci Special Head Neck* (2009) 31(10):1346–53. doi: 10.1002/hed.21097
9. Kellermann MG, Sobral LM, da Silva SD, Zecchin KG, Graner E, Lopes MA, et al. Myofibroblasts in the Stroma of Oral Squamous Cell Carcinoma Are Associated With Poor Prognosis. *Histopathology* (2007) 51(6):849–53. doi: 10.1111/j.1365-2559.2007.02873.x
10. Parajuli H, Teh MT, Abrahamsen S, Christoffersen I, Neppelberg E, Lybak S, et al. Integrin Alpha11 Is Overexpressed by Tumour Stroma of Head and Neck Squamous Cell Carcinoma and Correlates Positively With Alpha Smooth Muscle Actin Expression. *J Oral Pathol Med* (2017) 46(4):267–75. doi: 10.1111/jop.12493
11. Fujii N, Shomori K, Shiomi T, Nakabayashi M, Takeda C, Ryoke K, et al. Cancer-Associated Fibroblasts and CD163-Positive Macrophages in Oral Squamous Cell Carcinoma: Their Clinicopathological and Prognostic Significance. *J Oral Pathol Med* (2012) 41(6):444–51. doi: 10.1111/j.1600-0714.2012.01127.x
12. Marsh D, Suchak K, Moutasim KA, Vallath S, Hopper C, Jerjes W, et al. Stromal Features Are Predictive of Disease Mortality in Oral Cancer Patients. *J Pathol* (2011) 223(4):470–81. doi: 10.1002/path.2830
13. Bartel DP. MicroRNAs: Genomics, Biogenesis, Mechanism, and Function. *Cell* (2004) 116(2):281–97. doi: 10.1016/S0092-8674(04)00045-5
14. He L, Hannon GJ. Microrrnas: Small RNAs With a Big Role in Gene Regulation. *Nat Rev Genet* (2004) 5(7):522–31. doi: 10.1038/nrg1379
15. Esquela-Kerscher A, Slack FJ. Oncomirs - microRNAs With a Role in Cancer. *Nat Rev Cancer* (2006) 6(4):259–69. doi: 10.1038/nrc1840
16. Calin GA, Croce CM. MicroRNA Signatures in Human Cancers. *Nat Rev Cancer* (2006) 6(11):857–66. doi: 10.1038/nrc1997
17. Suzuki HI, Katsura A, Matsuyama H, Miyazono K. MicroRNA Regulons in Tumor Microenvironment. *Oncogene* (2015) 34(24):3085–94. doi: 10.1038/onc.2014.254
18. Tran N, O'Brien CJ, Clark J, Rose B. Potential Role of Micro-Rnas in Head and Neck Tumorigenesis. *Head Neck-J Sci Special Head Neck* (2010) 32(8):1099–111. doi: 10.1002/hed.21356
19. Min AJ, Zhu C, Peng SP, Rajthala S, Costea DE, Sapkota D. MicroRNAs as Important Players and Biomarkers in Oral Carcinogenesis. *BioMed Res Int* (2015) 2015:186904. doi: 10.1155/2015/186904
20. Sethi N, Wright A, Wood H, Rabbitts P. MicroRNAs and Head and Neck Cancer: Reviewing the First Decade of Research. *Eur J Cancer* (2014) 50(15):2619–35. doi: 10.1016/j.ejca.2014.07.012
21. Rajthala S, Min A, Parajuli H, Debnath KC, Ljokjel B, Hoven KM, et al. Profiling and Functional Analysis of microRNA Deregulation in Cancer-Associated Fibroblasts in Oral Squamous Cell Carcinoma Depicts an Anti-Invasive Role of microRNA-204 *via* Regulation of Their Motility. *Int J Mol Sci* (2021) 22(21). doi: 10.3390/ijms222111960
22. Yeh M, Oh CS, Yoo JY, Kaur B, Lee TJ. Pivotal Role of microRNA-138 in Human Cancers. *Am J Cancer Res* (2019) 9(6):1118–26.
23. Chan XHD, Nama S, Gopal F, Rizk P, Ramasamy S, Sundaram G, et al. Targeting Glioma Stem Cells by Functional Inhibition of a Prosurvival OncomiR-138 in Malignant Gliomas. *Cell Rep* (2012) 2(3):591–602. doi: 10.1016/j.celrep.2012.07.012
24. Manikandan M, Rao AKDM, Rajkumar KS, Rajaraman R, Munirajan AK. Altered Levels of miR-21, miR-125b-2*, miR-138, miR-155, miR-184, and miR-205 in Oral Squamous Cell Carcinoma and Association With Clinicopathological Characteristics. *J Oral Pathol Med* (2015) 44(10):792–800. doi: 10.1111/jop.12300
25. Brito BD, Lourenco SV, Damascena AS, Kowalski LP, Soares FA, Coutinho-Camillo CM. Expression of Stem Cell-Regulating miRNAs in Oral Cavity and Oropharynx Squamous Cell Carcinoma. *J Oral Pathol Med* (2016) 45(9):647–54. doi: 10.1111/jop.12424

26. Liu X, Jiang L, Wang A, Yu J, Shi F, Zhou X. MicroRNA-138 Suppresses Invasion and Promotes Apoptosis in Head and Neck Squamous Cell Carcinoma Cell Lines. *Cancer Lett* (2009) 286(2):217–22. doi: 10.1016/j.canlet.2009.05.030
27. Zhuang Z, Xie N, Hu J, Yu P, Wang C, Hu X, et al. Interplay Between DeltaNp63 and miR-138-5p Regulates Growth, Metastasis and Stemness of Oral Squamous Cell Carcinoma. *Oncotarget* (2017) 8(13):21954–73. doi: 10.18632/oncotarget.15752
28. Rajthala S, Dongre H, Parajuli H, Min A, Nginamau ES, Kvalheim A, et al. Combined *In Situ* Hybridization and Immunohistochemistry on Archival Tissues Reveals Stromal microRNA-204 as Prognostic Biomarker for Oral Squamous Cell Carcinoma. *Cancers (Basel)* (2021) 13(6). doi: 10.3390/cancers13061307
29. Locke M, Heywood M, Fawell S, Mackenzie IC. Retention of Intrinsic Stem Cell Hierarchies in Carcinoma-Derived Cell Lines. *Cancer Res* (2005) 65 (19):8944–50. doi: 10.1158/0008-5472.CAN-05-0931
30. Biddle A, Liang X, Gammon L, Fazil B, Harper LJ, Emich H, et al. Cancer Stem Cells in Squamous Cell Carcinoma Switch Between Two Distinct Phenotypes That Are Preferentially Migratory or Proliferative. *Cancer Res* (2011) 71 (15):5317–26. doi: 10.1158/0008-5472.CAN-11-1059
31. Kent WJ, Sugnet CW, Furey TS, Roskin KM, Pringle TH, Zahler AM, et al. The Human Genome Browser at UCSC. *Genome Res* (2002) 12(6):996–1006. doi: 10.1101/gr.229102
32. Chou CH, Shrestha S, Yang CD, Chang NW, Lin YL, Liao KW, et al. Mirtarbase Update 2018: A Resource for Experimentally Validated microRNA-Target Interactions. *Nucleic Acids Res* (2018) 46(D1):D296–302. doi: 10.1093/nar/gkx1067
33. Mierke CT, Fischer T, Puder S, Kunschmann T, Soetje B, Ziegler WH. Focal Adhesion Kinase Activity is Required for Actomyosin Contractility-Based Invasion of Cells Into Dense 3D Matrices. *Sci Rep* (2017) 7:42780. doi: 10.1038/srep42780
34. Parsons JT, Martin KH, Slack JK, Taylor JM, Weed SA. Focal Adhesion Kinase: A Regulator of Focal Adhesion Dynamics and Cell Movement. *Oncogene* (2000) 19(49):5606–13. doi: 10.1038/sj.onc.1203877
35. Sahai E, Astsaturov I, Cukierman E, DeNardo DG, Egeblad M, Evans RM, et al. A Framework for Advancing Our Understanding of Cancer-Associated Fibroblasts. *Nat Rev Cancer* (2020) 20(3):174–86. doi: 10.1038/s41568-019-0238-1
36. Li Z, Wang C, Jiao X, Lu Y, Fu M, Quong AA, et al. Cyclin D1 Regulates Cellular Migration Through the Inhibition of Thrombospondin 1 and ROCK Signaling. *Mol Cell Biol* (2006) 26(11):4240–56. doi: 10.1128/MCB.02124-05
37. Neumeister P, Pixley FJ, Xiong Y, Xie HF, Wu KM, Ashton A, et al. Cyclin D1 Governs Adhesion and Motility of Macrophages. *Mol Biol Cell* (2003) 14 (5):2005–15. doi: 10.1091/mbc.02-07-0102
38. Kawamoto M, Yamaji T, Saito K, Shirasago Y, Satomura K, Endo T, et al. Identification of Characteristic Genomic Markers in Human Hepatoma HuH-7 and Huh7.5.1-8 Cell Lines. *Front Genet* (2020) 11:546106. doi: 10.3389/fgene.2020.546106
39. Golubovskaya VM, Sumbler B, Ho B, Yemma M, Cance WG. MiR-138 and MiR-135 Directly Target Focal Adhesion Kinase, Inhibit Cell Invasion, and Increase Sensitivity to Chemotherapy in Cancer Cells. *Anticancer Agents Med Chem* (2014) 14(1):18–28. doi: 10.2174/18715206140114010811343 5
40. Jiang L, Liu XQ, Kolokythas A, Yu JS, Wang AX, Heidbreder CE, et al. Downregulation of the Rho GTPase Signaling Pathway is Involved in the microRNA-138-Mediated Inhibition of Cell Migration and Invasion in Tongue Squamous Cell Carcinoma. *Int J Cancer* (2010) 127(3):505–12. doi: 10.1002/ijc.25320
41. Liu X, Lv XB, Wang XP, Sang Y, Xu SB, Hu KS, et al. MiR-138 Suppressed Nasopharyngeal Carcinoma Growth and Tumorigenesis by Targeting the CCND1 Oncogene. *Cell Cycle* (2012) 11(13):2495–506. doi: 10.4161/cc.20898
42. Zeltz C, Alam J, Liu H, Erusappan PM, Hoschuetzky H, Molven A, et al. Alpha11beta1 Integrin is Induced in a Subset of Cancer-Associated Fibroblasts in Desmoplastic Tumor Stroma and Mediates *In Vitro* Cell Migration. *Cancers (Basel)* (2019) 11(6). doi: 10.3390/cancers11060765

Conflict of Interest: The authors declare that the research was conducted in the absence of any commercial or financial relationships that could be construed as a potential conflict of interest.

Publisher's Note: All claims expressed in this article are solely those of the authors and do not necessarily represent those of their affiliated organizations, or those of the publisher, the editors and the reviewers. Any product that may be evaluated in this article, or claim that may be made by its manufacturer, is not guaranteed or endorsed by the publisher.

frontiers | Frontiers in Oncology

SYSTEMATIC REVIEW
published: 28 April 2022
doi: 10.3389/fonc.2022.856831

Epidemiological Evidence Between Variants in Matrix Metalloproteinases-2, -7, and -9 and Cancer Risk

*Chenglu Huang[1], Suqin Xu[2], Zhilin Luo[1], Dong Li[1], Rui Wang[1] and Tianhu Wang[1]**

[1] Department of Thoracic Surgery, The Third Affiliated Hospital of Chongqing Medical University, Chongqing, China,
[2] Department of Radiology, Chongqing University Cancer Hospital, Chongqing, China

Background: Matrix metalloproteinases (*MMP*s), a kind of proteases, have a critical function in cancer occurrence, invasion, and migration. *MMP* gene variants (e.g., *MMP-2*, *MMP-7*, and *MMP-9*) can affect the biological functions of these enzymes and lead to the occurrence and progression of cancer, which has become a hot topic in recent years, but the corresponding results are still controversial. In this context, here, the meta-analysis was conducted for assessing the relations of variants in *MMP-2*, *MMP-7*, and *MMP-9* with the risk of various cancers.

Methods: PubMed, Web of Science, and Medline were systemically searched, and data were extracted from all eligible studies so as to investigate the susceptibility of *MMP-2*, *MMP-7*, and *MMP-9* to different types of cancers. The association between a variant in *MMP* and cancer susceptibility was analyzed through odds ratios (ORs) as well as 95% CIs. The Venice criteria and false-positive report probability (FPRP) were adopted to evaluate epidemiological evidence of significant associations discovered.

Results: The associations between the variants of *MMP*s and cancer risk in 36,530 cases and 41,258 controls were found, with 12 associations (*MMP-2* rs243865 with esophageal cancer and lung cancer, *MMP-7* rs11568818 with bladder and cervical cancer, and *MMP-9* rs3918242 with breast cancer) rated as strong associations for cancer risk and 7 and 15 as moderate and weak associations, respectively. These significant associations were mostly found in Asians.

Conclusions: These findings support the relations between variants of *MMP-2*, *MMP-7*, and *MMP-9* and various cancers risk, demonstrating the credibility of these relations.

Keywords: matrix metalloproteinases, variant, meta-analysis, gene, cancer

OPEN ACCESS

Edited by:
César López-Camarillo, Universidad Autónoma de la Ciudad de México, Mexico

Reviewed by:
Nosheen Masood, Fatima Jinnah Women University, Pakistan
Snjezana Ramic, Sestre Milosrdnice University Hospital Center, Croatia
Damir Danolić, University Hospital for Tumors, Croatia

****Correspondence:***
Tianhu Wang
650221@hospital.cqmu.edu.cn

Specialty section:
This article was submitted to Cancer Genetics, a section of the journal Frontiers in Oncology

Received: *17 January 2022*
Accepted: *31 March 2022*
Published: *28 April 2022*

Citation:
Huang C, Xu S, Luo Z, Li D, Wang R and Wang T (2022) Epidemiological Evidence Between Variants in Matrix Metalloproteinases-2, -7, and -9 and Cancer Risk. Front. Oncol. 12:856831. doi: 10.3389/fonc.2022.856831

INTRODUCTION

Cancer accounts for a major cause resulting in global mortality following ischemic heart disease, and the number of death cases and morbidity cases is increasing year by year, thus likely becoming the first in 2060 (1, 2). In previous works, *MMP*s are the most prominent family of proteinases

associated with tumorigenesis (3). They are the zn-dependent endopeptidases, which are responsible for degrading basement membrane (BM) and extracellular matrix (ECM), participating in tumor genesis and development (4, 5). Actually, the relationship between these enzymes and tumors is mainly manifested in mediating cell–cell and cell–stromal interactions, thus promoting tumor cell migration and angiogenesis. Here, it should be noted that the remodeling of ECM and BM can be considered an important tumor cell migration and invasion process. *MMP*s are responsible for degrading each BM and ECM protein component and breaking the cancer cell invasion barrier and have important functions in cancer migration and invasion, which have been thus regarded as the major proteases (6–8). According to the substrate and fragment homology, *MMP*s are divided into six categories, namely, collagenase, gelatinase, stroma degrading, stroma lysin, furin-activated *MMP*, and other secreted *MMP*s.

MMP-2, *MMP-7*, and *MMP-9* account for the three key components in *MMP* family. *MMP-2* is widely distributed *in vivo* and expressed in most cells including stromal cells, endothelial cells, and epithelial cells, with a relative molecular weight of 72,000, also known as gelatinase A, which can hydrolyze type IV, V, I, and III collagen, laminin, and elastin (9). *MMP-7*, which is called matrilysin as well, represents the smallest matrix metalloproteinase due to its lack of a carboxy-terminal heme-binding protein-like domain (10). Active *MMP-7* not only degrades ECM but also activates other potential forms of *MMP*s, such as *MMP-2* and *MMP-9*. As for *MMP-9* aka gelatinase B, its precursor can be secreted by monocytes, macrophages, neutrophils, vascular smooth muscle cells, endothelial cells, foam cells, fibroblasts, microglial cells, and tumor cells (11–13). Furthermore, it is activated by enzymatic hydrolysis at or near the 87th amino acid residues, which can hydrolyze various components of BM and ECM, such as collagen IV, thus playing a key role in cancer cell migration and invasion (14).

As early as 2002, Yu et al. discovered in their case–control research that *MMP-2* rs243865 was associated with a higher lung cancer (LC) susceptibility (odds ratio (OR) = 2.15, 95% CI = 1.70–2.71, $p < 0.05$) in Asian populations (15); however, in 2019, Chen et al. reported in their case–control research in the Asian populations that *MMP-2* rs243865 reduced LC susceptibility (OR = 0.54, 95% CI = 0.41–0.72, $p < 0.05$) (16). Moreover, in 2015, Zhang et al. found that *MMP-2* rs243865 had a decreased risk of esophageal squamous cell carcinoma (ESCC) (OR = 0.32, 95% CI = 0.10–0.89, $p = 0.02$) in a case–control study (17); interestingly, Eftekhary et al. revealed that *MMP-2* rs243865 had no association with risk of ESCC among the Asian populations (OR = 0.86, 95% CI = 0.39–1.93, $p = 0.718$) (18). Apart from that, in 2010, Peng et al. pointed out in their meta-analysis that *MMP-2* rs243865 was not related to colorectal cancer (CRC) (19). On the other hand, in 2015, according to Wu et al., they discovered in their meta-analysis that *MMP-2* rs243865 was a risk factor for CRC susceptibility, especially in Caucasians (20).

Although the relations between *MMP-2*, *MMP-7*, and *MMP-9* and various tumors risk had been demonstrated in previous studies, the conclusions were inconsistent. Therefore, in order to obtain more accurate conclusions, this integrative meta-analysis for evaluating the relations of *MMP-2*, *MMP-7*, and *MMP-9* variants with the risk of cancer was conducted.

MATERIALS AND METHODS

Literature Search

PubMed, Embase, and Web of Science were searched for identifying relatedarticlesfrominceptiontoJune20,2021,byadoptingthefollowing terms: ("tumor" or "malignant" or "malignancy" or "neoplasm" or "neoplasia" or "oncology" or "cancer" or "carcinoma" or "adenocarcinoma"), ("variant" or "variation" or "genotype" or "mutation" or "rs" or "polymorphism" or "single nucleotide polymorphism" or "SNP"), and ("matrix metalloproteinase" or "matrix metalloproteinases" or "MMP" or "MMPs" or "metalloproteinases" or "collagenase" or "gelatinase" or "matrilysin"). Furthermore, reference lists were also manually retrieved to discover eligiblearticles.

Criteria for Selection

Studies were selected by the following criteria: a) investigating associations between variants in *MMP-2*, *MMP-7*, and *MMP-9* and cancer risk by cohort, or case–control or cross-sectional studies in humans; b) being published in English; and c) providing case and control numbers, or available allele distribution and/or genotype number when necessary. Studies conforming to the following criteria were eliminated: a) not enough data and b) being in the form of meta-analyses, review articles, abstracts, editorials, letters to the editor, case reports, guidelines for management, and animal studies.

Data Extraction

Two authors (CH and SX) were responsible for data extraction; any disagreement between them was settled through mutual negotiation. The information extracted included the first author, country, race, publication year, tumor type, genetic variant, gene name, case and control numbers, and genotype distribution frequencies in cases and controls. In our study, the data of Asians and Caucasians, as well as those of different races in three genetic models, were mainly analyzed. For the mutation pattern of a genetic variant, https://www.ncbi.nlm.nih.gov/snp/ was browsed for confirmation.

Statistical Analysis

All data were obtained by Stata software, version 12.0 (Stata, College Station, TX, USA). The three genetic models were analyzed comprehensively, and ethnic subgroup analysis was performed where necessary. I^2 statistics and Cochran's Q test were applied in evaluating data heterogeneities from different articles, while heterogeneity was classified by I^2 value into three levels, ≤25%, 25%–50%, and ≥50%, which stood for little, moderate, and large heterogeneities, respectively. In addition, $P_Q < 0.1$ indicated that a random-effects model must be adopted; or else, a fixed-effect model should be utilized. In addition, the

robustness of the ORs with significant analyses was evaluated by sensitivity analysis, such as the first published study and studies deviated from the Hardy–Weinberg equilibrium (HWE) among controls. The small-study effect was analyzed by Egger's test, whereas potential publication bias by Begg's test ($p < 0.1$ is usually considered evidence for significant evidence of small-study effect or publication bias).

Evaluation of Cumulative Evidence

The Venice criteria were adopted for evaluating epidemiological evidence of obvious associations obtained from meta-analyses, which were graded as weak, moderate, and strong according to the replication of association, amount of evidence, and protection from bias. The A, B, or C grade was given according to the aforementioned criteria. Replication of association was evaluated through heterogeneity statistics, which was classified as grade A, B, or C depending on I^2 value (≤25%, 25%–50%, or ≥50%, respectively). The amount of evidence (grade A, B, or C) was evaluated through the overall genotype or allele number of control and case groups. (grade A: large scale evidence, minor genetic groups (alleles or genotypes) in cases and controls >1,000; grade B: moderate amount of evidence, minor genetic groups in cases and controls between 100 and 1,000; and grade C: little evidence, minor genetic groups in cases and controls <100). Protection from bias was mainly measured through bias tests and sensitivity analysis, like a single study (dataset), or the first published study, or studies that deviated from the HWE among controls. Grade A indicated no observable bias, and bias was unlikely to explain the presence of the association. Grade B suggested that there was considerable missing information on the identification of evidence, while grade C indicated that there was bias explaining the association. According to the Venice criteria, cumulative epidemiologic creditability for significant association was rated as a strong association if all three grades were A, moderate if a combination of A or B, and weak if any grade was C.

The presence of significant association that might be eliminated as the false-positive result by the false-positive report probability (FPRP) test was analyzed (21). Furthermore, the FPRP with a cutoff value of 0.20 and a prior probability concerning the significant association of 0.05 was calculated. As for FPRP values, <0.05, 0.05–0.20, and >0.20 indicated strong, moderate, and weak creditability of true association, respectively. Later, the FPRP test was conducted to reassess the credibility of the Venice criteria. In the case of strong evidence for true association evidenced by the FPRP test, cumulative evidence was upgraded from moderate to strong or from weak to moderate. In addition, in the case of weak evidence of true association, cumulative evidence was downgraded from strong to moderate or from moderate to weak. If the evidence for a true association was moderate, $0.05 < FPRP < 0.20$, the cumulative evidence was neither upgraded nor downgraded.

RESULTS

Characteristics of Eligible Studies

It was observed from **Figure 1** that PubMed, Embase, and Web of Science databases were systemically searched for identifying related articles, and altogether, 135 studies were obtained.

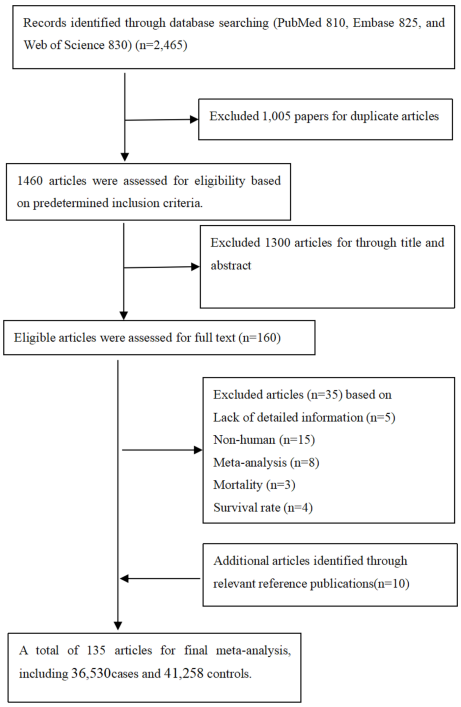

FIGURE 1 | Flow diagram of search strategy and study selection.

Among them, 23 articles were eliminated through abstract and keyword reading, while 12 articles were eliminated through full-text reading. Furthermore, 10 articles were selected from the references. Finally, 135 articles on *MMP-2*, *MMP-7*, and *MMP-9* polymorphisms related to cancer risk were included in the meta-analysis, among which 36,530 were cases and 41,258 were controls. Other than that, **Supplementary Table S2** shows basic characteristics of articles, including the first author, the publication year, cases and controls, cancer and genotype, ethnicity, and the rs number. In addition to that, in these papers, the relations between *MMP-2*, *MMP-7*, and *MMP-9* polymorphisms and the risk of a variety of cancers were evaluated.

Main Meta-Analyses

Meta-analyses were conducted for assessing the relations among variants in *MMP-2*, *MMP-7*, and *MMP-9* and cancer risk. These results are shown in **Table 1**. There were three variants remarkably related to cancer risk, including *MMP-2* rs243865, *MMP-7* rs11568818, and *MMP-9* rs3918242. To be specific, in our research, a significant association between *MMP-2* rs243865 and esophageal cancer risk in Asians was demonstrated (allelic model, OR = 0.751, 95% CI = 0.643–0.877, $p < 0.001$; dominant model, OR = 0.723, 95% CI = 0.607–0.862, $p < 0.001$). Furthermore, it was also revealed that *MMP-2* rs243865 had significant association with LC incidence among the overall populations under the allelic and dominant models (allelic model, OR = 0.654, 95% CI = 0.507–0.844, $p = 0.001$; dominant model, OR = 0.613, 95% CI = 0.457–0.823, $p = 0.001$). Apart from that, *MMP-2* rs243865 in the recessive, dominant, and allelic models showed obvious relations

TABLE 1 | Significant associations between variants in the *MMP-2*, *MMP-7*, and *MMP-9* and cancer risk.

Gene	Variant	Alleles	Cancer site	Ethnicity	MAF	Number evaluation		Risk of Meta-Analysis						Venice criteria	FPRP values	Credibility of evidence
						Studies	Sample size (cases/controls)	Genetic models	Effect model	OR (95% CI)	*p*-Value	*I2*	PQ			
MMP2	rs243865	TvsC	Esophageal	Asian	0.1565	4	2,850 (1,157/1,693)	Allelic	Fixed	0.751 (0.643–0.877)	<0.001	41.4	0.163	BBA	0.006	Strong
MMP2	rs243865	TvsC	Esophageal	Asian	0.1565	4	2,850 (1,157/1,693)	Dominant	Fixed	0.723 (0.607–0.862)	<0.001	46.9	0.13	BBA	0.007	Strong
MMP2	rs243865	TvsC	Lung	Overall	0.1679	5	4,734 (2,199/2,535)	Allelic	Random	0.654 (0.507–0.844)	0.001	72.1	0.006	ACC	0.045	Moderate
MMP2	rs243865	TvsC	Lung	Overall	0.1679	5	4,734 (2,199/2,535)	Dominant	Random	0.613 (0.457–0.823)	0.001	73.8	0.004	ACC	0.07	Weak
MMP2	rs243865	TvsC	Lung	Asian	0.1667	3	4,254 (1,909/2,345)	Allelic	Fixed	0.534 (0.468–0.610)	<0.001	0.0	0.837	AAA	5.60083E–07	Strong
MMP2	rs243865	TvsC	Lung	Asian	0.1667	3	4,254 (1,909/2,345)	Dominant	Fixed	0.484 (0.417–0.561)	<0.001	0.0	0.864	AAA	2.79371E–10	Strong
MMP2	rs243865	TvsC	Lung	Asian	0.1667	3	4,254 (1,909/2,345)	Recessive	Fixed	0.616 (0.385–0.985)	0.043	0.0	0.944	CAC	0.688	Weak
MMP2	rs243865	TvsC	Nasopharyngeal	Asian	0.1083	3	2,946 (1,381/1,565)	Dominant	Random	0.686 (0.492–0.957)	0.026	63.0	0.067	BCC	0.47	Weak
MMP2	rs243865	TvsC	Prostate	Overall	0.2044	6	1,433 (699/734)	Dominant	Fixed	1.365 (1.094–1.703)	0.006	7.1	0.371	BAA	0.122	Moderate
MMP2	rs243865	TvsC	Prostate	Asian	0.1535	3	732 (341/391)	Allelic	Fixed	1.480 (1.131–1.936)	0.004	0.0	0.868	BAA	0.13	Moderate
MMP2	rs243865	TvsC	Prostate	Asian	0.1535	3	732 (341/391)	Dominant	Fixed	1.657 (1.207–2.276)	0.002	0.0	0.962	BAA	0.114	Moderate
MMP7	rs11568818	CvsT	Bladder	Overall	0.291	4	2,377 (1,169/1,208)	Allelic	Fixed	1.204 (1.055–1.374)	0.006	0.0	0.405	AAA	0.1	Strong
MMP7	rs11568818	CvsT	Bladder	Overall	0.291	4	2,377 (1,169/1,208)	Recessive	Fixed	1.538 (1.198–1.974)	0.001	0.0	0.696	BAA	0.032	Strong
MMP7	rs11568818	CvsT	Bladder	Asian	0.2651	3	1,938 (929/1,009)	Allelic	Fixed	1.229 (1.056–1.431)	0.008	23.7	0.269	AAA	0.131	Strong
MMP7	rs11568818	CvsT	Bladder	Asian	0.2651	3	1,938 (929/1,009)	Recessive	Fixed	1.560 (1.166–2.087)	0.003	0.0	0.494	BAA	0.116	Moderate
MMP7	rs11568818	CvsT	Cervical	Asian	0.2896	3	1,179 (597/582)	Allelic	Fixed	1.372 (1.148–1.640)	0.001	0.0	0.583	BAA	0.012	Strong
MMP7	rs11568818	CvsT	Cervical	Asian	0.2896	3	1,179 (597/582)	Dominant	Fixed	1.381 (1.088–1.753)	0.008	52.8	0.12	BCC	0.168	Weak
MMP7	rs11568818	CvsT	Cervical	Asian	0.2896	3	1,179 (597/582)	Recessive	Fixed	1.664 (1.175–2.357)	0.004	52.7	0.121	BCA	0.22	Weak
MMP7	rs11568818	CvsT	Colorectal	Asian	0.1292	5	2,214 (1,045/1,169)	Allelic	Fixed	0.771 (0.629–0.945)	0.012	0.0	0.566	BAA	0.202	Weak
MMP7	rs11568818	CvsT	Colorectal	Asian	0.1292	5	2,214 (1,045/1,169)	Recessive	Fixed	0.450 (0.256–0.790)	0.005	12.6	0.285	CAC	0.546	Weak
MMP9	rs3918242	TvsC	Breast	Overall	0.1967	6	3,316 (1,656/1,660)	Allelic	Fixed	1.281 (1.134–1.447)	<0.001	29.2	0.216	AAA	0.001	Strong
MMP9	rs3918242	TvsC	Breast	Overall	0.1967	6	3,316 (1,656/1,660)	Dominant	Fixed	1.236 (1.065–1.434)	0.005	21.8	0.27	AAC	0.09	Weak

(Continued)

TABLE 1 | Continued

Gene	Variant	Alleles	Cancer site	Ethnicity	MAF	Number evaluation		Risk of Meta-Analysis						Venice criteria	FPRP values	Credibility of evidence
						Studies	Sample size (cases/controls)	Genetic models	Effect model	OR (95% CI)	*p*-Value	*I2*	PQ			
MMP9	rs3918242	TvsC	Breast	Overall	0.1967	6	3,316 (1,656/1,660)	Recessive	Fixed	1.681 (1.279–2.209)	<0.001	0.0	0.723	BAA	0.017	Strong
MMP9	rs3918242	TvsC	Breast	Asian	0.3042	3	1,196 (601/595)	Allelic	Fixed	1.501 (1.263–1.785)	<0.001	0.0	0.731	BAC	0.0002	Moderate
MMP9	rs3918242	TvsC	Breast	Asian	0.3042	3	1,196 (601/595)	Dominant	Fixed	1.526 (1.207–1.930)	<0.001	0.0	0.628	BAA	0.018	Strong
MMP9	rs3918242	TvsC	Breast	Asian	0.3042	3	1,196 (601/595)	Recessive	Fixed	1.710 (1.262–2.317)	0.001	0.0	0.917	BAA	0.049	Strong
MMP9	rs3918242	TvsC	Gastric	Asian	0.2385	3	1,128 (539/589)	Recessive	Fixed	1.612 (1.000–2.598)	0.05	0.0	0.551	CAA	0.712	Weak
MMP9	rs3918242	TvsC	Hepatocellular	Overall	0.1589	3	1,280 (657/623)	Recessive	Fixed	1.973 (1.068–3.645)	0.03	48.1	0.165	CBA	0.749	Weak
MMP9	rs3918242	TvsC	Lung	Overall	0.141	5	2,980 (1,539/1,447)	Allelic	Random	0.754 (0.570–0.999)	0.049	63.3	0.028	BCA	0.537	Weak
MMP9	rs3918242	TvsC	Lung	Overall	0.141	5	2,980 (1,539/1,447)	Recessive	Fixed	0.355 (0.177–0.712)	0.004	42.1	0.159	CCA	0.639	Weak
MMP9	rs3918242	TvsC	Lung	Caucasian	0.1496	3	1,890 (1,051/839)	Allelic	Fixed	0.798 (0.661–0.962)	0.018	0.0	0.502	BAA	0.276	Weak
MMP9	rs3918242	TvsC	Lung	Caucasian	0.1496	3	1,890 (1,051/839)	Recessive	Fixed	0.257 (0.118–0.561)	0.001	0.0	0.615	CAC	0.595	Weak
MMP9	rs3918242	TvsC	Oral	Overall	0.1406	3	1,545 (770/775)	Allelic	Fixed	1.309 (1.078–1.589)	0.007	26.8	0.255	BAA	0.118	Moderate
MMP9	rs3918242	TvsC	Oral	Overall	0.1406	3	1,545 (770/775)	Recessive	Fixed	3.497 (1.812–6.749)	<0.001	0.0	0.717	CAA	0.383	Weak

Allelics: minor allelic (bold) vs. major allelic. Venice criteria grades are for amount of evidence, replication of the association, and protection from bias. The prior probability of FPRP is 0.05, and the FPRP level of noteworthiness is 0.20. C, cytosine; T, thymine; OR, odds ratio; MAF, minor allelic frequency in control; FPRP, false-positive report probability.

with LC incidence among Asian populations (allelic model, OR = 0.534, 95% CI = 0.468–0.610, $p < 0.001$; dominant model, OR = 0.484, 95% CI = 0.417–0.561, $p < 0.001$; recessive model, OR = 0.616, 95% CI = 0.385–0.985, $p = 0.043$). *MMP-2* rs243865 was significantly related to nasopharyngeal cancer (NPC) risk among the Asian populations by the dominant model (OR = 0.686, 95% CI = 0.492–0.957, $p = 0.026$). With regard to prostate cancer (PCa), *MMP-2* rs243865 was significantly related to PCa incidence among the overall populations in the dominant model (OR = 1.365, 95% CI = 1.094–1.703, $p = 0.006$). Furthermore, *MMP-2* rs243865 was dramatically related to PCa incidence among the Asian populations (dominant model, OR = 1.657, 95% CI = 1.207–2.276, $p = 0.002$; allelic model, OR = 1.480, 95% CI = 1.131–1.936, $p = 0.004$).

For *MMP-7*, it was discovered that *MMP-7* rs11568818 was markedly related to bladder cancer susceptibility among the overall populations under the allelic and recessive models (allelic model, OR = 1.204, 95% CI = 1.055–1.374, $p = 0.006$; recessive model, OR = 1.538, 95% CI = 1.198–1.974, $p = 0.001$) instead of the dominant model; however, in Asians, *MMP-7* rs11568818 was obviously related to bladder cancer risk (allelic model, OR = 1.229, 95% CI = 1.056–1.431, $p = 0.008$; recessive model, OR = 1.560, 95% CI = 1.166–2.087, $p = 0.003$). Moreover, the *MMP-7* rs11568818 was evidently associated with a higher cervical cancer (CC) incidence in Asians (allelic model, OR = 1.372, 95% CI = 1.148–1.640, $p = 0.001$; dominant model, OR = 1.381, 95% CI = 1.088–1.753, $p = 0.008$; recessive model, OR = 1.664, 95% CI = 1.175–2.357, $p = 0.004$). In addition, it was also known that *MMP-7* rs11568818 under the recessive and allelic models was noticeably related to CRC incidence among the Asian populations (allelic model, OR = 0.771, 95% CI = 0.629–0.945, $p = 0.012$; recessive model, OR = 0.450, 95% CI = 0.256–0.790, $p = 0.005$).

MMP-9 rs3918242 was definitely relevant to breast cancer (BC) incidence among the overall populations (allelic model, OR = 1.281, 95% CI = 1.134–1.447, $p < 0.001$; dominant model, OR = 1.236, 95% CI = 1.065–1.434, $p = 0.005$; recessive model, OR = 1.681, 95% CI = 1.279–2.209, $p < 0.001$) and in Asians (allelic model, OR = 1.501, 95% CI = 1.263–1.785, $p < 0.001$; dominant model, OR = 1.526, 95% CI = 1.207–1.930, $p < 0.001$; recessive model, OR = 1.710, 95% CI = 1.262–2.317, $p = 0.001$) under three models. *MMP-9* rs3918242 was remarkably related to gastric cancer (GC) incidence among the Asian populations in the recessive model (OR = 1.612, 95% CI = 1.000–2.598, $p = 0.05$). Additionally, *MMP-9* rs3918242 was dramatically related to hepatocellular cancer (HCC) incidence among the overall populations in the recessive model (OR = 1.973, 95% CI = 1.068–3.645, $p = 0.03$). On the other hand, *MMP-9* rs3918242 was also markedly related to LC incidence in the recessive or allelic model in all populations (allelic model, OR = 0.754, 95% CI = 0.570–0.999, $p = 0.049$; recessive model, OR = 0.355, 95% CI = 0.177–0.712, $p = 0.004$). Furthermore, *MMP-9* rs3918242 was observably connected to LC incidence in the recessive and allelic models in Caucasians (recessive model, OR = 0.257, 95% CI = 0.118–0.561, $p = 0.001$; allelic model, OR = 0.798, 95% CI = 0.661–0.962, $p = 0.018$). Finally, it was revealed that *MMP-9* rs3918242 under the allelic and recessive models was remarkably related to oral cancer incidence among the overall populations (allelic model, OR = 1.309, 95% CI = 1.078–1.589, $p = 0.007$; recessive model, OR = 3.497, 95% CI = 1.812–6.749, $p < 0.001$).

In addition, in the current study, it can be seen that *MMP-2* rs243865 was not obviously related to the risk of certain cancer types in three models, such as BC, bladder cancer, CRC, GC, oral cancer, and lymphoma. *MMP-2* rs1053605 was not markedly related to LC incidence among the overall populations and Caucasians under three models, while *MMP-7* rs11568818 was not related to the risk of certain cancer types in three models, such as BC, GC, and LC. Furthermore, *MMP-9* rs3918242 was not related to the incidence of certain cancer types, like bladder cancer, CRC, and esophageal cancer. *MMP-9* rs17576 was not related to CRC incidence under three models in Asians.

Cumulative Evidence of Association

The details of the epidemiological evidence for three variants related to cancer risk can be observed in **Table 1**. Firstly, the Venice criteria were followed to evaluate these associations. As for the amount of evidence, 8, 19, and 7 associations were graded as grades A, B, and C, respectively, for further evaluating evidence credibility. With regard to replication of association, 24, 3, and 7 associations were graded as grades A, B, and C, respectively, for further assessment. As for the protection from bias, 25, 0, and 9 associations were graded as grades A, B, and C, respectively, for additional analysis. Five of the associations were rated as strong (*MMP-2* rs243865 among the Asian populations in the dominant and allelic models with LC risk, *MMP-7* rs11568818 in all populations or Asians under the allelic model with bladder cancer risk, and *MMP-9* rs3918242 in all populations under the allelic model with BC risk), 13 associations were rated as moderate (*MMP-2* rs243865 with esophageal cancer risk among the Asian populations in the dominant and allelic models and with PCa risk among the overall populations in the dominant model, as well as among the Asian populations in the dominant and allelic models; in addition, *MMP-7* rs11568818 was associated with bladder cancer risk among the Asian and overall populations in the recessive model with bladder cancer risk, *MMP-7* rs11568818 in Asians under the allelic model with CC risk, and *MMP-7* rs11568818 in Asians under the allelic model with CRC risk; furthermore, *MMP-9* rs3918242 was related to BC risk among Asian populations in the recessive or dominant model and among the overall populations in the recessive model, and *MMP-9* rs3918242 in all populations under the allelic model with oral cancer risk), and 16 associations were rated as weak (*MMP-2* rs243865 among Asian populations in the recessive model and among the overall populations in the dominant or allelic model with LC risk, *MMP-2* rs243865 in Asians under the dominant model with NPC risk, *MMP-7* rs11568818 in Asians under the dominant or recessive model with CC risk and among Asian population in the recessive model with CRC risk, *MMP-9* rs3918242 associated with BC risk among Asian populations in the allelic model and the overall populations in the dominant model, and *MMP-9* rs3918242 related to HCC risk among the

overall populations in the recessive model, to GC risk among Asian populations in the recessive model, and to LC risk among Caucasians or the overall populations in the recessive and allelic models, and in all populations under the recessive model with oral cancer risk) based on the Venice criteria.

By calculating FPRP values, the probability that nominally significant variants were truly related to cancer incidence was assessed. Of the above associations with cancer risk, 12 associations had a *p*-value of FPRP less than 0.05, while 10 associations were featured with a *p*-value from 0.05 to 0.2, and the *p*-value of the remaining 12 associations was greater than 0.2. Consequently, the cumulative evidence of association was reassessed. It was strong for *MMP-2* rs243865 with LC and esophageal cancer risk among the Asian populations in the dominant and allelic models. *MMP-7* rs11568818 was related to bladder cancer risk among the Asian populations in the allelic model, bladder cancer risk among the overall populations in the recessive or allelic model, and CC risk in Asians under the allelic model, whereas *MMP-9* rs3918242 was associated with BC risk among the Asian population in the dominant and recessive models and the overall populations in the recessive and allelic models (**Supplementary Figures S1–S12**); it was moderate for *MMP-2* rs243865 in all populations under the allelic model with LC risk, among the overall populations in the dominant model with PCa risk, and the Asian populations in the dominant and allelic models with PCa risk. Moreover, *MMP-7* rs11568818 in Asians under the recessive model was related to bladder cancer risk, while *MMP-9* rs3918242 was relevant to BC risk among the Asian populations in the allelic model and to oral cancer risk among the overall populations in the allelic model with oral cancer); it was weak for *MMP-2* rs243865 among the Asian populations with LC risk in the recessive model, among the overall populations with LC risk in the dominant model, and among the Asian population with NPC risk in the dominant model. *MMP-7* rs11568818 was related to CC risk among the Asian population in the recessive and dominant models, as well as with CRC risk among the Asian populations in the allelic and recessive models. *MMP-9* rs3918242 was associated with BC risk in all populations under the dominant model, GC risk in Asians under the recessive model, HCC risk in all populations under the recessive model, LC risk among the Caucasian and overall populations in the recessive and allelic models, and oral cancer risk in all populations under the allelic model (see **Table 1**).

Heterogeneity, Bias, and Sensitivity Analyses

Table 1 presents on heterogeneity, bias, and sensitivity analyses. There was low heterogeneity regarding the associations of *MMP-2* rs243865 (allelic model, $I^2 = 0.0\%$, $p = 0.837$; dominant model, $I^2 = 0.0\%$, $p = 0.864$; recessive model, $I^2 = 0.9\%$, $p = 0.944$) in Asians with LC risk, *MMP-2* rs243865 (dominant model, $I^2 = 7.1\%$, $p = 0.371$) in all populations with PCa risk, and *MMP-2* rs243865 (allelic model, $I^2 = 0.0\%$, $p = 0.405$; dominant model, $I^2 = 0.0\%$, $p = 0.696$) in Asians with PCa risk. Associations of *MMP-7* rs11568818 (allelic model, $I^2 = 0.0\%$, $p = 0.868$; recessive model, $I^2 = 0.0\%$, $p = 0.962$) were found in all populations and (allelic model, $I^2 = 23.7\%$, $p = 0.269$; recessive model, $I^2 = 0.0\%$, $p = 0.494$) in Asians with bladder cancer risk, *MMP-7* rs11568818 (allelic model, $I^2 = 0.0\%$, $p = 0.583$) in Asians with CC risk and (allelic model, $I^2 = 0.0\%$, $p = 0.566$; recessive model, $I^2 = 12.6\%$, $p = 0.285$) in Asians with CRC risk. Furthermore, associations of *MMP-9* rs3918242 (dominant model, $I^2 = 21.8\%$, $p = 0.27$; recessive model, $I^2 = 0.0\%$, $p = 0.723$) were found in all populations and in Asians (allelic model, $I^2 = 0.0\%$, $p = 0.731$; dominant model, $I^2 = 0.0\%$, $p = 0.628$; recessive model, $I^2 = 0.0\%$, $p = 0.917$) with BC risk (recessive model, $I^2 = 0.0\%$, $p = 0.551$) in Asians with GC risk, in Caucasians (allelic model, $I^2 = 0.0\%$, $p = 0.502$; recessive model, $I^2 = 0.0\%$, $p = 0.615$) with LC risk, and in all populations (recessive model, $I^2 = 0.0\%$, $p = 0.717$) with oral cancer risk; moderate heterogeneity was detected for relations of *MMP-2* rs243865 (allelic model, $I^2 = 41.4\%$, $p = 0.163$; dominant model, $I^2 = 46.9\%$, $p = 0.13$) in Asians with esophageal cancer risk and of *MMP-9* rs3918242 (allelic model, $I^2 = 29.2\%$, $p = 0.216$) in all populations with BC risk (recessive model, $I^2 = 48.1\%$, $p = 0.165$) and HCC risk and (recessive model, $I^2 = 42.1\%$, $p = 0.159$) with LC risk. Furthermore, the relation of *MMP-9* rs3918242 (allelic model, $I^2 = 26.8\%$, $p = 0.255$) in all populations with oral cancer risk was found; there was large heterogeneity regarding the associations of *MMP-2* rs243865 (allelic model, $I^2 = 72.1\%$, $p = 0.006$; dominant model, $I^2 = 73.8\%$, $p = 0.004$) in all populations with LC risk and in Asians (dominant model, $I^2 = 63\%$, $p = 0.067$) with NPC risk, *MMP-7* rs11568818 (dominant model, $I^2 = 52.8\%$, $p = 0.12$; recessive model, $I^2 = 52.7\%$, $p = 0.121$) in Asians with CC risk, and *MMP-9* rs3918242 (allelic model, $I^2 = 63.3\%$, $p = 0.028$) in all populations with LC risk. No significant publication bias was detected regarding the connections between *MMP* variants and cancer risk ($p > 0.10$), with the only exception of *MMP-2* rs243865 with LC risk among the overall populations in the dominant and allelic models. Sensitivity analysis was conducted for assessing the robustness of the significant associations. As a result, the summary ORs remained unchanged, despite deleting one single study, the first studies, or deviations from HWE among controls, with the only exception of *MMP-2* rs243865 with NPC risk among the Asian populations in dominant model, *MMP-7* rs11568818 with CC risk in Asians under the dominant model, and *MMP-9* rs3918242 with LC risk among the overall populations in the recessive model and with BC risk among the overall populations in the dominant model. In our sensitivity analyses, no significant correlation was observed for any of the three models, excluding works deviating from HWE among controls.

DISCUSSION

Although numerous studies have reported associations between *MMP-2*, *MMP-7*, and *MMP-9* variants and cancer risk, these results are highly controversial. Considering that, this study has the largest scale and is an integrative study that evaluates the relations of *MMP-2*, *MMP-7*, and *MMP-9* variants with cancer susceptibility. Relevant information was obtained in publications, and altogether 135 articles (36,530 cases and 41,258 controls) were collected for meta-analysis. In 2010, Peng et al. performed a meta-analysis involving 51 articles and over 40,000 participants (19) and found that *MMP-2*, *MMP-7*, and *MMP-9* variants are linked with the risk of cancer. Furthermore, compared with previous studies,

our study included more studies and variants, and then it was revealed that *MMP-2* rs243865 was associated with NPC and PCa risk, and *MMP-7* rs11568818 with bladder cancer, CC, and CRC risk. Furthermore, *MMP-9* rs3918242 was related to BC, GC, HCC, LC, and oral cancer risk. Then, whether the cumulative epidemiological evidence regarding such obvious associations was creditable combined with the FPRP test and Venice criteria was assessed. At last, 12 associations (*MMP-2* rs243865 with esophageal cancer and LC, *MMP-7* rs11568818 with bladder and CC, and *MMP-9* rs3918242 with BC) were rated as strong evidence for cancer risk, 7 as moderate evidence, and 15 as weak.

Located on chromosome 16q21, *MMP-2* gene contains 13 exons and 12 introns (22), which mainly degrade gelatin and type IV collagen, the main structural components of BM, so it has been identified as a critical marker for cancer occurrence and migration (23). *MMP-2* binds to integrin αvβ3 through the hemopexin domain and is essential for mesenchymal cell invasion activity (24). In addition, rs243865 polymorphism of the *MMP-2* promoter can affect mRNA and protein expression by changing its transcriptional activity and can lead to the occurrence of some cancers (25–28). However, certain transcription factors (TFs), like specificity protein-1 (SP-1) and activator protein-1 (AP-1), have a direct influence on *MMP-2* transcription (18, 29). Furthermore, the SP-1 binding region is inactivated by rs243865, resulting in reduced transcription and translation of *MMP-2* (30). This work suggested that rs243865 was related to the risk of esophageal and LC under the allelic and dominant models, with 1.249-fold and 1.277-fold reduced incidence of esophageal cancer among the Asian populations in the dominant and allelic models, and 1.516-fold (with a sample size of 4254) and 1.466-fold (with a sample size of 2850) reduced LC risk in the dominant and allelic models in Asians, rather than under the recessive model in Asians with esophageal cancer and the recessive model in all populations with LC. Here, it was important to emphasize the associations between the risk of esophageal cancer with such single-nucleotide polymorphism (SNP) among the Asian populations in the allelic and dominant models, which were upgraded from moderate to strong (FPRP < 0.05). *MMP-2* has been previously found to show overexpression within various human cancers, such as ESCC and LC (15, 31–33). A high expression level of *MMP-2* is a potentially unfavorable factor that predicts tumorigenesis, but rs243865 leads to a lower expression of *MMP-2* with lower cancer risk. Furthermore, the finding of Price et al. in 2001 that C>T polymorphism, which was located at −1,306 and destroyed the SP-1 promoter site (CCACC box), showed remarkably decreased activity of *MMP-2* promoter relative to the C allele was further confirmed in our study (30). Nonetheless, in our study, only the Asian populations were analyzed, and we failed to analyze other ethnic groups such as Caucasians due to insufficient data or a small sample size. Therefore, large-scale research on other races in the future is recommended, which may show that biological characteristics of *MMP-2* rs243865 may have differences in different ethnic groups.

MMP-7, located on human chromosome 11q21–q22, represents a small secretory protease that shows wide substrate specificity, which is responsible for degrading proteoglycans, elastin, type IV collagen, and fibronectin (34, 35). It cleaves non-matrix substrates on the cell surface, such as Fas ligand, E-cadherin, and pro-cancer TNF-α, also referred to as the "sheddase" effect (36, 37). Its level is related to tumor migration, invasion, and prognosis. SNP 181A>G (rs11568818) is located in the *MMP-7* promoter region known to influence gene expression. Our meta-analysis strongly indicated that rs11568818 could increase the risk of bladder cancer in all populations with a sample of 2,377 under both the allelic and recessive models (OR = 1.204, 95% CI = 1.055–1.374; OR = 1.538, 95% CI = 1.198–1.974) and in Asians with a sample of 1,938 under the allelic model (OR = 1.229, 95% CI = 1.056–1.431), while it also increased the risk of CC in Asians under the allelic model (OR = 1.372, 95% CI = 1.148–1.640). In this case, it can be seen that our results are inconsistent with those of some previous studies (38), which may be related to sample size, environment, and living habits. Furthermore, it should be pointed out that our results are more reliable due to the larger sample size. Interestingly, we upgraded the associations (*MMP-7* rs11568818 and CC among the Asian populations in the allelic model and bladder cancer among the overall populations in the recessive model) from moderate to strong. The amount of evidence explains the mechanism of grading two associations "BAA" and "BAA" based on the Venice criteria; due to the FPRP value <0.05, the associations were rated as strong. Moreover, the lack of data from Caucasians in this study should be expanded and be recommended so as to further demonstrate this association in the future.

MMP-9, also called type IV collagenase or gelatinase B, is the protease degrading type IV collagen (the main BM component). It has a critical function in distant metastasis of tumor cells because of the lysis activity of type IV collagen that disrupts the BM (39). *MMP-9* promoter 1562C>T (rs3918242) functional polymorphism predicts a higher *MMP-9* expression level (40). Promoter activity increases by 1.5 times in the MMP-9 T allele in comparison with the *MMP-9* C allele (7). In this case, it is indicated that rs3918242 plays a very important role in the generation and metastasis of tumors, which is consistent with our results. To be specific, our meta-analysis strongly suggested that rs3918242 elevated the BC risk among the overall populations in the recessive and allelic models with 1.681-fold and 1.281-fold, respectively, and among the Asian populations in the recessive and dominant models with 1.710-fold and 1.526-fold, accordingly. However, this study sample lacked Caucasian population analysis. In other words, this work was featured with a small sample size, which was the cause of focusing on the overall population. More research regarding such SNP in different races should be recommended.

There were 7 associations graded as moderate associations for cancer risk, including *MMP-2* rs243865 with LC risk and PCa risk, *MMP-7* rs11568818 with bladder cancer risk, and *MMP-9* rs3918242 with BC risk and oral cancer risk. These 7 associations were rated as moderate evidence due to high heterogeneity, publication bias, and a small-study effect based on the Venice criteria and FPRP values. Furthermore, large prospective studies should be performed to elucidate the relationships between these variants with cancer risk.

There were 15 associations rated as weakly associated with cancer risk. Among these associations, *MMP-2* rs243865 was connected

with LC risk and *MMP-9* rs3918242 with BC, HCC, LC, and oral cancer risk. They were all meaningful associations in all populations. Aside from that, other 7 associations were considered significant in Asians, including *MMP-2* rs243865 with LC risk and NPC risk, *MMP-7* rs11568818 with CC risk and CRC risk, and *MMP-9* rs3918242 with GC risk. However, 2 associations were regarded as significant in Caucasians, such as *MMP-9* rs3918242 with LC risk. In these variants, *MMP-2* rs243865 decreased the risk of LC by 1.387-fold under the dominant model in all populations with "ACC" based on the Venice criteria. Furthermore, a high degree of heterogeneity, a publication bias, or a small-study effect may explain why this variant was rated as weak evidence. Apart from that, *MMP-2* rs243865 decreased the risk of LC and the risk of NPC. Beyond that, *MMP-7* rs11568818 in Asians was associated with CRC risk with "BAA," and the FPRP value >0.2 led from moderate grade to weak grade, which was mainly due to the low amount of evidence, high heterogeneity of the data, a publication bias, a small-study effect, and HWE bias on the Venice criteria. Moreover, expanding the sample size and evaluating additional race groups of such variants are important to further investigate these associations.

In addition, the association was inconsistent according to different ethnic or genetic models. In terms of ethnicity, except for the analysis on the association of *MMP-9* rs3918242 with LC risk among the Europeans, the other subgroup analyses on associations were mainly conducted in the Asian populations, whereas subgroup analysis was not made since insufficient non-Asians were enrolled. This study adopted three genetic models to comprehensively assess the associations; patients' age, gender and other different genetic backgrounds, tumor subtypes, and environmental factors may be the variation source. More investigations into the above factors are necessary.

This study presented that three SNPs in two *MMP*s had no association with two cancers in any genetic model and/or ethnicity; of these, one SNP showed no relation with the risk of cancer (*MMP-2* rs243865 with BC) in meta-analyses that involved at least 2,000 cases and 2,000 controls, providing >85% power for detecting OR = 1.15 in the allelic model for the variant with type 1 error 0.05 and minor allelic frequency (MAF) 0.20 (**Supplementary Tables S3**, **S4**). Further research on this SNP with a similar sample size may not yield fruitful results. For the remaining SNPs, as these associations were characterized by low statistical power in the current sample size, further expanding the sample size or large meta-analyses on these associations are recommended.

Of course, in this study, there are some limitations: a) the literature collected in this study was in English, not in other languages, which may lead to bias; b) the subgroup analysis was performed only on Asians and Caucasians and under three genetic models, while other factors, such as age, gender, smoking, alcohol intake, and environment, were ignored, which might compromise our result reliability; c) only the susceptibility of associations between *MMP-2*, *MMP-7*, and *MMP-9* and cancer risk was assessed; furthermore, due to insufficient data, the influence of gene polymorphism on cancer progression and metastasis has not been evaluated. Regardless of the abovementioned limitations, the present work comprehensively investigated available publications to examine the functions of *MMP-2*, *MMP-7*, and *MMP-9* in cancers and will be valuable for future genetic studies.

The present work assessed cumulative epidemiological evidence supporting the obvious relations of *MMP*s with tumor susceptibility through integrating the FPRP test and Venice criteria. Finally, 12 associations (*MMP-2* rs243865 with esophageal cancer risk and LC risk, *MMP-7* rs11568818 with bladder risk and CC risk, and *MMP-9* rs3918242 with BC risk) were rated as strong evidence, 7 as moderate evidence, and 15 as weak. Analysis of the relations between *MMP*s variants and tumor susceptibility contributes to obtaining high-risk subjects for primary prevention. To sum up, this work reviews existing publications regarding *MMP* variations with tumor susceptibility. Our results offer valuable data to design future research to assess variants in *MMP* factors for cancer risk.

DATA AVAILABILITY STATEMENT

The original contributions presented in the study are included in the article/**Supplementary Material**. Further inquiries can be directed to the corresponding author.

AUTHOR CONTRIBUTIONS

CH and TW designed this work. CH and SX integrated and analyzed the data. CH and TW wrote this manuscript. CH, SX, ZL, DL, and RW finished the related tables and figures. CH and TW edited and revised the manuscript. All authors approved this manuscript.

SUPPLEMENTARY MATERIAL

The Supplementary Material for this article can be found online at: https://www.frontiersin.org/articles/10.3389/fonc.2022.856831/full#supplementary-material

REFERENCES

1. Mattiuzzi C, Lippi G. Current Cancer Epidemiology. *J Epidemiol Glob Health* (2019) 9:217–22. doi: 10.2991/jegh.k.191008.001
2. Acosta S, Johansson A, Drake I. Diet and Lifestyle Factors and Risk of Atherosclerotic Cardiovascular Disease-A Prospective Cohort Study. *Nutrients* (2021) 13:3822. doi: 10.3390/nu13113822
3. Kessenbrock K, Plaks V, Werb Z. Matrix Metalloproteinases: Regulators of the Tumor Microenvironment. *Cell* (2010) 141:52–67. doi: 10.1016/j.cell.2010.03.015
4. Rahimi Z, Rahimi Z, Shahsavandi MO, Bidoki K, Rezaei M. MMP-9 (-1562 C:T) Polymorphism as a Biomarker of Susceptibility to Severe Pre-Eclampsia. *biomark Med* (2013) 7:93–8. doi: 10.2217/bmm.12.95
5. Siddhartha R, Garg M. Molecular and Clinical Insights of Matrix Metalloproteinases Into Cancer Spread and Potential Therapeutic Interventions. *Toxicol Appl Pharmacol* (2021) 426:115593. doi: 10.1016/j.taap.2021.115593
6. Deryugina EI, Quigley JP. Tumor Angiogenesis: MMP-Mediated Induction of Intravasation- and Metastasis-Sustaining Neovasculature. *Matrix Biol* (2015) 44-46:94–112. doi: 10.1016/j.matbio.2015.04.004

7. Decock J, Paridaens R, Ye S. Genetic Polymorphisms of Matrix Metalloproteinases in Lung, Breast and Colorectal Cancer. *Clin Genet* (2008) 73:197–211. doi: 10.1111/j.1399-0004.2007.00946.x
8. Hua H, Li M, Luo T, Yin Y, Jiang Y. Matrix Metalloproteinases in Tumorigenesis: An Evolving Paradigm. *Cell Mol Life Sci* (2011) 68:3853–68. doi: 10.1007/s00018-011-0763-x
9. Visse R, Nagase H. Matrix Metalloproteinases and Tissue Inhibitors of Metalloproteinases: Structure, Function, and Biochemistry. *Circ Res* (2003) 92:827–39. doi: 10.1161/01.RES.0000070112.80711.3D
10. Fang F, Luo W, Yang M, Yang P, Yang X. Urinary Matrix Metalloproteinase-7 and Prediction of AKI Progression Post Cardiac Surgery. *Dis Markers* (2019) 2019:9217571. doi: 10.1155/2019/9217571
11. Joviliano EE, Ribeiro MS, Tenorio EJR. MicroRNAs and Current Concepts on the Pathogenesis of Abdominal Aortic Aneurysm. *Braz J Cardiovasc Surg* (2017) 32:215–24. doi: 10.21470/1678-9741-2016-0050
12. Sheu JR, Fong TH, Liu CM, Shen MY, Chen TL, Chang Y, et al. Expression of Matrix Metalloproteinase-9 in Human Platelets: Regulation of Platelet Activation in *In Vitro* and *In Vivo* Studies. *Br J Pharmacol* (2004) 143:193–201. doi: 10.1038/sj.bjp.0705917
13. Wilson SR, Gallagher S, Warpeha K, Hawthorne SJ. Amplification of MMP-2 and MMP-9 Production by Prostate Cancer Cell Lines *via* Activation of Protease-Activated Receptors. *Prostate* (2004) 60:168–74. doi: 10.1002/pros.20047
14. Maral S, Acar M, Balcik OS, Uctepe E, Hatipoglu OF, Akdeniz D, et al. Matrix Metalloproteinases 2 and 9 Polymorphism in Patients With Myeloproliferative Diseases: A STROBE-Compliant Observational Study. *Med (Baltimore)* (2015) 94:e732. doi: 10.1097/MD.0000000000000732
15. Yu C, Pan K, Xing D, Liang G, Tan W, Zhang L, et al. Correlation Between a Single Nucleotide Polymorphism in the Matrix Metalloproteinase-2 Promoter and Risk of Lung Cancer. *Cancer Res* (2002) 62:6430–3.
16. Chen GL, Wang SC, Shen TC, Tsai CW, Chang WS, Li HT, et al. The Association of Matrix Metalloproteinas-2 Promoter Polymorphisms With Lung Cancer Susceptibility in Taiwan. *Chin J Physiol* (2019) 62:210–6. doi: 10.4103/CJP.CJP_43_19
17. Zhang L, Xi RX, Zhang XZ. Matrix Metalloproteinase Variants Associated With Risk and Clinical Outcome of Esophageal Cancer. *Genet Mol Res* (2015) 14:4616–24. doi: 10.4238/2015.May.4.20
18. Eftekhary H, Ziaee AA, Yazdanbod M, Shahpanah M, Setayeshgar A, Nassiri M. The Influence of Matrix Metalloproteinase-2, -9, and -12 Promoter Polymorphisms on Iranian Patients With Oesophageal Squamous Cell Carcinoma. *Contemp Oncol (Pozn)* (2015) 19:300–5. doi: 10.5114/wo.2015.48569
19. Peng B, Cao L, Ma X, Wang W, Wang D, Yu L. Meta-Analysis of Association Between Matrix Metalloproteinases 2, 7 and 9 Promoter Polymorphisms and Cancer Risk. *Mutagenesis* (2010) 25:371–9. doi: 10.1093/mutage/geq015
20. Wu Z, Jiang P, Zulqarnain H, Gao H, Zhang W. Relationship Between Single-Nucleotide Polymorphism of Matrix Metalloproteinase-2 Gene and Colorectal Cancer and Gastric Cancer Susceptibility: A Meta-Analysis. *Onco Targets Ther* (2015) 8:861–9. doi: 10.2147/OTT.S78031
21. Wacholder S, Chanock S, Garcia-Closas M, El Ghormli L, Rothman N. Assessing the Probability That a Positive Report is False: An Approach for Molecular Epidemiology Studies. *J Natl Cancer Inst* (2004) 96:434–42. doi: 10.1093/jnci/djh075
22. Ye S. Polymorphism in Matrix Metalloproteinase Gene Promoters: Implication in Regulation of Gene Expression and Susceptibility of Various Diseases. *Matrix Biol* (2000) 19:623–9. doi: 10.1016/s0945-053x(00)00102-5
23. Stamenkovic I. Matrix Metalloproteinases in Tumor Invasion and Metastasis. *Semin Cancer Biol* (2000) 10:415–33. doi: 10.1006/scbi.2000.0379
24. Rupp PA, Visconti RP, Czirók A, Cheresh DA, Little CD. Matrix Metalloproteinase 2-Integrin Alpha(V)Beta3 Binding is Required for Mesenchymal Cell Invasive Activity But Not Epithelial Locomotion: A Computational Time-Lapse Study. *Mol Biol Cell* (2008) 19:5529–40. doi: 10.1091/mbc.e07-05-0480
25. Waleh NS, Murphy BJ, Zaveri NT. Increase in Tissue Inhibitor of Metalloproteinase-2 (TIMP-2) Levels and Inhibition of MMP-2 Activity in a Metastatic Breast Cancer Cell Line by an Anti-Invasive Small Molecule SR13179. *Cancer Lett* (2010) 289:111–8. doi: 10.1016/j.canlet.2009.08.006
26. Bourboulia D, Han H, Jensen-Taubman S, Gavil N, Isaac B, Wei B, et al. TIMP-2 Modulates Cancer Cell Transcriptional Profile and Enhances E-Cadherin/Beta-Catenin Complex Expression in A549 Lung Cancer Cells. *Oncotarget* (2013) 4:166–76. doi: 10.18632/oncotarget.801
27. Groblewska M, Mroczko B, Kozlowski M, Niklinski J, Laudanski J, Szmitkowski M. Serum Matrix Metalloproteinase 2 and Tissue Inhibitor of Matrix Metalloproteinases 2 in Esophageal Cancer Patients. *Folia Histochem Cytobiol* (2012) 50:590–8. doi: 10.5603/20327
28. Kapral M, Wawszczyk J, Jurzak M, Dymitruk D, Weglarz L. Evaluation of the Expression of Metalloproteinases 2 and 9 and Their Tissue Inhibitors in Colon Cancer Cells Treated With Phytic Acid. *Acta Pol Pharm* (2010) 67:625–9.
29. Singh N, Hussain S, Sharma U, Suri V, Nijhawan R, Bharadwaj M, et al. The Protective Role of the -1306C>T Functional Polymorphism in Matrix Metalloproteinase-2 Gene is Associated With Cervical Cancer: Implication of Human Papillomavirus Infection. *Tumour Biol* (2016) 37:5295–303. doi: 10.1007/s13277-015-4378-y
30. Price SJ, Greaves DR, Watkins H. Identification of Novel, Functional Genetic Variants in the Human Matrix Metalloproteinase-2 Gene: Role of Sp1 in Allele-Specific Transcriptional Regulation. *J Biol Chem* (2001) 276:7549–58. doi: 10.1074/jbc.M010242200
31. Samantaray S, Sharma R, Chattopadhyaya TK, Gupta SD, Ralhan R. Increased Expression of MMP-2 and MMP-9 in Esophageal Squamous Cell Carcinoma. *J Cancer Res Clin Oncol* (2004) 130:37–44. doi: 10.1007/s00432-003-0500-4
32. Yamashita K, Upadhay S, Mimori K, Inoue H, Mori M. Clinical Significance of Secreted Protein Acidic and Rich in Cystein in Esophageal Carcinoma and its Relation to Carcinoma Progression. *Cancer* (2003) 97:2412–9. doi: 10.1002/cncr.11368
33. Koyama H, Iwata H, Kuwabara Y, Iwase H, Kobayashi S, Fujii Y. Gelatinolytic Activity of Matrix Metalloproteinase-2 and -9 in Oesophageal Carcinoma; a Study Using *in Situ* Zymography. *Eur J Cancer* (2000) 36:2164–70. doi: 10.1016/s0959-8049(00)00297-5
34. Quantin B, Murphy G, Breathnach R. Pump-1 cDNA Codes for a Protein With Characteristics Similar to Those of Classical Collagenase Family Members. *Biochemistry* (1989) 28:5327–34. doi: 10.1021/bi00439a004
35. Wilson CL, Matrisian LM. Matrilysin: An Epithelial Matrix Metalloproteinase With Potentially Novel Functions. *Int J Biochem Cell Biol* (1996) 28:123–36. doi: 10.1016/1357-2725(95)00121-2
36. Haro H, Crawford HC, Fingleton B, Shinomiya K, Spengler DM, Matrisian LM. Matrix Metalloproteinase-7-Dependent Release of Tumor Necrosis Factor-Alpha in a Model of Herniated Disc Resorption. *J Clin Invest* (2000) 105:143–50. doi: 10.1172/JCI7091
37. Noë V, Fingleton B, Jacobs K, Crawford HC, Vermeulen S, Steelant W, et al. Release of an Invasion Promoter E-Cadherin Fragment by Matrilysin and Stromelysin-1. *J Cell Sci* (2001) 114:111–8. doi: 10.1242/jcs.114.1.111
38. Mao F, Niu XB, Gu S, Ji L, Wei BJ, Wang HB. The Association Between Matrix Metalloproteinase-7 Genetic Variant and Bladder Cancer Risk in a Chinese Han Population. *Clin Exp Med* (2019) 19:565–70. doi: 10.1007/s10238-019-00582-7
39. Przybylowska K, Kluczna A, Zadrozny M, Krawczyk T, Kulig A, Rykala J, et al. Polymorphisms of the Promoter Regions of Matrix Metalloproteinases Genes MMP-1 and MMP-9 in Breast Cancer. *Breast Cancer Res Treat* (2006) 95:65–72. doi: 10.1007/s10549-005-9042-6
40. Rahimi Z, Rahimi Z, Aghaei A, Vaisi-Raygani A. AT2R -1332 G:A Polymorphism and its Interaction With AT1R 1166 A:C, ACE I/D and MMP-9 -1562 C:T Polymorphisms: Risk Factors for Susceptibility to Preeclampsia. *Gene* (2014) 538:176–81. doi: 10.1016/j.gene.2013.12.013

Conflict of Interest: The authors declare that the research was conducted in the absence of any commercial or financial relationships that could be construed as a potential conflict of interest.

Publisher's Note: All claims expressed in this article are solely those of the authors and do not necessarily represent those of their affiliated organizations, or those of the publisher, the editors and the reviewers. Any product that may be evaluated in this article, or claim that may be made by its manufacturer, is not guaranteed or endorsed by the publisher.

frontiers | Frontiers in Oncology

REVIEW
published: 02 May 2022
doi: 10.3389/fonc.2022.870996

A Comprehensive Review on Function of miR-15b-5p in Malignant and Non-Malignant Disorders

Soudeh Ghafouri-Fard[1], *Tayyebeh Khoshbakht*[2], *Bashdar Mahmud Hussen*[3,4], *Hazha Hadayat Jamal*[5], *Mohammad Taheri*[6,7]* *and Mohammadreza Hajiesmaeili*[8,9]*

[1] Department of Medical Genetics, School of Medicine, Shahid Beheshti University of Medical Sciences, Tehran, Iran, [2] Men's Health and Reproductive Health Research Center, Shahid Beheshti University of Medical Sciences, Tehran, Iran, [3] Department of Pharmacognosy, College of Pharmacy, Hawler Medical University, Erbil, Iraq, [4] Center of Research and Strategic Studies, Lebanese French University, Erbil, Iraq, [5] Department of Biology, College of Education, Salahaddin University, Erbil, Iraq, [6] Urology and Nephrology Research Center, Shahid Beheshti University of Medical Sciences, Tehran, Iran, [7] Institute of Human Genetics, Jena University Hospital, Jena, Germany, [8] Skull Base Research Center, Loghman Hakim Hospital, Shahid Beheshti University of Medical Sciences, Tehran, Iran, [9] Critical Care Fellowship, Department of Anesthesiology, Loghman Hakim Hospital, Shahid Beheshti University of Medical Sciences, Tehran, Iran

OPEN ACCESS

Edited by:
Ondrej Slaby,
Central European Institute of Technology (CEITEC), Czechia

Reviewed by:
Francesca Lovat,
The Ohio State University, United States
Jie Li,
Chinese Academy of Medical Sciences and Peking Union Medical College, China

***Correspondence:**
Mohammad Taheri
mohammad.taheri@uni-jena.de
Mohammadreza Hajiesmaeili
mrhajiesmaeili@sbmu.ac.ir

Specialty section:
This article was submitted to Cancer Genetics, a section of the journal Frontiers in Oncology

Received: *07 February 2022*
Accepted: *05 April 2022*
Published: *02 May 2022*

Citation:
Ghafouri-Fard S, Khoshbakht T, Hussen BM, Jamal HH, Taheri M and Hajiesmaeili M (2022) A Comprehensive Review on Function of miR-15b-5p in Malignant and Non-Malignant Disorders. Front. Oncol. 12:870996. doi: 10.3389/fonc.2022.870996

miR-15b-5p is encoded by *MIR15B* gene. This gene is located on cytogenetic band 3q25.33. This miRNA participates in the pathogenesis of several cancers as well as non-malignant conditions, such as abdominal aortic aneurysm, Alzheimer's and Parkinson's diseases, cerebral ischemia reperfusion injury, coronary artery disease, dexamethasone induced steatosis, diabetic complications and doxorubicin-induced cardiotoxicity. In malignant conditions, both oncogenic and tumor suppressor impacts have been described for miR-15b-5p. Dysregulation of miR-15b-5p in clinical samples has been associated with poor outcome in different kinds of cancers. In this review, we discuss the role of miR-15b-5p in malignant and non-malignant conditions.

Keywords: miR-15b-5p, cancer, biomarker, expression, malignance

INTRODUCTION

microRNAs (miRNAs) are a category of non-coding RNA with sizes about 20-24 nucleotide which participate in post-transcriptional control of gene expression (1). This effect is exerted through modulation of stability and translation of mRNAs. The primary transcripts produced by RNA polymerase II have 5'-cap and 3'-polyadenylated tail. Then, Drosha ribonuclease III enzyme cleaves this transcript to make the stem-loop precursor miRNA with an estimated size of 70 nucleotides (2). Finally, this transcript is processed by the Dicer ribonuclease to make the mature miRNA which can be combined into the RNA-induced silencing complex. Through incorporation into this complex, miRNAs can recognize their target transcript in a base pairing-dependent process resulting in suppression of translation or destabilization of transcript (3).

MIR15B gene is located on cytogenetic band 3q25.33 and encodes hsa-mir-15b. This miRNA participates in the pathogenesis of several cancers as well as non-malignant conditions, including cardiovascular disorders, neuropsychiatric diseases and metabolic conditions. This miRNA has been reported to exert oncogenic or tumor suppressor effects in different malignancies. We have searched the literature and discussed the role of miR-15b-5p in malignant and non-malignant conditions.

MIR-15B-5P IN CANCERS

Cell Line Studies

In bladder cancer cell lines, the long non-coding RNA (lncRNA) MAGI2-AS3 acts as a molecular sponge for miR-15b-5p. In fact, MAGI2-AS3 exerts its tumor suppressor role in bladder cancer through decreasing level of this miRNA. Meanwhile, miR-15b-5p has been found to target the tumor suppressor gene CCDC19. Taken together, MAGI2-AS3/miR-15b-5p/CCDC19 axis has been revealed to regulate progression of bladder cancer (4).

An *in vitro* experiment in breast cancer cells has shown that miR-15b-5p silencing could restrain cell proliferation and invasiveness and induce apoptosis, while its up-regulation has exerted the opposite impacts. Notably, heparanase-2 (HPSE2) has been acknowledged as the target of miR-15b-5p in breast cancer cells, through which this miRNA applies its effect (5).

In cervical cancer cells, level of the tumor suppressor lncRNA FENDRR has been shown to be decreased. This lncRNA has binding sites for miR-15a-5p and miR-15b-5p, two miRNAs that can down-regulate expression of Tubulin alpha1A (TUBA1A). Taken together, FENDRR/miR-15a/b-5p/TUBA1A molecular route has been proved to regulate progression of cervical cancer (6).

Expression of miR-15b-5p has been reported to be surged in colon cancer cells. Treatment of HT-29 cells with a PNA against miR-15b-5p has been shown to reduce cell proliferation and activate the pro-apoptotic pathway (7). Another research in colon cancer cells has displayed that SIRT1 suppresses metastatic ability of cells through decreasing expression of miR-15b-5p. In fact, SIRT1 disrupts the regulatory effect of AP-1 on activation of expression of miR-15b-5p *via* deacetylating this activation factor. miR-15b-5p can target the transcript of a central enzyme in the fatty acid oxidation, namely acyl-CoA oxidase 1 (ACOX1). Taken together, SIRT1/miR-15b-5p/ACOX1 axis has been identified as a functional route in regulation of metastatic ability of colorectal cancer cells (8).

Figure 1 displays the oncogenic role of miR-15b-5p in bladder, breast, cervical, colorectal, liver, oral, ovarian, prostate and gastric cancers.

In contrast to the previously mentioned experiment in colorectal cancer cells (7), Zhao et al. have shown that miR-15b-5p has a tumor suppressor impact in this cancer. Notably, miR-15b-5p can enhance 5-fluorouracil (5-FU)-induced apoptosis in these cells and reversed the resistance of colorectal cancer cells to this therapeutic agent. Mechanistically, miR-15b-5p exerts this impact through modulating activity of the NF-κB signaling *via* decreasing NF-κB1 and IKK-α levels. miR-15b-5p has been found to target the anti-apoptosis transcript XIAP (9).

In vitro experiments in neuroblastoma cells have shown that up-regulation of miR-15a-5p, miR-15b-5p or miR-16-5p can reduce expression of MYCN transcript and N-Myc protein. On the other hand, suppression of these miRNAs could lead to enhancement of MYCN transcripts and N-Myc protein level, along with increasing half-life of its mRNA. The interaction between these miRNAs and MYCN mRNA has been proved through conducting immunoprecipitation and luciferase reporter assays. Notably, up-regulation of these miRNAs has diminished proliferation, migration, and invasiveness of neuroblastoma cells (17). **Figure 2** shows tumor suppressor

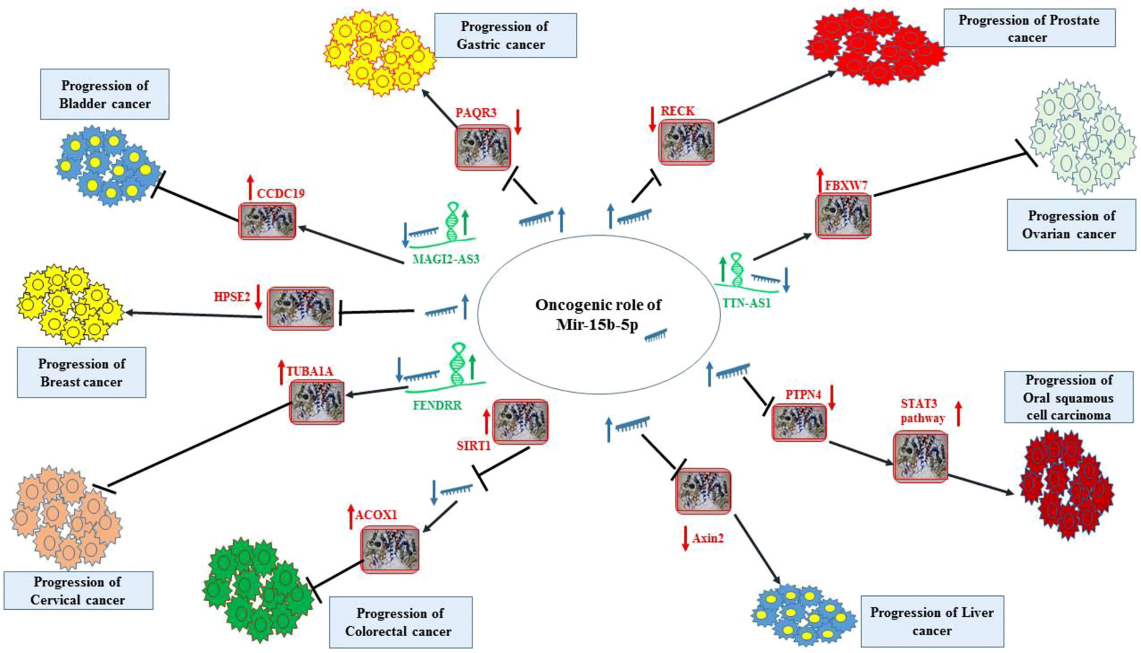

FIGURE 1 | Oncogenic effect of miR-15b-5p in bladder, breast, cervical, colorectal, liver, oral, ovarian, prostate and gastric cancers. Detailed information about the conducted experiments is shown in **Table 1**.

TABLE 1 | Summary of cell line studies on the role of miR-15b-5p in cancers (Δ, knock-down or deletion; MET, mesenchymal-epithelial transition).

Tumors	Interactions	Cell line	Function	Reference
Bladder cancer	MAGI2-AS3 and CCDC19	EJ, T24 and RT4, SV-HUC-1	↑↑ MAGI2-AS3 (which sponges mir-15b-5p): ↓ Proliferation, ↓ migration and ↓ invasion	(4)
Breast cancer	HPSE2	MDA-MB-231, MCF-7, 293T	Δ miR-15b-5p: ↓ proliferation, ↓ colony formation, ↓ migration and ↓ invasion, ↑ apoptosis	(5)
Cervical cancer	FENDRR, TUBA1A	HeLa, SiHa, CaSki, C33A, Ect1-E6E7	↑↑ FENDRR (which sponges mir-15b-5p): ↓ proliferation, ↓ migration and ↓ invasion, and ↓ cell viability, and ↑ apoptosis ↑↑ mir-15b-5p: ↑ proliferation, ↑ migration and ↑ invasion, and ↑ cell viability, and ↓ apoptosis	(6)
Colorectal cancer	NF-κB1 and IKK-α	NCM460, SW620, HCT116, DLD1, SW1116	↑↑ miR-15b-5p: ↑ sensitivity to 5-FU and ↑ apoptosis	(9)
	_	HT-29 cell line	R8-PNA-a15b molecule treatment: ↓ miR-15b-5p levels and ↑ inhibition of HT-29 cell growth associated with pro-apoptotic effects	(7)
	SIRT1, AP-1, ACOX1	HCT116, SW480, SW620, LoVo, Caco-2, HT-29	↑↑ SIRT1: ↓ migration and invasion and suppresses mir-15b-5p transcription *via* AP-1	(8)
	IL-17A, PD-L1, P65, NRF1	CT26, MC38, SW1116, HT29, SW480, SW620	↑↑ miR-15b-5p: ↓ PD-L1 protein level and ↑ anti-PD-1 sensitivity	(10)
	CERS6-AS1	FHC, Caco-2, T84, HCT-15	Δ CERS6-AS1 (whish sponges miR-15b-5p): ↓ proliferation, ↓ migration, ↓ invasion, ↓ EMT, and ↓ stemness	(11)
Gastric cancer	PAQR3	AGS, BGC-823, SGC-7901, MGC-803	↑↑ miR-15b-5p: ↑ migration and ↑ invasion	(12)
Glioblastoma multiforme	_	U251	Combo-therapy using PNA-a15b and SFN *via* interfering with miR-15b-5p could be used as a treatment for Glioblastoma multiforme to stimulate apoptosis.	(13)
Hepatocellular carcinoma	OIP5, AKT/mTORC1 and β-catenin signaling pathways	HepG2, Hep3B, SK-HEP-1, Chang liver and THLE2, Huh7	Δ OIP5 (a target of mir-15b-5p): ↓ migration, ↓ invasion and ↓ EMT process *via* mTORC1 and GSK-3β/β-catenin signaling	(12)
	H19 and CDC42/PAK1 signaling pathway	HepG2, SMMC-7721, Bel-7402, Huh-7, WRL-68, 293T	Δ H19 (which sponges mir-15b-5p): ↓ proliferation, migration, invasion, EMT and CDC42/PAK1 signaling pathway and ↑ apoptosis	(14)
	Rab1A	SMMC-7721, HepG2, Hep3B, HL-7702	↑↑ miR-15b-5p: ↓ cell growth, ↑ endoplasmic reticulum stress and apoptosis Δ miR-15b-5p: ↑ proliferation and ↓ apoptosis	(15)
Laryngeal cancer	TXNIP	HEP-2	↑↑ miR-15b-5p: ↑ cell growth *via* targeting TXNIP	(16)
Liver cancer	Axin2	HepG2 and Huh7, Hep3B and HCCLM3	↑↑ miR-15b-5p: ↑ Proliferation and ↑ invasion	(14)
Neuroblastoma	MYCN	SK-N-BE (2), NB-19, SH-EP Tet21N, CHLA-136	↑↑ miR-15b-5p: ↓ proliferation, ↓ migration, and ↓ invasion of NB cells	(17)
	SNHG16, PRPS1	neuroblastoma cells	Δ SNHG16 (which sponges mir-15b-5p): ↓ proliferation, and ↑ G0/G1 phase arrest	(18)
Non-small cell lung cancer	MEG8 and PSAT1	16HBE, A549, H1299, H1975, SPC-A1, and PC-9	Δ MEG8 (which sponges mir-15b-5p): ↓ proliferation, ↓ migration, and ↓ invasion	(19)
Oral squamous cell carcinoma	PTPN4, STAT3 pathway	SCC-4, UM-1, CAL-27, OSC-4	Δ mir-15b-5p: ↓ proliferation, ↓ migration, and ↓ invasion and ↑ apoptosis	(20)
Oral tongue squamous cell carcinoma	TRIM14	SCC25	↑↑ miR-15b: ↑ MET phenotypes and ↓ cisplatin-resistance *via* targeting TRIM14	(21)
Osteosarcoma	PDK4	hFOB1.19, MNNG-HOS, Saos-2, MG63, U-2OS	↑↑ miR-15b-5p: ↓ proliferation and the Warburg effect by suppressing PDK4 expression	(22)
	TRPM2-AS and PPM1D	OS cells	Δ TRPM2-AS (which sponges mir-15b-5p): ↓ viability, ↓ proliferation, ↓ migration and ↑ apoptosis	(23)
Ovarian cancer	TTN-AS1, FBXW7	A2780, OVCA429, IOSE80	↑↑ TTN-AS (which sponges mir-15b-5p): ↓ proliferation and ↓ colony formation, ↑ apoptosis	(24)
Prostate cancer	RECK	PCa cell lines (PC3 and 22RV1)	Δ miR-15b-5p: ↓ cell growth and invasion	(25)
	PVT1 and NOP2	DU 145, PC-3, RWPE-1	↑↑ PVT1 (which sponges mir-15b-5p): ↑ migration and ↑ invasion	(26)
Thyroid carcinoma	GDI2, MMP2 and MMP9	FTC133, SW1736, K1, Nthy-ori3-1	↑↑ mir-15b-5p: ↓ proliferation and ↓ invasion	(27)

↑ *Up-regulation;* ↓ *Down-regulation.*

role of miR-15b-5p in thyroid cancer, hepatocellular carcinoma, neuroblastoma, osteosarcoma and prostate cancer.

Animal Studies

Lovat et al. have produced miR-15b/16-2 knockout mice for the purpose of identification of the role of this cluster. This intervention has led to development of B-cell lymphomas by age 15–18 month possibly though modulation of expression of Cyclins D2 and D1, and IGF1R. These genes participate in the regulation of proliferation and antiapoptotic pathways. Taken together, this cluster has been shown to have a tumor suppressor role in mice models of B-cell lymphoma (28).

In xenograft models of bladder cancer, up-regulation of MAGI2-AS3 has reduced tumor volume possibly through decreasing expression of miR-15b-5p (4). Up-regulation of FENDRR, another miR-15b-5p-sponging lncRNA has exerted similar effects in xenograft models of cervical cancer (6). In colorectal cancer cells, a single study has shown that over-expression of miR-15b-5p improves sensitivity of cells to 5-FU (9). On the other hand, another study has indicated that SIRT1 decreases metastasis through suppression of miR-15b-5p transcription (8). Moreover, miR-15b-5p has been demonstrated to decrease expression of PD-L1, suppress tumorigenic potential of colorectal cancer cells and increase anti-PD-1 sensitivity in colitis-associated cancer and $APC^{min/+}$ models of colorectal cancer (10).

In an animal model of osteosarcoma, over-expression of miR-15b-5p has been associated with reduced cell proliferation (22).

Table 2 shows summary of animal studies on the role of miR-15b-5p in cancers.

Human Studies

Expression assays in clinical samples obtained from patients with bladder cancer, breast cancer, gastric cancer, oral squamous cell carcinoma and prostate cancer have shown up-regulation of miR-15b-5p. On the other hand, this miRNA has been found to be down-regulated in head and neck cancer squamous cell carcinomas, neublastoma and thyroid cancer samples. Different studies in colorectal cancer and hepatocellular carcinoma sample have shown contradictory expression patterns (**Table 3**). Moreover, dysregulation of expression of miR-15b-5p has been associated with poor clinical outcome in bladder cancer, breast cancer, head and neck/oral squamous cell carcinoma, hepatocellular carcinoma and neuroblastoma.

ROLE OF MIR-15B-5P IN NON-MALIGNANT CONDITIONS

Cell Line Studies

In vitro experiments in vascular smooth muscle cells (VSMCs) have shown that up-regulation of miR-15b-5p suppresses cell proliferation and induces apoptosis, while its knock down leads to opposite results. These effects are possibly mediated through suppression of ACSS2. Transfection of these cells with miR-15b-

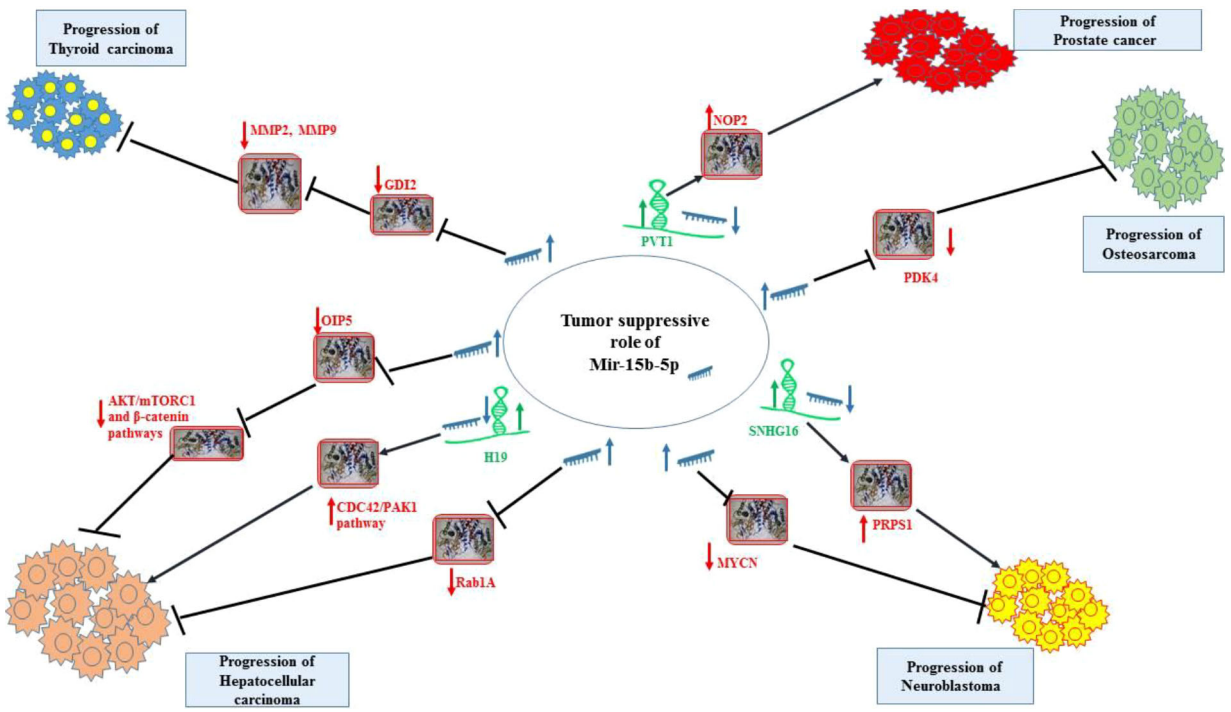

FIGURE 2 | Tumor suppressor role of miR-15b-5p in thyroid cancer, hepatocellular carcinoma, neuroblastoma, osteosarcoma and prostate cancer. Detailed information about the conducted experiments is shown in **Table 1**.

TABLE 2 | Summary of animal studies on the role of miR-15b-5p in cancers (Δ, knock-down or deletion).

Tumors	Animals	Results	Reference
Bladder cancer	4-week-old female BALB/C nude mic	↑↑ MAGI2-AS3: ↓ tumor volume and↓ tumor weight	(4)
Breast cancer	5-week-old female BALB/C nude mice	Δ miR-15b-5p: ↓ tumorigenic ability	(5)
Cervical cancer	6-week-old male BALB/C nude mice	↑↑ FENDRR (which sponges mir-15b-5p): ↓ tumor volume and ↓ tumor weight	(6)
Colorectal cancer	Four-week-old female athymic nude mice	↑↑ miR-15b-5p: ↑ sensitivity of colon cancer cells to 5-FU and ↑ apoptosis *via* the NF-κB pathway	(9)
	4-6 weeks old BALB/c nude mice	↑↑ SIRT1: ↓ metastasis by suppressing mir-15b-5p transcription *via* AP-1	(8)
	female BALB/c mice with two different groups control and blocking miR-15b-5p groups	Δ miR-15b-5p: ↑ tumorigenesis and ↑ PD-L1 levels	(10)
	BALB/c nude mice	Δ CERS6-AS1 (whish sponges miR-15b-5p): ↓ tumor growth	(11)
Hepatocellular carcinoma	Four-week-old female BALB/c nude mice	Δ OIP5 (a target of mir-15b-5p): ↓ tumor growth and ↓ metastasis	(12)
	Four-week-old male BALB/C nude mice	↑↑ miR-15b-5p: ↓ tumor growth, ↓ tumor volume and ↓ tumor weight	(15)
Neuroblastoma	Six-week-old NOD mice	↑↑ miR-15b-5p: ↓ tumor size and ↓ tumor weight	(17)
Non-small cell lung cancer	Balb/c nude mice	Δ MEG8 (which sponges mir-15b-5p): ↓ tumor growth	(19)
Oral squamous cell carcinoma	5-week-old female specific-pathogen-free mice	Δ mir-15b-5p: ↓ tumor growth and ↓ metastasis	(20)
Osteosarcoma	5-week-old male BALB/C nude mice	↑↑ miR-15b-5p: ↓ proliferation	(22)
Prostate cancer	PC3 xenograft tumor model	Δ miR-15b-5p: ↓ tumor volume and ↓ tumor weight	(25)

↑ *Up-regulation;* ↓ *Down-regulation.*

5p mimic or inhibitor has led to down-regulation and up-regulation of ACSS2 and PTGS2, respectively. Taken together, miR-15b-5p may increase apoptosis of aortic VSMCs and suppress their proliferation through influencing ACSS2/PTGS2 axis, thus participating in the pathoetiology of abdominal aortic aneurysm (35).

miR-15b-5p has also been shown to mediate the anti-amyloid effect of curcumin in an *in vitro* model of Alzheimer's disease through influencing expression of the amyloid precursor protein (36). Moreover, the antiangiogenic effect of isopimpinellin has been attributed to its impact on induction of miR-15b-5p expression and subsequent down-regulation of angiogenic stimulators (37).

In addition, miR-15b-5p has been shown to mediate the effects of LINC00473 in cerebral I/R injury. Experiments in a cellular model of cerebral I/R injury has shown down-regulation of LINC00473 in these cells. Up-regulation of this lncRNA has reversed the effects of oxygen glucose deprivation/reperfusion on cell viability and apoptosis as well as ROS levels. Mechanistically, LINC00473 acts as a molecular sponge for miR-15b-5p and miR-15a-5p and regulates expression of SRPK1 (38). **Table 4** shows summary of cell line studies on the role of miR-15b-5p in non-malignant conditions.

Animal Studies

Animal studies have highlighted the role of miR-15b-5p in different cellular processes and disorders such as angiogenesis, coronary artery disease, diabetic nephropathy, diabetic retinopathy, myocardial I/R injury, necroptosis and inflammation, Parkinson's disease and trachea inflammatory injury (**Table 5**). For instance, overexpression of miR-15b-5p has considerably suppressed arteriogenesis and angiogenesis in animal models through targeting AKT3. Remarkably, siRNA-mediated silencing of AKT3 has inhibited arteriogenesis and the rescue of blood perfusion following femoral ligation in animals (42). Another animal study has shown that silencing of the miR-15b-5p-sponging lncRNA MALAT1 decreases atherosclerotic process (43). miR-15b-5p has also been shown to affect diabetic nephropathy and retinopathy in animals. Assessment of transcriptome of high glucose-exposed mouse mesangial cells has shown the effect of miR-15b-5p and its downstream target BCL-2 in regulation of high glocose-induced apoptosis. Besides, db/db mice has been shown to have higher levels of urinary miR-15b-5p (47).

Human Studies

Different experiments in human samples obtained from patients with acute mountain sickness, asthma-COPD overlap, coronary artery disease, diabetic foot ulcers, diabetic nephropathy, late pulmonary complications, obstructive sleep apnea and Parkinson's disease have shown dysregulation of miR-15b-5p levels (**Table 6**).

This miRNA might participate in the pathoetiology of acute mountain sickness. Levels of miR-15b-5p in the saliva have been found to be higher in individuals being resistant to this condition compared to susceptible ones. Combination of levels of miR-134-3p and miR-15b-5p could discriminate between these two groups. Thus, salivary levels of miR-134-3p and miR-15b-5p have been suggested as non-invasive markers for prediction of acute mountain sickness prior to exposure to high altitude (71).

Although *in vitro* studies indicated possible role of miR-15b-5p in the pathogenesis of Alzheimer's disease (36), serum levels of miR-15b-5p were not significantly different between patients with Alzheimer's disease and healthy subjects (72).

miR-15b-5p has been among miRNA having lower expression in asthma-COPD overlap patients. This miRNA can distinguish between asthma-COPD overlap patients and individuals with either asthma or COPD. In fact, miR-15b-5p has been shown to be superior to other miRNAs in separation of patients with asthma-COPD overlap from similar conditions (73).

TABLE 3 | Summary of human studies on the role of miR-15b-5p in cancers (NB, Neuroblastoma; OS, Overall survival; ANCTs, adjacent non-cancerous tissues; TNM, tumor-node-metastasis; MSS, microsatellite stable; CRC, colorectal cancer; RFS, relapse-free survival; HCC, Hepatocellular carcinoma).

Tumors	Specimens	Expression (Tumor vs. Normal)	Kaplan-Meier analysis (as a result of dysregulation in mir-15b-5p)	Multivariate/Univariate cox regression	Clinicopathologic characteristics	Method by which RNA was detected	Reference
Bladder cancer	10 patients with and without BC included 3 healthy persons and 7 patients with other urologic diseases	upregulated	_	_	_	ExiLENT SYBR® Green master mix	(29)
	TCGA database 58 pairs of tumor tissues and ANCTs	upregulated	Poorer OS	_	_	PrimeScript RT-PCR kit	(4)
Breast cancer	6 pairs of tumor tissues and ANCTs TCGA databases	upregulated	Poorer OS	_	_	_	(5)
Cervical cancer	53 pairs of tumor tissues and ANCTs	Downregulation of FENDRR (which sponges mir-15b-5p)	_	_	_	SYBR Green kit	(6)
Colorectal cancer	23 pairs of tumor tissues and ANCTs TCGA database	downregulated	_	_	_	TransStart SYBR Green supermix	(9)
Colorectal cancer	94 tumor tissues	downregulation in SIRT1 which suppresses mir-15b-5p transcription *via* AP-1	_	_	_	_	(8)
	110 pairs of tumor tissues and ANCTs TCGA database: MSS CRC samples	downregulated	_	_	_	_	(10)
	GEPIA database	upregulation of CERS6-AS1 (which sponges mir-15b-5p)	_	_	_	_	(11)
Gastric cancer	40 pairs of tumor tissues and ANCTs 100 patients and 100 healthy controls	upregulated	_	_	degree of tumor invasion and lymph node metastasis and distant metastasis	PrimeScript™ RT reagent kit	(12)
Head and neck cancer squamous cell carcinomas	43 HNSCC patient in explorative phase 51 HNSCC patient in validation phase	downregulated	Shorter locoregional RFS	miR-15b-5p was found to be an independent predictive factor of LRC in HNSCC patients.	_	TaqMan stem-loop	(30)
Hepatocellular carcinoma	TCGA and GEO databases 991 HCC and 456 adjacent non-HCC tissue samples	upregulated	_	_	_	_	(31)
	GEO database (GSE36411: 42 pairs of tumor tissues and ANCTs)	Upregulation of OIP5 (a target of miR-15b-5p)	_	_	_	_	(12)
	46 pairs of tumor tissues and ANCTs	downregulated	_	_	_	SYBR Green	(14)
	Phase I: 6 pairs of tumor tissues and ANCTs (from 6 HCC patients) Phase II: 10 patients Phase III: 37 HCC patients, 29 cirrhosis patients, and 31 healthy controls	Overexpression in tumor tissues and preoperative plasmas, and downregulation in postoperative plasma	_	_	_	ALL-in-One™ miRNA qRT-PCR Detection Kit	(32)
	28 pairs of tumor tissues and ANCTs	upregulated	_	_	_	SYBR Premix Ex Taq II on an FTC-3000TM System	(15)
Hepatocellular carcinoma (HBV-related type)	GEO database GSE27462 (5 pairs of tumor tissues and ANCTs) GSE76903 (20 pairs of tumor tissues and ANCTs) GSE121248 (70 pairs of tumor tissues and ANCTs)	upregulated	Poorer OS	_	_	_	(33)

(Continued)

TABLE 4 | Summary of cell line studies on the role of miR-15b-5p in non-malignant conditions (Δ, knock-down or deletion; DOX, doxorubicin; H2S, Hydrogen sulfide; HG, High glucose; SHF, secondary hair follicle; ER, endoplasmic reticulum; EVs, extracellular vesicles).

Disease type	Interactions	Cell line	Function	Reference
Abdominal aortic aneurysm	ACSS2 and PTGS2	Human aortic VSMCs (T/G HA-VSMC cell line)	↑↑ miR-15b-5p: ↓ proliferation and ↑ apoptosis of aortic VSMCs *via* targeting the ACSS2/PTGS2 axis	(35)
Alzheimer's disease	amyloid precursor protein and amyloid-β	swAPP695-HEK293 cells and HEK293	Curcumin treatment: ↑ mir-15b-5p and ↓ amyloid precursor protein and ↓ amyloid-β	(36)
Angiogenesis	–	Human Umblical Vein Endothelial Cell (HUVEC)	Isopimpinellin: ↓ proliferation, ↓ invasion, ↓ migration, and tube formation *via* increasing mir-15b-5p levels and decreasing angiogenic stimulators	(37)
Asthma	YAP1	ASM cells	↑↑ miR-15b-5p: ↓ proliferation, migration, inflammatory response, and ECM deposition of TNF-α-induced ASM cells	(39)
Atherosclerosis	circCHFR and GADD45G	HUVECs	Upregulation of miR-15b-5p was found to reduce apoptosis, proinflammatory cytokine secretion, and improved cell survival *via* targeting GADD45G.	(40)
Cerebral I/R injury	LINC00473, SRPK1	Neuro-2a (N2a) cells	↑↑ LINC00473 (which sponges mir-15b-5p): ↑ cell viability, ↓ apoptosis and ↓ ROS level induced by OGD/R	(38)
Clopidogrel-induced liver injury	TLK1	HepG2 cells	Clopidogrel treatment: ↓ miR-15b and its target TLK1, which shows other molecules are involved in the regulation of TLK1 expression as a result of exposure to clopidogrel.	(41)
Coronary artery disease	AKT3	Human umbilical vein endothelial cells (HUVECs)	↑↑ miR-15b-5p: ↓ migration and ↓ proliferation of endothelial cells Δ miR-15b-5p: ↑ migration and ↑ proliferation of endothelial cells	(42)
Coronary atherosclerotic heart disease	MALAT1 and MAPK1, mTOR signaling pathway	HEK 293T cells	Δ MALAT1 (which sponges mir-15b-5p): ↑ cell viability, ↑ autophagy and ↓ development of CAD	(43)
Dexamethasone induced steatosis	ENST00000608794, PDK4	dexamethasone treated HepG2 cell lines	Δ ENST00000608794 (which sponges miR-15b-5p): ↓ dexamethasone induced steatosis ↑↑ miR-15b-5p: ↓ dexamethasone induced steatosis	(44)
Diabetic foot ulcers	IKBKB and WEE1	human keratinocytes	S. aureus: ↑ miR-15b-5p levels ↑↑ miR-15b-5p: ↓ DNA repair and ↓ inflammatory response	(45)
Diabetic nephropathy	JNK and Akt/mTOR pathway	HK-2 and HKC-5 cells	High glucose treatment: ↓ expression of miR-15b-5p in HK-2 cells ↑↑ miR-15b-5p: ↓ High glucose-induced apoptosis in HK-2 cells	(46)
	BCL-2	Mouse MCs (CRL1927) and human embryonic kidney (HEK) 293 cells	High glucose treatment: ↑ miR-15b-5p expression in mouse MCs, so ↑ mouse MC apoptosis by targeting BCL-2	(47)
Diabetic nephropathy	CDKN2B-AS1 and WNT2B	HMCs	Δ miR-15b-5p: ↑ viability, ↑ cell cycle progression, ↑ ECM accumulation, ↑ inflammatory response	(48)
	PDK4 and VEGFA	MPC5 cells	High-glucose treatment: ↓ mir-15b-5p in podocytes ↑↑ EVs-derived miR-15b-5p: ↓ MPC5 cell apoptosis and ↓ inflammation *via* reducing PDK4 and VEGFA	(49)
Diabetic retinopathy	circ_001209, COL12A1	human retinal vascular endothelial cells (HRVECs)	High-glucose treatment: ↑ circ_001209 (which sponges miR-15b-5p) levels, thus ↑ COL12A1 (a target of miR-15b-5p) levels ↑↑ miR-15b-5p: ↓ invasion, ↓ migration and ↓ tubular formation induced by HG	(50)
Diabetic retinopathy	TNFα, SOCS3 and IGFBP-3 l	Human REC	miR-15b was found to have a role in the inhibition of insulin resistance by decreased TNFα and SOCS3 signaling and increased IGFBP-3 levels, resulting in REC protection from hyperglycemia-induced apoptosis.	(51)
DOX-induced cardiotoxicity	Bmpr1a	H9c2 cardiomyocytes	↑↑ miR-15b-5p: ↑ DOX-induced apoptosis, ↑ oxidative stress and ↑ mitochondria damage	(52)
Endoplasmic reticulum stress mediated neurons apoptosis	Rab1A	HT22 cells	Sevoflurane exposure: ↓ cell viability, and ↑ apoptosis and ↑ ER stress *via* increasing mir-15b-5p levels, thus inhibiting Rab1A	(53)
Fracture	HCAR, VEGF and MMP13	BMSCs	HCAR sponges miR-15b-5p to regulate VEGF and MMP13, so induces endochondral bone repair in hypertrophic chondrocyte.	(54)
High glucose-induced podocyte injury	Sema3A	mouse podocytes	↑↑ mir-15b-5p: ↓ apoptosis, ↓ oxidative stress, and ↓ inflammatory response	(55)
Inductive property of DPCs in cashmere goat	lncRNA-599547, Wnt10b	dermal papilla cells (DPCs) of passage 3 of cashmere goat SHF	lncRNA-599547 (which sponges miR-15b-5p) showed strongly high levels in dermal papilla of cashmere goat SHF.	(56)
Myocardial infarction	circ-Ttc3, Arl2	cardiomyocytes and cardiac fibroblasts	High levels of f circ-Ttc3 (which sponges miR-15b) was found to protect cardiomyocytes against ischemia-related apoptotic death.	(57)

(Continued)

TABLE 3 | Continued

Tumors	Specimens	Expression (Tumor vs. Normal)	Kaplan-Meier analysis (as a result of dysregulation in mir-15b-5p)	Multivariate/Univariate cox regression	Clinicopathologic characteristics	Method by which RNA was detected	Reference
Liver cancer	69 pairs of tumor tissues and ANCTs	upregulated	Poorer OS	_	TNM stage and tumor capsular infiltration	SYBR Premix Ex Taq	(14)
Neuroblastoma	Two cohort: 88 NB patients and 105 NB patients	downregulated	Poorer OS	_	_	SYBR green mix (Bio-Rad) for mRNA expression or TaqMan Universal Fast PCR master mix	(17)
	46 neuroblastoma samples and 28 normal tissues	downregulated	_	_	_	_	(18)
Non-small cell lung cancer	37 pairs of tumor tissues and ANCTs	downregulated	_	_	_	_	(19)
Oral squamous cell carcinoma	TCGA database 37 pairs of tumor tissues and ANCTs	upregulated	Poorer OS	_	tumor stage, TNM stage, and tumor metastasis	SYBR Premix Ex Taq II	(20)
Ovarian cancer	TCGA and genotype-tissue expression (GTEx) databases	downregulation in TTN-AS1 which sponges mir-15b-5p	_	_	_	_	(24)
Prostate cancer	TCGA database: 495 patients and 52 pairs of tumor tissues and ANCTs	upregulated	_	_	age and Gleason score of patients with PCa	_	(25)
Squamous cell carcinoma	10 patients and 30 healthy controls	downregulated	_	_	_	_	(34)
Thyroid carcinoma	Cancer Genome Atlas project database: 509 patients and 58 healthy controls	downregulated	Poorer OS	_	_	_	(27)

TABLE 4 | Continued

Disease type	Interactions	Cell line	Function	Reference
Necroptosis and inflammation	TGFBR3, TGF-β pathway	HD11 and DT40	H2S exposure: ↑ oxidative stress and activates the TGF-β pathway by regulating miR-15b-5p/TGFBR3 axis miR-15b-5p is upregulated in H2S-induced necroptosis and inflammation.	(58)
Obstructive sleep apnea	PTGS1-NF-κB-SP1 signaling	human THP-1, HUVEC, and SH-SY5Y cell lines	Δ miR-15b-5p: ↑ IHR-induced oxidative stress and ↑ MAOA hyperactivity *via* targeting PTGS1-NF-κB-SP1 signaling in OSA patients	(59)
Osteoarthritis	LINC00662, GPR120	rat chondrocytes	LINC00662 is downregulated in osteoarthritis, so mir-15b-5p is upregulated and GPR120 is suppressed, thus inflammatory responses and apoptosis are induced.	(60)
Parkinson's disease	LINC00943 and RAB3IP	SK-N-SH cells	Δ LINC00943 (which sponges miR-15b-5p): ↓ MPP+-caused decrease of cell viability so reduced MPP+-induced neuronal damage	(61)
	SNHG1 and GSK3β	1-methyl-4-phenylpyridinium ion (MPP+)-treated SH-SY5Y cells	↑↑ SNHG1 (which sponges miR-15b-5p): ↑ MPP+ -induced cellular toxicity, ↓ cell viability *via* miR-15b-5p/GSK3β axis	(62)
	Akt3	293T cells and the human dopaminergic neuroblastoma SH-SY5Y cells	↑↑ miR-15b-5p: ↑ apoptosis by targeting Akt3 in an MPP+-induced PD cell model	(63)
	SNHG1, SIAH1	SH-SY5Y	↑↑ miR-15b-5p: ↓ α-synuclein aggregation and ↓ apoptosis *via* targeting SIAH1	(64)
Severe acute respiratory syndrome coronavirus 2	viral RdRp	–	↑↑ miR-15b-5p: ↓ viral infection and ↓ proliferation by targeting the RNA template component of SARS-CoV-2 RdRp	(65)
Skeletal muscle atrophy	lncIRS1 and IRS1	DF-1 cells	LncIRS1 (which sponges mir-15b-5p) was found to regulate myoblast proliferation and differentiation *in vitro via* increasing IRS1.	(66)
Tendon injury	circRNA-Ep400, FGF-1/7/9	293 T cells, fibroblasts and tenocytes	↑↑ M2 macrophage-derived circRNA-Ep400 (which sponges mir-15b-5p): ↑ fibrosis, ↑ proliferation, and ↑ migration	(67)

↑ *Up-regulation;* ↓ *Down-regulation.*

TABLE 5 | Summary of studies on the role of miR-15b-5p in non-malignant conditions (Δ, knock-down or deletion; MDA, malondialdehyde; ECs, endothelial cells; ACR, Albumin-to-Creatinine Ratio; H2S, Hydrogen sulfide).

Disease Type	Animal models	Results	Reference
Angiogenesis	zebrafish embryos	Isopimpinellin: ↓ intersegmental vessels	(37)
Coronary artery disease	8-10-week-old male C57BL/6 mice Mice were received agomiR-15b, agomiR-NC, or cholesterol-conjugated AKT3 siRNA by multi-point injections.	miR-15b-5p expression was decreased, because of a reduced expression in EC layer of collaterals and miR-15b-5p was mainly derived from ECs. ↑↑ miR-15b-5p: ↓ arteriogenesis and ↓ angiogenesis	(42)
Coronary atherosclerotic heart disease	Six-week old male ApoE–/–mice	Δ MALAT1 (which sponges mir-15b-5p): ↓ atherosclerosis	(43)
Diabetic nephropathy	5 db/m mice and 5 db/db mice	Higher urine miR-15b-5p levels were found in db/db mice. Urinary EV miR-15b-5p levels were positively associated with urinary ACR.	(47)
Diabetic retinopathy	80 Sprague–Dawley male rats	With increased levels of circ_001209 (which sponges miR-15b-5p) retinal thickness was thinner in diabetic rats, and apoptosis was enhanced.	(68)
Myocardial ischemia reperfusion injury	6-8 week-old male C57/B6 mice	Δ mir-15b-5p: ↓ arrhythmia, infarct extent and apoptosis, ↓ MDA content in the myocardial tissue by increasing levels of KCNJ2 (a target of mir-15b-5p)	(69)
Necroptosis and inflammation	40 one-day-old Ross 308 male broilers	H2S exposure: ↑ necroptosis and inflammation	(58)
Parkinson's disease	five-week-old male C57BL/6 mice	Δ miR-15b-5p: ↓ MPTP-induced apoptosis by regulating Akt3	(63)
Skeletal muscle atrophy	1-day-old chicks	LncIRS1 (which sponges mir-15b-5p) was found to regulate muscle mass and muscle fibre cross-sectional area.	(66)
Trachea inflammatory injury	Eighty one-day-old Ross 308 broilers divided into two groups (control group and H2S group)	H2S exposure: ↑ mir-15b-5p miR-15b-5p reduced ATF2 levels to mediate METs release, which induces trachea inflammatory damage	(70)

↑ *Up-regulation;* ↓ *Down-regulation.*

TABLE 6 | Summary of human studies on the role of miR-15b-5p in non-malignant conditions (CAD, coronary atherosclerotic heart disease; CCC, coronary collateral circulation; ACR, albumin-to-creatinine ratio; eGFR, Estimated Glomerular Filtration Rate; AMS, Acute mountain sickness; COPD, chronic obstructive pulmonary disease; ACO, asthma-COPD overlap; DN, diabetic nephropathy; OSA, obstructive sleep apnea; CPAP, continuous positive airway pressure; DFU, Diabetic foot ulcers; FS, foot skin).

Disease type	Numbers of clinical samples	Expression (Tumor vs. Normal)	Clinicopathologic characteristics of patients	Method by which RNA was detected	Reference
Acute mountain sickness	124 healthy men (75 AMS+ group and 49 AMS– group)	upregulated in AMS- group	_	iQ™5 Real-Time PCR Detection System	(71)
Alzheimer's disease	50 AD patients and 50 healthy controls	no significant differences	_	_	(72)
Asthma-COPD overlap	Cohort 1: 6 patients with ACO and 6 patients with asthma Cohort 2; 30 patients with asthma, 30 patients with COPD, or 30 patients with ACO	downregulated in ACO patients	_	miScript SYBR Green PCR Ki	(73)
Atherosclerosis	30 patients with atherosclerosis and 30 healthy controls	downregulated	_	SYBR Green PCR kit	(40)
Coronary artery disease	5 patients with poor CCC and 5 patients with good CCC 20 patients with poor CCC and 18 patients with good CCC and 18 healthy controls	upregulated in patients with poor CCC	miR-15b-5p was associated with insufficient coronary collateral artery function.	SYBR Premix Ex Taq qRT-PCR assays	(42)
Coronary atherosclerotic heart disease	GEO database (GSE18608: 10 CAD patients and 4 healthy controls 5 CAD patients and 5 healthy controls	downregulated	_	SYBR green	(43)
Diabetic foot ulcers	12 DFU and 12 FS specimens 6 DFU and 6 FS specimens (GEO database GSE80178)	upregulated in DFU	_	PerfeCTa® SYBR® Green SuperMix	(45)
Diabetic nephropathy	85 type 2 diabetic patients and 39 healthy controls	upregulated	Urinary EV miR-15b-5p levels were found to be positively associated with urinary ACR, negatively associated with eGFR, and correlated with rapid decline in kidney function in humans.	_	(47)
	34 DN patients and 34 healthy controls	downregulated	_	SYBR Green	(48)
Late pulmonary complications	20 Sulfur mustard-exposed individuals and 20 healthy controls	no differences	_	_	(74)
Obstructive sleep apnea	Discovery cohort: 16 OSA Patients and 8 healthy controls Validation cohort: 20 Primary Snoring, 45 Treatment-Naïve OSA Patients, and 13 OSA Patients on CPAP	downredulated in OSA patients	miR-15b-5p was negatively associated with an apnea hypopnea index	NGS (Illumina MiSeq platform) and SYBR Green PCR kit	(59)
Parkinson's disease	10 patients and 5 healthy controls	upregulated	_	ABI PRISM® 7500 Sequence Detection System	(63)

In some conditions, dysregulation of this miRNA has been associated with clinicopathological parameters. For instance, in patients with coronary artery disease, dysregulation of miR-15b-5p has been associated with insufficient coronary collateral artery function (42). Moreover, in diabetic nephropathy, Urinary exosomal levels of miR-15b-5p have been positively associated with urinary albumin-to-creatinine ratio, negatively associated with eGFR, and correlated with speedy failure in kidney function (47).

DISCUSSION

miR-15b-5p is an example of miRNAs with dual roels in the carcinogenesis. While it is a putative oncogenic miRNA in bladder cancer, breast cancer, gastric cancer, oral squamous cell carcinoma and prostate cancer, it has been found to be down-regulated in head and neck cancer squamous cell carcinomas, neublastoma and thyroid cancer samples as compared with corresponding non-cancerous samples (75). Moreover, in colorectal cancer and hepatocellular carcinoma, different studies have reported contradictory results.

This miRNA also participates in the pathogenesis of several non-malignant conditions, such as abdominal aortic aneurysm, Alzheimer's disease, Parkinson's disease, cerebral I/R injury, coronary artery disease, dexamethasone induced steatosis, diabetic complications and doxorubicin-induced cardiotoxicity.

miR-15b-5p has been shown to be sponged by several lncRNAs, namely MAGI2-AS3, H19, SNHG1, SNHG16, TTN-AS1, PVT1, FENDRR, SSTR5–AS1, MALAT1, ENST00000608794, CDKN2B-AS1, LINC00473, LINC00662, LINC00943, LncRNA-599547 and CDKN2B-AS1 as well as the circular RNA Circ_001209. Thus, lncRNAs and circRNAs can affect expression of this miRNA. Other possible regulatory mechanisms for modulation of expression levels of miR-15b-5p should be clarified in future studies.

NF-κB, STAT3, AKT/mTORC1, CDC42/PAK1 and β-catenin signaling pathways are signaling pathways that mediate the effects of miR-15b-5p in the carcinogenesis. Notably, this miRNA could regulate response of cancer cells to 5-FU and anti-PD-1 drugs. Thus, therapeutics modalities affecting expression of miR-15b-5p can be considered as possible ways to combat resistance to anti-cancer agents. Evidence from *in vitro* and *in vivo* studies indicates that therapeutic intervention with miR-15-5p levels can significantly influence pathological processes. Moreover, disease-associated abnormal expression pattern of this miRNA in the affected tissues potentiates it as a diagnostic biomarkers. Particularly, in bladder cancer, breast cancer, head and neck cancers, liver cancer, neuroblastoma, oral squamous cell carcinoma and thyroid cancer, abnormal expression of miR-15-5p has been associated with poor clinical outcomes indicating the role of this miRNA as a prognostic biomarker. It is expected that therapeutic modalities affect expression of miR-15-5p and amend disease-associated dysregulation of this miRNA. Therefore, expression pattern of miR-15-5p can be used to monitor disease status and response to therapeutic options.

Since both oncogenic and tumor suppressor roles have been reported for miR-15-5p, different miR-15-5p-targeting therapeutic targets can been applied in the field of cancer therapy. In tissues that this miRNA exerts tumor suppressor roles, exogenous miR-15-5p can be used to inhibit cell proliferation or induce apoptosis. This goal can be achieved by administration of chemically synthesized miR-15-5p mimics to induce expression of endogenous mature double-stranded miR-15-5p to restore function of this miRNA. Viral vectors expressing miR-15-5p are appropriate vectors for delivery of this miRNA to tumor cells. On the other hand, when miR-15-5p exerts oncogenic roles, antisense oligonucleotides and miR-15-5p sponges can be used for suppression of level of this miRNA. Although these strategies are putative therapeutic modalities for treatment of cancer, they have not been applied in the clinical setting yet.

CONCLUSION

While the prognostic impact of dysregulation of miR-15b-5p has been confirmed in different types of cancer, there is no explicit evidence for application of this miRNA as a diagnostic marker in cancers. Since miRNAs dysregulation in the circulation provides a potential way for early non-invasive diagnosis of cancer, future studies should focus on evaluation of expression levels of miR-15b-5p in different biofluids during the course of cancer to provide insights into diagnostic role of this miRNA in cancer.

AUTHOR CONTRIBUTIONS

SG-F wrote the manuscript and revised it. MT supervised and designed the study. TK, HJ, MH and BH collected the data and designed the figures and tables. All authors read and approved the submitted version.

FUNDING

This study was financially supported by Grant from Medical School of Shahid Beheshti University of Medical Sciences.

REFERENCES

1. Hussen BM, Hidayat HJ, Salihi A, Sabir DK, Taheri M, Ghafouri-Fard S. MicroRNA: A Signature for Cancer Progression. *Biomed Pharmacother = Biomed Pharmacother* (2021) 138:111528. doi: 10.1016/j.biopha.2021.111528
2. Ghafouri-Fard S, Shaterabadi D, Abak A, Shoorei H, Bahroudi Z, Taheri M, et al. An Update on the Role of miR-379 in Human Disorders. *Biomed Pharmacother = Biomed Pharmacother* (2021) 139:111553. doi: 10.1016/j.biopha.2021.111553
3. Ha M, Kim VN. Regulation of microRNA Biogenesis. *Nat Rev Mol Cell Biol* (2014) 15(8):509–24. doi: 10.1038/nrm3838
4. Wang F, Zu Y, Zhu S, Yang Y, Huang W, Xie H, et al. Long Noncoding RNA MAGI2-AS3 Regulates CCDC19 Expression by Sponging miR-15b-5p and Suppresses Bladder Cancer Progression. *Biochem Biophys Res Commun* (2018) 507(1-4):231–5. doi: 10.1016/j.bbrc.2018.11.013

5. Wu B, Liu G, Jin Y, Yang T, Zhang D, Ding L, et al. miR-15b-5p Promotes Growth and Metastasis in Breast Cancer by Targeting HPSE2. *Front Oncol* (2020) 10:108. doi: 10.3389/fonc.2020.00108
6. Zhu Y, Zhang X, Wang L, Zhu X, Xia Z, Xu L, et al. FENDRR Suppresses Cervical Cancer Proliferation and Invasion by Targeting miR-15a/B-5p and Regulating TUBA1A Expression. *Cancer Cell Int* (2020) 20(1):1–10. doi: 10.1186/s12935-020-01223-w
7. Gasparello J, Gambari L, Papi C, Rozzi A, Manicardi A, Corradini R, et al. High Levels of Apoptosis are Induced in the Human Colon Cancer HT-29 Cell Line by Co-Administration of Sulforaphane and a Peptide Nucleic Acid Targeting miR-15b-5p. *Nucleic Acid Ther* (2020) 30(3):164–74. doi: 10.1089/nat.2019.0825
8. Sun L-N, Zhi Z, Chen L-Y, Zhou Q, Li X-M, Gan W-J, et al. SIRT1 Suppresses Colorectal Cancer Metastasis by Transcriptional Repression of miR-15b-5p. *Cancer Lett* (2017) 409:104–15. doi: 10.1016/j.canlet.2017.09.001
9. Zhao C, Zhao Q, Zhang C, Wang G, Yao Y, Huang X, et al. miR-15b-5p Resensitizes Colon Cancer Cells to 5-Fluorouracil by Promoting Apoptosis *via* the NF-κb/XIAP Axis. *Sci Rep* (2017) 7(1):1–12. doi: 10.1038/s41598-017-04172-z
10. Liu C, Liu R, Wang B, Lian J, Yao Y, Sun H, et al. Blocking IL-17A Enhances Tumor Response to Anti-PD-1 Immunotherapy in Microsatellite Stable Colorectal Cancer. *J Immunother Cancer* (2021) 9(1):1–14. doi: 10.1136/jitc-2020-001895
11. Zhao SY, Wang Z, Wu XB, Zhang S, Chen Q, Wang DD, et al. CERS6-AS1 Contributes to the Malignant Phenotypes of Colorectal Cancer Cells by Interacting With miR-15b-5p to Regulate SPTBN2. *Kaohsiung J Med Sci* (2022) 38(5):403–414. doi: 10.1002/kjm2.12503. doi: 10.1002/kjm2.12503
12. Zhao C, Li Y, Chen G, Wang F, Shen Z, Zhou R. Overexpression of miR-15b-5p Promotes Gastric Cancer Metastasis by Regulating PAQR3. *Oncol Rep* (2017) 38(1):352–8. doi: 10.3892/or.2017.5673
13. Gasparello J, Papi C, Zurlo M, Gambari L, Rozzi A, Manicardi A, et al. Treatment of Human Glioblastoma U251 Cells With Sulforaphane and a Peptide Nucleic Acid (PNA) Targeting miR-15b-5p: Synergistic Effects on Induction of Apoptosis. *Molecules* (2022) 27(4):1299. doi: 10.3390/molecules27041299
14. Zhou Y, Fan R-G, Qin C-L, Jia J, Wu X-D, Zha W-Z. LncRNA-H19 Activates CDC42/PAK1 Pathway to Promote Cell Proliferation, Migration and Invasion by Targeting miR-15b in Hepatocellular Carcinoma. *Genomics* (2019) 111 (6):1862–72. doi: 10.1016/j.ygeno.2018.12.009
15. Yang Y, Hou N, Wang X, Wang L, Se C, He K, et al. miR-15b-5p Induces Endoplasmic Reticulum Stress and Apoptosis in Human Hepatocellular Carcinoma, Both *In Vitro* and *In Vivo*, by Suppressing Rab1A. *Oncotarget* (2015) 6(18):16227. doi: 10.18632/oncotarget.3970
16. Yu F, Lin Y, Tan G, Ai M, Gong H, Liu W, et al. Tumor-Derived Exosomal microRNA-15b-5p Augments Laryngeal Cancer by Targeting TXNIP. *Cell Cycle* (2022) 7:1–11. doi: 10.1080/15384101.2021.2022845
17. Chava S, Reynolds CP, Pathania AS, Gorantla S, Poluektova LY, Coulter DW, et al. miR-15a-5p, miR-15b-5p, and miR-16-5p Inhibit Tumor Progression by Directly Targeting MYCN in Neuroblastoma. *Mol Oncol* (2020) 14(1):180–96. doi: 10.1002/1878-0261.12588
18. Ge Y, Tan S, Bi J, Rao M, Yu Y, Tian L. SNHG16 Knockdown Inhibits Tumorigenicity of Neuroblastoma in Children *via* miR-15b-5p/PRPS1 Axis. *NeuroReport* (2020) 31(17):1225–35. doi: 10.1097/WNR.0000000000001537
19. Guo K, Qi D, Huang B. LncRNA MEG8 Promotes NSCLC Progression by Modulating the miR-15a-5p-miR-15b-5p/PSAT1 Axis. *Cancer Cell Int* (2021) 21(1):1–16. doi: 10.1186/s12935-021-01772-8
20. Liu X, Dong Y, Song D. Inhibition of microRNA-15b-5p Attenuates the Progression of Oral Squamous Cell Carcinoma *via* Modulating the PTPN4/STAT3 Axis. *Cancer Manage Res* (2020) 12:10559. doi: 10.2147/CMAR.S272498
21. Wang X, Guo H, Yao B, Helms J. miR-15b Inhibits Cancer-Initiating Cell Phenotypes and Chemoresistance of Cisplatin by Targeting TRIM14 in Oral Tongue Squamous Cell Cancer. *Oncol Rep* (2017) 37(5):2720–6. doi: 10.3892/or.2017.5532
22. Weng Y, Shen Y, He Y, Pan X, Xu J, Jiang Y, et al. The miR-15b-5p/PDK4 Axis Regulates Osteosarcoma Proliferation Through Modulation of the Warburg Effect. *Biochem Biophys Res Commun* (2018) 503(4):2749–57. doi: 10.1016/j.bbrc.2018.08.035
23. Cai Y, Yang Y, Zhang X, Ma Q, Li M. TRPM2-AS Promotes the Malignancy of Osteosarcoma Cells by Targeting miR-15b-5p/PPM1D Axis. *Cell Cycle* (2022) 8:1–16. doi: 10.1080/15384101.2022.2033414
24. Miao S, Wang J, Xuan L, Liu X. LncRNA TTN-AS1 Acts as Sponge for miR-15b-5p to Regulate FBXW7 Expression in Ovarian Cancer. *BioFactors* (2020) 46(4):600–7. doi: 10.1002/biof.1622
25. Chen R, Sheng L, Zhang HJ, Ji M, Qian WQ. miR-15b-5p Facilitates the Tumorigenicity by Targeting RECK and Predicts Tumour Recurrence in Prostate Cancer. *J Cell Mol Med* (2018) 22(3):1855–63. doi: 10.1111/jcmm.13469
26. Sun F, Wu K, Yao Z, Mu X, Zheng Z, Sun M, et al. Long Noncoding RNA PVT1 Promotes Prostate Cancer Metastasis by Increasing NOP2 Expression *via* Targeting Tumor Suppressor MicroRNAs. *OncoTargets Ther* (2020) 13:6755. doi: 10.2147/OTT.S242441
27. Zou J, Qian J, Fu H, Yin F, Zhao W, Xu L. MicroRNA−15b−5p Exerts its Tumor Repressive Role *via* Targeting GDI2: A Novel Insight Into the Pathogenesis of Thyroid Carcinoma. *Mol Med Rep* (2020) 22(4):2723–32. doi: 10.3892/mmr.2020.11343
28. Lovat F, Fassan M, Gasparini P, Rizzotto L, Cascione L, Pizzi M, et al. miR-15b/16-2 Deletion Promotes B-Cell Malignancies. *Proc Natl Acad Sci USA* (2015) 112(37):11636–41. doi: 10.1073/pnas.1514954112
29. Tölle A, Buckendahl L, Jung K. Plasma Mir−15b−5p and Mir−590−5p for Distinguishing Patients With Bladder Cancer From Healthy Individuals. *Oncol Rep* (2019) 42(4):1609–20. doi: 10.3892/or.2019.7247
30. Ahmad P, Sana J, Slávik M, Gurín D, Radová L, Gablo NA, et al. MicroRNA-15b-5p Predicts Locoregional Relapse in Head and Neck Carcinoma Patients Treated With Intensity-Modulated Radiotherapy. *Cancer Genomics Proteomics* (2019) 16(2):139–46. doi: 10.21873/cgp.20119
31. Pan WY, Zeng JH, Wen DY, Wang JY, Wang PP, Chen G, et al. Oncogenic Value of microRNA−15b−5p in Hepatocellular Carcinoma and a Bioinformatics Investigation. *Oncol Lett* (2019) 17(2):1695–713. doi: 10.3892/ol.2018.9748
32. Chen Y, Chen J, Liu Y, Li S, Huang P. Plasma miR-15b-5p, miR-338-5p, and miR-764 as Biomarkers for Hepatocellular Carcinoma. *Med Sci Monit* (2015) 21:1864. doi: 10.12659/MSM.893082
33. Xu J, Zhang J, Shan F, Wen J, Wang Y. SSTR5−AS1 Functions as a ceRNA to Regulate CA2 by Sponging Mir−15b−5p for the Development and Prognosis of HBV−Related Hepatocellular Carcinoma. *Mol Med Rep* (2019) 20 (6):5021–31. doi: 10.3892/mmr.2019.10736
34. Jin X, Chen Y, Chen H, Fei S, Chen D, Cai X, et al. Evaluation of Tumor-Derived Exosomal miRNA as Potential Diagnostic Biomarkers for Early-Stage Non–Small Cell Lung Cancer Using Next-Generation Sequencing. *Clin Cancer Res* (2017) 23(17):5311–9. doi: 10.1158/1078-0432.CCR-17-0577
35. Gan S, Mao J, Pan Y, Tang J, Qiu Z. Hsa−Mir−15b−5p Regulates the Proliferation and Apoptosis of Human Vascular Smooth Muscle Cells by Targeting the ACSS2/PTGS2 Axis. *Exp Ther Med* (2021) 22(5):1–8. doi: 10.3892/etm.2021.10642
36. Liu H-Y, Fu X, Li Y-F, Li X-L, Ma Z-Y, Zhang Y, et al. miR-15b-5p Targeting Amyloid Precursor Protein Is Involved in the Anti-Amyloid Effect of Curcumin in Swapp695-HEK293 Cells. *Neural Regen Res* (2019) 14(9):1603. doi: 10.4103/1673-5374.255979
37. Bhagavatheeswaran S, Ramachandran V, Shanmugam S, Balakrishnan A. Isopimpinellin Extends Antiangiogenic Effect Through Overexpression of miR-15b-5p and Downregulating Angiogenic Stimulators. *Mol Biol Rep* (2021) 49(1):279–91. doi: 10.1007/s11033-021-06870-4. doi: 10.1007/s11033-021-06870-4
38. Yao B, Ye L, Chen J, Zhuo S, Lin H. LINC00473 Protects Against Cerebral Ischemia Reperfusion Injury *via* Sponging miR-15b-5p and miR-15a-5p to Regulate SRPK1 Expression. *Brain Injury* (2021) 35(11):1462–71. doi: 10.1080/02699052.2021.1972156
39. Zeng S, Cui J, Zhang Y, Zheng Z, Meng J, Du J. MicroRNA-15b-5p Inhibits Tumor Necrosis Factor Alpha-Induced Proliferation, Migration, and Extracellular Matrix Production of Airway Smooth Muscle Cells *via* Targeting Yes-Associated Protein 1. *Bioengineered* (2022) 13(3):5396–406. doi: 10.1080/21655979.2022.2036890
40. Li Y, Wang B. Circular RNA circCHFR Downregulation Protects Against Oxidized Low-Density Lipoprotein-Induced Endothelial Injury *via* Regulation of microRNA-15b-5p/Growth Arrest and DNA Damage Inducible Gamma. *Bioengineered* (2022) 13(2):4481–92. doi: 10.1080/21655979.2022.2032967

41. Freitas RC, Bortolin RH, Lopes MB, Tamborlin L, Meneguello L, Silbiger VN, et al. Modulation of miR-26a-5p and miR-15b-5p Exosomal Expression Associated With Clopidogrel-Induced Hepatotoxicity in HepG2 Cells. *Front Pharmacol* (2017) 8:906. doi: 10.3389/fphar.2017.00906
42. Zhu L-P, Zhou J-P, Zhang J-X, Wang J-Y, Wang Z-Y, Pan M, et al. MiR-15b-5p Regulates Collateral Artery Formation by Targeting AKT3 (Protein Kinase B-3). *Arterioscler Thromb Vasc Biol* (2017) 37(5):957–68. doi: 10.1161/ATVBAHA.116.308905
43. Zhu Y, Yang T, Duan J, Mu N, Zhang T. MALAT1/miR-15b-5p/MAPK1 Mediates Endothelial Progenitor Cells Autophagy and Affects Coronary Atherosclerotic Heart Disease *via* mTOR Signaling Pathway. *Aging (Albany NY)* (2019) 11(4):1089. doi: 10.18632/aging.101766
44. Liu F, Chen Q, Chen F, Wang J, Gong R, He B. The lncRNA ENST00000608794 Acts as a Competing Endogenous RNA to Regulate PDK4 Expression by Sponging miR-15b-5p in Dexamethasone Induced Steatosis. *Biochim Biophys Acta (BBA)-Molecular Cell Biol Lipids* (2019) 1864(10):1449–57. doi: 10.1016/j.bbalip.2019.07.003
45. Ramirez HA, Pastar I, Jozic I, Stojadinovic O, Stone RC, Ojeh N, et al. Staphylococcus Aureus Triggers Induction of miR-15B-5P to Diminish DNA Repair and Deregulate Inflammatory Response in Diabetic Foot Ulcers. *J Invest Dermatol* (2018) 138(5):1187–96. doi: 10.1016/j.jid.2017.11.038
46. Shen H, Fang K, Guo H, Wang G. High Glucose-Induced Apoptosis in Human Kidney Cells was Alleviated by miR-15b-5p Mimics. *Biol Pharm Bull* (2019) 42(5):758–63. doi: 10.1248/bpb.b18-00951
47. Tsai Y-C, Kuo M-C, Hung W-W, Wu L-Y, Wu P-H, Chang W-A, et al. High Glucose Induces Mesangial Cell Apoptosis Through miR-15b-5p and Promotes Diabetic Nephropathy by Extracellular Vesicle Delivery. *Mol Ther* (2020) 28(3):963–74. doi: 10.1016/j.ymthe.2020.01.014
48. Chang J, Yu Y, Fang Z, He H, Wang D, Teng J, et al. Long non-Coding RNA CDKN2B-AS1 Regulates High Glucose-Induced Human Mesangial Cell Injury *via* Regulating the miR-15b-5p/WNT2B Axis. *Diabetol Metab Syndrome* (2020) 12(1):1–11. doi: 10.1186/s13098-020-00618-z
49. Zhao T, Jin Q, Kong L, Zhang D, Teng Y, Lin L, et al. microRNA-15b-5p Shuttled by Mesenchymal Stem Cell-Derived Extracellular Vesicles Protects Podocytes From Diabetic Nephropathy *via* Downregulation of VEGF/PDK4 Axis. *J Bioenerg Biomembr* (2021) 54:17–30. doi: 10.1007/s10863-021-09919-y
50. Li B, Zhang G, Wang Z, Yang Y, Wang C, Fang D, et al. C-Myc-Activated USP2-AS1 Suppresses Senescence and Promotes Tumor Progression *via* Stabilization of E2F1 mRNA. *Cell Death Dis* (2021) 12(11):1–14. doi: 10.1038/s41419-021-04330-2
51. Ye E-A, Steinle JJ. miR-15b/16 Protects Primary Human Retinal Microvascular Endothelial Cells Against Hyperglycemia-Induced Increases in Tumor Necrosis Factor Alpha and Suppressor of Cytokine Signaling 3. *J Neuroinflammation* (2015) 12(1):1–8. doi: 10.1186/s12974-015-0265-0
52. Gao ZF, Ji XL, Gu J, Wang XY, Ding L, Zhang H. microRNA-107 Protects Against Inflammation and Endoplasmic Reticulum Stress of Vascular Endothelial Cells *via* KRT1-Dependent Notch Signaling Pathway in a Mouse Model of Coronary Atherosclerosis. *J Cell Physiol* (2019) 234 (7):12029–41. doi: 10.1002/jcp.27864
53. Li Y, Xia H, Chen L, Zhang X. Sevoflurane Induces Endoplasmic Reticulum Stress Mediated Apoptosis Inmouse Hippocampal Neuronal HT22 Cells *via* Modulating miR-15b-5p/Rab1A Signaling Pathway. *Int J Clin Exp Pathol* (2017) 10(8):8270–80.
54. Bai Y, Gong X, Dong R, Cao Z, Dou C, Liu C, et al. Long non-Coding RNA HCAR Promotes Endochondral Bone Repair by Upregulating VEGF and MMP13 in Hypertrophic Chondrocyte Through Sponging miR-15b-5p. *Genes Dis* (2020). doi: 10.1016/j.gendis.2020.07.013
55. Fu Y, Wang C, Zhang D, Chu X, Zhang Y, Li J. miR-15b-5p Ameliorated High Glucose-Induced Podocyte Injury Through Repressing Apoptosis, Oxidative Stress, and Inflammatory Responses by Targeting Sema3A. *J Cell Physiol* (2019) 234(11):20869–78. doi: 10.1002/jcp.28691
56. Yin RH, Zhao SJ, Wang ZY, Zhu YB, Yin RL, Bai M, et al. LncRNA-599547 Contributes the Inductive Property of Dermal Papilla Cells in Cashmere Goat Through miR-15b-5p/Wnt10b Axis. *Anim Biotechnol* (2020) 14:1–15. doi: 10.1080/10495398.2020.1806860
57. Cai L, Qi B, Wu X, Peng S, Zhou G, Wei Y, et al. Circular RNA Ttc3 Regulates Cardiac Function After Myocardial Infarction by Sponging miR-15b. *J Mol Cell Cardiol* (2019) 130:10–22. doi: 10.1016/j.yjmcc.2019.03.007
58. Qianru C, Xueyuan H, Bing Z, Qing Z, Kaixin Z, Shu L. Regulation of H2S-Induced Necroptosis and Inflammation in Broiler Bursa of Fabricius by the miR-15b-5p/TGFBR3 Axis and the Involvement of Oxidative Stress in This Process. *J Hazard Mater* (2021) 406:124682. doi: 10.1016/j.jhazmat.2020.124682
59. Chen Y-C, Hsu P-Y, Su M-C, Chen T-W, Hsiao C-C, Chin C-H, et al. MicroRNA Sequencing Analysis in Obstructive Sleep Apnea and Depression: Anti-Oxidant and MAOA-Inhibiting Effects of miR-15b-5p and miR-92b-3p Through Targeting PTGS1-NF-κb-SP1 Signaling. *Antioxidants* (2021) 10 (11):1854. doi: 10.3390/antiox10111854
60. Lu M, Zhou E. Long Noncoding RNA LINC00662-miR-15b-5p Mediated GPR120 Dysregulation Contributes to Osteoarthritis. *Pathol Int* (2020) 70 (3):155–65. doi: 10.1111/pin.12875
61. Meng C, Gao J, Ma Q, Sun Q, Qiao T. LINC00943 Knockdown Attenuates MPP+-Induced Neuronal Damage *via* miR-15b-5p/RAB3IP Axis in SK-N-SH Cells. *Neurol Res* (2021) 43(3):181–90. doi: 10.1080/01616412.2020.1834290
62. Xie N, Qi J, Li S, Deng J, Chen Y, Lian Y. Upregulated lncRNA Small Nucleolar RNA Host Gene 1 Promotes 1-Methyl-4-Phenylpyridinium Ion-Induced Cytotoxicity and Reactive Oxygen Species Production Through miR-15b-5p/GSK3β Axis in Human Dopaminergic SH-SY5Y Cells. *J Cell Biochem* (2019) 120(4):5790–801. doi: 10.1002/jcb.27865
63. Zhu J, Xu X, Liang Y, Zhu R. Downregulation of microRNA-15b-5p Targeting the Akt3-Mediated GSK-3β/β-Catenin Signaling Pathway Inhibits Cell Apoptosis in Parkinson's Disease. *BioMed Res Int* (2021) 2021:8814862. doi: 10.1155/2021/8814862
64. Cory-Slechta D, Allen J, Conrad K, Marvin E, Sobolewski M. Developmental Exposure to Low Level Ambient Ultrafine Particle Air Pollution and Cognitive Dysfunction. *Neurotoxicology* (2018) 69:217–31. doi: 10.1016/j.neuro.2017.12.003
65. Sato A, Ogino Y, Tanuma S-i, Uchiumi F. Human microRNA hsa-miR-15b-5p Targets the RNA Template Component of the RNA-Dependent RNA Polymerase Structure in Severe Acute Respiratory Syndrome Coronavirus 2. *Nucleosides Nucleotides Nucleic Acids* (2021) 40(8):790–7. doi: 10.1080/15257770.2021.1950759
66. Li Z, Cai B, Abdalla BA, Zhu X, Zheng M, Han P, et al. LncIRS1 Controls Muscle Atrophy *via* Sponging miR-15 Family to Activate IGF1-PI3K/AKT Pathway. *J Cachexia Sarcopenia Muscle* (2019) 10(2):391–410. doi: 10.1002/jcsm.12374
67. Yu Y, Sun B, Wang Z, Yang M, Cui Z, Lin S, et al. Exosomes From M2 Macrophage Promote Peritendinous Fibrosis Posterior Tendon Injury *via* the MiR-15b-5p/FGF-1/7/9 Pathway by Delivery of circRNA-Ep400. *Front Cell Dev Biol* (2021) 1557. doi: 10.3389/fcell.2021.595911
68. Wang F, Zhang M. Circ_001209 Aggravates Diabetic Retinal Vascular Dysfunction Through Regulating miR-15b-5p/COL12A1. *J Trans Med* (2021) 19(1):1–12. doi: 10.1186/s12967-021-02949-5
69. Niu S, Xu L, Yuan Y, Yang S, Ning H, Qin X, et al. Effect of Down-Regulated miR-15b-5p Expression on Arrhythmia and Myocardial Apoptosis After Myocardial Ischemia Reperfusion Injury in Mice. *Biochem Biophys Res Commun* (2020) 530(1):54–9. doi: 10.1016/j.bbrc.2020.06.111
70. Song N, Wang W, Wang Y, Guan Y, Xu S, Guo M-y. Hydrogen Sulfide of Air Induces Macrophage Extracellular Traps to Aggravate Inflammatory Injury *via* the Regulation of miR-15b-5p on MAPK and Insulin Signals in Trachea of Chickens. *Sci Total Environment* (2021) 771:145407. doi: 10.1016/j.scitotenv.2021.145407
71. Huang H, Dong H, Zhang J, Ke X, Li P, Zhang E, et al. The Role of Salivary miR-134-3p and miR-15b-5p as Potential Non-Invasive Predictors for Not Developing Acute Mountain Sickness. *Front Physiol* (2019) 10:898. doi: 10.3389/fphys.2019.00898
72. Poursaei E, Abolghasemi M, Bornehdeli S, Shanehbandi D, Asadi M, Sadeghzadeh M, et al. Evaluation of Hsa-Let-7d-P, Hsa-Let-7g-5p and hsa-miR-15b-5p Level in Plasma of Patients With Alzheimer's Disease Compared to Healthy Controls. *Psychiatr Genet* (2022). doi: 10.1097/YPG.0000000000000303
73. Hirai K, Shirai T, Shimoshikiryo T, Ueda M, Gon Y, Maruoka S, et al. Circulating microRNA-15b-5p as a Biomarker for Asthma-COPD Overlap. *Allergy* (2021) 76(3):766–74. doi: 10.1111/all.14520
74. Salimi S, Noorbakhsh F, Faghihzadeh S, Ghaffarpour S, Ghazanfari T. Expression of miR-15b-5p, miR-21-5p, and SMAD7 in Lung Tissue of Sulfur Mustard-Exposed Individuals With Long-Term Pulmonary Complications. *Iranian J Allergy Asthma Immunol* (2019) 8:332–9. doi: 10.18502/ijaai.v18i3.1126

75. Taheri M, Noroozi R, Rakhshan A, Ghanbari M, Omrani MD, Ghafouri-Fard S. IL-6 Genomic Variants and Risk of Prostate Cancer. *Urol J* (2019) 16 (5):463–8. doi: 10.22037/uj.v0i0.4543

Conflict of Interest: The authors declare that the research was conducted in the absence of any commercial or financial relationships that could be construed as a potential conflict of interest.

Publisher's Note: All claims expressed in this article are solely those of the authors and do not necessarily represent those of their affiliated organizations, or those of the publisher, the editors and the reviewers. Any product that may be evaluated in this article, or claim that may be made by its manufacturer, is not guaranteed or endorsed by the publisher.

frontiers | Frontiers in Oncology

ORIGINAL RESEARCH
published: 12 May 2022
doi: 10.3389/fonc.2022.849242

A Novel and Robust Prognostic Model for Hepatocellular Carcinoma Based on Enhancer RNAs-Regulated Genes

Wei Zhang[1†], *Kegong Chen*[2,3†], *Wei Tian*[1], *Qi Zhang*[1], *Lin Sun*[1], *Yupeng Wang*[1], *Meina Liu*[1*] and *Qiuju Zhang*[1*]

[1] Department of Biostatistics, School of Public Health, Harbin Medical University, Harbin, China, [2] Department of Cardio-Thoracic Surgery, The Second Affiliated Hospital of Harbin Medical University, Harbin, China, [3] Department of Ultrasound, The First Affiliated Hospital of USTC, Division of Life Sciences and Medicine, University of Science and Technology of China, Hefei, China

Evidence has demonstrated that enhancer RNAs (eRNAs) play a vital role in the progression and prognosis of cancers, but few studies have focused on the prognostic ability of eRNA-regulated genes (eRGs) for hepatocellular carcinoma (HCC). Using gene expression profiles of HCC patients from the TCGA-LIHC and eRNA expression profiles from the enhancer RNA in cancers (eRic) data portal, we developed a novel and robust prognostic signature composed of 10 eRGs based on Lasso-penalized Cox regression analysis. According to the signature, HCC patients were stratified into high- and low-risk groups, which have been shown to have significant differences in tumor immune microenvironment, immune checkpoints, HLA-related genes, DNA damage repair-related genes, Gene-set variation analysis (GSVA), and the lower half-maximal inhibitory concentration (IC50) of Sorafenib. The prognostic nomogram combining the signature, age, and TNM stage had good predictive ability in the training set (TCGA-LIHC) with the concordance index (C-index) of 0.73 and the AUCs for 1-, 3-, and 5-year OS of 0.82, 0.77, 0.74, respectively. In external validation set (GSE14520), the nomogram also performed well with the C-index of 0.71 and the AUCs for 1-, 3-, and 5-year OS of 0.74, 0.77, 0.74, respectively. In addition, an important eRG (AKR1C3) was validated using two HCC cell lines (Huh7 and MHCC-LM3) *in vitro*, and the results demonstrated the overexpression of AKR1C3 is related to cell proliferation, migration, and invasion in HCC. Altogether, our eRGs signature and nomogram can predict prognosis accurately and conveniently, facilitate individualized treatment, and improve prognosis for HCC patients.

Keywords: hepatocellular carcinoma, enhancer RNAs, signature, prognosis, AKR1C3

OPEN ACCESS

Edited by:
Sabine Mihm,
University Medical Center Göttingen, Germany

Reviewed by:
Amin Mahpour,
Massachusetts General Hospital and Harvard Medical School, United States
Jian-Bing Wang,
Zhejiang University, China

***Correspondence:**
Meina Liu
liumeina369@163.com
Qiuju Zhang
qjzh_81@126.com

[†]*These authors have contributed equally to this work and share first authorship*

Specialty section:
This article was submitted to Cancer Genetics, a section of the journal Frontiers in Oncology

Received: *08 January 2022*
Accepted: *01 April 2022*
Published: *12 May 2022*

Citation:
Zhang W, Chen K, Tian W, Zhang Q, Sun L, Wang Y, Liu M and Zhang Q (2022) A Novel and Robust Prognostic Model for Hepatocellular Carcinoma Based on Enhancer RNAs-Regulated Genes. Front. Oncol. 12:849242. doi: 10.3389/fonc.2022.849242

1 INTRODUCTION

Hepatocellular carcinoma (HCC) is the most common type (approximately 90%) of primary liver cancer, which has already become the sixth most commonly diagnosed cancer (906,000 new cases) and the third leading cause of cancer death (830,000 deaths) worldwide in 2020 (1). Chronic infection of hepatitis B virus (HBV) or hepatitis C virus (HCV), cirrhosis, excessive alcohol consumption, and type 2 diabetes are the main risk factors for HCC (2). HCC has a very poor prognosis due to its advanced stage, rapid progression, high recurrence rate, and limited treatment options (3). Traditionally, tumor stage is a widely used basis for predicting the prognosis of patients with HCC (4, 5). However, prognosis in HCC is complex and highly heterogeneous (6, 7), patients in the same tumor stage may present significantly different prognosis. A valuable, accurate strategy is still an urgent need to predict HCC prognosis.

Previous research has proposed that serum biochemical biomarkers, such as hepatic growth factor, osteopontin, BALAD scoring model composed of alpha-fetoprotein (AFP), alpha-fetoprotein lens culinaris agglutin-3 (AFP-L3), and Des-γ-carboxy prothrombin (DCP) could be used for predicting prognosis (8–10). With the development of high-throughput sequencing technology, genes were considered to be important factors in predicting survival of patients with HCC (11–14). Furthermore, gene signatures based on multigene expression, and nomograms including gene signature and clinical information have been constructed for patients' prognosis in many published studies (15–17). However, it is still necessary to further mine omics data in combination with clinical characteristics to discover a novel and reliable prognostic model for HCC and guide patients' individualized treatment.

Enhancer RNAs (eRNAs) are non-coding RNAs transcribed by enhancers that mediate the activation of target genes (18, 19). In human cancers, eRNAs can contribute to the activation of oncogenes or oncogenic signaling pathways and can be induced by oncogenes or tumor suppressors to directly participate in tumor promotion or inhibition process (20–22). Furthermore, eRNAs can also bind to DNA, proteins (e.g., transcription factors, cofactors, RNA-binding proteins) to regulate their function and activity (23). Super-enhancers, the clusters of enhancers, also play prominent roles in dysregulation of oncogenes expression, tumor suppressor genes expression, process of tumorigenesis, and proliferation of cancer cells (23–25). Although some data portals have already annotated a mass of enhancers, the direct interaction between eRNA and its target genes has not been elaborated until researchers integrated data from TCGA and other projects (26–28) and developed eRic data portal including a global eRNA-gene regulatory network across 31 cancer types in 2019 (29). This portal facilitates a deeper investigation of relationships between eRNAs and cancers for biomedical researchers. However, few studies have focused on eRNA-regulated genes (eRGs) to construct prognostic models of HCC patients for the management of individualized treatment.

This study attempted to construct a novel prognostic gene signature composed of eRGs and nomogram combining the signature with clinical characteristics by using univariate and Lasso-penalized Cox regression analyses in TCGA-LIHC dataset and validate it in GSE14520 dataset. We demonstrated the application potential of the signature and nomogram through bioinformatics methods. In addition, we validated the effect of important eRG in the signature on cell proliferation, migration, and invasion of HCC using two HCC cell lines (Huh7 and MHCC-LM3) *in vitro*.

2 MATERIALS AND METHODS

2.1 Data Collection and Processing

Data used in this study were all publicly available. mRNA expression and clinical data of 374 LIHC patients were obtained from the Cancer Genome Atlas (TCGA) data portal (https://portal.gdc.cancer.gov/), and the eRNA expression profile across these TCGA samples as well as eRNA target genes were acquired from the enhancer RNA in cancers (eRic) data portal (https://hanlab.uth.edu/eRic/). The raw mRNA data in TCGA was processed to fragments per kilobase of transcript per million mapped reads (FPKM) and transformed based on log2 (log2FPKM). Patients with insufficient survival information or follow-up period less than 30 days were excluded, and 324 HCC samples were selected as the training set for subsequent analysis. Microarray dataset GSE14520 -GPL3921 includes 219 HCC patients with integral clinical information and survival time longer than 30 days were downloaded from the Gene Expression Omnibus (GEO) database (https://www.ncbi.nlm.nih.gov/geo/) as the external validation set.

2.2 Construction and Validation of eRGs Signature

In this section, we identified eRNAs related to survival in HCC patients and the target genes regulated by them. Based on the target genes, an eRGs signature was constructed and validated for predicting prognosis.

Kaplan-Meier analysis and univariate Cox regression were used to screen eRNAs related to survival in TCGA dataset, and only the eRNAs with $p < 0.05$ in both above analyses were selected. Then the target genes of these eRNAs were identified by referring to the eRic database.

The target genes of survival-related eRNAs in TCGA-LIHC were firstly subjected to univariate Cox regression analysis and genes with $p < 0.05$ were considered as the candidate prognostic eRGs. Subsequently, Lasso-penalized Cox regression analysis was performed to build the prognostic eRGs signature, and 10-fold cross-validation was carried out to determine the optimal penalty parameter using "glmnet" package in R. Then the prognostic eRGs signature was established, and the risk score of each patient can be calculated based on the corresponding coefficients of genes from the Lasso Cox regression model (β) and their expression level:

$$riskScore = \sum_{i=1}^{m} \beta_i \times Exp_i$$

where m is the number of the genes in signature, β_i is the coefficient from Lasso Cox analysis, Exp_i is the expression level of the eRGs in signature. The median risk score was used as the cutoff value to stratify the HCC patients into high risk and low risk groups. Thereafter, we performed a log-rank test to compare the survival rates between the two groups and plotted Kaplan-Meier survival curves using "survival" and "survminer" package in R. Time-dependent receiver operating characteristic (ROC) curves for 1-, 3-, and 5-year OS were also drawn based on the risk score using "timeROC" package in R to assess the prognostic performance of the signature. To validate the predictive capability and generalization of the eRGs signature, HCC patients in GSE14520 dataset with intact survival and clinical information were considered as the external validation set. Risk scores of these patients were calculated with the same model of prognostic eRGs signature, and Kaplan-Meier survival curves analysis and the ROC curves analysis were also conducted in this dataset.

2.3 Construction and Validation of Prognostic Nomogram

We performed univariate Cox regression and multivariable Cox regression analysis on the risk score of the gene signature and other clinical features (including age, TNM stage, AFP level, and BMI) in TCGA dataset to identify the independent prognostic factors, and factors with $p < 0.05$ were deemed statistically significant. The proportional hazard assumption of the model was tested by Schoenfeld residuals test. Then a nomogram based on these independent prognostic factors was developed using "rms" package in R to predict the overall survival time of HCC patients. Nomogram is a graphical representation of a complex mathematical formula (30). In medicine, a nomogram is usually used to graphically describe a statistical prognostic model that generates the probability of a particular individual's clinical events (such as cancer recurrence or overall survival), which can be conductive to personalized medicine (31). Calibration curves were utilized to investigate the consistency between the nomogram-predicted probabilities and the actual survival rates, and decision curves analysis (DCA) was conducted to assess the clinical predictive value of the nomogram. Furthermore, time-ROC curves were also plotted in TCGA dataset to evaluate the prognostic performance of the nomogram. Based on the nomogram in the training set, calibration curves analysis, DCA analysis and time-ROC curves analysis were all performed in the external validation set GSE14520 to further validate the results.

2.4 Enrichment Analyses and Gene-Set Variation Analysis

Gene Ontology (GO) and Kyoto Encyclopedia of Genes and Genomes (KEGG) enrichment analyses were performed with survival-related eRGs set, and terms with adjusted $p < 0.05$ were considered as significant enrichment. Gene Set Enrichment Analysis (GSEA) was also conducted on the genes in the survival-related signature to explore the potential pathways by using "clusterProfiler" package in R (32). After that, we applied gene-set variation analysis (GSVA) using "GSVA" package and "limma" package in R to identify the different pathways between the two different risk groups following the criteria of $|\log2FC| > 0.2$ and $p < 0.05$ (33). The annotated gene set used in GSEA and GSVA was "c5.all.v6.2.symbols.gmt", which can be downloaded from the Molecular Signatures Database (MSigDB).

2.5 Exploration of Immunotherapy Effect and Immune Landscape

Immune checkpoint inhibitors play an important role in the treatment of liver cancer (34), so we compared the differences in the expressions of some common immune checkpoints (CTLA4, PD-L1, TIGIT, and HAVCR2) between high risk patients and low risk patients using Wilcoxon rank-sum test. We also calculated the proportion of 22 immune-infiltrating cells in each patient using "Cell type Identification By Estimating Relative Subsets Of RNA Transcripts (CIBERSORT)" algorithm (35), and the patients with $p < 0.05$ were used for difference comparison in the two sub-groups. In addition, we utilized TIMER (Tumor Immune Estimation Resource) database to further explore the correlation between risk score and six immune cells including B cells, CD4+ T cells, CD8+ T cells, macrophages, neutrophils, and dendritic cells (36). Human leukocyte antigen (HLA) is the major histocompatibility complex (MHC) in human, which goes together with the function of human immune system. Therefore, we also validated the differences in HLA-related genes between the two groups.

2.6 Evaluation of Drug Sensitivity

Half maximal inhibitory concentration (IC50) is a widely used indicator to evaluate the sensitivity of drug therapy (37). Sorafenib, a targeted therapy drug, has been considered the standard treatment for patients with hepatocellular carcinoma (HCC) since 2007 (38). Therefore, we estimated the IC50 of Sorafenib in high- and low-risk patients and determined whether there is a difference in the sensitivity of different patients to sorafenib. The drug IC50 was estimated using "pRRophetic" package in R based on Genomics of Drug Sensitivity in Cancer (GDSC, https://www.cancerrxgene.org/) cell line expression data and TCGA-LIHC gene expression data (39, 40).

2.7 Identification of Transcription Factors Related to the Genes in Signature

Transcription factor (TF) list was downloaded from Cistrome (http://cistrome.org/), and the expression level of these TF were extracted from 324 TCGA-LIHC patients. Then we performed Spearman correlation test between the expression of eRGs in the signature and these TFs. The gene-TF pairs with absolute Spearman correlation coefficients > 0.4 and $p < 0.05$ were selected to further discussion.

2.8 *In Vitro* Experimental Validation of AKR1C3 in HCC Cell Lines

2.8.1 Cell Culture, Transfection and Sorafenib Treatment

Human hepatocellular carcinoma cell lines Huh7 and MHCC-LM3 were obtained from the Cell Bank of the Chinese Academy

of Sciences (Beijing, China), both types of cells were cultured in DMEM-6429 (Sigma, MO, USA) with 10% fetal bovine serum (FBS, HyClone, Logan, UT, USA). The siRNA sequences targeting AKR1C3 used in this study were as follows: si-AKR1C3-1:(5'-CCAAACACCAGUGUGUAAATT-3', 5'-UUU ACACACUGGUGUUUGGTT-3'); and si-AKR1C3-2:(5'-GGA ACUUUCACCAACAGAUTT-3', 5'-AUCUGUUGGUGAAA GUUCCTT-3') and negative controls (si-AKR1C3-NC); AKR1C3 overexpression plasmid:(5'-ATGGATTCCAAACA CCAGTGT-3', 5'-TTAATATTCATCTGAATATGG-3') and empty plasmids were regarded as negative controls (NC) purchased from the Nantong Biomics Biotechnologies company. Transfection was performed using Lipofectamine 3000 (Thermo Fisher Scientific, Inc) according to the manufacturers' instructions. The cells were harvested 48 hours after transfection. In addition, Sorafenib (8μM) was added to Huh7 and MHCC-LM3 cells prior the incubation.

2.8.2 Protein Extraction and Western Blot Analysis

Total protein was extracted using RIPA buffer and quantified with a BCA kit (Beyotime Biotechnology). Protein separation was performed using 10% SDS-PAGE and then transferred to PVDF membranes (Merck Millipore). Following being blocked with 5% non-fat milk for 2 h at 25°C, the PVDF membranes were incubated with AKR1C3(Abcam; 1:1000; ab209899) and GAPDH (Abcam; 1:5000; ab9485), and then incubated with a secondary antibody (Cell Signaling Technology) for 1 h. PVDF membranes were scanned by a chemiluminescence system.

2.8.3 Cell Viability and Colony Formation Assays

EdU cell proliferation assay was performed using a commercial EdU Kit (UE, China) according to the manufacturer's protocol. Images obtained from a fluorescence microscope (Leika, Germany) were analyzed using Image J. The colony formation assay was used to evaluate the cell clonogenic ability. The transfected Huh7 and MHCC-LM3 cells were seeded in a 35mm-diameter petri dish and cultured for up to 14 days, respectively. Cell colonies were fixed with 4% paraformaldehyde and stained with 0.1% crystal violet (Beyotime) for 20 minutes, the colonies were counted under a light microscope.

2.8.4 Transwell Assay

Cell invasion was evaluated by performing the Chamber matrigel invasion 24-well units (Costar) according to the manufacturer's instructions. The transfected cells were suspended in a serum-free medium and plated into the upper chamber of the transwell system with a pore size of 8 μm. The bottom chamber was filled with a medium containing 10% FBS. After incubation for 24 h, the migrated/invaded cells in the lower chamber (below the filter surface) were fixed in 4% paraformaldehyde, stained with crystal violet solution, and counted under a microscope.

2.8.5 Wound Scratch Assay

Wound scratch assays were used to assess the migratory ability of Huh7 and MHCC-LM3 cells *in vitro*. AKR1C3 downregulated Huh7 and MHCC-LM3 cells (including negative control cells) were planted in 3.5 cm dishes and grown until 80%–90% confluent. Then, a 100 μl yellow pipette tip was used to scratch the cell monolayers and the cells were maintained in DMEM-6429 medium. The area of the cell-free wound was measured with microscopy at 0 and 24 h.

2.8.6 CCK-8 Experiments

The CCK-8 assay (Dojindo, Japan) was performed to assess Huh7 and MHCC-LM3 cells proliferation. Cells were seeded at a density of 4×10^3 cells/well in 96 wells plates, then added 20 μl of CCK-8 reagent to each well of a 96-well plate, and incubated the cells for 2 h at 37°C. At 6, 24, 48, 72, and 96 h, cell viability was detected by scanning with a microplate reader (Tecan, Switzerland) at 450 nm.

2.9 Statistical Analysis

R software 3.6.3 was used for all data management and analyses in present study. Wilcoxon rank-sum test was used to compare the differences of quantitative variables, and Spearman correlation test was used to explore the correlation between variables. Schoenfeld residuals test was performed to test the proportional hazard assumption of Cox regression model. All the statistical tests were two-sided, and $p < 0.05$ were considered to be statistically significant.

3 RESULTS

3.1 Survival-Related eRNAs, eRGs and Prognostic Signature

The overall flow chart of our study is depicted in **Figure 1**. A total of 324 HCC patients from TCGA-LIHC were included as the training set, and 219 HCC patients from GSE14520-GPL3921 were used as the external validation set. The general clinical characteristics of the two datasets are exhibited in **Supplementary Table S1**.

eRNA expression profile data of 324 TCGA-LIHC patients were downloaded from the eRic data portal, and 457 eRNAs were obtained for K-M analysis and univariate Cox regression. Based on the results of survival analysis, 46 eRNAs were identified that were significantly associated with overall survival ($p < 0.05$). Then 95 target genes of the survival-related eRNAs were obtained by referring to the eRNA target genes list from the eRic database. The survival-related eRNAs and their target genes list are shown in **Supplementary Table S2**.

We conducted univariate Cox regression analysis on survival-related eRNAs target genes in training set, and 22 eRGs were significantly associated with overall survival ($p < 0.05$). After that, Lasso-Cox regression analysis was carried out to discover eRGs related to survival and construct a prognostic signature, which composed of 10 genes, including SSRP1, SSB, IGFBP4, SUOX, RDH16, G6PC, AKR1C3, NUP205, ADAMTS5, and RRAGD, and the correlation between these genes and their corresponding eRNAs are all significant (correlation coefficients larger than 0.3, $p < 0.0001$). Part of the results are shown in **Figure 2**, and the horizontal coordinate indicates the expression of genes in the signature, the vertical coordinate indicates the expression of their corresponding eRNAs. Other results have been shown in **Supplementary Figure S1**.

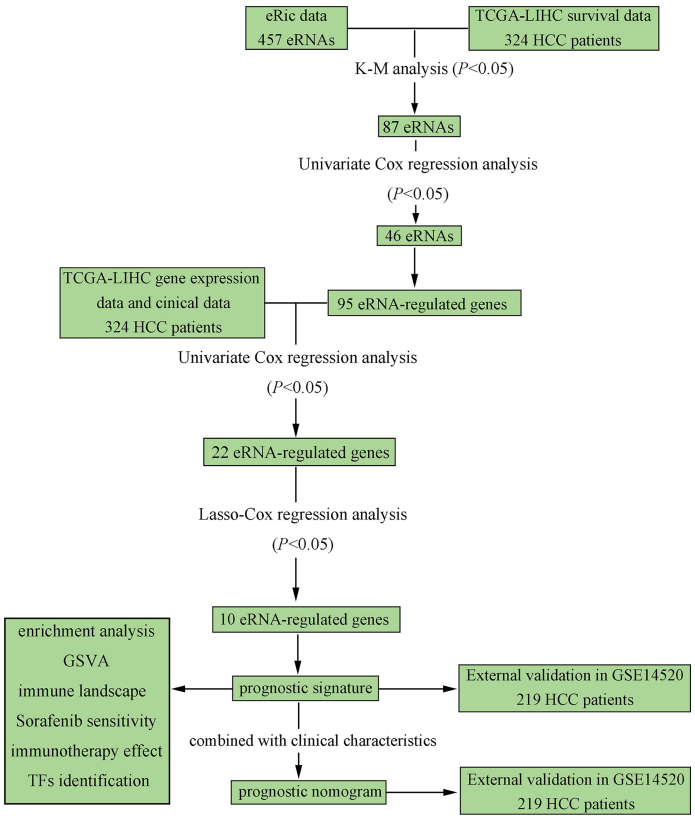

FIGURE 1 | Flowchart elaborating the scheme of construction and validation of prognostic signature and nomogram based on eRGs for HCC patients.

The risk score of each patient can be calculated by using the following formula based on the corresponding coefficients of genes: $riskScore = 0.2209 \times Exp_{SSRP1} + 0.1789 \times Exp_{SSB} + (-0.0131) \times Exp_{IGFBP4} + (-0.0522) \times Exp_{SUOX} + (-0.0053) \times Exp_{RDH16} + (-0.0356) \times Exp_{G6PC} + 0.0563 \times Exp_{AKR1C3} + 0.0106 \times Exp_{NUP205} + 0.4235 \times Exp_{ADAMTS5} + 0.0469 \times Exp_{RRAGD}$. Subsequently, we obtained all the risk scores of patients in the TCGA dataset and considered the median as the cutoff point to divide the patients into high- and low-risk groups. **Figure 3A** presents the expression profiles of 10 survival-related eRGs in the signature, and the expressions of 10 genes were all significantly different between the two groups (**Supplementary Figure S2**). Among them, the expressions of IGFBP4, SUOX, RDH16, and G6PC were lower in the high-risk group than those in the low-risk group, while the expressions of SSRP1, SSB, NUP205, AKR1C3, ADAMTS5, and RRAGD were higher in high-risk group. **Figure 3B** shows risk scores and survival status in the two groups. The Kaplan-Meier survival curves in the training set are shown in **Figure 3C**, which revealed that patients in the high-risk group had a significantly worse prognosis than those in the low-risk group ($p < 0.0001$). The time-dependent ROCs for 1-, 3-, and 5-year OS are exhibited in **Figure 3D**, and their AUCs (area under the ROC curve) were 0.79, 0.73, and 0.68, respectively. The C-index (concordance index) of the signature was 0.70. All the above results demonstrated that the signature composed of 10 eRGs poses a good prognostic performance.

Furthermore, the GSE14520 dataset was considered as the external validation data to confirm the performance of the eRGs signature. The expression of genes, risk scores, and survival status are shown in **Figures 4A, B**. The Kaplan-Meier survival curves were also significantly different ($p < 0.0001$) between the two different risk groups (**Figure 4C**). The AUCs of time-dependent ROCs for 1-, 3-, and 5-year OS were 0.71, 0.73, 0.67, respectively (**Figure 4D**), and the C-index was 0.68. Taken together, these results suggested that the signature had a good capability of predicting survival.

3.2 Prognostic Nomogram

Univariate Cox regression analysis and multivariate Cox regression analysis were used to identify the prognostic factors in TCGA training set, and the risk score of the eRGs signature was a crucial independent prognostic predictor (**Figure 5A**). The results of Schoenfeld residuals test can be found in **Figure S3** (the global Schoenfeld test $p = 0.29$), which indicated that the Cox model satisfied the proportional hazard assumption. Then a nomogram containing age, TNM stage, and risk score was established to predict 1-, 3-, and 5-year survival based on the training set (**Figure 5B**). We conducted a series of internal

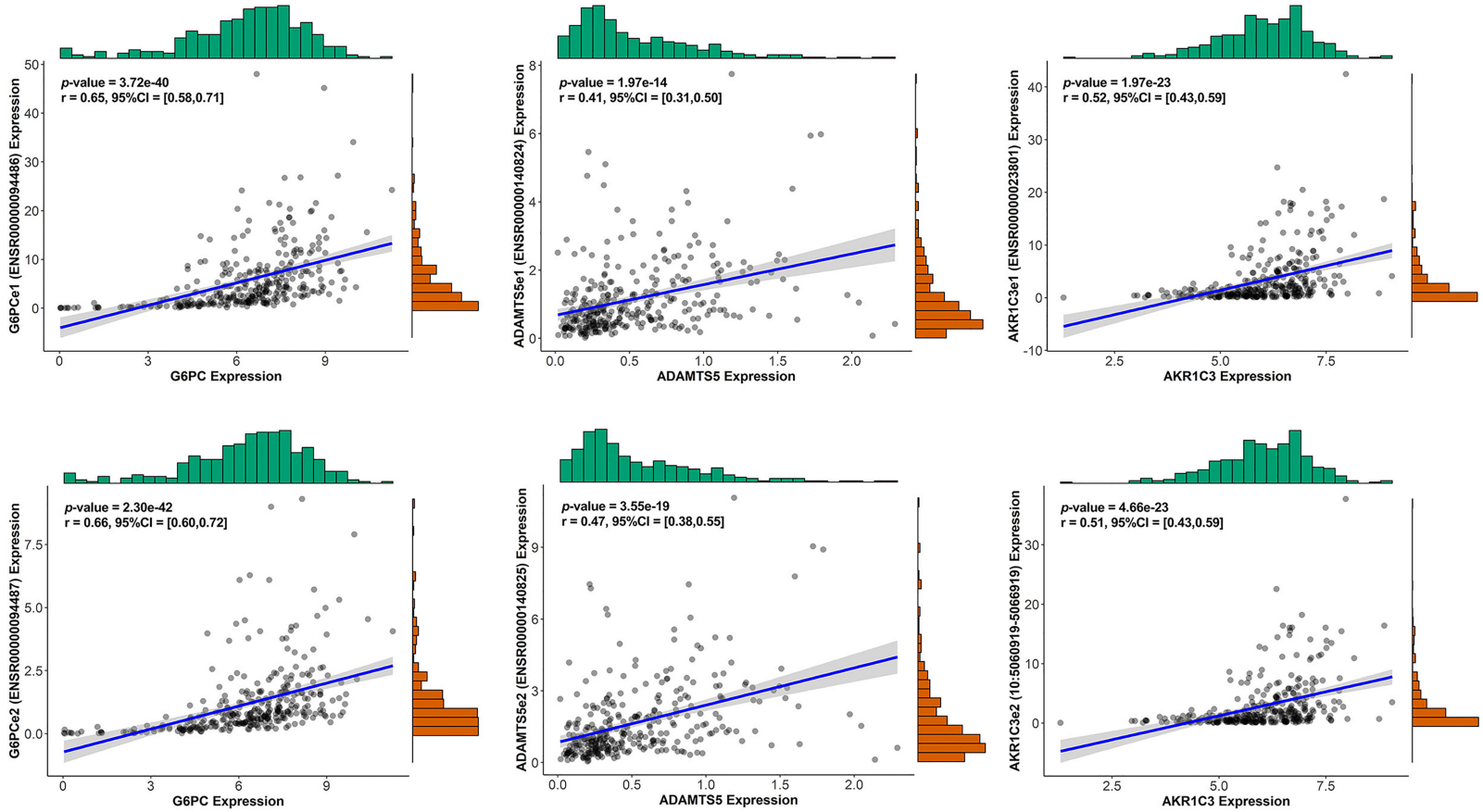

FIGURE 2 | The correlation between genes in the signature and their corresponding eRNA (part results).

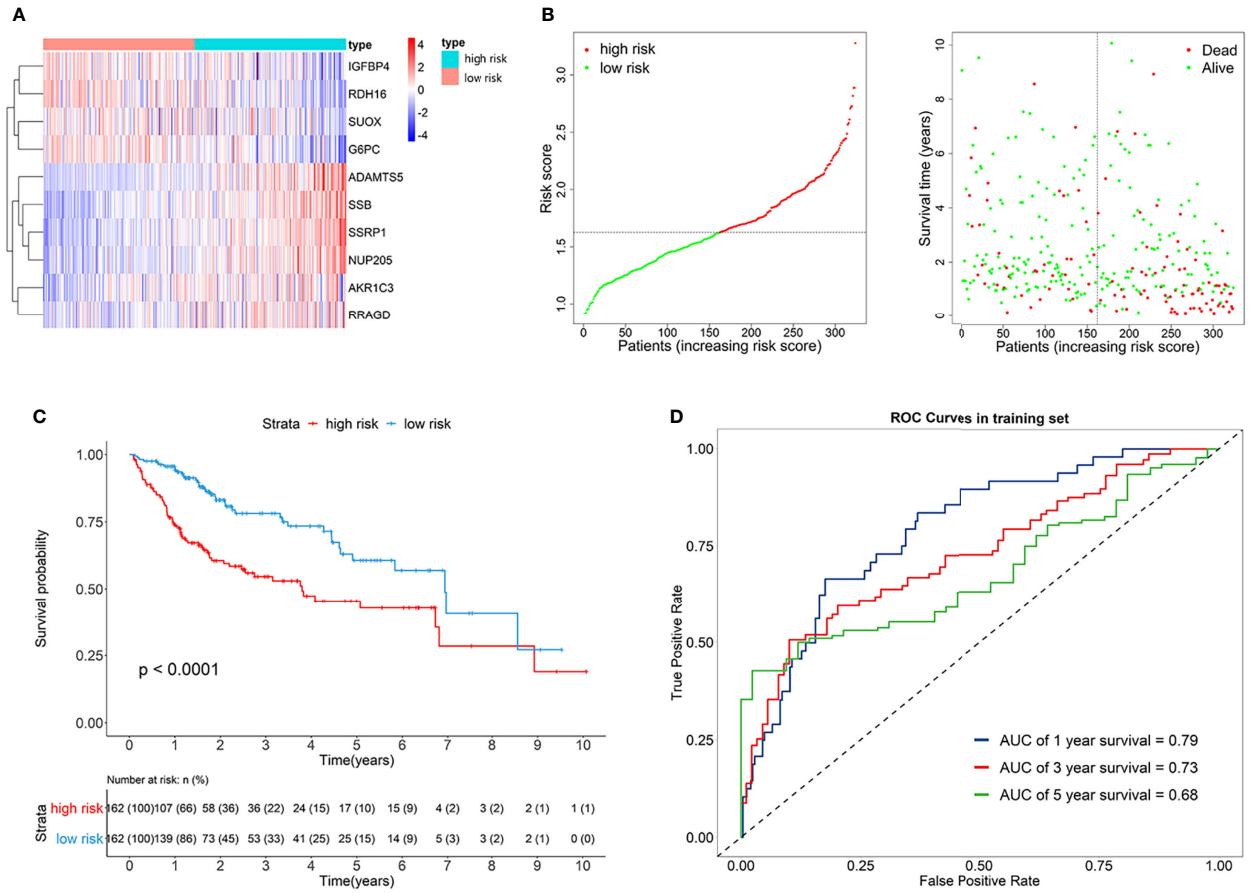

FIGURE 3 | **(A)** Heatmap of the signature genes expression profiles in training set, and the colors represent centered and scaled log2FPKM value in the row direction (FPKM is defined as fragments per kilobase of transcript per million mapped reads); **(B)** Survival status distribution of patients in high risk and low risk group; **(C)** Kaplan-Meier curves of the signature for high risk and low risk group in training set; **(D)** Time-dependent ROC curves of the signature for 1-, 3-, 5-year overall survival in training set.

validation on the performance of the nomogram. Calibration curves presented good concordance between the nomogram-predicted survival and the actual survival of 1-, 3-, and 5-year (**Figure 5C**). The C-index of the nomogram was 0.73. Time-dependent ROC curves at 1-, 3-, and 5-year were exhibited in **Figure 5D**, and AUCs of the nomogram at 1-, 3-, and 5-year were 0.82, 0.77, 0.74, respectively. Furthermore, the model with signature had significantly higher AUC values than the model without signature, which suggested that our eRGs signature and nomogram possessed an excellent prognostic performance. DCA curves of the nomogram for 1-, 3-, 5-year survival in training set are shown in **Figure 5E**, which demonstrates that the nomogram had a high net benefit.

The prognostic performance of nomogram was also validated in GEO validation set. Kaplan-Meier survival curves of the nomogram in TCGA training set and GEO validation set were presented in **Supplementary Figures S4A, B**, and the curves also significantly different ($p < 0.0001$) between the high-risk and low-risk group. The C-index of the nomogram in validation set was 0.71. AUCs of the nomogram at 1-, 3-, and 5-year were 0.74, 0.77, 0.74, respectively, and significantly larger than that model without signature (**Supplementary Figure S4D**). In addition, calibration curves, ROC curves, and DCA curves (**Supplementary Figures S4C, E**) in GEO validation set were all further confirmation that the nomogram had a good predictive value and clinical application value.

3.3 Pathways and Mechanism Analyses

We performed GO and KEGG enrichment analysis on the survival-related eRGs and identified 28 GO terms and two KEGG pathways (**Supplementary Table S3** and **Figure S5**). These survival-related eRGs were enriched in steroid metabolic process, lipid transport, carbohydrate catabolic process, coenzyme metabolic process, oxidoreductase activity, and other GO terms. The enriched KEGG pathways were ABC transporters and steroid hormone biosynthesis. The single gene GSEA results can be seen in **Figures 6A, B**, **Supplementary Figure S6** and **Supplementary Table S4** exhibit the different pathways between

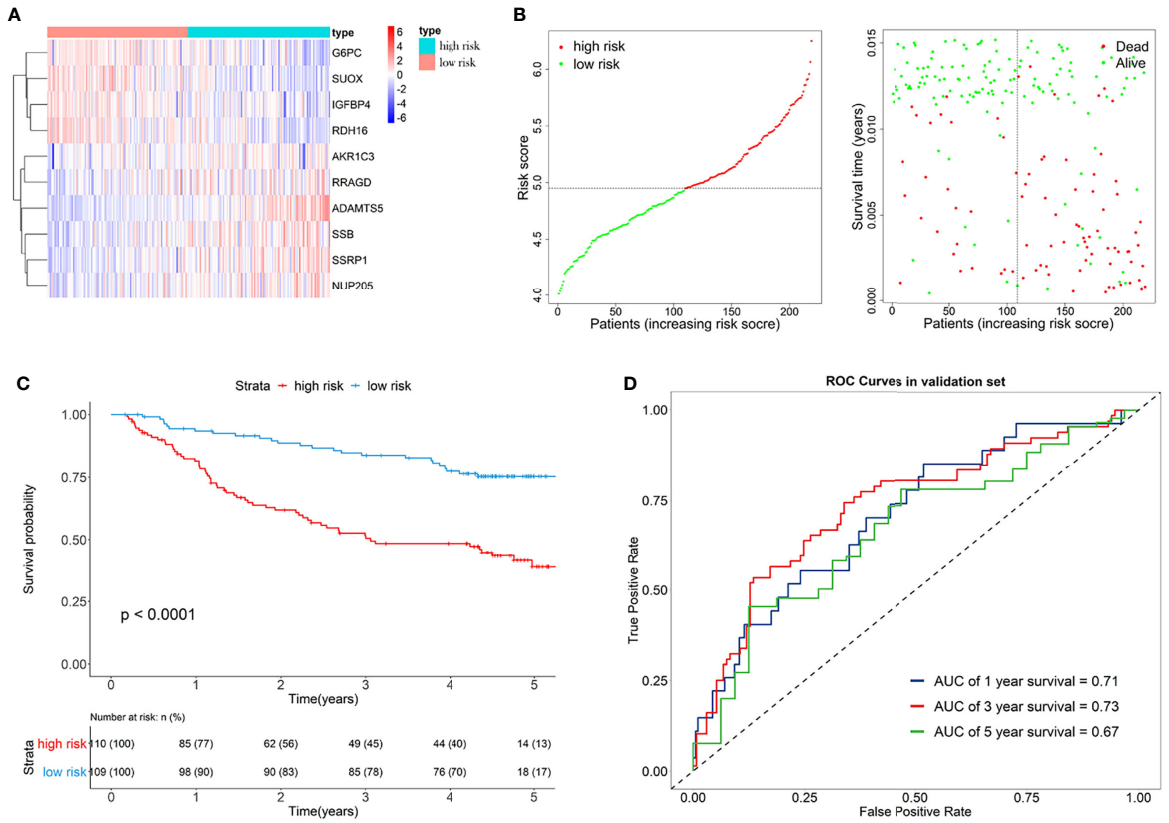

FIGURE 4 | **(A)** Heatmap of the signature genes expression profiles in validation set, and the colors represent centered and scaled log2FPKM value in the row direction (FPKM is defined as fragments per kilobase of transcript per million mapped reads); **(B)** Survival status distribution of patients in high risk and low risk group; **(C)** Kaplan-Meier curves of the signature for high risk and low risk group in validation set; **(D)** Time-dependent ROC curves of the signature for 1-, 3-, 5-year overall survival in validation set.

the high-risk and low-risk group. The up-regulated pathways in high-risk patients were pathogenic Escherichia coli infection, cell cycle, DNA replication, mismatch repair, spliceosome, and ribosome. In comparison, the down-regulated pathways in high-risk patients were fatty acid metabolism, drug metabolism cytochrome P450, steroid hormone biosynthesis, primary bile acid biosynthesis, PPAR signaling pathway, complement and coagulation cascades, amino acid metabolism, linoleic acid metabolism, etc.

3.4 Immune Landscape

eRGs we identified were associated with immune function, and G6PC, SSRP1, NUP205, ADAMTS5, and RRAGD were all related to immune response or process, so we further explored the relationship between risk scores and immune landscape.

Macrophages and T cells had a large proportion in the immune infiltration of TCGA HCC patients (**Figure 7A**). The compositions of immune infiltration were significantly different between the two risk groups. The proportions of B cells naïve, Macrophages M2, Monocytes, NK cells resting, T cells gamma delta were lower in the high-risk group than those in the low-risk group, while dendritic cells resting, Macrophages M0, T cells follicular helper had higher proportions in the high-risk group (**Figure 7B**). The abundances of B cells, CD4+ T cells, CD8+ T cells, macrophages, neutrophils, and dendritic cells were estimated based on Timer algorithm, and they were all significantly correlated with risk score (Spearman correlation test, $p < 0.0001$, **Figure 7D**). In addition, it can be seen from **Figure 7C** that, except for HLA-B, HLA-C, HLA-E, HLA-F, and HLA-G, the expression levels of HLA-related genes were significantly different between the two groups with a higher expression in the high-risk group.

3.5 Drug Sensitivity, Immunotherapy Effect and Transcription Factors

The expressions of four common immune checkpoints (CTLA4, PD-L1, TIGIT, and HAVCR2) were all significantly lower in the low-risk group than high-risk group ($p < 0.05$), which indicated that low-risk patients may have better outcomes when treated with immune checkpoint inhibitors (**Figure 8A**). There was a significant difference in IC50 of Sorafenib between the two different risk groups, and low-risk patients have a lower IC50,

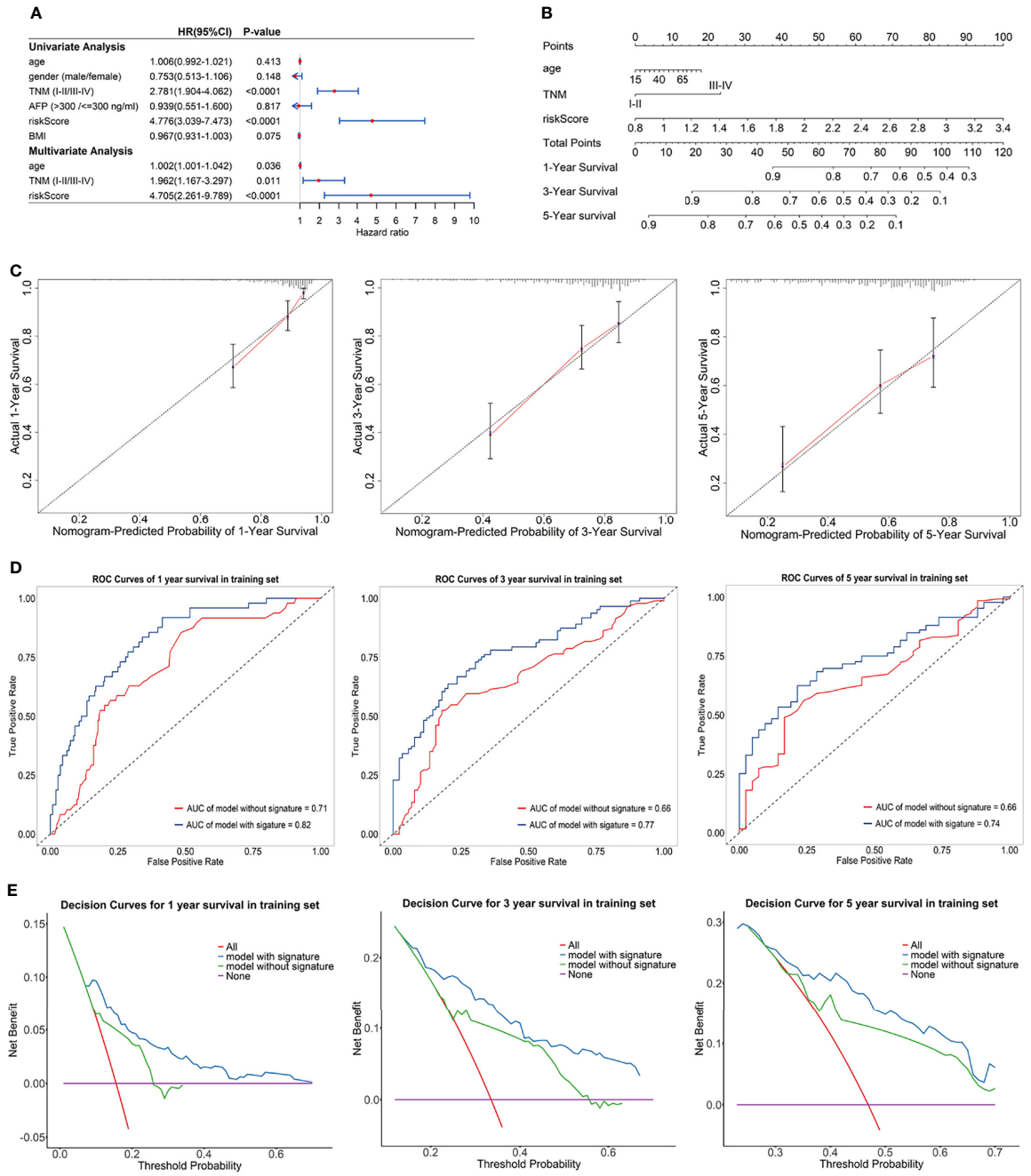

FIGURE 5 | **(A)** Forest plot for univariate Cox regression analysis and multivariate Cox regression analysis; **(B)** Nomogram predicting 1-, 3-, 5-year survival probability; **(C)** Calibration curves of the nomogram for 1-, 3-, 5-year overall survival in training set; **(D)** Time-dependent ROC curves of the nomogram for 1-, 3-, 5-year overall survival in training set; **(E)** DCA curves of the nomogram for 1-, 3-, 5-year overall survival in training set.

which suggested that patients in the low-risk group may be more sensitive to Sorafenib (**Figure 8B**).

We downloaded a list of 318 TFs from Cistrome and identified 14 TFs related to the genes in prognostic signature (**Supplementary Table S5**). The network diagram of the correlation between TFs and genes is shown in **Figure 8C**, and SSRP1, SSB, NUP205, and RDH16 have more co-expressed TFs with positive correlations. Furthermore, we also compared the differences of DNA damage repair related genes (PMS2, EPVAM, MLH1, and MSH2) between the high-risk group and low-risk

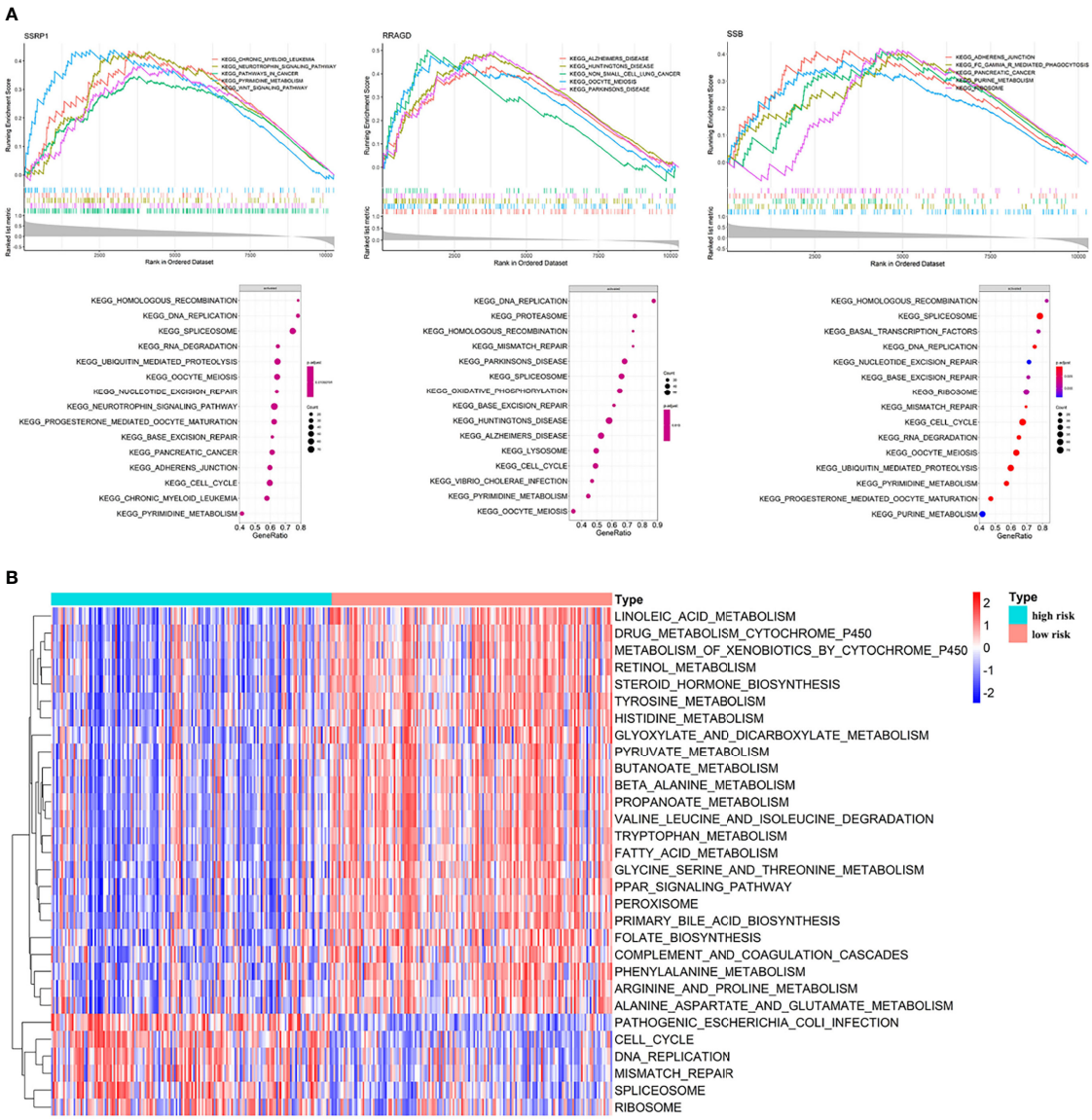

FIGURE 6 | Enrichment analyses. **(A)** Single gene GSEA results; **(B)** GSVA results: different pathways between high risk patients and low risk patients.

group, and the expressions of these genes were all significantly higher in the high-risk group than low-risk group (**Figure 8D**).

3.6 Experimental Confirmation of AKR1C3 *In Vitro* on Two HCC Cell Lines

We utilized the UCSC Genome Browser (http://genome.ucsc.edu/index.html) visualized the location of AKR1C3 and relative enhancers (**Figure 9A**). The AKR1C3 located on chromosome 10:5094414-5107686, and the enhancers associated with AKR1C3 located on chromosome 10:5060919-5067935. After transfection with AKR1C3-specific siRNA in Huh7 and MHCC-LM3 cell lines, both of the two selected siRNAs could significantly decrease AKR1C3 expression compared with control cells according to the western blot analysis (**Figure 9B**). EdU staining and colony formation assays were applied to assess the effect of si-AKR1C3-transfection on proliferation. The results indicated that compared with the control (si-NC), the si-AKR1C3 significantly reduced cell viability (**Figure 9C**) and the number of colony formations (**Figure 9D**). We further explored the effects of AKR1C3 on migration and invasion capacity of Huh7 and MHCC-LM3 cells *via* Transwell chamber assays. The migration and invasion abilities were significantly inhibited in si-AKR1C3-1 and si-AKR1C3-2 groups compared to the si-NC group (**Figures 9E, F**). Consistently, the wound healing assay revealed that the si-NC group

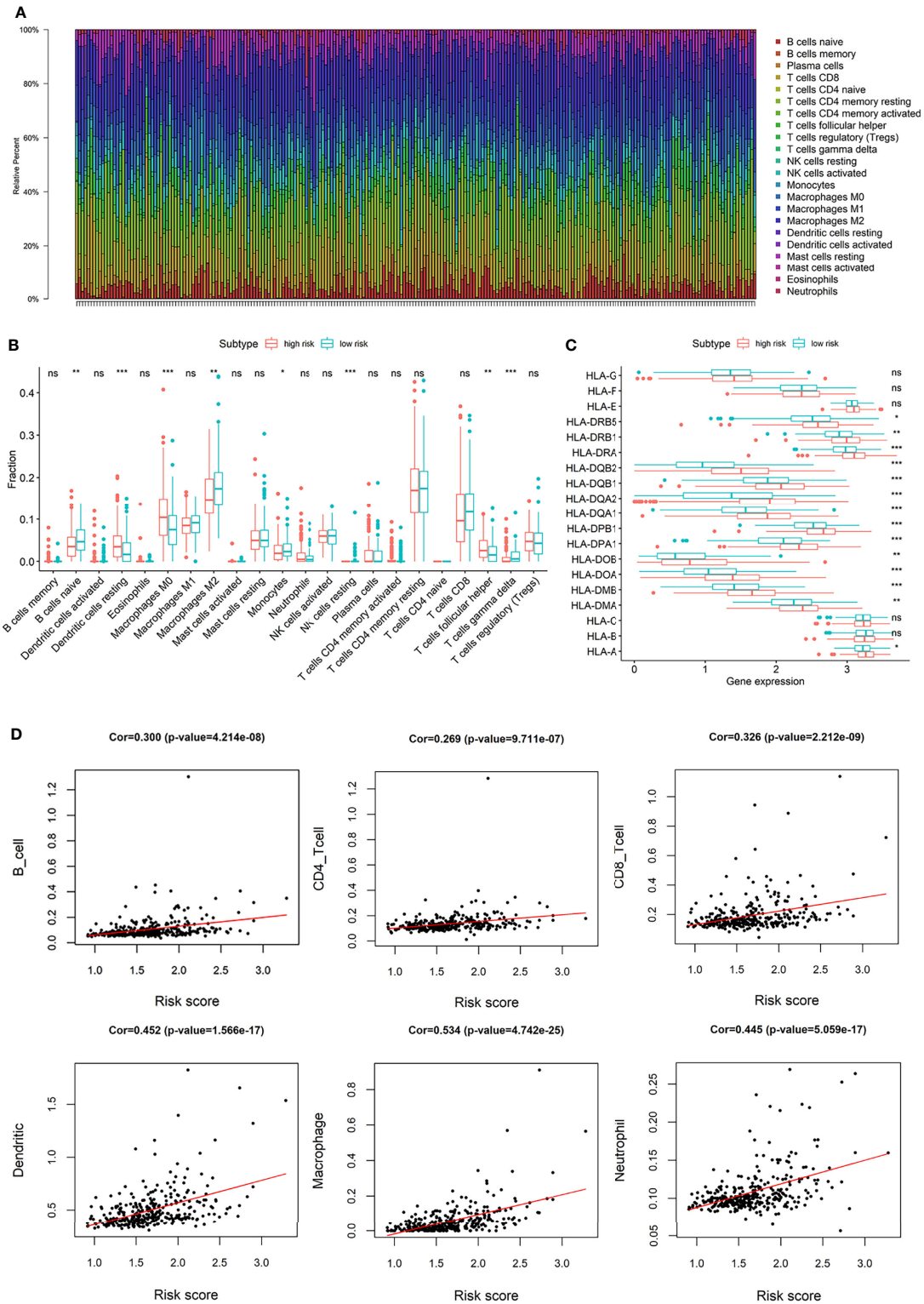

FIGURE 7 | **(A)** The composition of immune infiltrating cells in TCGA-LIHC patients; **(B)** Differences of immune infiltration cells between high and low risk group; **(C)** Differences of HLA-related genes between high and low risk group; **(D)** The correlation between risk score and the abundances of B cells, CD4+ T cells, CD8+ T cells, macrophages, neutrophils, and dendritic cells. (*p < 0.05; **p < 0.01; ***p < 0.001; "ns" means "no significant difference").

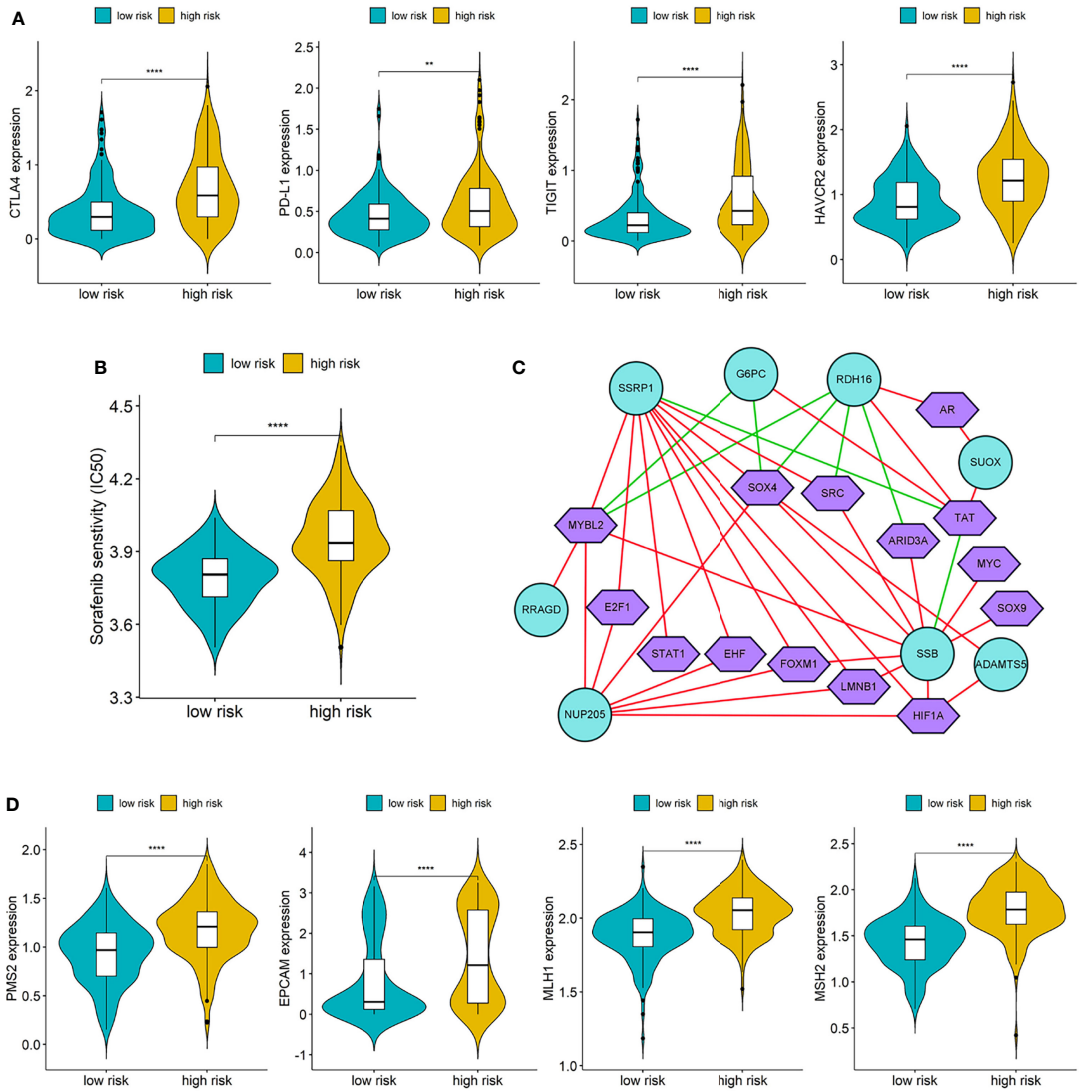

FIGURE 8 | **(A)** Differences of immune checkpoints between high risk group and low risk group; **(B)** Difference of Sorafenib sensitivity (IC50) between high risk and low risk patients; **(C)** The network diagram of the correlation between TFs and genes in the prognostic signature. Green circles represent genes in the signature and purple polygons represent TFs. The red lines indicate positive correlation and the green lines indicate negative correlation; **(D)** Differences of DNA damage repair related genes between high and low risk group. (**p < 0.01; ****p < 0.0001).

had a higher efficiency at closing the wound width than those in the AKR1C3 silencing group (**Figure 9G**). AKR1C3 overexpression promoted and silencing inhibited protein expression (**Figure 10A**) and cell proliferation (**Figure 10B**). In comparison with the control group and sorafenib groups, the si-AKR1C3-1 plus sorafenib groups showed significantly decreased cell proliferation rate, then it is of note that the AKR1C3 plus sorafenib groups further enhanced cell proliferation rate compared with the sorafenib groups (**Figure 10C**). Altogether, these experimental results suggested that the knockdown of AKR1C3 inhibited the cell proliferation, migration, and invasion in HCC cell lines, which indicated that AKR1C3 plays a key role in HCC cell proliferation and aggressiveness.

4 DISCUSSION

Enhancer RNAs (eRNAs) regulate the expression of oncogenes or tumor suppressors and play a prominent role in the tumorigenesis, progression, and proliferation of cancers, which could be used as potential and valuable diagnostic, prognostic, and therapeutic markers for cancers. Considering this, we attempted to establish a novel and robust signature based on eRGs to provide a new perspective for prognostic prediction and optimization of personalized treatment in HCC patients for the first time.

In this study, we identified a signature including 10 survival-related eRGs (SSRP1, SSB, IGFBP4, SUOX, RDH16, G6PC,

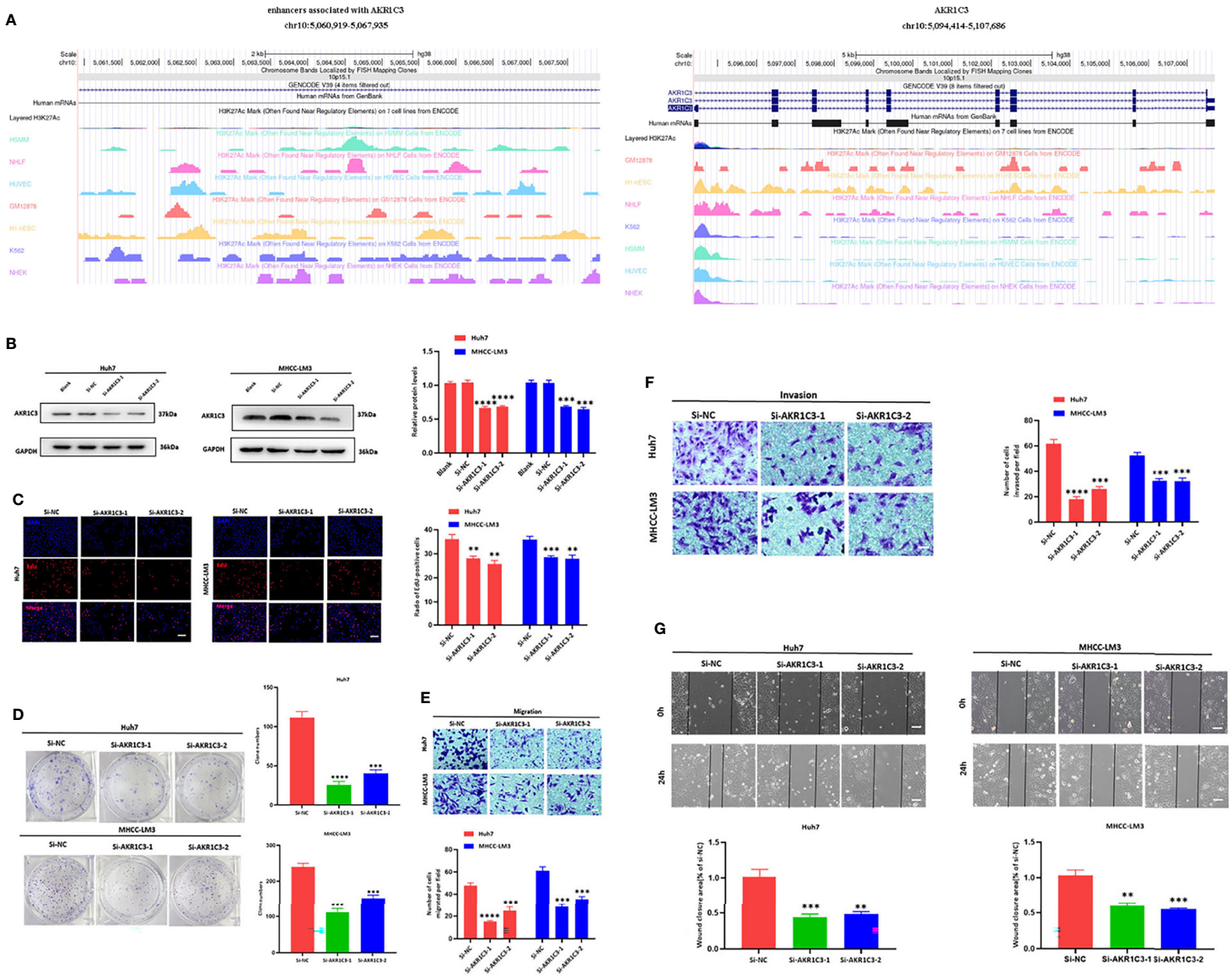

FIGURE 9 | **(A)** The locations of AKR1C3 and enhancers associated with AKR1C3 on chromosome. **(B)** Western blot analysis to examine the efficiency of the AKR1C3 knockdown. **(C)** Proliferation ability in AKR1C3 knockdown Huh7 and MHCC-LM3 cells by EdU staining. **(D)** Colony-forming abilities in AKR1C3 knockdown Huh7 and MHCC-LM3 cells by clonogenic assays. **(E, F)** Transwell assays to detect the migration and invasive capacities in AKR1C3 knockdown Huh7 and MHCC-LM3 cells. **(G)** Wound-healing assay was performed to measure the migration ability of various cells as indicated. Magnification, × 200 **(C, E, F)**, × 40 **(G)**. Scale bar, 100 mm **(C, E, F)**, 500 mm **(G)**. Data were shown as mean ± SD of at least three independent experiments. (**p < 0.01; ***p < 0.001; ****p < 0.0001).

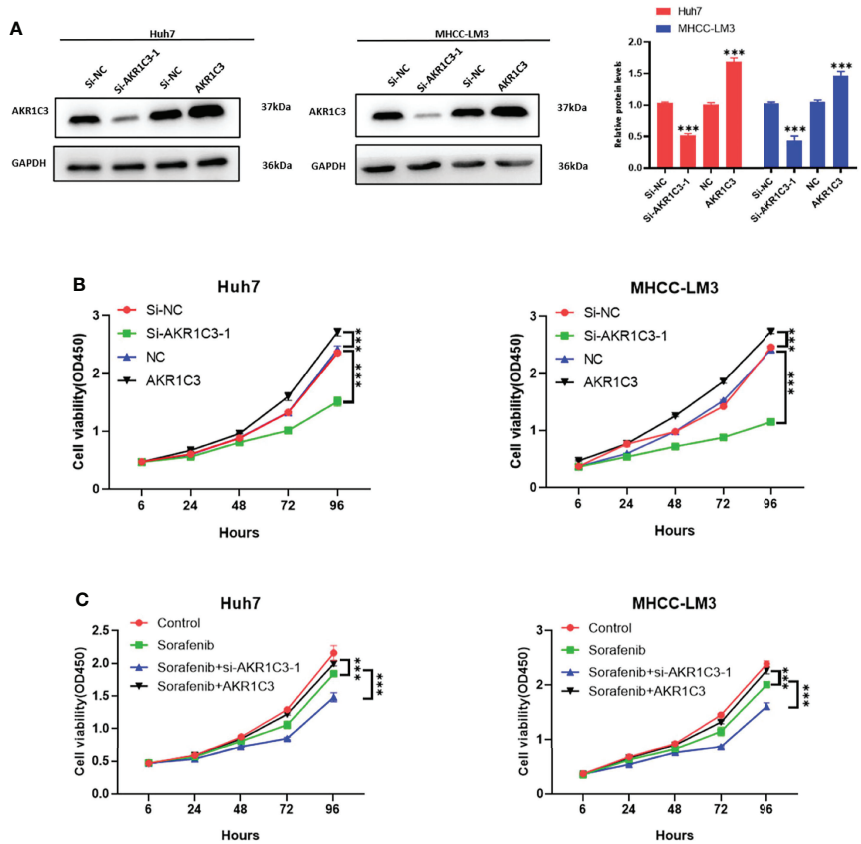

FIGURE 10 | **(A)** Western blot analysis to examine the efficiency of the AKR1C3 knockdown and overexpression. **(B, C)** Proliferation curves were determined in AKR1C3 knockdown and overexpression Huh7 and MHCC-LM3 cells by cell counting kit-8 (CCK-8) assays in normal culture conditions and sorafenib sensitivity experiment. Data were shown as mean ± SD of at least three independent experiments. (***p < 0.001).

AKR1C3, NUP205, ADAMTS5, and RRAGD). The signature stratified HCC patients into high- and low-risk groups, and patients in the high-risk group significantly tended to have a poorer prognosis. Previous studies have already constructed different signatures for predicting the overall survival in HCC patients (41–43). The comparison of the AUCs for 1-, 3-, 5-year overall survival of our eRGs signature and those of previous signatures were presented in **Table 1**. Obviously, our signature has a better prognostic value than others, especially in external validation dataset, which indicates that our signature is more robust. Furthermore, we found that the signature was an independent prognostic factor, which can combine age and TNM stage to establish a nomogram. The calibration curves of the nomogram indicated that the predicted outcomes were in good agreement with the actual outcomes in training set and validation set. Furthermore, time-dependent ROC curves exhibited that the sensitivity and specificity of model with signature were significantly improve compared with those of

TABLE 1 | Comparison of AUCs for prognostic signatures in different studies.

	Our study	Zhang et al. (2020) (41)	Li et al. (2017) (42)	Zhang et al. (2020) (43)
Signature	10-genes	14-genes	3-genes	8-genes
Training set	TCGA (n = 324)	TCGA (n = 312)	TCGA (n = 360)	TCGA (n = 361)
1-year AUC	0.79	0.71	0.73	0.77
3-year AUC	0.73	0.74	0.71	0.75
5-year AUC	0.68	0.64	0.69	0.75
Validation set	GSE14520 (n = 219)	GSE14520 (n = 225)	GSE14520 (n = 209)	GSE14520 (n = 221)
1-year AUC	0.71	0.64	0.65	0.66
3-year AUC	0.73	0.59	0.62	0.66
5-year AUC	0.67	0.65	0.62	0.67

the model with signature. According to the nomogram, clinicians can predict the prognosis of HCC patients and provide appropriate individualized treatment to improve their quality of life.

Genes in the signature and their corresponding eRNAs were all significantly correlated. Among them, ENSR00000052553 is the cancer-type-specific eRNA of HCC, which regulates the expression of SUOX and RDH16, and can be considered as a potential target eRNA for further treatment studies of HCC. In addition, G6PC, AKR1C3, and ADAMTS5 were all regulated by two neighbor eRNAs, which indicated that the enhancers at those locations may cluster into super-enhancers. Studies have already demonstrated that super-enhancers play a significant role in oncogene activation, process of tumorigenesis, and tumor cell proliferation (23–25), so our findings may lay the groundwork for investigating the mechanism of super enhancers in HCC.

Compared with the low-risk group, four genes (IGFBP4, SUOX, RDH16, and G6PC) of the prognostic signature downregulated in the high-risk group, while the other six genes (SSRP1, SSB, NUP205, AKR1C3, ADAMTS5, and RRAGD) upregulated conversely. IGFBP4 is the smallest member of human insulin-like growth factors binding proteins (IGFBPs) (44), which is involved in the inhibition of oncogenic pathways and exerts a powerful tumor suppressor function in HCC cells. It also had been demonstrated that low expression of IGFBP4 is associated with poor prognosis in HCC patients (45). SUOX was found to decrease with the progression of HCC and considered as an independent prognostic factor for overall survival and time to recurrence in HCC patients (46). RDH16 is a tumor-suppressing gene, and it had been reported that downregulation of RDH16 occurs in approximately 90% of primary HCC patients with poor prognosis (47). In addition, RDH16 was also contained in a robust twelve-gene signature for predicting survival of HCC patients (48). The deficiency of G6PC can cause glycogen storage disease type Ia (GSD-Ia), which may lead to HCC (49). A previous study has identified G6PC as a potential prognostic target in clear cell renal cell carcinoma, and its low expression associated with poor survival and aggressive progression (50). SSRP1 can regulate the proliferation and metastasis of HCC, its aberrant overexpression is related to higher serum AFP level, larger tumor size, and higher T stage of HCC patients. It has been considered as a prognostic biomarker associated with CD8+ T cell infiltration in HCC, and patients with higher expression of SSRP1 have shorter overall survival and faster recurrence (51, 52). SSB plays a significant role in DNA replication (53), its overexpression may promote the proliferation of HCC cells. Xiong et al. suggested that the upregulation of NUP205 correlated with severe TNM stage and poor survival, which demonstrated that it can be seen as a biomarker for prognostic prediction in HCC patients (54). It was found that higher ADAMTS5 expression had a significant association with development and poorer survival of HCC, and its impact on prognosis was specific for HCC among other cancer types from TCGA project (55). Furthermore, ADAMTS5 was also identified as a prominent gene in a hypoxia-related and immune-associated prognosis signature for HCC (56). RRAGD can promote cell proliferation, invasion, migration, aerobic glycolysis, and Warburg effect (an important characteristic of cancer cell metabolism) of HCC. Upregulation of RRAGD is associated with poor prognosis (57).

AKR1C3 consisted of 323 amino acids with a predicted molecular weight of 36,853 Da Like other AKR enzymes it is a soluble monomeric NAD(P)(H) dependent oxidoreductase, the enzyme that converts carbonyl groups into secondary alcohols (58). Overexpression of AKR1C3 is usually associated with prostate cancer progression, aggressiveness, and resistance to AR-targeted therapies (59). According to a previous clinical study, upregulation of AKR1C3 is an indicator of poor prognosis in HPV16-associated and HPV-negative oropharyngeal squamous cell carcinoma (OPSCC) (60). The results from our bioinformatics analysis were confirmed by a series of experiments, and we found that the silence of AKR1C3 in Huh7 and MHCC-LM3 cells can significantly inhibit HCC cell viability, clone formation, migration, invasion ability, and wound closure potential. In addition, AKR1C3 may be regulated by super-enhancers based on our study. All the above indicated that AKR1C3 is an important eRG related to the progression and prognosis of HCC, which may be a potential biomarker for HCC treatment and intervention.

The enrichment results presented that survival-related eRGs were enriched in ATPase activity, lipid transporter activity, steroid hormone biosynthesis, and ABC transporters, etc. GSVA identified a number of significant pathways that may affect prognostic outcomes of HCC patients. The downregulation of fatty acid metabolism, drug metabolism cytochrome P450, steroid hormone biosynthesis, primary bile acid biosynthesis, complement and coagulation cascades, PPAR signaling pathway, and the upregulation of cell cycle, DNA replication may be the mechanism for poorer prognosis of HCC. Therefore, our enrichment results provide new insights into the deeper investigation of molecular mechanisms and the development of targeted drugs for HCC patients.

Immune microenvironment plays an important role in the occurrence and development of tumors, which has attracted attentions of researchers. According to our results, immune infiltration and HLA may be considered important factors in exploring the specific mechanism and improving the outcomes of HCC patients. Immune checkpoints have received a great deal of attention in cancer treatment in recent years. We checked the differences of expression of immune checkpoints (CTLA4, PD-L1, TIGIT, and HAVCR2) between the high-risk group and low-risk group, and found that they all had higher expression in the high-risk group, which was in line with previous study (61).

Although Sorafenib is the standard systemic therapeutic agent available in HCC patients, the mechanism of drug resistance and the existence of heterogeneity make patients have different drug treatment effects. So, we estimated IC50 of Sorafenib in the two groups and found that the low-risk patients performed better to Sorafenib, which may contribute to the efficient and rational medication of HCC patients. Co-expression analysis of genes and TFs showed that SSRP1 and SSB, NUP205 had positive correlations with their co-expression TFs, while G6PC and RDH16 were negatively correlated with their co-expression

TFs. Meanwhile, expression of SSRP1, SSB, and NUP205 were all positively correlated with risk score, and expression of G6PC and RDH16 were negatively correlated with risk score. These findings suggested that eRNAs may bind to these TFs to regulate the expression of genes in the prognostic signature, which seemed to shed light on the investigation of HCC pathological mechanism and therapeutic targets.

Taken together, some advantages of our study deserve to be underscored. First, we constructed prognostic signature and nomogram for HCC based on eRGs for the first time, and the model performed a better predictive ability and provided a novel direction for the underlying pathological mechanism of HCC. Second, we identified survival-related eRNAs directly in HCC patients rather than select them from differential expressed eRNAs between patients and normal controls, so that more comprehensive information can be considered. Third, signature composed of specific genes is more economical and practical than whole-genome sequencing, and easy to routinely test. Fourth, the visualization of the nomogram is more convenient to assist clinicians in predicting patients' prognosis and customizing individualized treatment plans. Last but not least, we confirmed the role of AKR1C3 in the progression and invasion of HCC through a series of *in vitro* experiments. Nonetheless, some limitations still exist in this study. Firstly, the external validation set was also from a public database, and a multicenter cohort study is needed to further prove the generalizability of the models. Secondly, only one eRG in the signature was experimentally verified in the present study, and other eRGs should be validated in the future studies. Thirdly, the regulatory relationships between eRNAs and their target genes from the eRic database used in our study were generated based on data-driven correlations, and their biological regulatory relationships need to be confirmed by rigorous experiments. Finally, multi-omics data such as methylation, long non-coding RNA, and proteomics should be integrated and analyzed to comprehensively elucidate biological regulatory networks.

5 CONCLUSION

Our study has been the first attempt to identify a prognostic signature composed of eRGs for HCC. We also constructed a nomogram incorporating the signature and clinical characteristics to predict overall survival of HCC patients accurately and robustly, which has been validated in external dataset. The signature and nomogram both performed good prognostic ability. AKR1C3 may be a potential biomarker for HCC treatment and intervention through a series of *in vitro* experiments. The findings of this study have significant practical implications in terms of providing a deeper insight into the investigation of pathogenesis of HCC, optimizing individualized treatment, and improving the prognosis of HCC patients.

DATA AVAILABILITY STATEMENT

The datasets presented in this study can be found in online repositories. The names of the repository/repositories and accession number(s) can be found below: The Cancer Genome Atlas (TCGA) (https://portal.gdc.cancer.gov/); enhancer RNA in cancers (eRic) (https://hanlab.uth.edu/eRic/); Gene Expression Omnibus, GSE14520 -GPL3921.

AUTHOR CONTRIBUTIONS

Conceptualization, WZ and WT; methodology, WZ and KC; software, WZ; validation, QiZ; formal analysis, WZ and WT; investigation, LS and YW; resources, KC; data curation, WZ and KC; writing—original draft preparation, WZ and KC; writing—review and editing, QiuZ; visualization, WZ; supervision, QiuZ; project administration, LS and YW; funding acquisition, ML. All authors have read and agreed to the published version of the manuscript.

FUNDING

This work was supported by the National Science and Technology Major Project (2016ZX08011005), the National Natural Science Foundation of China (82073666), and the National Natural Science Foundation of China (82003556).

ACKNOWLEDGMENTS

We are very grateful to the staff who provided TCGA, GEO database and other online resources for providing us with a research foundation.

SUPPLEMENTARY MATERIAL

The Supplementary Material for this article can be found online at: https://www.frontiersin.org/articles/10.3389/fonc.2022.849242/full#supplementary-material

REFERENCES

1. Sung H, Ferlay J, Siegel RL, Laversanne M, Soerjomataram I, Jemal A, et al. Global Cancer Statistics 2020: GLOBOCAN Estimates of Incidence and Mortality Worldwide for 36 Cancers in 185 Countries. *CA: Cancer J Clin* (2021) 71(3):209–49. doi: 10.3322/caac.21660
2. Singal AG, Elserag HB. Hepatocellular Carcinoma From Epidemiology to Prevention: Translating Knowledge Into Practice. *Clin Gastroenterol Hepatol* (2015) 13:2140–51. doi: 10.1016/j.cgh.2015.08.014
3. Rastogi A. Changing Role of Histopathology in the Diagnosis and Management of Hepatocellular Carcinoma. *World J Gastroenterol* (2018) 24(35):4000–13. doi: 10.3748/wjg.v24.i35.4000

4. Llovet J, Brú C, Bruix J. Prognosis of Hepatocellular Carcinoma: The BCLC Staging Classification. *Semin Liv Dis* (1999) 19(3):329-38. doi: 10.1055/s-2007-1007122
5. Yau T, Tang VY, Yao TJ, Fan ST, Lo CM, Poon RT. Development of Hong Kong Liver Cancer Staging System With Treatment Stratification for Patients With Hepatocellular Carcinoma. *Gastroenterology* (2014) 146(7):16917–700.e3. doi: 10.1053/j.gastro.2014.02.032
6. Li L, Wang H. Heterogeneity of Liver Cancer and Personalized Therapy. *Cancer Lett* (2016) 379(2):191–7. doi: 10.1016/j.canlet.2015.07.018
7. Yang JD, Roberts LR. Epidemiology and Management of Hepatocellular Carcinoma. *Infect Dis Clin North Am* (2010) 24:899–919. doi: 10.1016/j.idc.2010.07.004
8. Pan HW, Ou YH, Peng SY, Liu SH, Lai PL, Lee PH, et al. Overexpression of Osteopontin Is Associated With Intrahepatic Metastasis, Early Recurrence, and Poorer Prognosis of Surgically Resected Hepatocellular Carcinoma. *Cancer* (2003) 98(1):119–27. doi: 10.1002/cncr.11487
9. Giordano S, Columbano A. Met as a Therapeutic Target in HCC: Facts and Hopes. *J Hepatol* (2014) 60:442–52. doi: 10.1016/j.jhep.2013.09.009
10. Toyoda H, Kumada T, Kiriyama S, Sone Y, Tanikawa M, Hisanaga Y, et al. Prognostic Significance of Simultaneous Measurement of Three Tumor Markers in Patients With Hepatocellular Carcinoma. *Clin Gastroenterol Hepatol* (2006) 4(1):111–7. doi: 10.1016/S1542-3565(05)00855-4
11. He Q, Lin Z, Wang Z, Huang W, Tian D, Liu M, et al. SIX4 Promotes Hepatocellular Carcinoma Metastasis Through Upregulating YAP1 and C-MET. *Oncogene* (2020) 39(50):7279–95. doi: 10.1038/s41388-020-01500-y
12. Huang W, Yu D, Wang M, Han Y, Lin J, Wei D, et al. ITGBL1 Promotes Cell Migration and Invasion Through Stimulating the TGF-β Signalling Pathway in Hepatocellular Carcinoma. *Cell Prolif* (2020) 53(7):e12836. doi: 10.1111/cpr.12836
13. Hong X, Luo H, Zhu G, Guan X, Jia Y, Yu H, et al. SSR2 Overexpression Associates With Tumorigenesis and Metastasis of Hepatocellular Carcinoma Through Modulating EMT. *J Cancer* (2020) 11(19):5578–87. doi: 10.7150/jca.44788
14. Wang TH, Yu CC, Lin YS, Chen TC, Yeh CT, Liang KH, et al. Long Noncoding RNA CPS1-IT1 Suppresses the Metastasis of Hepatocellular Carcinoma by Regulating HIF-1α Activity and Inhibiting Epithelial-Mesenchymal Transition. *Oncotarget* (2016) 7(28):43588–603. doi: 10.18632/oncotarget.9635
15. Zhang Z, Weng W, Huang W, Wu B, Zhou Y, Zhang J, et al. A Novel Molecular-Clinicopathologic Nomogram to Improve Prognosis Prediction of Hepatocellular Carcinoma. *Aging* (2020) 12(13):12896–920. doi: 10.18632/aging.103350
16. Liu GM, Xie WX, Zhang CY, Xu JW. Identification of a Four-Gene Metabolic Signature Predicting Overall Survival for Hepatocellular Carcinoma. *J Cell Physiol* (2020) 235:1624–36. doi: 10.1002/jcp.29081
17. Zhao QJ, Zhang J, Xu L, Liu FF. Identification of a Five-Long Non-Coding RNA Signature to Improve the Prognosis Prediction for Patients With Hepatocellular Carcinoma. *World J Gastroenterol* (2018) 24:3426–39. doi: 10.3748/wjg.v24.i30.3426
18. Kim TK, Hemberg M, Gray JM, Costa AM, Bear DM, Wu J, et al. Widespread Transcription at Neuronal Activity-Regulated Enhancers. *Nature* (2010) 465(7295):182–7. doi: 10.1038/nature09033
19. Li W, Notani D, Rosenfeld MG. Enhancers as Non-Coding RNA Transcription Units: Recent Insights and Future Perspectives. *Nat Rev Genet* (2016) 17:207–7. doi: 10.1038/nrg.2016.4
20. Li W, Hu Y, Oh S, Ma Q, Merkurjev D, Song X, et al. Condensin I and II Complexes License Full Estrogen Receptor α-Dependent Enhancer Activation. *Mol Cell* (2015) 59(2):188–202. doi: 10.1016/j.molcel.2015.06.002
21. Hsieh CL, Fei T, Chen Y, Li T, Gao Y, Wang X, et al. Enhancer RNAs Participate in Androgen Receptor-Driven Looping That Selectively Enhances Gene Activation. *Proc Natl Acad Sci USA* (2014) 111(20):7319–24. doi: 10.1073/pnas.1324151111
22. Melo CA, Drost J, Wijchers PJ, van de Werken H, de Wit E, Oude Vrielink JA, et al. eRNAs Are Required for P53-Dependent Enhancer Activity and Gene Transcription. *Mol Cell* (2013) 49(3):524–35. doi: 10.1016/j.molcel.2012.11.021
23. Lee JH, Xiong F, Li W. Enhancer RNAs in Cancer: Regulation, Mechanisms and Therapeutic Potential. *RNA Biol* (2020) 17:1550–9. doi: 10.1080/15476286.2020.1712895
24. Hnisz D, Schuijers J, Lin CY, Weintraub AS, Abraham BJ, Lee TI, et al. Convergence of Developmental and Oncogenic Signaling Pathways at Transcriptional Super-Enhancers. *Mol Cell* (2015) 58(2):362–70. doi: 10.1016/j.molcel.2015.02.014
25. Lovén J, Hoke HA, Lin CY, Lau A, Orlando DA, Vakoc CR, et al. Selective Inhibition of Tumor Oncogenes by Disruption of Super-Enhancers. *Cell* (2013) 153(2):320–34. doi: 10.1016/j.cell.2013.03.036
26. Andersson R, Gebhard C, Miguel-Escalada I, Hoof I, Bornholdt J, Boyd M, et al. An Atlas of Active Enhancers Across Human Cell Types and Tissues. *Nature* (2014) 507(7493):455–61. doi: 10.1038/nature12787
27. ENCODE Project Consortium. An Integrated Encyclopedia of DNA Elements in the Human Genome. *Nature* (2012) 489(7414):57–74. doi: 10.1038/nature11247
28. Bernstein BE, Stamatoyannopoulos JA, Costello JF, Ren B, Milosavljevic A, Meissner A, et al. The NIH Roadmap Epigenomics Mapping Consortium. *Nat Biotechnol* (2010) 28(10):1045–8. doi: 10.1038/nbt1010-1045
29. Zhang Z, Lee JH, Ruan H, Ye Y, Krakowiak J, Hu Q, et al. Transcriptional Landscape and Clinical Utility of Enhancer RNAs for eRNA-Targeted Therapy in Cancer. *Nat Commun* (2019) 10(1):4562. doi: 10.1038/s41467-019-12543-5
30. Grimes DA. The Nomogram Epidemic: Resurgence of a Medical Relic. *Ann Internal Med* (2008) 149:273–5. doi: 10.7326/0003-4819-149-4-200808190-00010
31. Balachandran VP, Gonen M, Smith JJ, DeMatteo RP. Nomograms in Oncology: More Than Meets the Eye. *Lancet Oncol* (2015) 16:e173–80. doi: 10.1016/s1470-2045(14)71116-7
32. Subramanian A, Tamayo P, Mootha VK, Mukherjee S, Ebert BL, Gillette MA, et al. Gene Set Enrichment Analysis: A Knowledge-Based Approach for Interpreting Genome-Wide Expression Profiles. *Proc Natl Acad Sci USA* (2005) 102(43):15545–50. doi: 10.1073/pnas.0506580102
33. Hnzelmann S, Castelo R, Guinney J. GSVA: Gene Set Variation Analysis for Microarray and RNA-Seq Data. *BMC Bioinf* (2013) 14:7–7. doi: 10.1186/1471-2105-14-7
34. Liu X, Qin S. Immune Checkpoint Inhibitors in Hepatocellular Carcinoma: Opportunities and Challenges. *Oncology* (2019) 24:S3. doi: 10.1634/theoncologist.2019-IO-S1-s01
35. Newman AM, Liu CL, Green MR, Gentles AJ, Feng W, Xu Y, et al. Robust Enumeration of Cell Subsets From Tissue Expression Profiles. *Nat Methods* (2015) 12(5):453–7. doi: 10.1038/nmeth.3337
36. Li T, Fan J, Wang B, Traugh N, Chen Q, Liu JS, et al. TIMER: A Web Server for Comprehensive Analysis of Tumor-Infiltrating Immune Cells. *Cancer Res* (2017) 77(21):e108–e110. doi: 10.1158/0008-5472.CAN-17-0307
37. Aykul S, Martinez-Hackert E. Determination of Half-Maximal Inhibitory Concentration Using Biosensor-Based Protein Interaction Analysis. *Analytic Biochem* (2016) 508:97–103. doi: 10.1016/j.ab.2016.06.025
38. Llovet JM, Ricci S, Mazzaferro V, Hilgard P, Gane E, Blanc JF, et al. Sorafenib in Advanced Hepatocellular Carcinoma. *N Engl J Med* (2008) 359(4):378–90. doi: 10.1056/NEJMoa0708857
39. Geeleher P, Cox N, Huang RS. Prrophetic: An R Package for Prediction of Clinical Chemotherapeutic Response From Tumor Gene Expression Levels. *PloS One* (2014) 9(9):e107468. doi: 10.1371/journal.pone.0107468
40. Yang W, Soares J, Greninger P, Edelman EJ, Lightfoot H, Forbes S, et al. Genomics of Drug Sensitivity in Cancer (GDSC): A Resource for Therapeutic Biomarker Discovery in Cancer Cells. *Nucleic Acids Res* (2013) 41(Database issue):D955–61. doi: 10.1093/nar/gks1111
41. Zhang BH, Yang J, Jiang L, Lyu T, Kong LX, Tan YF, et al. Development and Validation of a 14-Gene Signature for Prognosis Prediction in Hepatocellular Carcinoma. *Genomics* (2020) 112(4):2763–71. doi: 10.1016/j.ygeno.2020.03.013
42. Li B, Feng W, Luo O, Xu T, Cao Y, Wu H, et al. Development and Validation of a Three-Gene Prognostic Signature for Patients With Hepatocellular Carcinoma. *Sci Rep* (2017) 7(1):5517. doi: 10.1038/s41598-017-04811-5
43. Zhang FP, Huang YP, Luo WX, Deng WY, Liu CQ, Xu LB, et al. Construction of a Risk Score Prognosis Model Based on Hepatocellular Carcinoma Microenvironment. *World J Gastroenterol* (2020) 26(2):134–53. doi: 10.3748/wjg.v26.i2.134
44. Chelius D, Baldwin MA, Lu X, Spencer EM. Expression, Purification and Characterization of the Structure and Disulfide Linkages of Insulin-Like

Growth Factor Binding Protein-4. *J Endocrinol* (2001) 168:283–96. doi: 10.1677/joe.0.1680283
45. Lee YY, Mok MT, Kang W, Yang W, Tang W, Wu F, et al. Loss of Tumor Suppressor IGFBP4 Drives Epigenetic Reprogramming in Hepatic Carcinogenesis. *Nucleic Acids Res* (2018) 46(17):8832–47. doi: 10.1093/nar/gky589
46. Jin GZ, Yu WL, Dong H, Zhou WP, Gu YJ, Yu H, et al. SUOX Is a Promising Diagnostic and Prognostic Biomarker for Hepatocellular Carcinoma. *J Hepatol* (2013) 59(3):510–7. doi: 10.1016/j.jhep.2013.04.028
47. Zhu YH, Li JB, Wu RY, Yu Y, Li X, Li ZL, et al. Clinical Significance and Function of RDH16 as a Tumor-Suppressing Gene in Hepatocellular Carcinoma. *Hepatol Res Off J Jap Soc Hepatol* (2020) 50(1):110–20. doi: 10.1111/hepr.13432
48. Ouyang G, Yi B, Pan G, Chen X. A Robust Twelve-Gene Signature for Prognosis Prediction of Hepatocellular Carcinoma. *Cancer Cell Int* (2020) 20:207. doi: 10.1186/s12935-020-01294-9
49. Cho JH, Lee YM, Bae SH, Chou JY. Activation of Tumor-Promoting Pathways Implicated in Hepatocellular Adenoma/Carcinoma, A Long-Term Complication of Glycogen Storage Disease Type Ia. *Biochem Biophys Res Commun* (2020) 522:1–7. doi: 10.1016/j.bbrc.2019.11.061
50. Xu WH, Xu Y, Tian X, Anwaier A, Liu WR, Wang J, et al. Large-Scale Transcriptome Profiles Reveal Robust 20-Signatures Metabolic Prediction Models and Novel Role of G6PC in Clear Cell Renal Cell Carcinoma. *J Cell Mol Med* (2020) 24(16):9012–27. doi: 10.1111/jcmm.15536
51. Luo G, Xu J, Xia Z, Liu S, Liu H, He K, et al. SSRP1 Is a Prognostic Biomarker Correlated With CD8(+) T Cell Infiltration in Hepatocellular Carcinoma (HCC). *BioMed Res Int* (2021) 2021:9409836. doi: 10.1155/2021/9409836
52. Ding Q, He K, Luo T, Deng Y, Wang H, Liu H, et al. SSRP1 Contributes to the Malignancy of Hepatocellular Carcinoma and Is Negatively Regulated by miR-497. *Mol Ther J Am Soc Gene Ther* (2016) 24(5):903–14. doi: 10.1038/mt.2016.9
53. Pandita RK, Chow TT, Udayakumar D, Bain AL, Cubeddu L, Hunt CR, et al. Single-Strand DNA-Binding Protein SSB1 Facilitates TERT Recruitment to Telomeres and Maintains Telomere G-Overhangs. *Cancer Res* (2015) 75 (5):858–69. doi: 10.1158/0008-5472.Can-14-2289
54. Xiong DD, Feng ZB, Lai ZF, Qin Y, Liu LM, Fu HX, et al. High Throughput circRNA Sequencing Analysis Reveals Novel Insights Into the Mechanism of Nitidine Chloride Against Hepatocellular Carcinoma. *Cell Death Dis* (2019) 10(9):658. doi: 10.1038/s41419-019-1890-9
55. Zhu Z, Xu J, Wu X, Lin S, Li L, Ye W, et al. *In Silico* Identification of Contradictory Role of ADAMTS5 in Hepatocellular Carcinoma. *Technol Cancer Res Treat* (2021) 20:1533033820986826. doi: 10.1177/1533033820986826
56. Hu B, Yang XB, Sang XT. Development and Verification of the Hypoxia-Related and Immune-Associated Prognosis Signature for Hepatocellular Carcinoma. *J Hepatocell Carcinom* (2020) 7:315–30. doi: 10.2147/jhc.S272109
57. Ding L, Liang X. Ras Related GTP Binding D Promotes Aerobic Glycolysis of Hepatocellular Carcinoma. *Ann Hepatol* (2021) 23:100307. doi: 10.1016/j.aohep.2021.100307
58. Jin Y, Penning TM. Aldo-Keto Reductases and Bioactivation/Detoxication. *Annu Rev Pharmacol Toxicol* (2007) 47:263–92. doi: 10.1146/annurev.pharmtox.47.120505.105337
59. Liu C, Yang JC, Armstrong CM, Lou W, Liu L, Qiu X, et al. AKR1C3 Promotes AR-V7 Protein Stabilization and Confers Resistance to AR-Targeted Therapies in Advanced Prostate Cancer. *Mol Cancer Ther* (2019) 18 (10):1875–86. doi: 10.1158/1535-7163.Mct-18-1322
60. Huebbers CU, Verhees F, Poluschkin L, Olthof NC, Kolligs J, Siefer OG, et al. Upregulation of AKR1C1 and AKR1C3 Expression in OPSCC With Integrated HPV16 and HPV-Negative Tumors Is an Indicator of Poor Prognosis. *Int J Cancer* (2019) 144(10):2465–77. doi: 10.1002/ijc.31954
61. Liu Z, Jiao D, Liu L, Zhou X, Yao Y, Li Z, et al. Development and Validation of a Robust Immune-Related Risk Signature for Hepatocellular Carcinoma. *Medicine* (2021) 100(10):e24683. doi: 10.1097/md.0000000000024683

Conflict of Interest: The authors declare that the research was conducted in the absence of any commercial or financial relationships that could be construed as a potential conflict of interest.

Publisher's Note: All claims expressed in this article are solely those of the authors and do not necessarily represent those of their affiliated organizations, or those of the publisher, the editors and the reviewers. Any product that may be evaluated in this article, or claim that may be made by its manufacturer, is not guaranteed or endorsed by the publisher.

frontiers | Frontiers in Oncology

REVIEW
published: 26 May 2022
doi: 10.3389/fonc.2022.826113

Three-Dimensional 3D Culture Models in Gynecological and Breast Cancer Research

*Yarely M. Salinas-Vera[1], Jesús Valdés[1], Yussel Pérez-Navarro[2], Gilberto Mandujano-Lazaro[3], Laurence A. Marchat[3], Rosalio Ramos-Payán[4], Stephanie I. Nuñez-Olvera[5], Carlos Pérez-Plascencia[6] and César López-Camarillo[2]**

[1] Departamento de Bioquímica, Centro de Investigación de Estudios Avanzados (CINVESTAV-IPN), Ciudad de Mexico, Mexico, [2] Posgrado en Ciencias Genómicas, Universidad Autónoma de la Ciudad de Mexico, Ciudad de Mexico, Mexico, [3] Programa en Biomedicina Molecular y Red de Biotecnología, Instituto Politécnico Nacional, Ciudad de Mexico, Mexico, [4] Facultad de Ciencias Químico Biológicas, Universidad Autónoma de Sinaloa, Culiacán Sinaloa, Mexico, [5] Departamento de Biología Celular y Fisiología, Instituto de Investigaciones Biomédicas, Universidad Nacional Autónoma de México, Ciudad de México, Mexico, [6] Laboratorio de Genómica, Instituto Nacional de Cancerología, Ciudad de México, Mexico

OPEN ACCESS

Edited by:
Elzbieta Pluciennik, Medical University of Lodz, Poland

Reviewed by:
Allen Thayakumar Basanthakumar, Dana–Farber Cancer Institute, United States
Giorgia Imparato, Center for Advanced Biomaterials for Healthcare (IIT), Italy

***Correspondence:**
César López-Camarillo
cesar.lopez@uacm.edu.mx
orcid.org/0000-0002-9417-2609

Specialty section:
This article was submitted to Cancer Genetics, a section of the journal Frontiers in Oncology

Received: *30 November 2021*
Accepted: *20 April 2022*
Published: *26 May 2022*

Citation:
Salinas-Vera YM, Valdés J, Pérez-Navarro Y, Mandujano-Lazaro G, Marchat LA, Ramos-Payán R, Nuñez-Olvera SI, Pérez-Plascencia C and López-Camarillo C (2022) Three-Dimensional 3D Culture Models in Gynecological and Breast Cancer Research. Front. Oncol. 12:826113. doi: 10.3389/fonc.2022.826113

Traditional two-dimensional (2D) monolayer cell cultures have long been the gold standard for cancer biology research. However, their ability to accurately reflect the molecular mechanisms of tumors occurring *in vivo* is limited. Recent development of three-dimensional (3D) cell culture models facilitate the possibility to better recapitulate several of the biological and molecular characteristics of tumors *in vivo*, such as cancer cells heterogeneity, cell-extracellular matrix interactions, development of a hypoxic microenvironment, signaling pathway activities depending on contacts with extracellular matrix, differential growth kinetics, more accurate drugs response, and specific gene expression and epigenetic patterns. In this review, we discuss the utilization of different types of 3D culture models including spheroids, organotypic models and patient-derived organoids in gynecologic cancers research, as well as its potential applications in oncological research mainly for screening drugs with major physiological and clinical relevance. Moreover, microRNAs regulation of cancer hallmarks in 3D cell cultures from different types of cancers is discussed.

Keywords: 3D cultures, breast cancer, gynecological cancers, microRNAs, therapy response

INTRODUCTION

Three-dimensional (3D) cell cultures are a breakthrough for gynecological and breast cancer research as they mimic the 3D architecture of primary tumors. For a long time, oncology research was based on 2D monolayer cultures, where cells grown on a flat solid surface. However, this culture model has limitations, such as the absence of cell-cell and cell- extracellular matrix (ECM) interactions, and tumor microenvironment, as well as unlimited access to nutrients, oxygen, and metabolites (1, 2). Additionally, cells cultured in 2D modify their morphology and cause cytoskeletal rearrangements, acquiring artificial polarity, which in turn leads to aberrant gene and protein expression (**Figure 1A**) (3, 4). On the other hand, 3D cultures promote cell-cell and cell-ECM interactions (5). This culture model better recapitulates the characteristics of tumor cells *in vivo*,

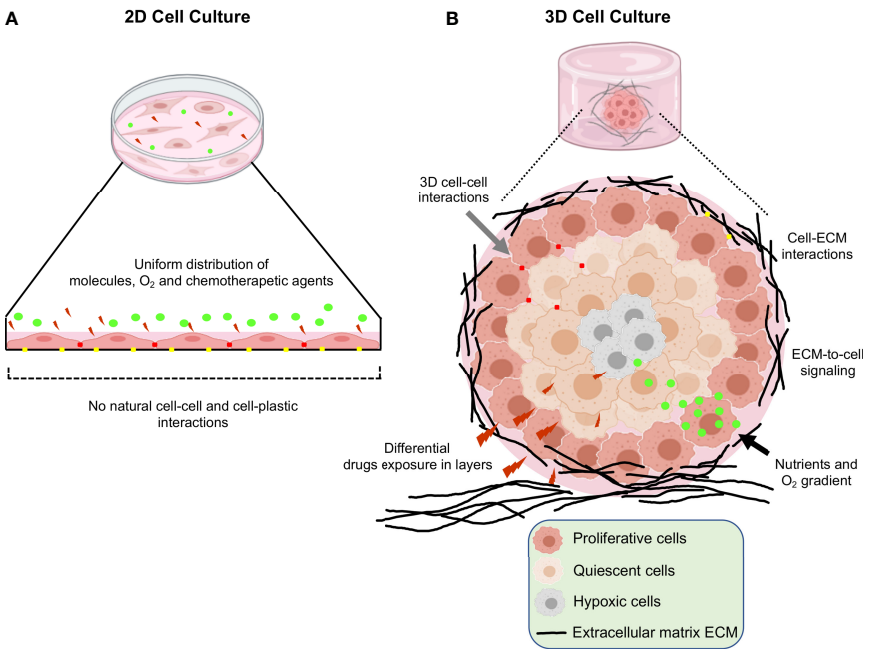

FIGURE 1 | Schematic representation of the main differences between 2D and 3D cell cultures. **(A)** Traditional 2D cell culture in which flattened cells grown in a monolayer at the bottom of plastic plates. Reduced cell-cell interactions, unlimited exposure to nutrients, oxygen and drugs are limitations of this type of cultures. **(B)** 3D cell culture systems; in which increased cell-cell and cell-extracellular matrix interactions, limited access to nutrients, oxygen, and heterogeneity in the drugs interactions leads to better recapitulation of the tumor microenvironment occurring *in vivo*.

such as cell heterogeneity, hypoxia, growth kinetics, signaling pathway activity and gene expression patterns (6, 7). Moreover, in 3D cultures the morphology and polarity of tumor cells are maintained, and a concentration gradient of O_2, nutrients and metabolic waste is generated, making them an ideal model to study tumor cells behavior (**Figure 1B**) (8, 9). Several reports showed the advantages of using 3D culture systems for gynecological cancer studies, as they allow the evaluation of the effect of the extracellular matrix on the tumor, reducing the existing breach between 3D culture models and *in vivo* models (**Table 1**).

The development of 3D cultures and its more generalized utilization have permitted the evaluation of changes in gene expression mechanisms relative to 2D conditions, mainly in mRNA transcriptomes. However, scarce data on postranscriptional control of gene expression represented by microRNAs (miRNAs) have been studied in 3D cancer cell cultures. MiRNAs are small non-coding RNAs of about 21-25 nucleotides in length that function as

TABLE 1 | Advantages and disadvantages of using 3D versus 2D culture.

Characteristic	2D	3D			Reference
		Spheroids	Organotypic	Organoid	
Support	Plastic, polycarbonate	Low-adherence plastic plates	Extracellular matrix *in vitro*	Extracellular matrix *in vitro*	(10, 11)
Duration of cultivation	long-term culture	Short-term culture	Short-term culture	Robust and stable in long-term culture	(12)
Interaction and communication	N/A	Cell-cell interactions	Cell-cell and cell-matrix 3D interactions	Cell-cell, cell-stroma and cell-matrix 3D interactions	(13)
Cell forms	Flat and extensible	Natural cellular structure preserved	Natural cellular structure preserved	Natural cellular structure preserved	(14)
Cell junctions	Less common	More common (cell-cell communication)	More common (cell-cell communication)	More common (cell-cell communication)	(2)
Maintain	Easy to maintain and passage	Easy to maintain	Easy to maintain	Difficult to maintain and expensive	(12)
Drug response	Cells more sensitive to treatment	Cells more sensitive to treatment	Cells less sensitive to treatment	Cells less sensitive to treatment	(6, 8)
Reproducibility	High reproducibility	High reproducibility	High reproducibility	Lack of reproducibility due to patient heterogeneity	(9)

negative regulators of gene expression at the post-transcriptional level (15). The miRNAs contain a seed region corresponding to 2-7 nucleotides, which binds by bases complementarity to conserved sites in the 3' untranslated regions (UTR) of target mRNAs, resulting in mRNA degradation or translation repression (16). Increasing evidence shows that miRNAs regulate diverse processes involved in cancer progression, such as, cell proliferation, apoptosis, invasion, metastasis, and drug resistance (17, 18). Due to their high stability, miRNAs are also being tested in clinical trials as therapeutic agents for treatment of oncological patients (19). The objective of this review is to address the 3D modeling systems in cancer research, as well as potential applications in gynecological and breast cancers, because they are main oncological diseases affecting the female population. Finally, the differential regulation of miRNAs in 3D cultured breast and gynecological cancer cells is addressed, in order to understand its biological functions and if they could be potential therapeutic targets.

TYPES OF 3D CULTURE SYSTEMS IN CANCER

Nowadays, 3D culture systems are divided into three categories: spheroids, organotypic cultures and organoid models. Spheroids are commonly referred to cultures in which cancer cell lines grown in low-adherence plastic plates or over inert substrates like agarose with continuous agitation, in which no ECM is utilized as substrates. In contrast, 3D organotypic cultures of cancer cell lines are *in vitro* systems in which the cells are cultured on commercial matrigel containing extracellular matrix proteins which provides a semi-solid support simulating some features of the *in vivo* tumor microenvironment such as cell-cell and cell-ECM interactions which activate cell signaling. On the other hand, the organoids which are generally *ex vivo* systems mainly patient-derived explants (PDE), are cultured on matrigel that simulate the extracellular matrix and facilitate drug testing in intact human tumors. In the next sections, we will discuss the different types of 3D culture systems.

Spheroids Models

Spheroids are cell aggregates that can be grown in suspension, for example on low-adhesion plastic plates or over inert substrates such as agarose with continuous agitation without the presence of matrigel (11). The suspension culture method was developed in 1970 by Sutherland and coworkers (20). They used an *in vitro* 3D model system to recreate the complexities of the multicellular tumor to study the response of tumor cells to radiotherapy. In this method, ultra-low attachment plates are used or standard plastic plates coated with inert substrates, for example, agar or poly-2-hydroxyethyl methacrylate (poly-HEMA), which prevents cells from adhering to the surface of the wells, forcing cells to aggregate and form spheroids (21). On the other hand, the system from spinner flasks consists of cells suspension and a shaker element that maintains continuous movement. The liquid flow not only prevents cell adhesion, but also ensures uniform distribution of nutrients and oxygen in cells. This method produces high yields of spheroids (22, 23) (**Figure 2A**).

Organotypic Cultures of Cancer Cell Lines

The 3D culture systems or organotypic models are generated by *in vitro* culturing cancer cell lines in a semisolid extracellular matrix under defined culture medium conditions (**Figure 2B**) (24, 25). They are an attractive model as they recapitulate the characteristics of tumor cells *in vivo* with respect to growth kinetics, cellular heterogeneity, signaling pathway activity. Additionally, it has been shown that gene expression in 3D cultures is much closer to clinical expression profiles than those observed in traditional 2D monolayer culture (6). Interestingly, organotypic cultures show diverse morphologies depending on the inherent nature of the cell and culture conditions, for example, in breast cancer three different morphologies have been observed depending on the molecular subtype of the cell line, such as mass, grape bunch and stellate (26). Moreover, to further understand cancer biology, they have developed 3D co-culture models in order to effectively model the influences of the tumor microenvironment on drug efficacy. Thus, organotypic models possess features more appropriate for high-throughput screening assays compared to 2D conditions (9) (**Figure 2B**).

Organoid Models

Organoids are 3D systems that have been established for cancer research as they recapitulate the genotype, phenotype and cellular behavior of parental tissues (27). These innovative cultures models can be developed from both induced pluripotent stem cells (iPSCs), and tumor tissues (28, 29). Organoids established from induced pluripotent stem cells (iPSCs) begins with the isolation and culture of malignant cells from a primary or metastatic tumor sample (30, 31) (**Figure 2C**). Subsequently, reprogramming is carried out through gene transfer of SOX2, KLF4, c-MYC, and OCT4 transcription factors by means of retroviruses or lentiviruses (32). These cells then differentiate into the cell type of origin of the initial tumor. Differentiated iPSC-derived cells can be used to derive organoids. However, iPSC-derived organoids have major disadvantages because their efficacy depends on the type of cancer and the presence or absence of oncogenic mutations potentially selecting for the growth of tumor subclones and the loss of genetic heterogeneity of the tumor from which they are derived (33). In general, it is more practical to grow tumor organoids directly from tumor tissue. On the other hand, cancer tissue-derived organoids are established from the collection of tumor tissue after biopsy and placed on a matrigel-coated surface where it is embedded within the matrigel (34) (**Figure 2C**). The main advantage of this system is the preservation of the original tumor tissue architecture, including cellular and non-cellular components of the tumor microenvironment and cell-cell interactions However, the main disadvantage is the lack of reproducibility due to tumor heterogeneity (9, 35).

3D CULTURES SYSTEMS IN GYNECOLOGICAL CANCERS

Traditional 2D cell cultures and animal models represent the experimental mainstay for gynecologic cancer research. However, their ability to reflect mechanisms occurring *in vivo* is limited. This

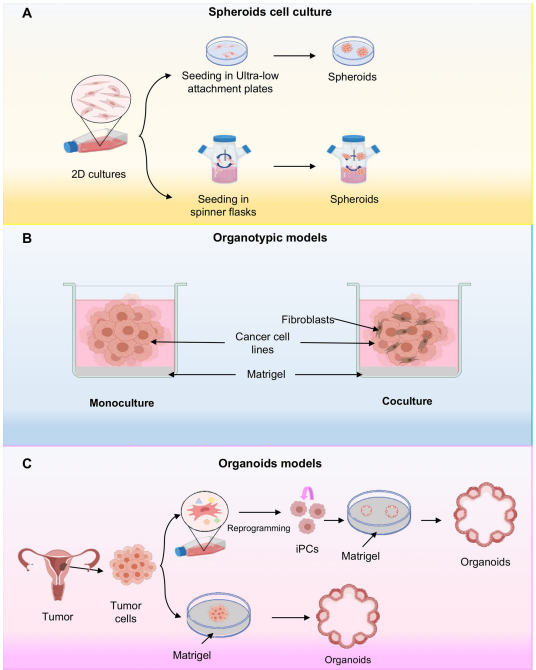

FIGURE 2 | Three-dimensional cell cultures. **(A)** Scheme representing the cellular spheroids grown in ultra-low attachment plates. In this system, cancer cells are deposited on an ultralow fixation plate that prevents sticking and allowing the grown of cells in suspension; or alternatively they are placed in spinning flasks and subjected to gravitational forces also inducing the spheroids formation. **(B)** Schematic representing organotypic models, where organotypic models have been generated in monoculture or in combination with fibroblasts cocultures. **(C)** Representative schematic of organoid establishment from pluripotent stem cells (iPSCs) and cancer cells. The iPSCs first undergo reprogramming, followed by directed differentiation, and are then seeded into an extracellular matrix in a specific culture medium to initiate organoid culture. The tumor tissue organoids were processed to remove excess fat and necrotic cells and cut into small pieces. They are then seeded on Matrigel.

is because the cellular models lack the tumor microenvironment and associated cellular interactions, which limits their application to clinical practice and research. Therefore, the development of technologies such as 3D culture will provide a novel alternative for gynecologic cancer research, as it allows to replicate several critical features of tissues including tumor morphology, differentiation, polarity, proliferation rate, gene expression, cell heterogeneity, and nutrient and oxygen gradients (2).

3D CULTURES SYSTEMS IN CERVICAL CANCER

Cervical cancer is the fourth most common cancer among women globally and therapy resistance is still a major problem to treat the disease (36). Hence, it is necessary to develop novel drugs and therapeutic approaches, as almost all drugs used today suffer from serious side effects due to drug resistance and lack of selectivity towards tumors (37). Recently, there has been an increasing interest in the development of 3D *in vitro* tumor models based on human cancer cells to accurately reproduce the characteristics of human cancer tissues (38). For instance, Zhao and coworkers demonstrated increased paclitaxel chemoresistance and proliferation rate in 3D cultures compared to traditional monolayer (2D) cultures of HeLa cells. In addition, HeLa cells increased the expression of matrix metalloproteinase (MMP) protein in 3D cultures (39). Similarly, Baek N and coworkers demonstrated increased resistance to doxorubicin in 3D cultures of HeLa cells compared to 2D cultures, resulting in higher IC50 values 11.2 and 9.6 μM of doxorubicin in 3D cultures at day 3 and 5, respectively, compared to monolayer cultures 1.0 μM of doxorubicin. The observed differences to doxorubicin sensitivity with respect to 2D and 3D cultures is due to monolayer cultured cells being well oxygenated, resulting in the rapid accumulation of reactive oxygen species (ROS) when exposed to DXR. In contrast, cells in the spheroid core are under hypoxic conditions, which makes them much more resistant (40). It has been shown that some plant constituents have anticancer activities, for example, Zataria essential oil (ZEO) is one of the useful essential oils that possesses extensive biological activities. The major components of ZEO have been shown to decrease the viability of breast cancer cells (41). Azadi M and coworkers demonstrated that ZEO treatment promotes inhibition of cell proliferation and promotes apoptosis in the TC1 cervical cancer cell line TC1 in both monolayer (2D) and multicellular spheroids (3D). In addition, ZEO was effective in tilting the cytokine balance in favor of T helper 1 through increased secretion of TNF-α, IFN-γ, IL-2 and decreased IL-4 (**Figure 3**) (42). It has been shown that bidirectional crosstalk between tumor and stroma plays an important role in the response

to therapy. De Gregorio V and coworkers developed an organotypic cervical tumor model where they established this crosstalk, they developed two models 1) composed of primary human cervical fibroblasts (HCFs) embedded in the ECM, to produce normal cervical stroma (NCIS) and 2) composed of cervical cancer-associated fibroblasts (CCAFs), generating cervical cancer stroma (CCIS). They demonstrated increased gene expression of early viral E6 and E7 genes in SiHa cells when cultured in CCSI. Therefore, organotypic models of cancer can help to better understand cancer progression and establish novel anti-cancer therapeutic targets directed to tumor stroma and cancer cells (43).

MicroRNAs Modulation in 3D Cervical Cancer Cultures

As major regulators of gene expression, its expected that miRNAs expression could be modulated in the 3D cultures, as several studies reported (44). The miR-143/145 cluster has been found downregulated in cervical cancer and overexpression of miR-143 or miR-145 inhibits cell viability, proliferation, migration, and invasion, in monolayers and 3D cultures of HeLa cervical cancer cell line. Furthermore, transfection of miRNA-145 increased pMLC levels by targeting the MYPT1 subunit of myosin regulatory phosphatase (45). Moreover, it has been shown that extracellular vesicles (EVs) secreted by 3D cultured tumor cells differ in terms of secretion dynamics and essential signaling molecular contents (RNA and DNA) compared to EVs derived from monolayer 2D cultures. These data suggested that EV small RNAs derived from 3D cultures may reflect EVs RNAs derived from *in vivo* tissues (46). Indeed, this is because cells in monolayer completely differ from the *in vivo* state where cells grow in 3D, in terms of cell morphology, cell-to-cell interactions, growth behavior and interactions with the extracellular matrix (1, 47). Thippabhotla and coworkers demonstrated that miRNAs expression profile of extracellular vesicles derived from 3D culture of HeLa cervical cancer cell line exhibited a high similarity of about 96% with circulating extracellular vesicles obtained from the plasma of cervical cancer patients, compared with the expression profile of EVs miRNAs derived from HeLa cell line growing in 2D. On the other hand, they demonstrated that culture and growth conditions do not affect genomic information, carried by EVs secretion, by DNA sequencing analysis (48). Currently, the number of studies focusing in the generation of organoids from primary cervical tissue is scarce. Recently, Lõhmussaar K, and coworkers established a protocol to generate 3D organoids from cervical tissue from both the endocervix and ectocervix that stably recapitulate cervical tissue. These organoids generated differential responses to chemotherapeutic agents, such as carboplatin, cisplatin, and gemcitabine, and grew as xenografts in mice (33, 49).

3D CULTURES SYSTEMS IN OVARIAN CANCER

Ovarian cancer (OC) is considered the most lethal gynecological cancer due to its high metastatic potential and resistance to

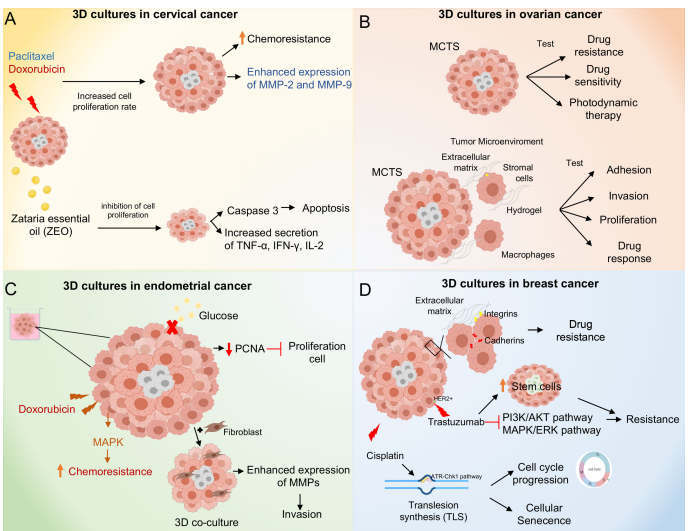

FIGURE 3 | Molecular mechanisms activated in 3D culture systems. **(A)** 3D cultures of cervical cancer cells result in paclitaxel and doxorubicin chemoresistance through increased proliferation rate and overexpression of MMP-2 and 9. Zataria essential oil treatment inhibits cell proliferation in 3D cultures and induces apoptosis through activation of caspase 3. **(B)** 3D culture systems in ovarian cancer. The Multicellular Tumor Spheroids (MCTS) allow testing of drug and photodynamic therapies. The co-culture of MCTS with stromal cells and macrophages in combination with hydrogels as scaffold, allow to mimic the tumor microenvironment providing a model to test adhesion, invasion, proliferation processes as well as drug response. **(C)** 3D cultures systems in endometrial cancer. Doxorubicin treatment induces chemoresistance through activation of the MAPK pathway. Moreover, 3D cultures of endometrial cancer co-cultured with fibroblasts promote invasion through overexpression of MMPs. **(D)** 3D cultures systems in breast cancer. Spheroids of breast cancer cells exhibit cell-cell and extracellular cell-matrix interactions promoting drug resistance. Cisplatin treatment promotes cell cycle progression and cellular senescence through up-regulation of trans-lesion DNA polymerase (TLS) expression and activation of the ATR-Chk1 pathway. Trastuzumab treatment induces resistance in 3D cultures through inhibition of PI3K/AKT and ERK/MAPK pathways, in addition to an increase in stem cells subpopulations.

chemotherapeutic agents; because of these several studies have been dedicated to demonstrating the importance and influence of 3D cell cultures in the characterization and study of the OC. Due to the above, the need has arisen to develop culture supports and 3D cultures models that allow to mimic the tumor microenvironment to have greater efficiency when testing drugs, this because the use of *in vitro* screening methods on tissue culture polystyrene (TCPS) does not mimic the microenvironment of aggregates *in vivo* when evaluating the response to drugs (50). Additionally, the characteristics genotypic and phenotypic between the different cell lines, can lead to development different morphologies in the formation of spheroids and influence resistance or sensitivity in drug testing, obtaining variable results in the study between 2D and 3D models (51). Hirst and coworkers showed an increase in gene expression associated with hypoxia, drug resistance and stem cell markers in a Multicellular Tumor Spheroids (MCTS) model from epithelial ovarian cancer (EOC), interestingly, they identified that FDA-approved drugs as licofelone and glafenine reversed the gene expression found in MCST (52). The use of different techniques allows to optimize the development of tumor spheroids in OC; the co-culture between OC and mesothelial cells, promotes and facilitates OC spheroid formation in a 3D model, showing a structure of spheroids larger in 3D co-culture than OC cells in a monoculture (53). On the other hand, Angiotensin II (AGII) and its receptor AGTR1 enhanced the formation and increased the growth of OVCA429, and Isogenic highly metastatic OC (HM) tumor spheroids (54). Hydrogel supports made with Poly ethylene glycol-maleimide (PEG-MAL) allow emulation of the omentum, which has made it possible to evaluate resistance to drugs such as Pacitaxel and Mafosfamide as well as the sensitivity to drugs such as Carboplatin, Doxorubicin and LY2606368 in MCTS of SKOV-3 and Ovarian Carcinoma Ascites Spheroids (OCAS) patient-derived models, indicating a greater efficiency and potential use of 3D hydrogel omentum-based MCTS model in drug resistance and sensitivity tests compared with TCPS in OC patients (50). An 3D organotypic model omentum-based using OVCAR4 cells, showed that 3D organotypic models are a suitable tool to evaluate the delivery systems of potential nano-drugs using anti-metastatic nanoparticles with low toxicity such as RAPTA-C [Rutheniumdichloride (p-cymene) PTA] in order to optimize and increase the sensitivity in the treatment of OC (55). On the other hand, Verteporfin, a photosensitizer, was encapsulated efficiently within nanostructured lipid carriers, showing a greater sensitivity to light exposure and a higher cytotoxic effect after treatment in OVCAR3 and SKOV3 spheroids, demonstrating the application of 3D models in the search of photodynamic therapeutic prospects in OC therapy (56). The development and use of organoids models emerged as an alternative in the study of OC due to the limitations in the use of the spheroid models of cell lines. Organoids from EOC, particularly, fallopian tubes and ovarian surface epithelial cells organoids, are the main EOC organoid models used to study ovarian carcinogenesis; however, the lack of microenvironment is one of the principal limitations in the use of organoids because of that several anti-angiogenic, stromal-affecting, and immunotherapy drugs cannot be tested; the combination with the use of microfluid platform, could offer a partial solution to limitation previously mentioned (57).

The tumor microenvironment (TME) is a fundamental part in tumor development and progression, organotypic models consisting of stromal cells, such as human primary mesothelial cells (HPMC) or fibroblasts, and microfluidic models, could be a partial solution to the limitation of 2D culture. Regard 3D organotypic human mesothelium models, the key factors are the use of different ECM proteins and two mainly stromal primary cells, the purpose of this model is to study and identify potential molecules against adhesion, invasion, proliferation, and drug response on OC. The microfluidic 3D model is subjected to a continuous flow of growth factors and nutrients in order to mimic the TME by the flow of peritoneal fluid originated by OC, this model is useful mainly to evaluate the influence of macrophage infiltration in the TME development and its effect on the adhesion, tumorigenicity, proliferation, progression and trancoelomic metastasis in OC (58). The Tumor-associated macrophages (TAM) are key pieces to the survival and proliferation of free detached tumor cells from the primary tumor to form spheroids in early steps of transcoelomic metastasis, Long and coworkers established an *in vitro* spheroid formation assay with a co-culture system composed by GDP+F4/80+CD206+TAMs from an isolated of spheroids of ovarian cancer-bearing donor tomatoIysM-cre mouse, mixed with ID8 cells in a medium with matrigel. The model could support the lack of a tumor microenvironment in 3D models, particularly in the study of the effects of macrophage infiltration on the development and progression tumor (59). Additionally, a hetero-spheroid model, with OVCAR3 OC cells, Ovarian cancer stem cells (CSC) and CD68+ macrophages showed an increase in the expression of CD206, a M2 macrophage marker, IL-10 and WNT5B, in addition to presenting an increase in ALDH+ population and resistance to carboplatin treatment, showing a greater invasive capacity in CDS/M2 spheroids compared with OVCAR3/M0 spheroids, indicating the influence of macrophages in the modulation of the microenvironment of peritoneal fluid in the modulation of the WNT signaling and their relation with the development and progression in OC (60). Ward Rashidi and coworkers showed an increase in the population of ALDH+ from Passage 0 to 6 in an OC 3D hanging drop spheroid model of CSCs; interestingly, an increase in cisplatin resistance was observed in all spheroids serial passage, conversely, a reduction on the cell viability was observed in cells treated with 673A, an ALDH inhibitor, these finding highlights the usefulness of OC 3D model in the study of chemoresistance and tumorigenicity (61).

The gene expression profiles allow the comparative analysis of genotypic and phenotypic features between 2D and 3D cultures, as well as in primary OC tumors. An analysis of transcriptomic profiles in organotypic 3D model identified 1,182 genes differentially expressed. A comparison with primary tumors found 144 common genes that were deregulated in early metastatic colonization. The analysis of cell pathways identified

the matrisome, core matrisome, ECM glycoproteins, ECM organization, matrisome associated, focal adhesion and integrin 1 as the main proteins and pathways modulated (62). In the same context, Paullin and coworkers performed a comparative transcriptomic analysis between 2D versus 3D spheroid OC models using HEY cells treated with TGFβ in order to induce the EMT. Results showed a different gene expression profile between models, among them, genes related to chemotherapy resistance (ARK1C1), ECM remodeling (PRSS35) and EMT enhancer transcription factors (SNAI1, SNAI2, ZEB2, TCF3 and SIXI) showed a differential gene expression in 3D compared with 2D culture. In relation to transcriptional networks modulated in 3D spheroids, analysis of the results identified sub-networks that include genes related to response to stress oxidative (PRDX2, CAT, SOD1 and GST01) and transcripts modulated related to heat shock response (HSP90AA1, HSPB1 and HSF1) that may contribute to stabilization of oncogenes and drug resistance (63) (**Figure 3**).

MicroRNAs Regulation in 3D Ovarian Cancer Cell Cultures

The 3D models can also help to study regulatory mechanisms in OC mediated by miRNAs, in this context, Yoshimura and coworkers evaluated the effect of miR-99a-5p, an microRNA overexpressed in EOC, in peritoneal dissemination, using human peritoneal mesothelial cells (HPMCs) treated with EOC-derived exosomes. Results showed that overexpression of miR-99a-5p in HMPCs promoted the EOC invasion by affecting HPMCs by fibronectin and vitronectin upregulation suggesting that it could be considered as an EOC biomarker in serum and a potential therapeutic target (64). Altogether, reports indicate various advantages of the use of the 3D models culture models for the study and characterization of the development, progression, invasion and treatments of ovarian cancer.

3D CULTURES SYSTEMS IN ENDOMETRIAL CANCER

Endometrial cancer is the most prevalent gynecologic malignancy and a leading cause of morbidity and mortality in females (65). Endometrial cancer has been classified into two main groups, type I or type II, according to their clinicopathologic and molecular characteristics; estrogen-dependent type 1 endometrioid adenocarcinomas account for 80% of cases and are associated with endometrial hyperplasia with characteristic mutations in KRAS, PIK3CA and PTEN whereas type 2 tumors are of non-endometrioid histology, are estrogen-independent, are associated with endometrial atrophy and usually have mutations in TP53 and HER-2 (66, 67). Nowadays, there are several preclinical models in endometrial cancer to evaluate drug efficacy and predict patient outcomes. These include traditional monolayer 2D cultures, organoids, spheroids and animal models. However, some models present limitations (68, 69). For example, Chitcholtan and coworkers demonstrated reduced proliferation in 3D cultures of Ishikawa, RL95-2, EN-1078D and KLE endometrial cancer cell lines compared to 2D cultures, which correlated with decreased expression of the proliferative protein marker PCNA. In addition, altered metabolic phenotypes were observed, including decreased glucose uptake, independent of glucose transporter (GLUT) expression, and down-regulation of vascular epidermal growth factor (VEGF) secretion (70). Together, these data demonstrate that 3D cultures can affect the proliferation and metabolic behavior of endometrial cancer cells compared to 2D cells. Thus, the use of these *in vitro* models to assess the drug response in preclinical trials is important. The 3D cultures of RL95-2 and KLE endometrial cancer cell lines showed increased resistance to doxorubicin compared to 2D cultures, this was due to MAPK inactivation (71). Likewise, it has been shown that deletion of the ETS translocation variant 4 (ETV4), a candidate factor controlling ER genomic binding in endometrial cancer cells, led to decreased growth in 3D cultures of the Ishikawa endometrial cancer cell line (72). Nevertheless, one of the main limitations of these systems is the lack of incorporation of non-epithelial cells, which is why 3D co-cultures are now being developed, incorporating both stromal and epithelial cells. For this reason, 3D co-cultures are now being developed, incorporating both stromal and epithelial cells. These spheroids are phenotypically comparable to endometrial cancer tissue *in vivo*. In other study, Al-Juboori and coworkers performed a proteomic analysis to assess the biological relevance of spheroids in 3D co-culture (HESC/Ishikawa), they found 591 common proteins and canonical pathways that are closely related to endometrial biology in the 3D co-culture model compared to human endometrial tissue (73). On the other hand, the influence of fibroblasts on the invasion of endometrial cancer cells in 3D cultures has been analyzed, showing that Ishikawa endometrial cancer cells co-cultured with fibroblasts in 3D show a high invasion capacity and over-express proteins such as metalloproteinases (MMPs) and plasminogen activators (PA), compared to 3D cultures without fibroblasts (74). Other types of 3D preclinical models relevant to endometrial cancer patients are patient-derived organoids, patient-derived xenografts and patient-derived explants (75). Maru, Y and coworkers established a Matrigel bilayer organoid culture (MBOC) in gynecological tumors, demonstrating that the recovered organoids basically retained the characteristics of the original tumors (76).

3D CULTURES SYSTEMS IN BREAST CANCER

Breast cancer is a major public health problem due to its high incidence and mortality, being the most common cancer in women worldwide (77). The search for new drugs against breast cancer remains an important field in cancer research. However, the results of the effectiveness of treatments obtained *in vitro* have not been reproduced in the clinic. This is largely because most pre-clinical studies are generated from 2D cultures that do not resemble the "true biology" of the tumor *in vivo* (78,

79). In an early study, dit Faute and coworkers demonstrated that 3D cultures resulted in decreased proliferative rate of both MCF-7 breast cancer cell line and multi-resistant cells (MDR-MCF-7), reduced drug sensitivity of MCF-7 cells, and did not affect the resistance of MDR-MCF-7 cells. In addition, transmission electron microscopy assays demonstrated that MCF-7 cells grown as spheroids had a junctional system involving E-cadherin, tight-junctions and desmosomes, promoting drug resistance. Interestingly, in MCF-7 multi-resistant cell spheroids, cell cohesion was mostly due to membrane interdigitations, induced invasive properties (80). Another study group tested the sensitivity of cisplatin of the MCF-7 cell line grown in 2D and 3D cultures. Similarly, they demonstrated that resistance to cisplatin was mainly generated in 3D cultures which seems to be generated by interactions with the tumor microenvironment. Interestingly, it was demonstrated that 3D-cultured cells were able to progress through the S-cell cycle phase, due to the upregulation of translesion (TLS) DNA polymerase expression and the activation of the ATR-Chk1 pathway. Furthermore, co-treatment with a pharmacological ATR inhibitor (VE-821) generated a response to cisplatin (81).

In other study, Lovitt and coworkers found that spheroids cells displayed more chemoresistance to doxorubicin corresponding to higher IC50 values than conventional monolayer cells in MCF-7 and MDA-MB-23 breast cancer cell lines, mediated by cell-to-ECM interactions. Interestingly, inhibition of integrin signaling in combination with doxorubicin reduced the viability of breast cancer cells (82). Recently, a 3D-μTP culture system was established; it was manufactured by seeding tumor and/or fibroblast cells on biodegradable porous microcarriers in a dynamic culture system (83). Similarly, the efficacy of doxorubicin (DOX) was evaluated in two different 3D cancer models: microtissue (3D-μTP) versus spheroid, both models were formed by co-culturing MCF-7 cell line with fibroblasts. It was demonstrated that the 3D-μTP model showed increased DOX diffusion and decreased cell viability compared to spheroid. Moreover, they demonstrated that, beside multi-cellularity, the presence of a cell-assembled ECM in the 3D-μTP model also played a crucial role in modulating the drug response (84). Another effective treatment for breast cancer is trastuzumab, a recombinant humanized monoclonal antibody targeting human epidermal growth factor receptor 2 (HER2), a gene frequently amplified in 30% of breast cancer cases, and associated with poor prognosis in breast cancer patients (85). Several studies have demonstrated that trastuzumab significantly improved the prognosis of breast cancer patients with HER2 overexpression (86). This is because trastuzumab inhibits several signaling pathways, such as phosphatidylinositol 3-kinase (PI3K)-AKT serine/threonine kinase 1 and mitogen activated protein kinase (MEK)/extracellular signal regulated kinase (ERK) (87). Tatara and coworkers demonstrated that 3D cultures better simulate the cytological and biochemical responses to trastuzumab-induced apoptosis and resistance to trastuzumab associated with the PIK3CA mutation compared to 2D cultures. They observed increased expression of poly (ADP-ribose) polymerase (PARP) cleaved only in PIK3CA-wt lines grown in 3D in response to trastuzumab, but not in PIK3CA-wt or PIK3CA-mt lines grown in 2D (88).

Likewise, Gangadhara and coworkers demonstrated that breast cancer cell lines grown in 3D Matrigel-based culture system showed resistance to trastuzumab compared to 2D cultures, generated by AKT/MAPK extracellular matrix-mediated signaling. Interestingly, MAPK suppression in 3D cultures restoring the therapeutic response (89). Finally, Rodriguez and coworkers demonstrated that the hypoxic environment developed in the spheroids modulates the response to Trastuzumab in the breast cancer cell line HER2+. Furthermore, the acquired resistance to Trastuzumab in 3D cultures was associated with an increase in the population of cancer stem cells (90). Another anti-tumor chemotherapeutic agent is the taxane paclitaxel (Ptx) which binds to- and stabilizes cytoskeleton microtubules resulting in mitosis inhibition (91). Recently, new strategies have been described that allow the drug to accumulate at the site of the tumor and simultaneously decrease the concentration in the rest of the body, thus avoiding serious side effects, such as bone marrow suppression and neurotoxicity (92). This targeted drug delivery can be achieved by magnetic drug targeting (MDT). Lugert and coworkers developed Ptx-functionalized super paramagnetic iron oxide (SPION) nanoparticles coated with lauric acid (LA) and human serum albumin (HSA; SPION LA-HSA-Ptx) and analyzed their efficacy in different breast cancer cell lines cultured in 2D and 3D. They demonstrated that the binding of the antiproliferative and antitumor agent Ptx to the biocompatible and magnetically susceptible carrier SPION LA-HSA was effective in different breast cancer cell lines and did not influence the cytotoxic efficacy of the chemotherapeutic drug. Furthermore, they found not significant differences between the 2D and 3D culture systems (93).

On the other hand, compounds of natural origin with anti-cancer activity have been investigated. An example is Ginger (Zingiber officinale Roscoe). Ginger is the rhizome of plants in the Zingiberaceae family and has been widely used as a medicinal plant for thousands of years, due to its phenolic compounds, [4], [6], [8], and [10]-gingerols (94). It has been demonstrated that gingerols, have multiple anti-cancer effects, inhibiting the cellular proliferation of MDA-MB-231 triple negative breast cancer cells compared to non-tumor cells (95). Therefore, Fuzer and coworkers analyzed the anti-cancer activity of [10]-gingerol in breast cancer HMT-3522 cells growing in lr-ECM in 3D culture. They demonstrated that [10]-gingerol promoted cytotoxicity in linear HMT-3522 (T4-2) cells compared to non-malignant S1 cells. Furthermore, [10]-gingerol induced apoptosis in the HMT-3522 (T4-2) cell line in breast cancer (96).

Interestingly, extracellular matrix signals have been demonstrated to play a crucial role in apoptotic sensitivity in response to chemotherapeutic agents for non-malignant and malignant breast cell lines in 2D and 3D culture (97, 98). This is largely because cells grown in 3D adopt morphologies similar to those of tissues *in vivo*. Kenny and coworkers analyzed the morphological phenotype of 25 of these breast cell lines grown in

2D and 3D cultures, and their gene expression profiles under these same conditions. They demonstrated that breast cancer cell lines grown in 2D did not show different morphologies, however, when grown in 3D they adopted four different morphologies called: Round, Massive, Grape-like and Stellate. Furthermore, the 3D microenvironment produced significant changes in the gene expression profiles of these cancer cell lines (26). In particular, genes encoding proteins involved in signal transduction were over-expressed in 3D cell cultures compared to 2D cultures. Therefore, it is important to understand that cancer is a complex process that depends both on the behavior of the cancer cells and on the function of the non-malignant supporting cells in the tumor microenvironment (99). Tumor-associated mesenchymal stromal cells (TA-MSC) are a major component of the tumor microenvironment; they contribute to cancer progression by promoting metastasis, vascularization of the tumor and contribute to cancer cell resistance to chemotherapy (100). One way to study these TA-MSC is through 3D cell cultures, because cell signaling, and drug responses differ when cells are cultured on rigid 2D substrates or using 3D cell culture systems that more closely mimic the tumor microenvironment (101). Blache and coworkers demonstrated that secretions from the 3D-cultured MDA-MB-231 breast cancer cell line convert mesenchymal stromal cells (MSC) to MSC-AT, generating an immunomodulatory phenotype that is particularly prominent in response to bone-tropic cancer cells (102). The development of 3D cultures allows us to understand the molecular mechanisms of drug resistance and the biology of breast cancer (**Figure 3D**).

MicroRNAs Regulation in 3D Breast Cancer Cell Cultures

The expression and function of miRNAs in breast cancer cells have long been derived from 2D cultures, which lack the tumor microenvironment. However, recently the expression of miRNAs in 3D versus 2D cultures in different breast cancer cell lines has been described. For example, Nguyen and coworkers analyzed the expression profile of miRNAs in 3D compared to 2D cultures in the MCF-7 (non-invasive) and MDA-MB-231 (invasive) breast cancer cell lines. They showed that 49 miRNAs were differentially expressed in the MCF-7 cell line in 3D cultures compared to 2D, of those 24 were upregulated and 25 were downregulated. Whereas, in the MDA-MB231 cell line, 28 miRNAs were differentially expressed, with 22 miRNAs upregulated and 6 miRNAs downregulated. In addition, two miR-200 family members, miR-141 and miR-429 were overexpressed only in 3D cultures in the MCF-7 cell line. Overexpression of miR-429 in MDA-MB231 cells attenuated their invasive stellate morphology in 3D culture. This suggests that the differential expression profile between the two cell lines is probably due to miRNAs regulating mass morphology in the MCF-7 cell line and invasive stellate morphology in MDA-MB231 cells (25). Furthermore, it has been shown that the expression profiles of miRNAs in MDA-MB-231 cell line cultured in 3D are like the changes reported in highly invasive breast tumors. For example, miR-146a-5p, which regulates cancer progression or miR-210, which is over-expressed in response to hypoxia in breast cancer. Suggesting that 3D cultures better mimic tumors *in vivo* than traditional 2D culture (103).

On the other hand, the use of natural compounds in the treatment of cancer is increasing. Such is the case of silibinin, which is a natural flavonoid, and the anticancer and chemopreventive effects of silibinin have been demonstrated in different types of cancer (104). Yazdi and coworkers analyzed the effect of silibinin on cell viability and miRNA expression in 3D and 2D cultures of the T47D breast cancer cell line. They demonstrated that the 3D cultures show higher drug resistance, similar to what occurs *in vivo* and is largely due to the fact that the cells are in different stages of growth, including proliferation, hypoxia, apoptosis, necrosis and quiescent phase. Furthermore, they demonstrated that silibinin promotes apoptosis in both 3D and 2D cultures. Finally, they demonstrated decreased expression of miR-21, miR-15a, and miR-141, in silibinin-treated cells in 3D and 2D cultures of the T47D cell line (105).

3D CULTURES APPLICATIONS IN GYNECOLOGICAL AND BREAST CANCER TRANSLATIONAL RESEARCH

3D culture models in gynecological and breast cancer provide a valuable platform to investigate the molecular processes leading to uncontrolled cell proliferation and metastasis which may allow for novel drugs discovery. This is of utmost importance, because resistance to chemo- and radiotherapy is common in patients with gynecological and breast cancer, in indeed a large proportion of patients undergo excessively toxic treatments with no or minimal therapeutic benefit (106). The utilization of 3D cultures and organoids will help to predict the responsiveness of patients to treatments and will allow tailoring specific treatments for each patient, resulting in personalized therapies. For example, Boretto, M and coworkers developed organoid cultures derived from endometrial cancer patients as preclinical models for screening drugs, for screening drugs, such as paclitaxel, 5-fluorouracil, carboplatin, doxorubicin) and everolimus (mTOR inhibitor), showed patient-specific responses (107). Furthermore, the STAT3 transcription factor inhibitor, BBI608 (Napabucasin), strongly inhibited the growth of patient-derived organoids through inhibition of growth receptor tyrosine kinase (108).

On the other hand, one of the main characteristics of ovarian cancer is its genetic heterogeneity, so differential responses to drugs in ovarian cancer have to be expected. The development of organoids derived from individual ovarian cancer lines will allow screening for different drugs, for example, the HGS-3.1 organoid line was sensitive to gemcitabine, adavosertib, carboplatin and paclitaxel and resistant to drugs targeting the PI3K/AKT/mTOR pathway, while the HGS-23 line showed a pattern of sensitivity to the opposite drugs. Furthermore, organoids have been demonstrated to capture tumor heterogeneity (106). The radiosensitivity of cervical cancer organoids has been investigated.

Nakajima, A and coworkers demonstrated that organoid growth was inhibited in a dose-dependent manner one week after irradiation. Radiosensitivity was patient-specific and matched the response of the xenografted tumor and the patient. Interestingly, hypoxia-inducible factor 1α (HIF-1α) target gene expression was up-regulated in organoids derived from resistant cancer tissues. HIF-1α protein levels increased several hours after irradiation (109). Finally, breast cancer organoids reflect tumor heterogeneity, it has been observed that breast cancer organoids can achieve 60% or more similarity of characteristics and gene profile expression with tumors *in vivo* (110). Furthermore, breast cancer organoids can be used as an effective *in vitro* model for the study of personalized treatment. Garcia-Davis, S and coworkers evaluated the antitumor effect of *laurinterol*, the main compound of an ethanolic extract of *Laurencia johnstonii* on breast cancer organoids. They found a dose-dependent inhibition of metabolic activity, as well as morphological and nuclear changes characteristic of apoptosis. However, they observed a heterogeneous response that was associated with the individual response of each human tumor sample, being associated with intratumoral heterogeneity (111). Recently, Carter and coworkers developed an experimental protocol to infect breast cancer organoid cultures with oncolytic viruses and compared the oncolytic effects of a measles vaccine virus (MeV) and a vaccinia virus (GLV), genetically modified, allowing enzymatic conversion of the 5-fluorocytosine (5-FC) prodrug into the cytotoxic compounds 5-fluorouracil (5-FU) and 5-fluorouridine monophosphate (5-FUMP), to investigate the effects of oncolytic virotherapy. They demonstrated that oncolytic viruses significantly inhibited cell viability in organoid cultures derived from breast cancer tissue. Thus, the model provides a promising *in vitro* method to aid further testing of virotherapeutic vectors for *in vivo* use (112).

At present, breast and gynecological cancer organoids represent an optimal model for the compression of tumor biology, and their applications in the screening of new tumor drugs has significantly contributed to clinical applications (113). However, although promising breast and gynecological cancer organoids have some limitations such as: i) they lack the complete technology to simultaneously connect organoids and tumor microenvironment, ii) the generation of breast and gynecological cancer organoids from patients are mainly surgical tissue or puncture, however, it is believed that some of the cellular heterogeneity of *in vivo* tumors is lost in the sampling process and iii) they lack mesenchymal cells, so they do not have nervous and vascular system, presenting some differences with solid tumors (114, 115). These limitations must be overcome in the immediate future of 3D and organoids technologies to contribute to the advance of the field. In the future, 3D and organoid culture models combined with recent biotechnological progress will offer exciting improvements for the precise application of this technology.

CONCLUSIONS

Although 2D cultures have been used for a long time, they do not reflect the biology of cancer, making them an inefficient model to study the processes associated with cellular responses to chemotherapeutic exposure. On the other hand, the establishment of 3D cultures are potentially a better approach in the search for new biomarkers and new treatment strategies in breast and gynecological cancer, due to their physiological relevance bringing us closer to the goal of personalized medicine. The main contributions of 3D cultures in gynecological and breast cancer can be summarized as follows i) they have improved our understanding of cancer biology, ii) they have helped to better understand the molecular mechanisms of drug resistance by the identification on novel players in these processes, iii) they capture phenotypic heterogeneity, iv) they modify gene expression and cell behavior in a similar way to *in vivo* condition, v) and they mimic the tumor micro-environment in a similar way to *in vivo* tumors. In conclusion the development of 3D culture models in breast and gynecologic cancer will help to further understand cancer biology and to develop new drugs and predict drug response to address poor response rates and improve survival outcomes in patients.

AUTHOR CONTRIBUTIONS

CL-C, YS-V, JV, LM, and RR-P conceived and designed the review. CL-C, YS-V, JV, YP-N, GM-L, LM, RR-P, and SN-O performed the literature review and were involved in the writing and revision of the manuscript. YS-V, YP-N, CP-P, and GM-L prepared all the figures. All authors have read and agreed to the published version of the manuscript.

FUNDING

This research was funded by Consejo Nacional de Ciencia y Tecnologia (CONACYT), Mexico, Grant FORDECYT-PRONACES/51207/2020. Convenio I1200/189/2020. YS-V and SN-O received scholarships 754782 and 789774, respectively, from CONACYT, Mexico.

ACKNOWLEDGMENTS

We acknowledge to Universidad Autonoma de la Ciudad de Mexico for support.

REFERENCES

1. Pampaloni F, Reynaud EG, Stelzer EH. The Third Dimension Bridges the Gap Between Cell Culture and Live Tissue. *Nat Rev Mol Cell Biol* (2007) 8:839–45. doi: 10.1038/nrm2236
2. Cukierman E, Pankov R, Stevens DR, Yamada KM. Taking Cell-Matrix Adhesions to the Third Dimension. *Science.* (2001) 294:1708–12. doi: 10.1126/science.1064829
3. Mseka T, Bamburg JR, Cramer LP. ADF/cofilin Family Proteins Control Formation of Oriented Actin-Filament Bundles in the Cell Body to Trigger Fibroblast Polarization. *J Cell Sci* (2007) 120:4332–44. doi: 10.1242/jcs.017640

4. Weiswald LB, Bellet D, Dangles-Marie V. Spherical Cancer Models in Tumor Biology. *Neoplasia*. (2015) 17:1–15. doi: 10.1016/j.neo.2014.12.004
5. Baal N, Widmer-Teske R, McKinnon T, Preissner KT, Zygmunt MT. *In Vitro* Spheroid Model of Placental Vasculogenesis: Does it Work? *Lab Invest* (2009) 89:152–63. doi: 10.1038/labinvest.2008.126
6. Friedrich J, Seidel C, Ebner R, Kunz-Schughart LA. Spheroid-Based Drug Screen: Considerations and Practical Approach. *Nat Protoc* (2009) 4:309–24. doi: 10.1038/nprot.2008.226
7. Baker BM, Chen CS. Deconstructing the Third Dimension: How 3D Culture Microenvironments Alter Cellular Cues. *J Cell Sci* (2012) 125:3015–24. doi: 10.1242/jcs.079509
8. Mehta G, Hsiao AY, Ingram M, Luker GD, Takayama S. Opportunities and Challenges for Use of Tumor Spheroids as Models to Test Drug Delivery and Efficacy. *J Control Release* (2012) 164:192–204. doi: 10.1016/j.jconrel.2012.04.045
9. Nath S, Devi GR. Three-Dimensional Culture Systems in Cancer Research: Focus on Tumor Spheroid Model. *Pharmacol Ther* (2016) 163:94–108. doi: 10.1016/j.pharmthera.2016.03.0137
10. Kleinman HK, Philp D, Hoffman MP. Role of the Extracellular Matrix in Morphogenesis. *Curr Opin Biotechnol* (2003) 14:526–32. doi: 10.1016/j.copbio.2003.08.002
11. Katt ME, Placone AL, Wong AD, Xu ZS, Searson PC. *In Vitro* Tumor Models: Advantages, Disadvantages, Variables, and Selecting the Right Platform. *Front Bioeng Biotechnol* (2016) 4:12. doi: 10.3389/fbioe.2016.00012
12. Yang J, Huang S, Cheng S, Jin Y, Zhang N, Wang Y. Application of Ovarian Cancer Organoids in Precision Medicine: Key Challenges and Current Opportunities. *Front Cell Dev Biol* (2021) 9:701429. doi: 10.3389/fcell.2021.701429
13. Rosso F, Giordano A, Barbarisi M, Barbarisi A. From Cell-ECM Interactions to Tissue Engineering. *J Cell Physiol* (2004) 199:174–80. doi: 10.1002/jcp.10471
14. Antoni D, Burckel H, Josset E, Noel G. Three-Dimensional Cell Culture: A Breakthrough *In Vivo*. *Int J Mol Sci* (2015) 16:5517–27. doi: 10.3390/ijms16035517
15. Calin GA, Croce CM. MicroRNA Signatures in Human Cancers. *Nat Rev Cancer* (2006) 6:857–66. doi: 10.1038/nrc1997
16. Lin S, Gregory RI. MicroRNA Biogenesis Pathways in Cancer. *Nat Rev Cancer* (2015) 15:321–33. doi: 10.1038/nrc3932
17. Lerner RG, Petritsch C. A microRNA-Operated Switch of Asymmetric-to-Symmetric Cancer Stem Cell Divisions. *Nat Cell Biol* (2014) 16:212–4. doi: 10.1038/ncb2924
18. Pencheva N, Tavazoie SF. Control of Metastatic Progression by microRNA Regulatory Networks. *Nat Cell Biol* (2013) 15:546–54. doi: 10.1038/ncb2769
19. Bouchie A. First microRNA Mimic Enters Clinic. *Nat Biotechnol* (2013) 31:577. doi: 10.1038/nbt0713-577
20. Sutherland RM, McCredie JA, Inch WR. Growth of Multicell Spheroids in Tissue Culture as a Model of Nodular Carcinomas. *J Natl Cancer Inst* (1971) 46:113–20.
21. Kelm JM, Timmins NE, Brown CJ, Fussenegger M, Nielsen LK. Method for Generation of Homogeneous Multicellular Tumor Spheroids Applicable to a Wide Variety of Cell Types. *Biotechnol Bioeng* (2003) 83:173–80. doi: 10.1002/bit.10655
22. Lin RZ, Chang HY. Recent Advances in Three-Dimensional Multicellular Spheroid Culture for Biomedical Research. *Biotechnol J* (2008) 3:1172–84. doi: 10.1002/biot.200700228
23. Hoarau-Véchot J, Rafii A, Touboul C, Pasquier J. Halfway Between 2D and Animal Models: Are 3d Cultures the Ideal Tool to Study Cancer-Microenvironment Interactions? *Int J Mol Sci* (2018) 19:181. doi: 10.3390/ijms19010181
24. Lee GY, Kenny PA, Lee EH, Bissell MJ. Three-Dimensional Culture Models of Normal and Malignant Breast Epithelial Cells. *Nat Methods* (2007) 4:359–65. doi: 10.1038/nmeth10157
25. Nguyen HT, Li C, Lin Z, Zhuang Y, Flemington EK, Burow ME, et al. The microRNA Expression Associated With Morphogenesis of Breast Cancer Cells in Three-Dimensional Organotypic Culture. *Oncol Rep* (2012) 28 (1):117–26. doi: 10.3892/or.2012.1764
26. Kenny PA, Lee GY, Myers CA, Neve RM, Semeiks JR, Spellman PT, et al. The Morphologies of Breast Cancer Cell Lines in Three-Dimensional Assays Correlate With Their Profiles of Gene Expression. *Mol Oncol* (2007) 1:84–96. doi: 10.1016/j.molonc.2007.02.004
27. Messner S, Agarkova I, Moritz W, Kelm JM. Multi-Cell Type Human Liver Microtissues for Hepatotoxicity Testing. *Arch Toxicol* (2013) 87:209–13. doi: 10.1007/s00204-012-0968-2
28. Xu H, Lyu X, Yi M, Zhao W, Song Y, Wu K. Organoid Technology and Applications in Cancer Research. *J Hematol Oncol* (2018) 11:116. doi: 10.1186/s13045-018-0662-9
29. Lancaster MA, Knoblich JA. Organogenesis in a Dish: Modeling Development and Disease Using Organoid Technologies. *Science*. (2014) 345:1247125. doi: 10.1126/science.1247125
30. Clevers HC. Organoids: Avatars for Personalized Medicine. *Keio J Med* (2019) 68:95. doi: 10.2302/kjm.68-006-ABST
31. Kim J, Hoffman JP, Alpaugh RK, Rhim AD, Reichert M, Stanger BZ, et al. An iPSC Line From Human Pancreatic Ductal Adenocarcinoma Undergoes Early to Invasive Stages of Pancreatic Cancer Progression. *Cell Rep* (2013) 3:2088–99. doi: 10.1016/j.celrep.2013.05.036
32. Takahashi K, Yamanaka S. A Decade of Transcription Factor-Mediated Reprogramming to Pluripotency. *Nat Rev Mol Cell Biol* (2016) 17:183–93. doi: 10.1038/nrm.2016.8
33. Papapetrou EP. Patient-Derived Induced Pluripotent Stem Cells in Cancer Research and Precision Oncology. *Nat Med* (2016) 22:1392–401. doi: 10.1038/nm.4238
34. Kondo J, Endo H, Okuyama H, Ishikawa O, Iishi H, Tsujii M, et al. Retaining Cell-Cell Contact Enables Preparation and Culture of Spheroids Composed of Pure Primary Cancer Cells From Colorectal Cancer. *Proc Natl Acad Sci USA* (2011) 108:6235–40. doi: 10.1073/pnas.1015938108
35. Ritter CA, Perez-Torres M, Rinehart C, Guix M, Dugger T, Engelman JA, et al. Human Breast Cancer Cells Selected for Resistance to Trastuzumab *In Vivo* Overexpress Epidermal Growth Factor Receptor and ErbB Ligands and Remain Dependent on the ErbB Receptor Network. *Clin Cancer Res* (2007) 13:4909–19. doi: 10.1158/1078-0432.CCR-07-0701
36. Vu M, Yu J, Awolude OA, Chuang L. Cervical Cancer Worldwide. *Curr Probl Cancer* (2018) 42:457–65. doi: 10.1016/j.currproblcancer.2018.06.003
37. Newell H, Sausville E. Cytotoxic Drugs: Past, Present and Future. *Cancer Chemother Pharmacol* (2016) 77:1. doi: 10.1007/s00280-015-2917-2
38. Horning JL, Sahoo SK, Vijayaraghavalu S, Dimitrijevic S, Vasir JK, Jain TK, et al. 3-D Tumor Model for *In Vitro* Evaluation of Anticancer Drugs. *Mol Pharm* (2008) 5:849–62. doi: 10.1021/mp800047v
39. Zhao Y, Yao R, Ouyang L, Ding H, Zhang T, Zhang K, et al. Three-Dimensional Printing of Hela Cells for Cervical Tumor Model *In Vitro*. *Biofabrication* (2014) 6:35001. doi: 10.1088/1758-5082/6/3/035001
40. Baek N, Seo OW, Kim M, Hulme J, An SS. Monitoring the Effects of Doxorubicin on 3D-Spheroid Tumor Cells in Real-Time. *Onco Targets Ther* (2016) 9:7207–18. doi: 10.2147/OTT.S112566
41. Salehi F, Behboudi H, Kavoosi G, Ardestani SK. Monitoring ZEO Apoptotic Potential in 2D and 3D Cell Cultures and Associated Spectroscopic Evidence on Mode of Interaction With DNA. *Sci Rep* (2017) 7:2553. doi: 10.1038/s41598-017-02633-z
42. Azadi M, Jamali T, Kianmehr Z, Kavoosi G, Ardestani SK. *In-Vitro* (2D and 3D Cultures) and *in-Vivo* Cytotoxic Properties of Zataria Multiflora Essential Oil (ZEO) Emulsion in Breast and Cervical Cancer Cells Along With the Investigation of Immunomodulatory Potential. *J Ethnopharmacol* (2020) 257:112865. doi: 10.1016/j.jep.2020.112865
43. De Gregorio V, La Rocca A, Urciuolo F, Annunziata C, Tornesello ML, Buonaguro FM, et al. Modeling the Epithelial-Mesenchymal Transition Process in a 3D Organotypic Cervical Neoplasia. *Acta Biomater* (2020) 116:209–22. doi: 10.1016/j.actbio.2020.09.006
44. Pasquinelli AE. MicroRNAs and Their Targets: Recognition, Regulation and an Emerging Reciprocal Relationship. *Nat Rev Genet* (2012) 13:271–82. doi: 10.1038/nrg3162
45. González-Torres A, Bañuelos-Villegas EG, Martínez-Acuña N, Sulpice E, Gidrol X, Alvarez-Salas LM. MYPT1 is Targeted by miR-145 Inhibiting Viability, Migration and Invasion in 2D and 3D HeLa Cultures. *Biochem Biophys Res Commun* (2018) 507:348–54. doi: 10.1016/j.bbrc.2018.11.039
46. Taylor DD, Gercel-Taylor C. MicroRNA Signatures of Tumor-Derived Exosomes as Diagnostic Biomarkers of Ovarian Cancer. *Gynecol Oncol* (2008) 110:13–21. doi: 10.1016/j.ygyno.2008.04.033

47. Li Y, Kilian KA. Bridging the Gap: From 2D Cell Culture to 3D Microengineered Extracellular Matrices. *Adv Healthc Mater* (2015) 4:2780–96. doi: 10.1002/adhm.201500427
48. Thippabhotla S, Zhong C, He M. 3D Cell Culture Stimulates the Secretion of *In Vivo* Like Extracellular Vesicles. *Sci Rep* (2019) 9:13012. doi: 10.1038/s41598-019-49671-3
49. Lõhmussaar K, Oka R, Espejo Valle-Inclan J, Smits M, Wardak H, Korving J, et al. Patient-Derived Organoids Model Cervical Tissue Dynamics and Viral Oncogenesis in Cervical Cancer. *Cell Stem Cell* (2021) 28:1380–1396.e6. doi: 10.1016/j.stem.2021.03.012
50. Brooks EA, Gencoglu MF, Corbett DC, Stevens KR, Peyton SR. An Omentum-Inspired 3D PEG Hydrogel for Identifying ECM-Drivers of Drug Resistant Ovarian Cancer. *APL Bioeng* (2019) 3:026106. doi: 10.1063/1.5091713
51. Heredia-Soto V, Redondo A, Berjón A, Miguel-Martín M, Díaz E, Crespo R, et al. High-Throughput 3-Dimensional Culture of Epithelial Ovarian Cancer Cells as Preclinical Model of Disease. *Oncotarget.* (2018) 9:21893–903. doi: 10.18632/oncotarget.25098
52. Hirst J, Pathak HB, Hyter S, Pessetto ZY, Ly T, Graw S, et al. Licofelone Enhances the Efficacy of Paclitaxel in Ovarian Cancer by Reversing Drug Resistance and Tumor Stem-Like Properties. *Cancer Res* (2018) 78:4370–85. doi: 10.1158/0008-5472.CAN-17-3993
53. Shishido A, Mori S, Yokoyama Y, Hamada Y, Minami K, Qian Y, et al. Mesothelial Cells Facilitate Cancer Stem–Like Properties in Spheroids of Ovarian Cancer Cells. *Oncol Rep* (2018) 40:2105–14. doi: 10.3892/or.2018.6605
54. Zhang Q, Yu S, Lam MMT, Poon T, Sun L, Jiao Y, et al. Angiotensin II Promotes Ovarian Cancer Spheroid Formation and Metastasis by Upregulation of Lipid Desaturation and Suppression of Endoplasmic Reticulum Stress. *J Exp Clin Cancer Res* (2019) 38:116. doi: 10.1186/s13046-019-1127-x
55. Lu M, Henry CE, Lai H, Khine YY, Ford CE, Stenzel MH. A New 3D Organotypic Model of Ovarian Cancer to Help Evaluate the Antimetastatic Activity of RAPTA-C Conjugated Micelles. *Biomater Sci* (2019) 7:1652–60. doi: 10.1039/c8bm01326h
56. Michy T, Massias T, Bernard C, Vanwonterghem L, Henry M, Guidetti M, et al. Verteporfin-Loaded Lipid Nanoparticles Improve Ovarian Cancer Photodynamic Therapy *In Vitro* and *In Vivo*. *Cancers (Basel)* (2019) 11:1760. doi: 10.3390/cancers11111760
57. Dumont S, Jan Z, Heremans R, Van Gorp T, Vergote I, Timmerman D. Organoids of Epithelial Ovarian Cancer as an Emerging Preclinical *In Vitro* Tool: A Review. *J Ovarian Res* (2019) 12:105. doi: 10.1186/s13048-019-0577-2
58. Watters KM, Bajwa P, Kenny HA. Organotypic 3d Models of the Ovarian Cancer Tumor Microenvironment. *Cancers (Basel)* (2018) 10:265. doi: 10.3390/cancers10080265
59. Long L, Yin M, Min W. 3d Co-Culture System of Tumor-Associated Macrophages and Ovarian Cancer Cells. *Bio Protoc* (2018) 8:e2815. doi: 10.21769/BioProtoc.2815
60. Raghavan S, Mehta P, Xie Y, Lei YL, Mehta G. Ovarian Cancer Stem Cells and Macrophages Reciprocally Interact Through the WNT Pathway to Promote Pro-Tumoral and Malignant Phenotypes in 3D Engineered Microenvironments. *J Immunother Cancer* (2019) 7:190. doi: 10.1186/s40425-019-0666-1
61. Ward Rashidi MR, Mehta P, Bregenzer M, Raghavan S, Fleck EM, Horst EN, et al. Engineered 3d Model of Cancer Stem Cell Enrichment and Chemoresistance. *Neoplasia.* (2019) 21:822–36. doi: 10.1016/j.neo.2019.06.005
62. Mitra S, Tiwari K, Podicheti R, Pandhiri T, Rusch DB, Bonetto A, et al. Transcriptome Profiling Reveals Matrisome Alteration as a Key Feature of Ovarian Cancer Progression. *Cancers (Basel)* (2019) 11:1513. doi: 10.3390/cancers11101513
63. Paullin T, Powell C, Menzie C, Hill R, Cheng F, Martyniuk CJ, et al. Spheroid Growth in Ovarian Cancer Alters Transcriptome Responses for Stress Pathways and Epigenetic Responses. *PloS One* (2017) 12:e0182930. doi: 10.1371/journal.pone.0182930
64. Yoshimura A, Sawada K, Nakamura K, Kinose Y, Nakatsuka E, Kobayashi M, et al. Exosomal miR-99a-5p Is Elevated in Sera of Ovarian Cancer Patients and Promotes Cancer Cell Invasion by Increasing Fibronectin and Vitronectin Expression in Neighboring Peritoneal Mesothelial Cells. *BMC Cancer* (2018) 18:1065. doi: 10.1186/s12885-018-4974-57
65. Mahdy H, Casey MJ, Crotzer D. Endometrial Cancer. In: *StatPearls*. Treasure Island (FL: StatPearls (2021).
66. Bokhman JV. Two Pathogenetic Types of Endometrial Carcinoma. *Gynecol Oncol* (1983) 15:10–7. doi: 10.1016/0090-8258(83)90111-7
67. Murali R, Soslow RA, Weigelt B. Classification of Endometrial Carcinoma: More Than Two Types. *Lancet Oncol* (2014) 15:e268–78. doi: 10.1016/S1470-2045(13)70591-6
68. Van Nyen T, Moiola CP, Colas E, Annibali D, Amant F. Modeling Endometrial Cancer: Past, Present, and Future. *Int J Mol Sci* (2018) 19:2348. doi: 10.3390/ijms19082348
69. Grun B, Benjamin E, Sinclair J, Timms JF, Jacobs IJ, Gayther SA, et al. Three-Dimensional *In Vitro* Cell Biology Models of Ovarian and Endometrial Cancer. *Cell Prolif* (2009) 42(2):219–28. doi: 10.1111/j.1365-2184.2008.00579.x
70. Chitcholtan K, Asselin E, Parent S, Sykes PH, Evans JJ. Differences in Growth Properties of Endometrial Cancer in Three Dimensional (3D) Culture and 2D Cell Monolayer. *Exp Cell Res* (2013) 319:75–87. doi: 10.1016/j.yexcr.2012.09.012
71. Chitcholtan K, Sykes PH, Evans JJ. The Resistance of Intracellular Mediators to Doxorubicin and Cisplatin Are Distinct in 3D and 2D Endometrial Cancer. *J Transl Med* (2012) 10:38. doi: 10.1186/1479-5876-10-38
72. Rodriguez AC, Vahrenkamp JM, Berrett KC, Clark KA, Guillen KP, Scherer SD, et al. ETV4 Is Necessary for Estrogen Signaling and Growth in Endometrial Cancer Cells. *Cancer Res* (2020) 80:1234–45. doi: 10.1158/0008-5472.CAN-19-1382
73. Al-Juboori AAA, Ghosh A, Jamaluddin MFB, Kumar M, Sahoo SS, Syed SM, et al. Proteomic Analysis of Stromal and Epithelial Cell Communications in Human Endometrial Cancer Using a Unique 3d Co-Culture Model. *Proteomics.* (2019) 19:e1800448. doi: 10.1002/pmic.201800448
74. Tanaka R, Saito T, Ashihara K, Nishimura M, Mizumoto H, Kudo R. Three-Dimensional Coculture of Endometrial Cancer Cells and Fibroblasts in Human Placenta Derived Collagen Sponges and Expression Matrix Metalloproteinases in These Cells. *Gynecol Oncol* (2003) 90:297–304. doi: 10.1016/s0090-8258(03)00335-4
75. Collins A, Miles GJ, Wood J, MacFarlane M, Pritchard C, Moss E. Patient-Derived Explants, Xenografts and Organoids: 3-Dimensional Patient-Relevant Pre-Clinical Models in Endometrial Cancer. *Gynecol Oncol* (2020) 156:251–9. doi: 10.1016/j.ygyno.2019.11.020
76. Maru Y, Tanaka N, Itami M, Hippo Y. Efficient Use of Patient-Derived Organoids as a Preclinical Model for Gynecologic Tumors. *Gynecol Oncol* (2019) 154:189–98. doi: 10.1016/j.ygyno.2019.05.005
77. Siegel RL, Miller KD, Fuchs HE, Jemal A. Cancer Statistics, 2021. *CA Cancer J Clin* (2021) 71(1):7–33. doi: 10.3322/caac.21654
78. Weeber F, Ooft SN, Dijkstra KK, Voest EE. Tumor Organoids as a Pre-Clinical Cancer Model for Drug Discovery. *Cell Chem Biol* (2017) 24:1092–100. doi: 10.1016/j.chembiol.2017.06.012
79. Miller DH, Sokol ES, Gupta PB. 3d Primary Culture Model to Study Human Mammary Development. *Methods Mol Biol* (2017) 612:139–47. doi: 10.1007/978-1-4939-7021-6_10
80. dit Faute MA, Laurent L, Ploton D, Poupon MF, Jardillier JC, Bobichon H. Distinctive Alterations of Invasiveness, Drug Resistance and Cell-Cell Organization in 3D-Cultures of MCF-7, a Human Breast Cancer Cell Line, and its Multidrug Resistant Variant. *Clin Exp Metastasis* (2002) 19:161–8. doi: 10.1023/a:10145948255027
81. Gomes LR, Rocha CRR, Martins DJ, Fiore A, Kinker GS, Bruni-Cardoso A, et al. ATR Mediates Cisplatin Resistance in 3D-Cultured Breast Cancer Cells *via* Translesion DNA Synthesis Modulation. *Cell Death Dis* (2019) 10:459. doi: 10.1038/s41419-019-1689-8
82. Lovitt CJ, Shelper TB, Avery VM. Doxorubicin Resistance in Breast Cancer Cells Is Mediated by Extracellular Matrix Proteins. *BMC Cancer* (2018) 18:41. doi: 10.1186/s12885-017-3953-6
83. Urciuolo F, Garziano A, Imparato G, Panzetta V, Fusco S, Casale C, et al. Biophysical Properties of Dermal Building-Blocks Affects Extra Cellular Matrix Assembly in 3D Endogenous Macrotissue. *Biofabrication.* (2016) 8:15010. doi: 10.1088/1758-5090/8/1/015010
84. Brancato V, Gioiella F, Imparato G, Guarnieri D, Urciuolo F, Netti PA. 3D Breast Cancer Microtissue Reveals the Role of Tumor Microenvironment on

the Transport and Efficacy of Free-Doxorubicin In Vitro. *Acta Biomater* (2018) 75:200–12. doi: 10.1016/j.actbio.2018.05.055
85. Figueroa-Magalhães MC, Jelovac D, Connolly R, Wolff AC. Treatment of HER2-Positive Breast Cancer. *Breast.* (2014) 23:128–36. doi: 10.1016/j.breast.2013.11.011
86. Genuino AJ, Chaikledkaew U, The DO, Reungwetwattana T, Thakkinstian A. Adjuvant Trastuzumab Regimen for HER2-Positive Early-Stage Breast Cancer: A Systematic Review and Meta-Analysis. *Expert Rev Clin Pharmacol* (2019) 12:815–24. doi: 10.1080/17512433.2019.1637252
87. Yakes FM, Chinratanalab W, Ritter CA, King W, Seelig S, Arteaga CL. Herceptin-Induced Inhibition of Phosphatidylinositol-3 Kinase and Akt Is Required for Antibody-Mediated Effects on P27, Cyclin D1, and Antitumor Action. *Cancer Res* (2002) 62:4132–41.
88. Tatara T, Mukohara T, Tanaka R, Shimono Y, Funakoshi Y, Imamura Y, et al. 3d Culture Represents Apoptosis Induced by Trastuzumab Better Than 2D Monolayer Culture. *Anticancer Res* (2018) 38:2831–9. doi: 10.21873/anticanres.12528
89. Gangadhara S, Smith C, Barrett-Lee P, Hiscox S. 3D Culture of Her2+ Breast Cancer Cells Promotes AKT to MAPK Switching and a Loss of Therapeutic Response. *BMC Cancer* (2016) 16:345. doi: 10.1186/s12885-016-2377-z
90. Rodríguez CE, Berardi DE, Abrigo M, Todaro LB, Bal de Kier Joffé ED, Fiszman GL. Breast Cancer Stem Cells are Involved in Trastuzumab Resistance Through the HER2 Modulation in 3D Culture. *J Cell Biochem* (2018) 119:1381–91. doi: 10.1002/jcb.26298
91. Alqahtani FY, Aleanizy FS, El Tahir E, Alkahtani HM, AlQuadeib BT. Paclitaxel. *Profiles Drug Subst Excip Relat Methodol* (2019) 44:205–38. doi: 10.1016/bs.podrm.2018.11.001
92. Tietze R, Zaloga J, Unterweger H, Lyer S, Friedrich RP, Janko C, et al. Magnetic Nanoparticle-Based Drug Delivery for Cancer Therapy. *Biochem Biophys Res Commun* (2015) 468:463–70. doi: 10.1016/j.bbrc.2015.08.022
93. Lugert S, Unterweger H, Mühlberger M, Janko C, Draack S, Ludwig F, et al. Cellular Effects of Paclitaxel-Loaded Iron Oxide Nanoparticles on Breast Cancer Using Different 2D and 3D Cell Culture Models. *Int J Nanomed* (2018) 14:161–80. doi: 10.2147/IJN.S187886
94. Haniadka R, Rajeev AG, Palatty PL, Arora R, Baliga MS. Zingiber Officinale (Ginger) as an Anti-Emetic in Cancer Chemotherapy: A Review. *J Altern Complement Med* (2012) 18:440–4. doi: 10.1089/acm.2010.0737
95. Almada da Silva J, Becceneri AB, Sanches Mutti H, Moreno Martin AC, Fernandes da Silva MF, Fernandes JB, et al. Purification and Differential Biological Effects of Ginger-Derived Substances on Normal and Tumor Cell Lines. *J Chromatogr B Analyt Technol BioMed Life Sci* (2012) 903:157–62. doi: 10.1016/j.jchromb.2012.07.013
96. Fuzer AM, Lee SY, Mott JD, Cominetti MR. [10]-Gingerol Reverts Malignant Phenotype of Breast Cancer Cells in 3D Culture. *J Cell Biochem* (2017) 118:2693–9. doi: 10.1002/jcb.25906
97. Weaver VM, Lelièvre S, Lakins JN, Chrenek MA, Jones JC, Giancotti F, et al. Beta4 Integrin-Dependent Formation of Polarized Three-Dimensional Architecture Confers Resistance to Apoptosis in Normal and Malignant Mammary Epithelium. *Cancer Cell* (2002) 2:205–16. doi: 10.1016/s1535-6108(02)00125-3
98. Roberts S, Peyman S, Speirs V. Current and Emerging 3d Models to Study Breast Cancer. *Adv Exp Med Biol* (2019) 1152:413–27. doi: 10.1007/978-3-030-20301-6_22
99. Maman S, Witz IP. A History of Exploring Cancer in Context. *Nat Rev Cancer* (2018) 18:359–76. doi: 10.1038/s41568-018-0006-7
100. Karnoub AE, Dash AB, Vo AP, Sullivan A, Brooks MW, Bell GW, et al. Mesenchymal Stem Cells Within Tumour Stroma Promote Breast Cancer Metastasis. *Nature.* (2007) 449:557–63. doi: 10.1038/nature06188
101. Rijal G, Li W. 3D Scaffolds in Breast Cancer Research. *Biomaterials.* (2016) 81:135–56. doi: 10.1016/j.biomaterials.2015.12.016
102. Blache U, Horton ER, Xia T, Schoof EM, Blicher LH, Schönenberger A, et al. Mesenchymal Stromal Cell Activation by Breast Cancer Secretomes in Bioengineered 3D Microenvironments. *Life Sci Alliance* (2019) 2: e201900304. doi: 10.26508/lsa.201900304
103. Balachander GM, Rajashekar B M, Sarashetti P, Rangarajan A, Chatterjee K. MiRNomics Reveals Breast Cancer Cells Cultured on 3D Scaffolds Better Mimic Tumors in Vivo Than Conventional 2d Culture. *ACS Biomater Sci Eng* (2018) 4:116–27. doi: 10.1021/acsbiomaterials.7b00694
104. Kim TH, Woo JS, Kim YK, Kim KH. Silibinin Induces Cell Death Through Reactive Oxygen Species-Dependent Downregulation of Notch-1/ERK/Akt Signaling in Human Breast Cancer Cells. *J Pharmacol Exp Ther* (2014) 349:268–78. doi: 10.1124/jpet.113.207563
105. Yazdi Rouholamini SE, Moghassemi S, Maharat Z, Hakamivala A, Kashanian S, Omidfar K. Effect of Silibinin-Loaded Nano-Niosomal Coated With Trimethyl Chitosan on miRNAs Expression in 2D and 3D Models of T47D Breast Cancer Cell Line. *Artif Cells Nanomed Biotechnol* (2018) 46(3):524–35. doi: 10.1080/21691401.2017.1326928
106. Kopper O, de Witte CJ, Lõhmussaar K, Valle-Inclan JE, Hami N, Kester L, et al. An Organoid Platform for Ovarian Cancer Captures Intra- and Interpatient Heterogeneity. *Nat Med* (2019) 25:838–49. doi: 10.1038/s41591-019-0422-6
107. Boretto M, Maenhoudt N, Luo X, Hennes A, Boeckx B, Bui B, et al. Patient-Derived Organoids From Endometrial Disease Capture Clinical Heterogeneity and are Amenable to Drug Screening. *Nat Cell Biol* (2019) 21:1041–51. doi: 10.1038/s41556-019-0360-z
108. Girda E, Huang EC, Leiserowitz GS, Smith LH. The Use of Endometrial Cancer Patient-Derived Organoid Culture for Drug Sensitivity Testing Is Feasible. *Int J Gynecol Cancer* (2017) 27:1701–7. doi: 10.1097/IGC.0000000000001061
109. Nakajima A, Endo H, Okuyama H, Kiyohara Y, Kimura T, Kamiura S, et al. Radiation Sensitivity Assay With a Panel of Patient-Derived Spheroids of Small Cell Carcinoma of the Cervix. *Int J Cancer* (2015) 136:2949–60. doi: 10.1002/ijc.29349
110. Jardé T, Lloyd-Lewis B, Thomas M, Kendrick H, Melchor L, Bougaret L, et al. Wnt and Neuregulin1/ErbB Signalling Extends 3D Culture of Hormone Responsive Mammary Organoids. *Nat Commun* (2016) 7:13207. doi: 10.1038/ncomms13207
111. García-Davis S, Viveros-Valdez E, Díaz-Marrero AR, Fernández JJ, Valencia-Mercado D, Esquivel-Hernández O, et al. Antitumoral Effect of Laurinterol on 3D Culture of Breast Cancer Explants. *Mar Drugs* (2019) 7:201. doi: 10.3390/md17040201
112. Carter ME, Hartkopf AD, Wagner A, Brucker S Y, Berchtold S, Lauer UM, et al. A Three-Dimensional Organoid Model of Primary Breast Cancer to Investigate the Effects of Oncolytic Virotherapy. *Front Mol Biosci* (2022) 9:826302. doi: 10.3389/fmolb.2022.826302
113. Huch M, Knoblich JA, Lutolf MP, Martinez-Arias A. The Hope and the Hype of Organoid Research. *Development.* (2017) 144:938–41. doi: 10.1242/dev.150201
114. Weigelt B, Ghajar CM, Bissell MJ. The Need for Complex 3D Culture Models to Unravel Novel Pathways and Identify Accurate Biomarkers in Breast Cancer. *Adv Drug Deliv Rev* (2014) 69-70:42–51. doi: 10.1016/j.addr.2014.01.001
115. Fernández-Periáñez R, Molina-Privado I, Rojo F, Guijarro-Muñoz I, Alonso-Camino V, Zazo S, et al. Basement Membrane-Rich Organoids With Functional Human Blood Vessels are Permissive Niches for Human Breast Cancer Metastasis. *PloS One* (2013) 8:e72957. doi: 10.1371/journal.pone.0072957

Conflict of Interest: The authors declare that the research was conducted in the absence of any commercial or financial relationships that could be construed as a potential conflict of interest.

frontiers | Frontiers in Oncology

ORIGINAL RESEARCH
published: 16 June 2022
doi: 10.3389/fonc.2022.813158

Genomic Features of Solid Tumor Patients Harboring *ALK/ROS1/NTRK* Gene Fusions

Yinghuan Dai[1], Ping Liu[2], Wenlong He[3], Lizhen Yang[3], Yang Ni[4,5], Xuejiao Ma[4,5], Furong Du[4,5], Chao Song[4,5], Yang Liu[6]* and Yi Sun[1]**

[1] Department of Pathology, The Second Xiangya Hospital, Central South University, Changsha, China, [2] Department of Oncology, The Second Xiangya Hospital, Central South University, Changsha, China, [3] Department of Respiratory and Critical Care Medicine, The Second Xiangya Hospital, Central South University, Changsha, China, [4] State Key Laboratory of Translational Medicine and Innovative Drug Development, Jiangsu Simcere Diagnostics Co., Ltd., Nanjing, China, [5] Department of Medicine, Nanjing Simcere Medical Laboratory Science Co., Ltd., Nanjing, China, [6] Department of Thoracic Surgery, The First Affiliated Hospital of China Medical University, Shenyang, China

The fusions of receptor tyrosine kinase (RTK) involving anaplastic lymphoma kinase (*ALK*), c-ros oncogene 1 (*ROS1*), and neurotrophic receptor tyrosine kinase (*NTRK*) represent the potential targets of therapeutic intervention for various types of solid tumors. Here, the genomic features of 180 Chinese solid tumor patients with *ALK*, *ROS1*, and *NTRK* fusions by next generation sequencing (NGS) were comprehensively characterized, and the data from 121 patients in Memorial Sloan Kettering Cancer Center (MSKCC) database were used to compare. We found that *ALK*, *ROS1*, and *NTRK* fusions were more common in younger female patients ($p<0.001$) and showed a higher expression of programmed death ligand 1 (PD-L1). The gene-intergenic fusion and the fusion with rare formation directions accounted for a certain proportion in all samples and 62 novel fusions were discovered. Alterations in *TP53* and *MUC16* were common in patients with RTK fusions. The mutational signatures of patients were mainly distributed in COSMIC signature 1, 2, 3, 15 and 30, while had a higher frequency in copy number variations (CNVs) of individual genes, such as *IL-7R*. In the MSKCC cohort, patients with fusions and CNVs showed shorter overall survival than those with only fusions. Furthermore, the differentially mutated genes between fusion-positive and -negative patients mainly concentrated on MAPK signaling and FOXO signaling pathways. These results may provide genomic information for the personalized clinical management of solid tumor patients with *ALK*, *ROS1*, and *NTRK* fusions in the era of precision medicine.

Keywords: *ALK*, *ROS1*, *NTRK*, gene fusion, next generation sequencing, mutational signature, copy number variants, programmed death ligand 1

OPEN ACCESS

Edited by:
Ondrej Slaby, Central European Institute of Technology (CEITEC), Czechia

Reviewed by:
Pasqualino De Antonellis, University of Toronto, Canada
Guan Wang, Sichuan University, China

****Correspondence:***
Yi Sun
sunyixiangya2@126.com
Yang Liu
liuydoctor911@163.com
Chao Song
chao.song@simceredx.com

Specialty section:
This article was submitted to Cancer Genetics, a section of the journal Frontiers in Oncology

Received: *11 November 2021*
Accepted: *19 April 2022*
Published: *16 June 2022*

Citation:
Dai Y, Liu P, He W, Yang L, Ni Y, Ma X, Du F, Song C, Liu Y and Sun Y (2022) Genomic Features of Solid Tumor Patients Harboring ALK/ROS1/NTRK Gene Fusions. Front. Oncol. 12:813158. doi: 10.3389/fonc.2022.813158

INTRODUCTION

Chromosomal inversions, deletions or translocations leading to the constitutive activation of receptor tyrosine kinase (RTK) drive tumorigenesis across different malignancies (1, 2). The prevalence of RTK fusions involving anaplastic lymphoma kinase (*ALK*), c-ros oncogene 1 (*ROS1*), and neurotrophic receptor tyrosine kinase (*NTRK*) ranges from 0.3% to 5% in solid

tumors and tyrosine kinase inhibitors (TKIs) are the standard treatment modality for the first-line setting of patients with advanced cancer harboring such fusions (3–5). Currently, multiple *ALK* fusion partners have been identified, of which echinoderm microtubule-associated protein-like 4 (*EML4*) is the most frequent, with nine variants occurring in nearly 80% of all the *ALK* fusion cases of non-small cell lung cancer (NSCLC) (6–8). Meanwhile, many different 5′ gene partners have been identified in the fusion with 3′ regions of *ROS1*. These fusions are discovered in adult glioblastoma, paediatric glioma, NSCLC, and inflammatory myofibroblastic tumor (IMTs) (4, 9). Additionally, approximately 80 *NTRK* fusion partners have also been described (10, 11). Although the frequency of *NTRK* fusions is low, they are ubiquitous in rare cancer types, such as mammary analog secretory carcinoma and infantile fibrosarcoma (12–15).

In recent years, a lot of clinical trials on treatments targeting specific molecular mechanisms like *ALK*, *ROS1*, and *NTRK* fusions have been conducted. Small molecule inhibitors for *ALK*, *ROS1*, and *NTRK* fusions, such as crizotinib, brigatinib, lorlatinib, entrectinib and larotrectinib, have been approved by the US Food and Drug Administration (FDA) for different cancer types (16–20). Despite the potential benefit from identifying these fusions, it remains unclear whether the tumors with *ALK*, *ROS1*, and *NTRK* fusions represent a distinct, although rare, disease subtype that should be detected early for targeted therapy. Herein, a comprehensive study was carried out to characterize the molecular and clinicopathological characteristics, and prognosis of solid tumor patients with *ALK*, *ROS1*, and *NTRK* fusions.

MATERIALS AND METHODS

Sample Collection

In this study, the sequencing data of 7,537 solid tumor samples from the database of Simcere Diagnostics, Co. Ltd. (Nanjing, China) for genomic profiling between June 2019 and November 2020 were retrospectively analyzed, including lung cancer (n=3001), liver cancer (n=762), soft tissue sarcoma (n=281), bile duct carcinoma (n=232), esophageal cancer (n=155), breast cancer (n=154), melanoma (n=125), gallbladder carcinoma (n=121), bone tumor (n=59) and other unspecified tumors (n=2647) (**Table 1**). All patients signed written informed consents. The formalin fixed, paraffin-embedded (FFPE) tissue samples were selected for analysis, and peripheral blood samples were collected as the control. Here, 121 *ALK*, *ROS1*, and *NTRK* fusion-positive cancer patients from the MSK-IMPACT Clinical Sequencing Cohort (MSKCC, Nat Med 2017), which was composed of 10,945 samples, were used as the compared cohort.

DNA Extraction, Library Construction and Sequencing

DNA was extracted from unstained FFPE sections with more than 20% tumor cells according to the manufacturer's protocol. Library construction was performed using the KAPA Library Preparation kit. The concentration of the library was assessed using the Invitrogen Qubit4.0, and the inserted size was examined on the Agilent 4200 TapeStation. Next generation sequencing (NGS) was performed on the Illumina Novaseq 6000 system at an average depth of 1000X with a panel of 539 cancer-related genes (**Supplementary Table 1**). Genomic alterations,

TABLE 1 | Patients' characteristics according to the presence or absence of *ALK*, *ROS1*, and *NTRK* fusions.

Characteristics	ALK/ROS1/NTRK fusion negative (n=7357)	ALK/ROS1/NTRK fusion positive (n=180)	*p*	ALK fusion positive (n=103)	*p*	ROS1 fusion positive (n=40)	*p*	NTRK fusion positive (n=37)	*p*
Age, years*			0.0002		0.0166		0.0091		0.1514
Median	61	55		57		53.5		56.5	
Range	0-107	3-83		15-82		32-77		3-83	
Gender**			0.0137		0.1906		0.0006		0.8671
Female	2949	89		48		27		14	
Male	4404	91		55		13		23	
Pathology			<0.0001		<0.0001		0.0005		<0.0001
Bile duct carcinoma	229	3		0		1		2	
Bone tumor	56	3		1		0		2	
Breast cancer	152	2		0		0		2	
Esophageal cancer	153	2		1		1		0	
Gallbladder carcinoma	118	3		0		0		3	
Lung cancer	2865	136		93		33		10	
Liver cancer	757	5		0		1		4	
Melanoma	122	3		0		1		2	
Soft tissue sarcoma	270	11		6		0		5	
Others	2635	12		2		3		7	

*The values of p were based on Fisher's exact test or Mann-Whitney tests. *In terms of age, the total number of patients was 7260 due to lack of information. **Regarding the gender, the total number of patients was 7533 due to lack of information.*

including single nucleotide variants (SNVs), copy number variations (CNVs), small insertions, deletions and gene arrangements were covered. The tumor mutation burden (TMB) and microsatellite status (MSI) were also calculated by NGS.

Statistical Analysis

The Fisher's exact test and Mann-Whitney test were used to assess the association of *ALK*, *ROS1*, and *NTRK* fusions with age, gender, and cancer types. To assess the probability of gene fusions in various cancer types, odds ratios (ORs) and relative 95% confidence intervals (CIs) were calculated. The overall survival (OS) was analyzed using the Kaplan-Meier method, and survival curves (mutational signature, SNVs, and CNVs) were compared using the log-rank test. Fisher's exact test was used to evaluate the association of genomic characteristics with the proportion of PD-L1 expression, with 1% and 50% as the cutoff value. All statistical tests were two-sided, and $p < 0.05$ was considered statistically significant.

RESULTS

Patient Characteristics

There were 103 (1.37%) cases harboring *ALK* rearrangements in 7,537 solid tumor patients, including lung cancer (n=93), soft tissue sarcoma (n=6), bone tumor (n=1), esophagus cancer (n=1) and other unspecified tumors (n=2). *ROS1* rearrangements were detected in 40 cases (0.53%), among whom 33 cases suffered from lung cancer (**Table 1**). 37 cases (0.49%) harbored *NTRK* fusions, including 9 cases of *NTRK1* fusions, 2 cases of *NTRK2* fusions, and 26 cases of *NTRK3* fusions.

Through NGS, a total of 180 patients were found to harbor *ALK/ROS1/NTRK* fusions and were set as *ALK/ROS1/NTRK* fusion-positive group (n=180), while those without *ALK/ROS1/NTRK* fusions were as *ALK/ROS1/NTRK* fusion-negative group (n=7357). As shown in **Table 1**, *ALK/ROS1/NTRK* fusions were more common in young patients ($p<0.001$). However, no age bias was presented in patients with *NTRK* fusion ($p>0.05$). There was a higher *ALK/ROS1/NTRK* fusion-positive frequency in females than males ($p=0.0137$), and subgroup analysis further showed that the *ROS1* fusion-positive rate in females was significantly higher than that in males ($p=0.0006$), but not *ALK* fusion ($p=0.1906$) and *NTRK* fusion ($p=0.8671$). The incidence of RTK fusions in soft tissue sarcoma and bone tumor was significantly higher than that in liver cancer ($p<0.05$). Meanwhile, the rates of RTK fusions in bile duct carcinoma and liver cancer was much lower than that in lung cancer ($p<0.05$, OR=0.285) (**Supplemental Figure 1**).

Molecular Features of *ALK* Fusion-Positive Tumors

Of 103 *ALK* fusion-positive samples, a total of 491 variants were identified, including frame InDel, missense mutations, nonsense mutations and splicing mutations. *TP53* alterations (26%) were the most common, followed by *MUC16* (11%), *HUWE1* (10%), *ARID2* (10%), and *ALK* (10%). Other genomic alterations included *NOTCH3* (6%), *MTOR* (6%), *KMT2C* (6%), *KDM5C* (6%), and *DICER1* (6%) (**Figure 1A**). The median TMB was 2.21 mut/Mb (0-33.82 mut/Mb). Although MSI status was available in 47% of patients, there was a higher proportion of microsatellite stability (MSS) in the tumors bearing *ALK* fusions. In the MSKCC cohort, totally 94 mutations occurred in 53 *ALK* fusion-positive cases, suggesting *TP53* and *ALK* were the most frequently altered genes (**Figure 1B**).

Analysis of mutational signatures showed that C>T transition were the most common, followed by C>A and C>G transitions (**Figure 1C**). The probability of T>G and T>A transitions was the lowest, consistent with COSMIC signature 1 identified in most cancer samples. Accordingly, our results were highly in accordance with MSKCC findings that C>T transition was the most frequently mutation (**Figure 1D**). Additionally, the breakpoints corresponding to *ALK* fusion in the sequencing data of these patients were also identified. Most of breakpoints were located at the intron between exon 19 and exon 20 of *ALK* gene. In the *ALK* cohort, *EML4-ALK* fusion accounted for 67%, *ALK-EML4* fusion for 6%, and others for the remaining 27%. Coexistence of these fusions was present in 26 patients (25%). 89 out of 103 patients had an *EML4-ALK* fusion, with variant 1 (v1, E13:A20), variant 2 (v2, E20:A20), variant 3 (v3, E6:A20) and variant 5 (v5, E2:A20) detected in 31, 8, 37 and 1 patients, respectively (**Figure 1E**). Sixteen novel *ALK* fusion partners identified were shown in **Supplementary Table 2**.

Notably, in our cohort, the mutations at the site of *ALK* resistance were detected. The gatekeeper L1196M (4/103) was present in crizotinib-resistant cases, while the solvent-front *G1202R* mutation (2/103) was highly resistant to crizotinib, as well as to next-generation ALK inhibitors (21).

Molecular Features of *ROS1* Fusion-Positive Tumors

Genomic alterations in *ROS1* fusion-positive samples (n=40) were shown in **Figure 2A**. The median TMB was 2.94 mut/Mb with a range of 0-25 mut/Mb. 61% of *ROS1* fusion-positive tumors harboring MSI data showed MSS, while only one case showed MSI-L. The frequency of *TP53* mutations was obviously the highest (54%), followed by *MUC16* (29%), *LRP18* (14%), *FAT1* (14%), *CARD11* (14%), and *ARID18* (14%) mutations. We further compared our results with the MSKCC cohort that included 43 *ROS1* fusion-positive cases harboring 155 mutations. *TP53* was the most frequently altered gene in the MSKCC cohort, followed by *MLL2* instead of *MUC16* (**Figure 2B**). Analysis of their mutational signatures showed that C>T transition was the most prevalent, followed by T>A and T>C transitions (**Figure 2C**). The T>G transition showed the lowest frequency. This pattern was also consistent with COSMIC signature 1. Moreover, C>T transition also occurred most frequently in the MSKCC cohort (**Figure 2D**).

Then we identified the breakpoints and partner genes of the *ROS1* fusion in the sequencing data of these patients. In our cohort, *CD74* was the most common *ROS1* fusion partner (33%), followed by *EZR* (25%), *SDC4* (8%), *TPM3* (6%) and more (**Figure 2E**). *ROS1* fusions were formed *via* intra chromosomes, most frequently occurring in *ROS1* introns 31, 32, 33, while less

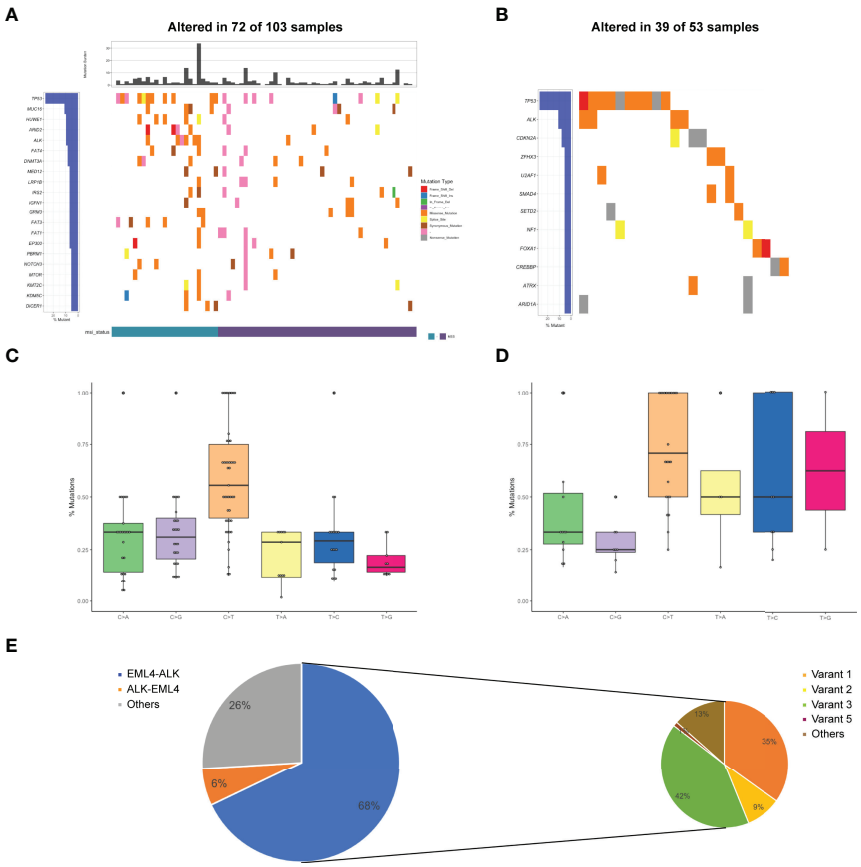

FIGURE 1 | Mutational profiles and partners of *ALK* fusion-positive patients. **(A)** The oncoprint of the somatic SNVs in 103 patients harboring *ALK* fusion in our study. **(B)** The oncoprint of the somatic SNVs in 53 patients harboring *ALK* fusion in the MSKCC database. **(C)** Mutational signatures of *ALK* fusion-positive patients in our cohort. **(D)** Mutational signatures of *ALK* fusion-positive patients in the MSKCC cohort. **(E)** Distribution of *ALK* fusion partners and *EML4-ALK* variants. MSI, microsatellite instability.

frequently in other exons and introns (**Figure 2F**). Meanwhile, *ROS1* most frequently fused to intron 6 of *CD74*, intron 9 of *EZR*, intron 2 of *SDC4*, and intron 7 of *TPM3* (**Figure 2G**). We also identified 11 novel *ROS1* fusion partners (**Supplementary Table 2**). Mutations resulting in substitutions at solvent-front residues (G2032R) of *ROS1* were identified in one *CD74-ROS1* fusion case. The *G2032R* mutation had been reported to introduce steric hindrance and diminish high-affinity crizotinib binding (22).

Molecular Features of *NTRK* Fusion-Positive Tumors

Among 37 *NTRK* fusion-positive cases (0.49%, 37/7537), 479 variants were totally identified in our cohort (**Figure 3A**). The median TMB was 4.41 mut/Mb, with the peak value of 93.38 mut/Mb. In the cases with MSI data, only one case bearing rearrangements was MSI-H and the others were MSS.

The heatmap of somatic mutations showed that *TP53* was the most altered gene (81%), followed by *MUC16* (33%), *TERT* (22%), *LRP1B* (22%), *SPTA1* (19%), *SMARCA4* (19%), *FAT1* (19%), and *EGFR* (19%) mutations. By analysis of the MSKCC cohort that comprised 25 *NTRK* fusion-positive cases harboring 299 mutations, *TP53* was also found to be the most frequently altered gene, followed by *SYK* but not *MUC16* (**Figure 3B**). Analysis of the mutational signatures showed that C>T transition occurred most frequently, followed by C>A transition (**Figure 3C**). The other transitions were at a low frequency. As shown in **Figure 3D**, the frequency of C>T transition in the MSKCC cohort was the highest, even higher than ours, which might be associated with different ethnicities and diets.

The positive rates of *NTRK* fusions were generally low in a wide range of cancers and tended to be enriched among rare cancers. By analyzing its partner genes, we found the proportion of *NTRK3* partner genes was the highest (76%), followed by *NTRK1* (17%), and *NTRK2* (7%). Meanwhile, 35 novel *NTRK* fusions were identified (**Supplementary Table 2**). Notably, *G709C* mutation resulting in amino acid substitutions was identified in the *QKI-NTRK2* fusion case, which involved the regions of the xDFG motif and was paralogous to *G1269* (*ALK*) substitutions (23).

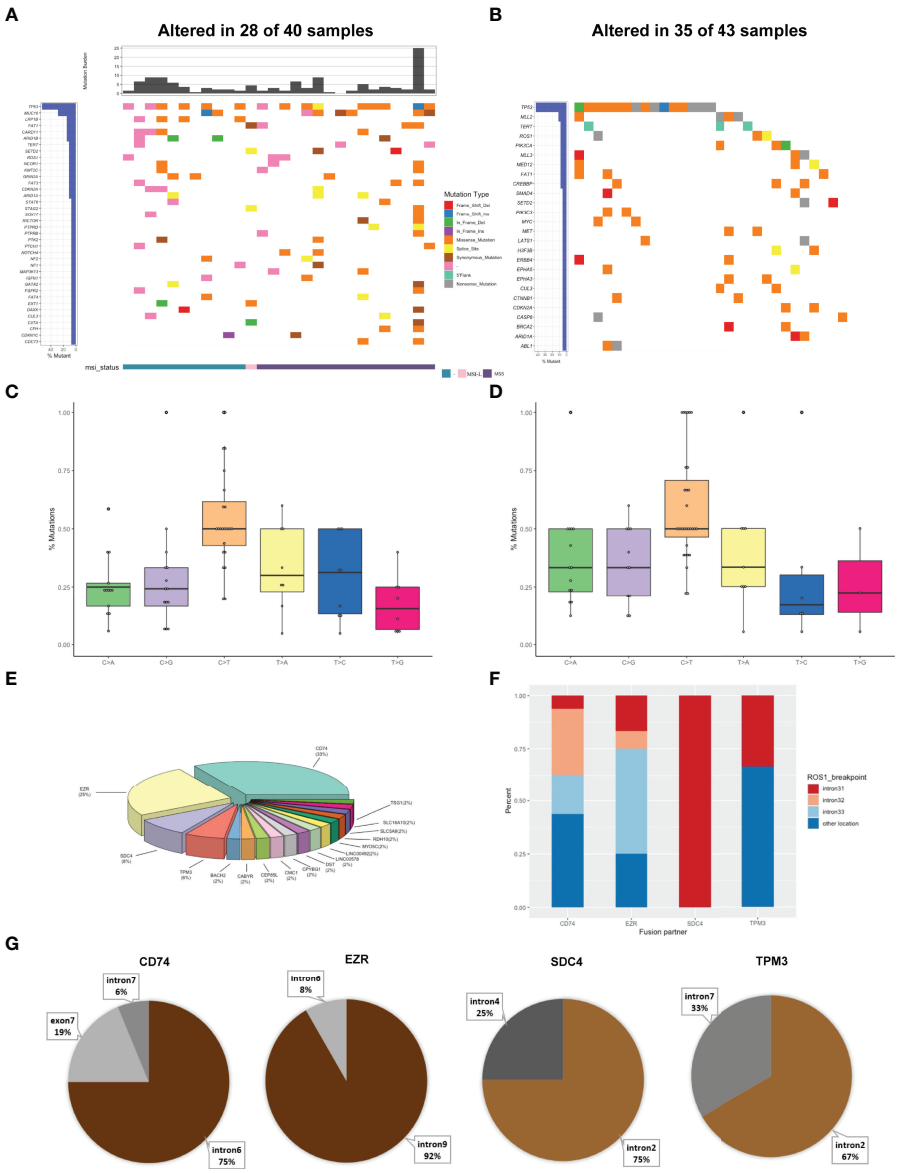

FIGURE 2 | Mutational profiles and partners of *ROS1* fusion-positive patients. **(A)** The oncoprint of the somatic SNVs in 40 patients harboring *ROS1* fusion in our study. **(B)** The oncoprint of the somatic SNVs in 43 patients harboring *ROS1* fusion in the MSKCC database. **(C)** Mutational signatures of *ROS1* fusion-positive patients in our cohort. **(D)** Mutational signatures of *ROS1* fusion-positive patients in the MSKCC cohort. **(E)** Distribution of *ROS1* fusion partners. **(F)** Distribution of fusion breakpoint positions in the most common *ROS1* fusions including *CD74-ROS1*, *EZR-ROS1*, *SDC4-ROS1*, and *TPM3-ROS1*. **(G)** Distribution of breakpoint locations for *ROS1* fusion partner genes, including *CD74*, *EZR*, *SDC4*, and *TPM3*.

Classification of *ALK*, *ROS1*, and *NTRK* Fusion Events

As shown in **Figure 4A**, a total of 225 gene fusions were identified in 180 samples, in which coexistence was present in 41 cases. These fusions occurred mostly in chromosomes, with a few occurring between adjacent chromosomes (**Figure 4B**). These fusions were classified into two categories based on the genome annotation containing the breakpoint regions (**Figure 4C**): gene-gene (91.1%) and gene-intergenic (8.9%). The gene-intergenic fusions accounted for 3.1% of *ALK* fusions, 6.3% of *ROS1* fusions, and 28.2% of *NTRK* fusions. Based on the gene breakpoint regions, we discovered 14% fusions harboring rare fusion directions, namely "upstream-upstream-breakpoint" cases (8%) and "downstream-downstream-breakpoint" cases (6%) (**Figure 4D**). Due to lack of chimeric transcripts, they were set aside in most fusion analyses as being unlikely to be functionally relevant.

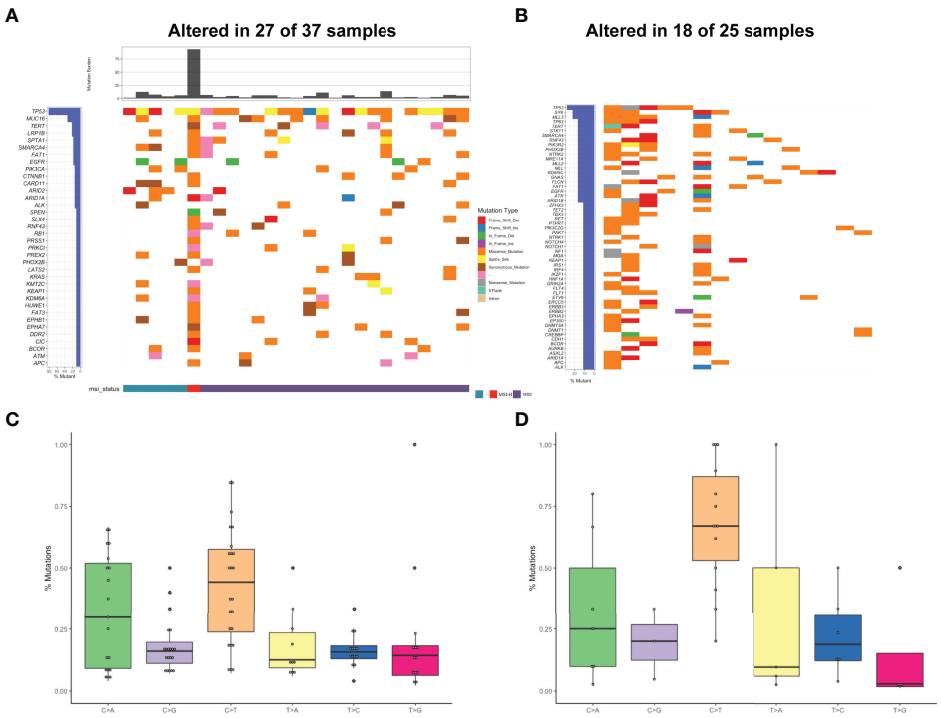

FIGURE 3 | Mutational profiles and partners of *NTRK* fusion-positive patients. **(A)** The oncoprint of the somatic SNVs in 37 patients harboring *NTRK* fusion in our study. **(B)** The oncoprint of the somatic SNVs in 25 patients harboring *NTRK* fusion in the MSKCC database. **(C)** Mutational signatures of *NTRK* fusion positive patients in our cohort. **(D)** Mutational signatures of *NTRK* fusion-positive patients in the MSKCC cohort.

Impacts of *ALK*, *ROS1*, and *NTRK* Positivity on the Prognosis

In this study, we used Signature Multivariate Analysis (SigMA), a computational tool, to call the mutational signatures, which could accurately detect the mutational signatures associated with homologous recombination deficiency from targeted gene panels (24). Using deconstructSigs R package to extract the mutational signatures, we identified the presence of signature 1 (Sig 1) in 18.2% (22/121), signature 3 (Sig 3) in 11.6% (14/121), signature 30 (Sig 30) in 9.9% (12/121), and signature 2 in 9% (11/121) of the patients in our cohort (**Figure 5A**). Likewise, Sig 1, signature 7 (Sig 7), signature 15 (Sig 15), and Sig 30 were detected in 25.8% (24/93), 6.5% (6/93), 8.6% (8/93), and 6.5% (6/93) of the MSKCC samples, respectively (**Figure 5B**).

A previous study indicated that Sig 3 positivity was indicative of clinical benefits (25), so we analyzed the association of Sig 1, Sig 7, Sig 15, and Sig 30 positive patients with clinical benefits. Sig 1 and Sig 15 were apparently not associated with prolonged OS (**Figure 5B**). Sig 7 and Sig 30 positive patients showed slightly longer OS than others, but without statistical significance. Interestingly, some fusion samples were absent of SNVs. On this basis, we examined whether fusion-positive samples without SNVs could indicate clinical benefits. Unfortunately, the absence of SNVs did not make a significant difference in OS (**Supplemental Figure 2A**).

CNVs in Patients With *ALK*, *ROS1*, and *NTRK* Fusions

CNVs were found in 50% of 180 samples. About 11% of the patients in our cohort harbored *MYC* CNVs, which may be a candidate for tumor genesis and progression (26). In addition, CNVs of *CDKN2A*, *CDKN2B*, *MCL1*, *MDM2*, and *IRS2* have been reported to be associated with prognosis (27–31). CNVs of these genes were also found in fusion-positive samples from the MSKCC database (**Figure 6**). Interestingly, we found that CNVs of *IL7R* showed a high frequency. Moreover, the CNVs in fusion-positive samples were related to poor prognosis (p=0.01) (**Supplemental Figure 2B**), which needed more data to verify.

PD-L1 Expression in *ALK*, *ROS1*, and *NTRK* Fusion-Positive Tumors

Over-expression of *ALK* fusion protein increased PD-L1 expression, while anti-PD-1 antibody (immunotherapy) was effective in both crizotinib sensitive and resistant NSCLC cells (32). Hence, we examined the expression of PD-L1 in our cohort. A total of 3337 patients were eligible after excluding those without PD-L1 expression. PD-L1 immunohistochemistry testing was performed using the SP263 antibody. In our cohort, PD-L1 expression was higher in tumors with *ALK* (p=0.0017) and *ROS1* (p=0.0036) fusions than fusion-negative tumors at 1% cutoff. However, PD-L1 expression between *NTRK*

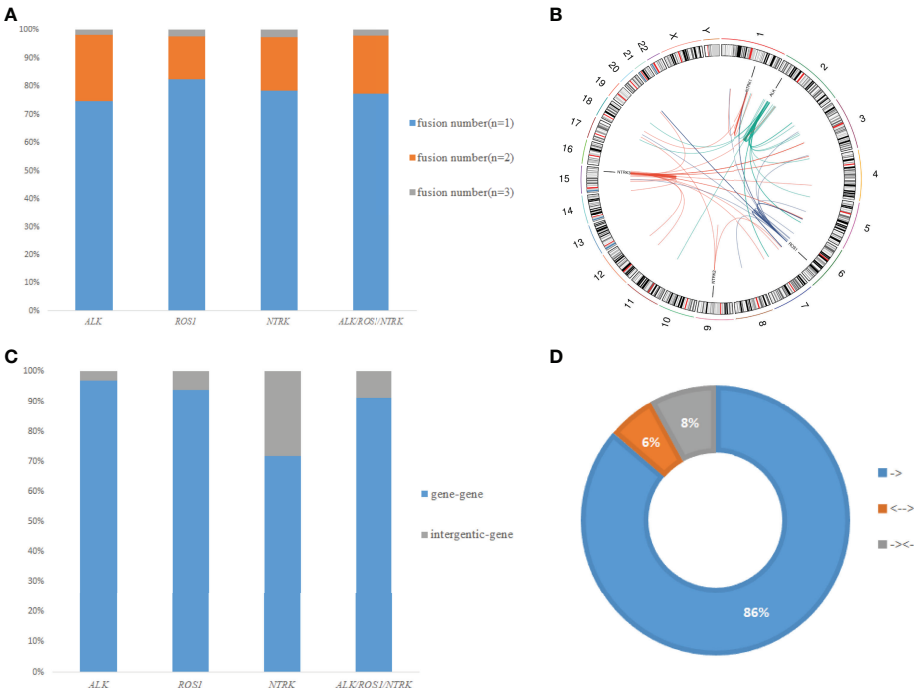

FIGURE 4 | Classification of fusion events. **(A)** Distribution of different fusion numbers (n=1, 2, 3) in our study. **(B)** A circos plot of 225 gene fusions identified in all patients. **(C)** Distribution of different fusion types (gene-gene and gene-intergenic). **(D)** Distribution of fusions with different formation directions.

fusion-positive and -negative tumors showed no statistical difference (p=0.052). RTK fusions including *ALK*, *ROS1*, and *NTRK* exhibited a higher PD-L1 expression than fusion-negative tumors (p<0.0001). Using ≥50% cutoff, a higher PD-L1 positivity was also observed in tumors with *ALK* (p=0.0484), but not *ROS1* (p=0.2827), *NTRK* (p=1), or RTK fusions (p=0.0961) (**Table 2**). These results indicated that PD-L1 expression from different RTK fusion-positive tumors may have different predictive values for benefiting from immune checkpoint inhibitors (ICIs) in solid tumors.

Aberrations in Relevant Signaling Pathways

The signaling pathway analysis of *NTRK/ROS1/ALK* fusion-positive and -negative patients exhibited significant dysregulations in well-defined pathways, namely MAPK and FOXO pathways (**Figure 7**). According to prior reports, MAPK pathway regulates cell proliferation, differentiation, apoptosis, and migration, while FOXO signaling pathway is related to cell cycle, apoptosis, autophagy, metabolism, oxidation, immune response, and stem cell maintenance (33, 34). We found that the MAPK signaling pathway was altered in 60% of fusion-positive patients and 57.9% of negative patients. Fusion-positive patients had a higher frequency of mutations in *EML4*, *ALK*, *FGF10*, and *HRAS*, while the rates of *EGFR*, *ERBB2*, and *KRAS* were higher in fusion-negative patients. Differential frequencies of *IRS2*, *IL7R*, and *PLK1* mutations resulted in dysregulation of the FOXO1 signaling pathway between these two groups.

DISCUSSION

By analyzing the genomic landscape of patients with *ALK*, *ROS1*, and *NTRK* fusions, a relatively high frequency of *TP53* mutation, MSS status, and different TMB levels (*NTRK*>*ALK*/*ROS1*) were found, supported by previous studies (7, 9, 35, 36). In our cohort, the frequency of *MUC16* mutations was secondary to *TP53*. *MUC16* mutations appeared to be associated with the therapeutic and prognostic factors and were expected to be a biomarker to guide immunotherapy (37, 38). In terms of mutational signatures, *ALK*, *ROS1*, and *NTRK* fusion-positive patients showed similar point mutant characteristics, and the C>T transition was most common, followed by C>A transition. This pattern was consistent with COSMIC Sig 1 that had been found in most cancer types (39). Furthermore, survival curves suggested that Sig 7 and Sig 30 may be associated with a favorable prognosis in some way, which needed more data to verify.

Accumulating evidence has suggested that CNVs might be a potential biomarker or prognostic factor for tumor treatment. Apart from the genes with a high frequency of copy number amplification, such as *MYC* and *MDM2*, we identified some genes with copy number loss, such as *CDKN2A* and *CDKN2B*. *CDKN2A/B* deletions were independent prognostic markers for

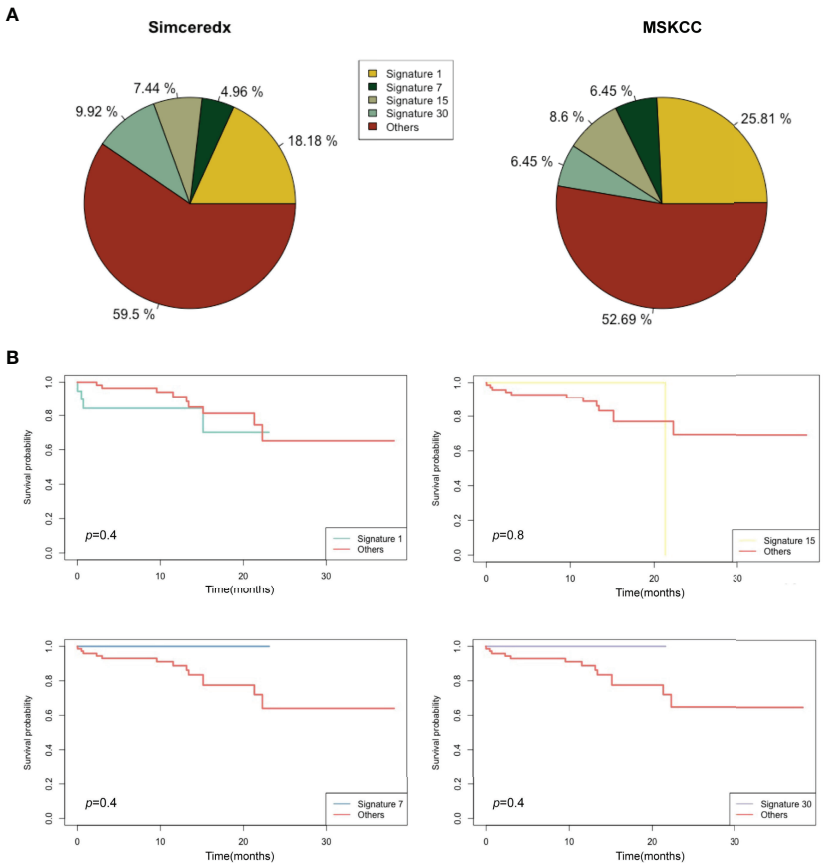

FIGURE 5 | Mutational signatures of *ALK/ROS1/NTRK* fusion-positive patients. **(A)** Distribution of mutational signatures in all patients harboring *ALK/ROS1/NTRK* fusions in our study and that from the MSKCC database. **(B)** Kaplan-Meier graph for survival probability according to Sig 1, Sig 7, Sig 15, and Sig 30 status.

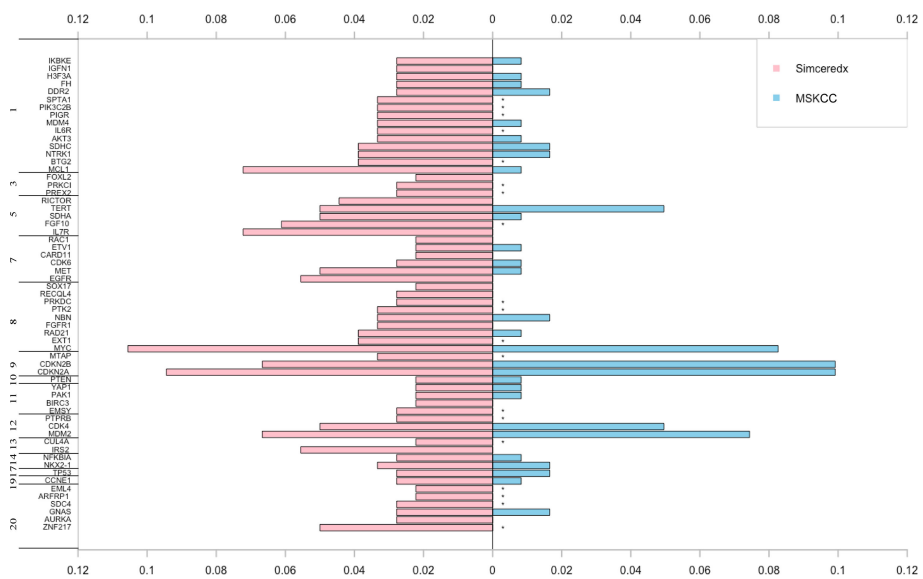

FIGURE 6 | The pink and blue bars represent CNV events occurring in *ALK/ROS1/NTRK* fusion-positive patients in our cohort and MSKCC cohort, respectively. *represents the genes not covered in the MSKCC panel.

TABLE 2 | Summary of PD-L1 expression in patients with *ALK*, *ROS1*, and *NTRK* fusions, n (%).

Variables		1% Cutoff			50% Cutoff		
		≥1%	<1%	*p*	≥50%	<50%	*p*
ALK fusion	Positive	23 (63.89)	13 (36.11)	0.0017	6 (16.67)	30 (83.33)	0.0484
	Negative	1246 (32.99)	2055 (67.01)		244 (7.39)	3057 (92.61)	
ROS1 fusion	Positive	11 (78.57)	3(21.43)	0.0036	2 (14.29)	12 (85.71)	0.2827
	Negative	1258 (37.86)	2065 (62.14)		248 (7.46)	3075 (92.54)	
NTRK fusion	Positive	11 (61.11)	7 (38.89)	0.0520	1 (5.56)	17 (94.44)	1.0000
	Negative	1258 (37.90)	2061 (62.10)		249 (7.50)	3070 (92.50)	
ALK/ROS1/NTRK fusion	Positive	45 (66.18)	23 (33.82)	<0.0001	9 (13.24)	59 (86.76)	0.0961
	Negative	1224 (37.44)	2045 (62.56)		241 (7.37)	3028 (92.63)	

The values of p were based on Fisher's exact test.

both adult and paediatric lymphoblastic leukaemia (40). *MDM2* amplification was associated with poor clinical outcomes and significantly increased tumor growth rates with anti-PD-1/PD-L1 immunotherapy (41). This information is important for guiding clinical treatment. We observed that fusion-positive patients without CNVs had a favorable prognosis. Notably, the pathogenic *IL-7R* CNVs exist in 7% of Chinese patients with fusions, which is higher than that in the Western population (0%). *IL7R* was previously reported to be amplified in various cancers, with the function of mediating potential tumor promotion, and high levels of *IL-7R* may be associated with poor prognosis (42). Currently, the risk factors for *IL-7R*-mutant fusions are unknown. Future studies should focus on how diet and ethnic differences increase the risk of *IL-7R* mutations.

Of the 180 fusion-positive samples by NGS, *EML4* and *CD74* were the most common *ALK* and *ROS1* fusion partners, respectively. *EML4-ALK* occurred mainly in the forms of three variants: variant 1, variant 2, and variant 3 (43, 44). Diverse *ROS1* fusion partners were identified, and the top four fusion partners were *CD74*, *EZR*, *SDC4*, and *TPM3*. As the most common ROS1 fusion partner, CD74 had a frequency similar to the previous ones (9, 45). There were no high-frequency partner genes occurring in *NTRK* fusions, which might be related to the high incidence of *NTRK* fusions in rare tumors. We also detected some novel *ALK/ROS1/NTRK* fusion partners, such as *LPIN1* and *SMARCC1* (*ALK*), *SLC16A10* and *CRYBG1* (*ROS1*), *SDK1* and *GYPA* (*NTRK3*). These results suggested that the NGS-based evaluation for *ALK/ROS1/NTRK* fusions was accurate and comprehensive. Compared with traditional methods, such as IHC, FISH, and Sanger sequencing, NGS had unique advantages in detecting unknown fusion partners and identifying accurate breakpoints. However, the rare fusions remain clinically interesting, further studies are needed to confirm these observations in preclinical and clinical studies.

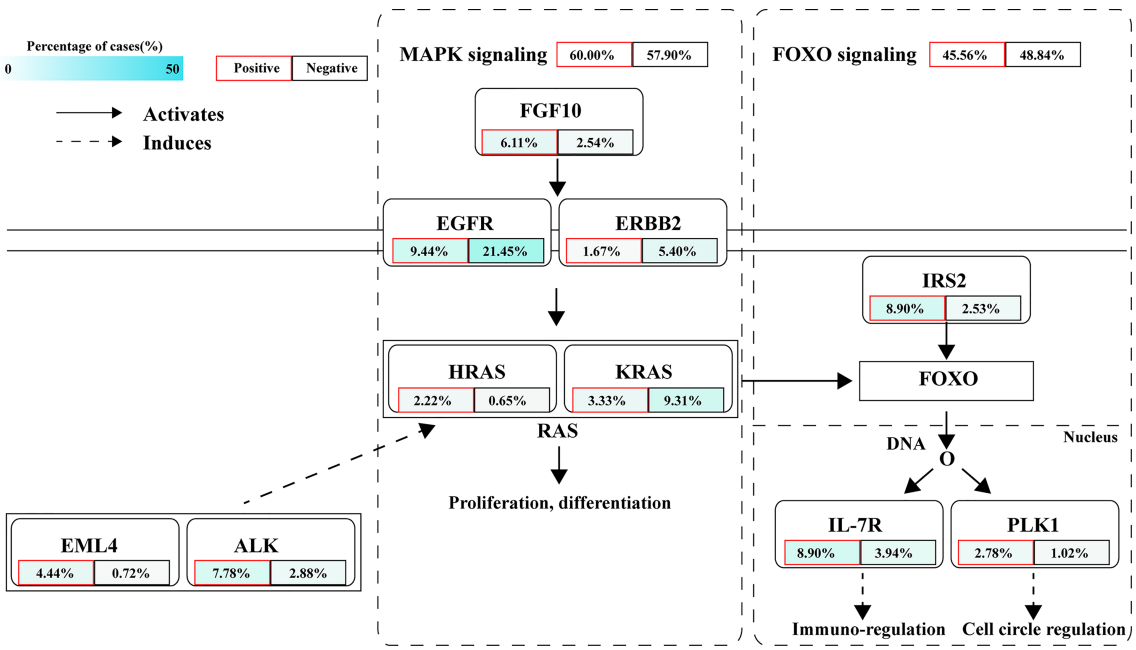

FIGURE 7 | Frequently deregulated signaling pathways in *ALK/ROS1/NTRK* fusion-positive patients.

A previous study reported the impacts of gene-intergenic and intergenic-intergenic fusions on the upregulation of their target genes (46). Therefore, we classified the fusions in our cohort into two categories: gene-gene fusion and gene-intergenic fusion. Neither intergenic sequence-*ALK* nor coexistence of fusions showed a significant effect on the benefit from crizotinib treatment (47). However, a substantial portion of chimeric transcripts was produced by gene-intergenic fusions. The impact of such intergenic breakpoints on transcriptome has been unclear. Meanwhile, these fusions with rare fusion directions mostly coexisted with classic fusions, and their clinical significance was currently unknown, even though a portion of them harboring kinase domains. Future research may focus on investigating the clinical role of gene-intergenic fusions and fusions with rare fusion directions in cancers.

PD-L1 protein expression in tumor cells emerged as the first potential predictive biomarker for sensitivity to ICIs (48). In our cohort, 44.27% of the patients had clinically relevant information in PD-L1 expression. Consistent with the literature, we observed a significantly higher expression of PD-L1 in the *ALK* fusion-positive cohort. Of note, the expression of PD-L1 in the *ROS1* or *NTRK* fusion-positive cohort was similar to that in the fusion-negative cohort. However, other data suggested that immune escape may confer a higher PD-L1 expression in NSCLC patients with an aggressive tumor phenotype, leading to a poor prognosis with TKI therapy (40). Moreover, the differentially mutated genes between fusion-positive and fusion-negative samples were mainly enriched in the MAPK and FOXO signaling pathways. The mutational frequency of individual gene varied greatly between fusion-positive and fusion-negative samples, but with similar mutational frequency in the whole signaling pathways.

In conclusion, we characterized the genomic landscape of solid tumor patients with *ALK*, *ROS1*, and *NTRK* fusions and 62 novel fusions were discovered, which may provide more clinically actionable targets for cancer therapy to a great extent. Although the gene-intergenic fusion and fusion with rare fusion directions accounted for a certain proportion of all fusion samples, the clinical significance of these fusions remained to be unclear, thus RTK-targeted therapy should be explored further in solid tumors in the future. Notably, the frequency of CNVs was high and associated with a poor prognosis in fusion-positive patients, highlighting the importance of CNVs as a potential biomarker or prognostic factor for cancer therapy. PD-L1 high-expression was more common in the *ALK* fusion-positive cohort than that in the fusion-negative cohort, leading us to hypothesize that ICIs might bring clinical benefits to the solid tumor patients harboring RTK fusions. Collectively, all these findings may provide genomic information for personalized clinical management of patients with *ALK*, *ROS1*, and *NTRK* fusions in the era of precision medicine.

DATA AVAILABILITY STATEMENT

The datasets presented in this study can be found in online repositories. The names of the repository/repositories and accession number(s) can be found below: GenBank, submission #2562890.

ETHICS STATEMENT

Ethical review and approval was not required for the study on human participants in accordance with the local legislation and institutional requirements. The patients/participants provided their written informed consent to participate in this study.

AUTHOR CONTRIBUTIONS

YD, CS, YL and YS contributed to conception and design of the study. YD wrote the first draft of the manuscript. PL, WH, LY wrote sections of the manuscript. YN, XM and FD organized the database and performed the statistical analysis. CS, YL and YS contributed to edit and review the manuscript. All authors approved the submitted version.

FUNDING

This study was supported by Hunan Principal Project "The molecular mechanism of the reversion of glioma differentiation induced by Toll-like receptor 4 activation of Notch signal pathway" (ID: 2019JJ40422).

SUPPLEMENTARY MATERIAL

The Supplementary Material for this article can be found online at: https://www.frontiersin.org/articles/10.3389/fonc.2022.813158/full#supplementary-material

REFERENCES

1. Stransky N, Cerami E, Schalm S, Kim JL, Lengauer C. The Landscape of Kinase Fusions in Cancer. *Nat Commun* (2014) 5:4846. doi: 10.1038/ncomms5846
2. Shaw AT, Hsu PP, Awad MM, Engelman JA. Tyrosine Kinase Gene Rearrangements in Epithelial Malignancies. *Nat Ret Cancer* (2013) 13:772–87. doi: 10.1038/nrc3612
3. Chia PL, Mitchell P, Dobrovic A, John T. Prevalence and Natural History of ALK Positive Non-Small-Cell Lung Cancer and the Clinical Impact of Targeted Therapy With ALK Inhibitors. *Clin Epidemiol* (2014) 6:423–32. doi: 10.2147/CLEP.S69718
4. Drilon A, Jenkins C, Iyer S, Schoenfeld A, Keddy C, Davare MA. ROS1-Dependent Cancers- Biology, Diagnostics and Therapeutics. *Nat Ret Clin Oncol* (2021) 18:35–55. doi: 10.1038/s41571-020-0408-9
5. Okamura R, Boichard A, Kato S, Sicklick JK, Bazhenova L, Kurzrock R. Analysis of NTRK Alterations in Pan-Cancer Adult and Pediatric Malignancies: Implications for NTRK-Targeted Therapeutics. *JCO Precis Oncol* (2018) 2018:PO.18.00183. doi: 10.1200/PO.18.00183

6. Sabir SR, Yeoh S, Jackson G, Bayliss R. EML4-ALK Variants: Biological and Molecular Properties, and the Implications for Patients. *Cancers* (2017) 9:118. doi: 10.3390/cancers9090118
7. Liu S, Huang T, Liu M, He W, Zhao Y, Yang L, et al. The Genomic Characteristics of ALK Fusion Positive Tumors in Chinese NSCLC Patients. *Front Oncol* (2020) 10:726. doi: 10.3389/fonc.2020.00726
8. Noh KW, Lee MS, Lee SE, Song JY, Shin HT, Kim YJ, et al. Molecular Breakdown: A Comprehensive View of Anaplastic Lymphoma Kinase (ALK)-Rearranged Non-Small Cell Lung Cancer. *J Pathol* (2017) 243:307–19. doi: 10.1002/path.4950
9. Cui M, Han Y, Li P, Zhang J, Ou Q, Tong X, et al. Molecular and Clinicopathological Characteristics of ROS1-Rearranged Non-Small-Cell Lung Cancers Identified by Next-Generation Sequencing. *Mol Oncol* (2020) 14:2787–95. doi: 10.1002/1878-0261.12789
10. Farago AF, Taylor MS, Doebele RC, Zhu VW, Kummar S, Spira AI, et al. Clinicopathologic Features of Non-Small-Cell Lung Cancer Harboring an NTRK Gene Fusion. *JCO Precis Oncol* (2018) 2018:PO.18.00037. doi: 10.1200/PO.18.00037
11. Kummar S, Lassen UN. TRK Inhibition: A New Tumor-Agnostic Treatment Strategy. *Target Oncol* (2018) 13:545–56. doi: 10.1007/s11523-018-0590-1
12. Assi T, Rassy E, Nassereddine H, Farhat F, Karak FE, Kattan J, et al. TRK Inhibition in Soft Tissue Sarcomas: A Comprehensive Review. *Semin Oncol* (2020) 47:73–84. doi: 10.1053/j.seminoncol.2020.02.009
13. Skalova A, Vanecek T, Sima R, Laco J, Weinreb I, Perez-Ordonez B, et al. Mammary Analogue Secretory Carcinoma of Salivary Glands, Containing the ETV6-NTRK3 Fusion Gene: A Hitherto Undescribed Salivary Gland Tumor Entity. *Am J Surg Pathol* (2010) 34:599–608. doi: 10.1097/PAS.0b013e3181d9efcc
14. Bourgeois JM, Knezevich SR, Mathers JA, Sorensen PH. Molecular Detection of the ETV6-NTRK3 Gene Fusion Differentiates Congenital Fibrosarcoma From Other Childhood Spindle Cell Tumors. *Am J Surg Pathol* (2000) 24:937–46. doi: 10.1097/00000478-200007000-00005
15. Zhao R, Yao F, Xiang C, Zhao J, Shang Z, Guo L, et al. Identification of NTRK Gene Fusions in Lung Adenocarcinomas in the Chinese Population. *J Pathol Clin Res* (2021) 7:375–84. doi: 10.1002/cjp2.208
16. Rodig SJ, Shapiro GI. Crizotinib, a Small-Molecule Dual Inhibitor of the C-Met and ALK Receptor Tyrosine Kinases. *Curr Opin Investig Drugs* (2010) 11:1477–90.
17. Markham A. Brigatinib: First Global Approval. *Drugs* (2017) 77:1131–5. doi: 10.1007/s40265-017-0776-3
18. Kuang S, Leighl NB. Lorlatinib in ALK-Rearranged Lung Cancer. *Cancer Cell* (2021) 39:25–7. doi: 10.1016/j.ccell.2020.12.017
19. Marcus L, Donoghue M, Aungst S, Myers CE, Helms WS, Shen G, et al. FDA Approval Summary: Entrectinib for the Treatment of NTRK Gene Fusion Solid Tumors. *Clin Cancer Res* (2021) 27:928–32. doi: 10.1158/1078-0432.CCR-20-2771
20. Scott LJ. Larotrectinib: First Global Approval. *Drugs* (2019) 79:201–6. doi: 10.1007/s40265-018-1044-x
21. McCoach CE, Le AT, Gowan K, Jones K, Schubert L, Doak A, et al. Resistance Mechanisms to Targeted Therapies in ROS1(+) and ALK(+) Non-Small Cell Lung Cancer. *Clin Cancer Res* (2018) 24:3334–47. doi: 10.1158/1078-0432.CCR-17-2452
22. Wu X, Fu Y, Wang Y, Wan S, Zhang J. Gaining Insight Into Crizotinib Resistance Mechanisms Caused by L2026M and G2032R Mutations in ROS1 *via* Molecular Dynamics Simulations and Free-Energy Calculations. *J Mol Model* (2017) 23:141. doi: 10.1007/s00894-017-3314-z
23. Drilon A. TRK Inhibitors in TRK Fusion-Positive Cancers. *Ann Oncol* (2019) 30:viii23–30. doi: 10.1093/annonc/mdz282
24. Gulhan DC, Lee JJ, Melloni GEM, Cortés-Ciriano I, Park PJ. Detecting the Mutational Signature of Homologous Recombination Deficiency in Clinical Samples. *Nat Genet* (2019) 51:912–9. doi: 10.1038/s41588-019-0390-2
25. Farkkila A, Gulhan DC, Casado J, Jacobson CA, Nguyen H, Kochupurakkal B, et al. Immunogenomic Profiling Determines Responses to Combined PARP and PD-1 Inhibition in Ovarian Cancer. *Nat Commun* (2020) 11:1459. doi: 10.1038/s41467-020-15315-8
26. Lourenco C, Resetca D, Redel C, Lin P, MacDonald AS, Ciaccio R, et al. MYC Protein Interactors in Gene Transcription and Cancer. *Nat Rev Cancer* (2021) 21:579–91. doi: 10.1038/s41568-021-00367-9
27. Chen WS, Bindra RS, Mo A, Hayman T, Husain Z, Contessa JN, et al. CDKN2A Copy Number Loss Is an Independent Prognostic Factor in HPV-Negative Head and Neck Squamous Cell Carcinoma. *Front Oncol* (2018) 8:95. doi: 10.3389/fonc.2018.00095
28. Zhao Y, Li Y, Lu H, Chen J, Zhang Z, Zhu ZZ. Association of Copy Number Loss of CDKN2B and PTCH1 With Poor Overall Survival in Patients With Pulmonary Squamous Cell Carcinoma. *Clin Lung Cancer* (2011) 12:328–34. doi: 10.1016/j.cllc.2011.02.007
29. Yin J, Li Y, Zhao H, Qin Q, Li X, Huang J, et al. Copy-Number Variation of MCL1 Predicts Overall Survival of Non-Small-Cell Lung Cancer in a Southern Chinese Population. *Cancer Med* (2016) 5:2171–9. doi: 10.1002/cam4.774
30. Sawada R, Maehara R, Oshikiri T, Nakamura T, Itoh T, Kodama Y, et al. MDM2 Copy Number Increase: A Poor Prognostic, Molecular Event in Esophageal Squamous Cell Carcinoma. *Hum Pathol* (2019) 89:1–9. doi: 10.1016/j.humpath.2019.04.002
31. Huang F, Chang H, Greer A, Hillerman S, Reeves KA, Hurlburt W, et al. IRS2 Copy Number Gain, KRAS and BRAF Mutation Status as Predictive Biomarkers for Response to the IGF-1r/IR Inhibitor BMS-754807 in Colorectal Cancer Cell Lines. *Mol Cancer Ther* (2015) 14:620–30. doi: 10.1158/1535-7163.MCT-14-0794-T
32. Ota K, Azuma K, Kawahara A, Hattori S, Iwama E, Tanizaki J, et al. Induction of PD-L1 Expression by the EML4-ALK Oncoprotein and Downstream Signaling Pathways in Non-Small Cell Lung Cancer. *Clin Cancer Res* (2015) 21:4014–21. doi: 10.1158/1078-0432.CCR-15-0016
33. Guo YJ, Pan WW, Liu SB, Shen ZF, Xu Y, Hu LL. ERK/MAPK Signalling Pathway and Tumorigenesis. *Exp Ther Med* (2020) 19:1997–2007. doi: 10.3892/etm.2020.8454
34. Farhan M, Wang H, Gaur U, Little PJ, Xu J, Zheng W. FOXO Signaling Pathways as Therapeutic Targets in Cancer. *Int J Biol Sci* (2017) 13:815–27. doi: 10.7150/ijbs.20052
35. Pietrantonio F, Di Nicolantonio F, Schrock AB, Lee J, Tejpar S, Sartore-Bianchi A, et al. ALK, ROS1, and NTRK Rearrangements in Metastatic Colorectal Cancer. *J Natl Cancer Inst* (2017) 109:1–10. doi: 10.1093/jnci/djx089
36. Gatalica Z, Xiu J, Swensen J, Vranic S. Molecular Characterization of Cancers With NTRK Gene Fusions. *Mod Pathol* (2019) 32:147–53. doi: 10.1038/s41379-018-0118-3
37. Aithal A, Rauth S, Kshirsagar P, Shah A, Lakshmanan I, Junker WM, et al. MUC16 as a Novel Target for Cancer Therapy. *Expert Opin Ther Targets* (2018) 22:675–86. doi: 10.1080/14728222.2018.1498845
38. Li X, Pasche B, Zhang W, Chen K. Association of MUC16 Mutation With Tumor Mutation Load and Outcomes in Patients With Gastric Cancer. *JAMA Oncol* (2018) 4:1691–8. doi: 10.1001/jamaoncol.2018.2805
39. Alexandrov LB, Nik-Zainal S, Wedge DC, Aparicio SA, Behjati S, Biankin AV, et al. Signatures of Mutational Processes in Human Cancer. *Nature* (2013) 500:415–21. doi: 10.1038/nature12477
40. Zhang W, Kuang P, Liu T. Prognostic Significance of CDKN2A/B Deletions in Acute Lymphoblastic Leukaemia: A Meta-Analysis. *Ann Med* (2019) 51:28–40. doi: 10.1080/07853890.2018.1564359
41. Fang W, Zhou H, Shen J, Li J, Zhang Y, Hong S, et al. MDM2/4 Amplification Predicts Poor Response to Immune Checkpoint Inhibitors: A Pan-Cancer Analysis. *ESMO Open* (2020) 5:e000614. doi: 10.1136/esmoopen-2019-000614
42. Barata JT, Durum SK, Seddon B. Flip the Coin: IL-7 and IL-7R in Health and Disease. *Nat Immunol* (2019) 20:1584–93. doi: 10.1038/s41590-019-0479-x
43. Soda M, Choi YL, Enomoto M, Takada S, Yamashita Y, Ishikawa S, et al. Identification of the Transforming EML4-ALK Fusion Gene in Non-Small-Cell Lung Cancer. *Nature* (2007) 448:561–6. doi: 10.1038/nature05945
44. Gristina V, La Mantia M, Iacono F, Galvano A, Russo A, Bazan V. The Emerging Therapeutic Landscape of ALK Inhibitors in Non-Small Cell Lung Cancer. *Pharmaceuticals* (2020) 13:474. doi: 10.3390/ph13120474
45. Huang RSP, Haberberger J, Sokol E, Schrock AB, Danziger N, Madison R, et al. Clinicopathologic, Genomic and Protein Expression Characterization of 356 ROS1 Fusion Driven Solid Tumors Cases. *Int J Cancer* (2021) 148:1778–88. doi: 10.1002/ijc.33447

46. Yun JW, Yang L, Park HY, Lee CW, Cha H, Shin HT, et al. Dysregulation of Cancer Genes by Recurrent Intergenic Fusions. *Genome Biol* (2020) 21:166. doi: 10.1186/s13059-020-02076-2
47. Cai C, Tang Y, Li Y, Chen Y, Tian P, Wang Y, et al. Distribution and Therapeutic Outcomes of Intergenic Sequence-ALK Fusion and Coexisting ALK Fusions in Lung Adenocarcinoma Patients. *Lung Cancer* (2021) 152:104–8. doi: 10.1016/j.lungcan.2020.12.018
48. Davis AA, Patel VG. The Role of PD-L1 Expression as a Predictive Biomarker: An Analysis of All US Food and Drug Administration (FDA) Approvals of Immune Checkpoint Inhibitors. *J Immunother Cancer* (2019) 7:278. doi: 10.1186/s40425-019-0768-9
49. Su S, Dong ZY, Xie Z, Yan LX, Li YF, Su J, et al. Strong Programmed Death Ligand 1 Expression Predicts Poor Response and *De Novo* Resistance to EGFR Tyrosine Kinase Inhibitors Among NSCLC Patients With EGFR Mutation. *J Thorac Oncol* (2018) 13:1668–75. doi: 10.1016/j.jtho.2018.07.016

Conflict of Interest: Authors YN, XM, FD, and CS were employed by Jiangsu Simcere Diagnostics Co., Ltd. And Nanjing Simcere Medical Laboratory Science Co., Ltd.

The remaining authors declare that the research was conducted in the absence of any commercial or financial relationships that could be construed as a potential conflict of interest.

Publisher's Note: All claims expressed in this article are solely those of the authors and do not necessarily represent those of their affiliated organizations, or those of the publisher, the editors and the reviewers. Any product that may be evaluated in this article, or claim that may be made by its manufacturer, is not guaranteed or endorsed by the publisher.

frontiers | Frontiers in Oncology

ORIGINAL RESEARCH
published: 20 June 2022
doi: 10.3389/fonc.2022.862216

Clinical Diagnostic and Prognostic Potential of *NDRG1* and *NDRG2* in Hepatocellular Carcinoma Patients

Shaohua Xu[1], *Ruihuan Gao*[1], *Yidan Zhou*[1], *Ying Yang*[1], *Yi Zhang*[1], *Qianyuan Li*[2], *Chunhua Luo*[2] *and Song-Mei Liu*[*,1]

[1] *Department of Clinical Laboratory, Center for Gene Diagnosis & Program of Clinical Laboratory, Zhongnan Hospital of Wuhan University, Wuhan, China,* [2] *The First College of Clinical Medical Science, Three Gorges University, Hubei, China*

Background: Primary liver cancer is still the most common lethal malignancy. The N-myc downstream-regulated gene family (*NDRG1–4*) is a group of multifunctional proteins associated with carcinogenesis. However, systematic evaluation of the diagnostic and prognostic values of *NDRG1* or *NDRG2* expression in liver cancer is poorly investigated.

Method: The gene expression matrix of liver hepatocellular carcinoma (LIHC) was comprehensively analyzed by the "limma" and "Dseq2" R packages. The Gene Ontology (GO) and Gene Set Enrichment Analysis (GSEA) were used to identify the biological functional differences. A single-sample GSEA (ssGSEA) was conducted to quantify the extent of immune cell infiltration. Finally, the clinical and prognostic information of LIHC patients was systematically investigated using Kaplan–Meier analysis and logistic and Cox regression analysis.

Results: Compared with normal tissues, *NDRG1* expression was higher, whereas *NDRG2* expression was lower in tumor tissues (P <0.001). The area under the receiver operator characteristic curve (AUROC) of *NDRG1* and *NDRG2* for LIHC was 0.715 and 0.799, respectively. Kaplan–Meier analysis revealed that *NDRG1* and *NDRG2* were independent clinical prognostic biomarkers for the overall survival (OS, P = 0.001 and 2.9e–06), progression-free interval (PFI, P = 0.028 and 0.005) and disease-specific survival (DSS, P = 0.027 and P <0.001). The C-indexes and calibration plots of the nomogram suggest that *NDRG1* and *NDRG2* have an effective predictive performance for OS (C-index: 0.676), DSS (C-index: 0.741) and PFI (C-index: 0.630) of liver cancer patients. The mutation rate of *NDRG1* in liver cancer reached up to 14%, and DNA methylation levels of *NDRG1* and *NDRG2* promoters correlated significantly with clinical prognosis.

Conclusions: The mRNA expression and DNA methylation of *NDRG* superfamily members have the potential for LIHC diagnosis and prognosis *via* integrative analysis from multiple cohorts.

Keywords: LIHC, prognosis, *NDRG1*, *NDRG2*, hepatocellular carcinoma, methylation, Kaplan–Meier

OPEN ACCESS

Edited by:
Ondrej Slaby,
Central European Institute of Technology (CEITEC), Czechia

Reviewed by:
Qianqian Song,
Wake Forest School of Medicine, United States
Jungshan Chang,
Taipei Medical University, Taiwan

****Correspondence:***
Song-Mei Liu
smliu@whu.edu.cn

Specialty section:
This article was submitted to Cancer Genetics, a section of the journal Frontiers in Oncology

Received: *25 January 2022*
Accepted: *11 May 2022*
Published: *20 June 2022*

Citation:
Xu S, Gao R, Zhou Y, Yang Y, Zhang Y, Li Q, Luo C and Liu S-M (2022) Clinical Diagnostic and Prognostic Potential of NDRG1 and NDRG2 in Hepatocellular Carcinoma Patients. Front. Oncol. 12:862216. doi: 10.3389/fonc.2022.862216

INTRODUCTION

Primary liver cancer is the fourth leading cause of cancer-related deaths worldwide, characterized by an insidious onset and a low rate of early diagnosis (1). In China, liver hepatocellular carcinoma (LIHC) is the most common type of primary liver cancer and typically results from chronic hepatitis B virus infection (2). Despite the recent advances in diagnostic and therapy, the 5-year relative survival rate of LIHC remains to be only 12% (3). Currently, LIHC contributes to over half of the new deaths, and it is predicted to rise continuously in the next decade (4). Therefore, identifying potential biomarkers that improve diagnostic accuracy and prognostic prediction is critical.

Increasing evidence indicates that disturbance of proto-oncogenes and tumor suppressor genes results in hepatocarcinogenesis, which is a complicated pathophysiological process (5). Viral infection and metabolic stress induce genetic and epigenetic alterations through cell cycle turnover and the inflammatory environment (6). The N-myc downstream-regulated gene (*NDRG1–4*) family, a hypoxia-associated protein, has been involved in cell proliferation and differentiation, stress responses, tumor progression, and metastasis (7–9). *NDRG1* is involved in cellular skeleton modification and organ development and can be induced by hypoxia and DNA damage (7, 10). *NDRG2* is highly expressed in dendritic cells and maintains activated leukocyte adhesion (11). Moreover, *NDRG3* could promote cell growth and angiogenesis and participate in the lactate-dependent hypoxia signaling pathway (12). *NDRG4* is exclusively expressed in the embryonic stage and regulates the proliferation and growth of nerve cells and cardiomyocytes (13). Of note, abnormal expression of *NDRG1* or *NDRG2* has been found in different cancer types, such as in esophageal cancer, colorectal cancer, breast cancer, prostate cancer, and hepatocellular carcinoma, and is significantly associated with poor prognosis (10, 14–16). Existing data indicate that *NDRG1* is upregulated and *NDRG2* is downregulated in LIHC. However, a few studies focused on the diagnostic and prognostic values of *NDRG1* or *NDRG2* in LIHC, and their potential mechanisms in LIHC remain unknown.

Here, the diagnostic and prognostic significance of *NDRG1* and *NDRG2* were systematically identified in LIHC using RNA-seq data from the TCGA database. We first comprehensively analyzed the gene expression matrix of LIHC and then applied bioinformatics methods (namely, Gene Ontology (GO) terms, Kyoto Encyclopedia of Genes and Genomes (KEGG) pathway analysis, and Gene Set Enrichment Analysis (GSEA)) to explore the underlying biological mechanism. Secondly, we analyzed DNA mutation and methylation in *NDRG1* or *NDRG2*, and explored the relevance between immune cells and *NDRG1* or *NDRG2* expression by the single sample GSEA (ssGSEA). Moreover, clinical and follow-up information of LIHC patients were used for Kaplan–Meier analysis, and logistic and Cox regression analysis. Finally, we plotted a nomogram for the prognosis prediction of the patients. Taken together, this study revealed that *NDRG1* or *NDRG2* could be a potential diagnostic and prognostic biomarker for LIHC.

MATERIALS AND METHODS

Data Source

RNA-seq data for pan-cancer analysis were retrieved from the UCSC XENA (https://xenabrowser.net/datapages/) (17, 18). The mRNA expression datasets (GSE14520, GSE25097, and GSE36376) were obtained from the GEO database (https://www.ncbi.nlm.nih.gov/geo/) to further validate the results of pan-cancer analysis in LIHC patients. Meanwhile, we also collected the data for NDRG1 and NDRG2 protein expression from the Human Protein Atlas (HPA) (https://www.proteinatlas.org/). The mRNA expression matrix file of TCGA-LIHC and the corresponding clinical data were collected from the TCGA website (https://portal.gdc.cancer.gov/repository), and level-3 HTSeq-FPKM data were transformed into TPM (transcripts per million reads) for subsequent analyses. A total of 371 patient information was used, while unavailable or unknown clinical information was excluded.

Clinical Specimen Collection, RNA isolation, and qPCR

Thirty-two pairs of fresh-frozen tissues (LIHC tissues and their adjacent tissues) were collected from the Zhongnan Hospital of Wuhan University with informed consent and approval from the hospital ethics committee. cDNA was synthesized from total RNA using the PrimeScript RT Reagent Kit (Vazyme, R333-01, China). The SYBR Prime Script RT-PCR kit (Vazyme, Q712-02, China) was used for qPCR on a CFX96 Connect Real-Time System (Bio-Rad, America). The primer sequences were as follows: *NDRG1*-F, 5′-GAAGTGGTCCACACCTACCG-3′; *NDRG1*-R, 5′-GTCCGCCATCTTGAGGAGAG-3′; *NDRG2*-F, 5′-GCCCAGCGATCCTTACCTAC-3′; *NDRG2*-R, 5′-TGCAAGCTGGTCCAGAGATG-3′; *GAPDH*-F, 5′-GGAGCGAGATCCCTCCAAAAT-3′; and *GAPDH*-R, 5′-GGCTGTTGTCATACTTCTCATGG-3′.

Identification of the *NDRG1* and *NDRG2* Expression Profile

The raw expression profiles from GEO datasets were preprocessed by R software (version 4.0.5) and differentially analyzed by running the "limma" R package (version 3.46.0). Gene expression data of LIHC case samples were stratified into high- and low-expression groups based on the median expression of *NDRG1* and *NDRG2*, respectively. The expression analysis between high- and low-expression groups was performed using the "DESeq2" R package (19) (version 3.18.1; http://www.Rproject.org). Genes with the threshold for $|\log2FoldChange| > 0.5$ and adjusted $P < 0.05$ were regarded as statistically significant.

Functional Annotation and Enrichment Analysis

R package ClusterProfiler (version 3.14.3) was applied to GO term analysis, KEGG pathway analysis, and GSEA to elucidate the function and pathway differences between the high- and low-

expression groups (20, 21). Here, the curated gene sets (c2.cp.v7.2.symbols.gmt) from MSigDB Collections were selected as reference gene sets for GSEA. A permutation test with 1,000 iterations was used to identify pathways that had changed significantly. Significant pathway enrichment was identified by a false discovery rate (FDR) <0.25 and *P*-value <0.05.

Single-Sample GSEA (ssGSEA) for Immune Infiltration Analysis

The ssGSEA was conducted using the GSVA R package (3.6.3) to quantify the tumor immune infiltration levels in 24 types of immune cells (22) and the marker of which was obtained from a previous study (23). Next, Spearman's correlation analysis was conducted to evaluate the associations of *NDRG1* and *NDRG2* expression with immune cell infiltration, and the Wilcoxon rank-sum test was used to investigate the enrichment scores of immune infiltration levels between high- and low-*NDRG1* and *NDRG2* expression groups.

DNA Mutations and Methylation Analysis

The cBio Cancer Genomics Portal (http://cbioportal.org) was applied to analyze *NDRG* family alterations in the TCGA-LIHC sample, which is an interactive exploration website of multidimensional cancer genomic datasets (24). The DNA CpG methylation of *NDRG1* and *NDRG2* in TCGA was also analyzed by MethSurv (https://biit.cs.ut.ee/methsurv/) to explore the relevance between the CpG methylation level and prognostic values (25).

Statistical Analysis

The R software (version 4.0.5) was used for all statistical analysis and graphical plotting. Scatter plot analysis was performed using the Wilcoxon rank-sum test. Non-parametric survival analysis was performed by the Kaplan–Meier method and log-rank test. Correlation analysis was evaluated using the Spearman's coefficient. The Wilcoxon signed rank test, Kruskal–Wallis test, and Chi-Squared test were used to assess the clinicopathological features between high- and low-expression groups. The diagnostic performance of *NDRG1* or *NDRG2* expression was tested by the Area Under the Receiver Operator Characteristic Curve (AUROC). Univariate and multivariate analyses using Cox proportional hazard modeling were performed to estimate the death risk. Unless stated otherwise, $P < 0.05$ (two-sided) was considered statistically significant.

RESULTS

NDRG1 Was Upregulated and *NDRG2* Was Downregulated in LIHC

We used pan-cancer RNA-seq data from the UCSC XENA to evaluate the mRNA expression levels of *NDRG1* and *NDRG2* in diverse human cancers. As shown in **Figure 1A**, the mRNA expression of *NDRG1* and *NDRG2* was found to be significantly different ($P < 0.001$) in almost all tumor types, including LIHC. To further verify the above results, we performed common differential expression gene analysis among the three selected GEO datasets (GSE14520, GSE25097, and GSE3637), and *NDRG1* and *NDRG2* were found to be two of the 843 overlapping genes (|log2FoldChange| >0.5, P*adj* <0.05) (**Figure 1B**). As shown in **Figures 1C, D**, the results from GSE14520 showed that *NDRG1* mRNA was highly expressed in LIHC tissues compared to the adjacent normal tissues ($p < 0.001$), and *NDRG2* mRNA was markedly downregulated in LIHC tissues ($P < 0.001$).

To further validate NDRG1 and NDRG2 protein expression in LIHC, we analyzed the NDRG1 and NDRG2 expression profiles in the HPA database (**Figure 1E**). The immunohistochemical staining from HPA also showed that NDRG1 and NDRG2 proteins were expressed in a pattern consistent with the mRNA-level changes in LIHC tissues. At the experimental level, we analyzed *NDRG1* and *NDRG2* mRNA expression by qPCR in 32 pairs of LIHC tissues (**Figures 1F, G**). The qPCR results again indicated the high expression of *NDRG1* ($P < 0.001$) and low expression of *NDRG2* ($P < 0.001$) in LIHC tissues.

DNA Mutation and Methylation of *NDRG1* or *NDRG2* for LIHC Prognosis

Next, we analyzed the mutation frequencies of *NDRG1* or *NDRG2* in TCGA-LIHC using the cBioPortal online tool. As shown in **Figure 2A**, a high mutation rate of *NDRG1* (up to 14%) was observed in LIHC patients, while other *NDRG* family genes (*NDRG2*, *NDRG3*, and *NDRG4*) were rarely mutated (less than 2%). Moreover, we analyzed the DNA methylation levels of *NDRG1* and *NDRG2* (**Figures 2B, C**) and the prognostic values (**Figure 2D**) of single CpG in TCGA-LIHC *via* MethSurv©2017. As a result, they showed that cg15393676 in *NDRG1* (**Figure 2B**), and cg16409562 and cg04359602 in *NDRG2* (**Figure 2C**) showed the highest methylation in their promoter regions. The DNA methylation level has been negatively correlated with the gene expression level. As shown in **Figure 2D**, LIHC patients with hypermethylation in *NDRG1* and hypomethylation in *NDRG2* could have a better clinical prognosis, which supported our mRNA expression results.

Furthermore, we explored the relationship between the expression of *NDRG1* or *NDRG2* and DNA repair and methyltransferase genes. As shown in **Figure 2E**, *NDRG1* expression has a strong positive correlation with DNA repair genes and methyltransferase genes in LIHC. As shown in **Figure 2F**, we found that *NDRG2* expression has a markable positive correlation with only a few RNA methyltransferase genes and DNA repair genes, but not with DNA methyltransferase in LIHC. This suggests that *NDRG1* may indirectly affect the development and progression of LIHC by regulating epigenetic status.

NDRG1- or *NDRG2*-Related Differentially Expressed Genes

The enrolled 371 LIHC tumor samples from the TCGA dataset were stratified into high- and low-expression groups according to *NDRG1 or NDRG2* median values (cut-off value of 50%),

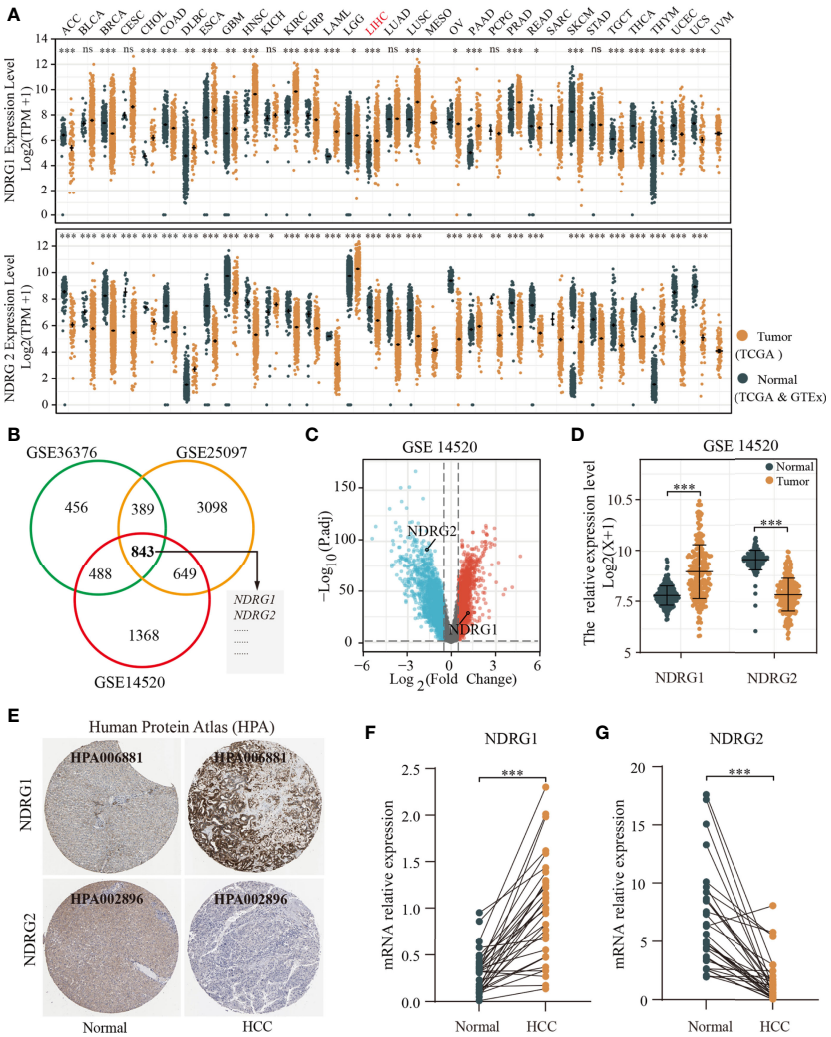

FIGURE 1 | Differential mRNA expression profiles of *NDRG1 or NDRG2* in different cancer types. **(A)** The expression levels of *NDRG1* and *NDRG2* in different cancer types were analyzed based on the TCGA database. **(B)** Venn plots of DEGs (| log2FoldChange>0.5 and adjusted *P* <0.05) identified in three GEO databases. **(C)** The volcano plots for all the coding genes obtained in the GSE14520 database. Red and blue dots represent up-regulated DEGs and down-regulated DEGs, respectively. **(D)** The scatter diagram of *NDRG1* and *NDRG2* mRNA expression levels in GSE14520 database. **(E)** The protein expression of *NDRG1* and *NDRG2* in LIHC was obtained from the Human Protein Atlas (HPA, https://www.proteinatlas.org/). **(F, G)** The expression levels of *NDRG1* and *NDRG2* were obtained by qPCR assay in liver carcinoma and para-carcinoma tissues. **P* < 0.05; ***P* < 0.01; ****P* < 0.001. ns, no significance.

respectively. The identified differentially expressed genes (DEGs) (|log2FoldChange| >0.5, *Padj* <0.05) between different cohorts were illustrated by the volcano plot. A total of 3,547 genes (2,322 upregulated and 1,225 downregulated) were identified as DEGs in the high-*NDRG1* group (**Figure 3A**), and 3,216 genes (1,204 upregulated and 2,012 downregulated) in the high-*NDRG2* group (**Figure 3B**). As shown in **Figure 3C**, 1,345 overlapping DEGs were found between the *NDRG1* and *NDRG2* groups based on the TCGA-LIHC dataset.

To predict the function of *NDRG1*- and *NDRG2*-related DEGs, we conducted GO and KEGG pathway analysis using 1,345 overlapping DEGs by the "ClusterProfiler" R package (version 3.14.3). As shown in **Figures 3D–G**, we found that *NDRG1*- and *NDRG2*-related DEGs were involved in many biological processes, namely, retinol metabolism, bile secretion, fatty acid degradation, chemical carcinogenesis, amino acid metabolism, PPAR signaling pathway, and the cytochrome p450 pathway.

NDRG1- or *NDRG2*-Related Signaling Pathways

To identify *NDRG1*- and *NDRG2*-related signaling pathways, the GSEA was then conducted between low- and high-expression groups, based on significant differences (*P*-value <0.05, FDR <0.25) in the enrichment of the MSigDB Collection [c2.cp.v7.2.symbols.gmt (curated)]. Here, the most significant enrichment was selected according to the Normalized Enrichment Score (NES). As shown in **Figure 4**, GSEA results

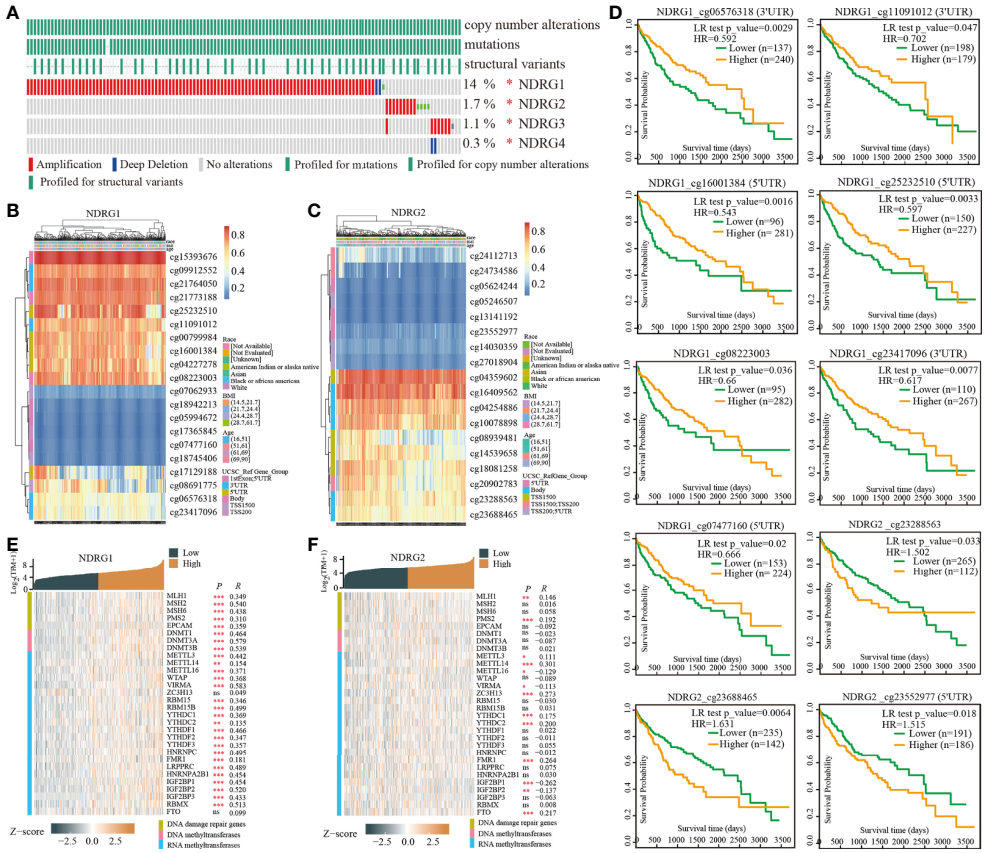

FIGURE 2 | The analysis of DNA mutation and methylation of *NDRG1 or NDRG2*. **(A)** The overview of DNA mutation of the *NDRGs* family genes, mapped by cBioPortal (http://www.cbioportal.org/). **(B, C)** The DNA methylation clustered expression of *NDRG1* and *NDRG2* by using MethSurv©2017 (https://biit.cs.ut.ee/methsurv/). Red to blue represents a high to low expression. **(D)** The significantly prognostic values of the promoter CpGs in *NDRG1* and *NDRG2* obtained from MethSurv©2017. **(E, F)** The heatmaps of *NDRG1* and *NDRG2* expression in relation to DNA repair genes and methyltransferases. *$P < 0.05$, **$P < 0.01$, ***$P < 0.001$. NS, no significance.

showed that the *NDRG1*-related signaling pathway is involved in the PLK1 pathway, complement cascade, complement and coagulation cascades, and fatty acid metabolism (**Figure 4A**), while the *NDRG2*-related signaling pathway is involved in fatty acid metabolism, oxidation by cytochrome p450, retinol metabolism, and eukaryotic translation elongation (**Figure 4B**).

Correlation Between *NDRG1* or *NDRG2* Expression and Immune Infiltration

The tissue microenvironment is vital for tumor cells. Therefore, we first assessed the infiltration of 24 types of immune cells in LIHC using the ssGSEA method from the R package "GSVA", and subsequently evaluated the relationship between *NDRG1* or *NDRG2* mRNA expression and immune cell infiltration by Spearman's analysis. As shown in **Figure 5**, T helper cell 2 (Th2) (r = 0.366, P <0.001), follicular helper T cells (TFH) (r = 0.211, P <0.001), and NK CD56 bright cells (r = 0.202, P <0.001) showed a positive correlation with *NDRG1* expression, while dendritic cells (DC) (r = −0.285, P <0.001), cytotoxic cells (r = −0.218, P <0.001), and pre-dendritic cells (pDC) (r = −0.233, P <0.001) showed a negative correlation with *NDRG1* expression (**Figures 5A, C**). The expression of *NDRG2* was negatively correlated with TFH (r = −0.261, P <0.001), Th2 cells (r = −0.250, P <0.001), NK CD56 bright cells (r = −0.240, P <0.001), and positively correlated with T helper cell 17 (Th17) (r = 0.206, P <0.001) and NK cells (r = 0.147, P <0.004) (**Figures 5B, D**).

Correlation Between *NDRG1* or *NDRG2* Expression and Clinicopathological Characteristics

The clinicopathological characteristics of LIHC patients with differential *NDRG1* and *NDRG2* expression are listed in **Table 1**. There was a significant difference in the distribution of BMI (P = 0.018), T stages (P = 0.031), pathologic stages (P = 0.016), residual tumor (P = 0.008), and histological grade (P = 0.027) between the high- and low-*NDRG1* groups. We also further evaluated the correlation between *NDRG1* or *NDRG2* expression and clinicopathological characteristics by logistic regression analysis (**Table 2**). As a result, we found markedly positive correlations of *NDRG1* expression with clinical T stage (P = 0.004), histological grade (P = 0.005), and AFP concentration (P <0.001).

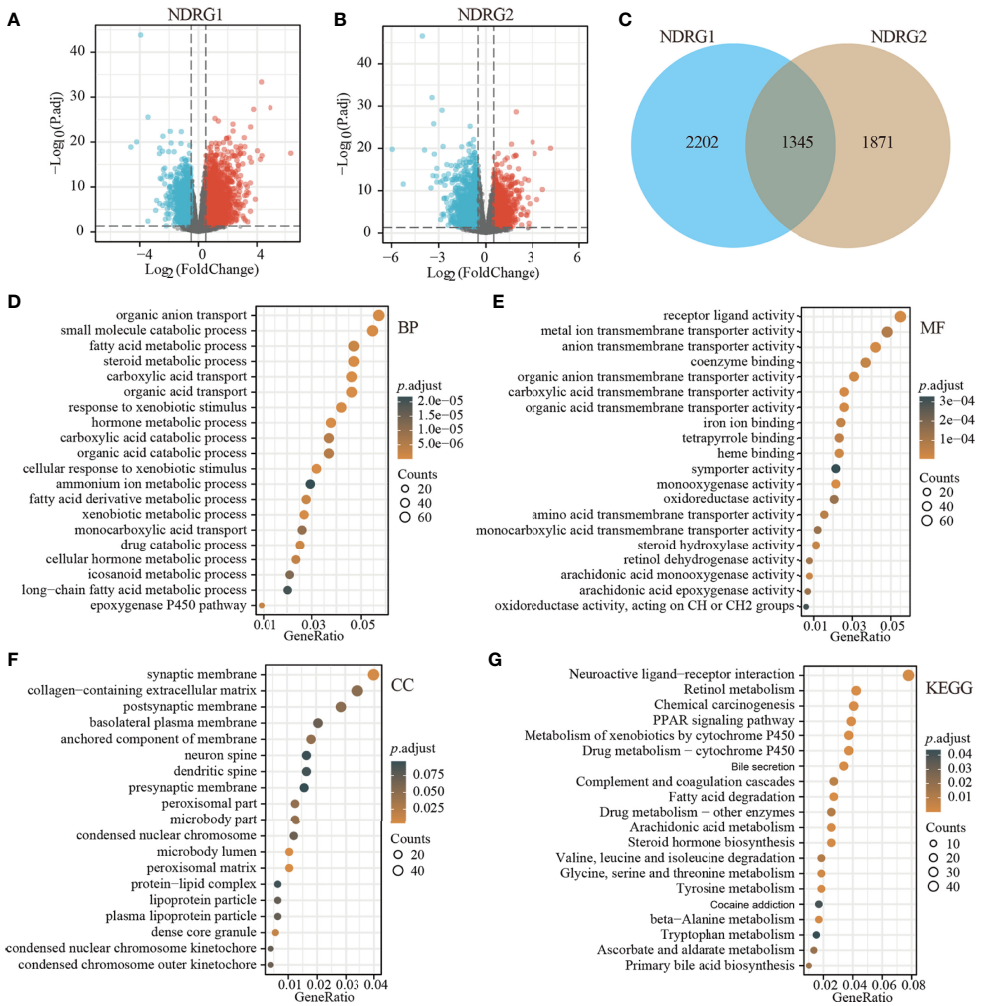

FIGURE 3 | Identification of DEGs in LIHC tissues with low- and high-expressed *NDRG1* and *NDRG2* groups. **(A, B)** Volcano plot of DEGs between low- and high-*NDRG1* and *NDRG2* expression groups based on the TCGA & GTEx datasets. **(C)** Venn diagram of the identified DEGs between low- and high-*NDRG1* and *NDRG2* expression groups. **(D–G)** The plots for the results of enriched GO terms and KEGG pathway analysis using the "ClusterProfiler" R package. The x-axis represents the proportion of DEGs, and different circle sizes represent the number of DEGs.

Diagnosis and Prognosis Values of *NDRG1* or *NDRG2* for LIHC

As shown in **Figure 6A**, the AUROC of *NDRG1* and *NDRG2* is 0.715 and 0.799, respectively. The results of AUROC indicated that the expression of *NDRG1* or *NDRG2* had high sensitivity and specificity for LIHC diagnosis. Next, Kaplan–Meier (K–M) analysis was performed to verify the prediction of *NDRG1* or *NDRG2* on clinical outcomes. As shown in **Figures 6B–E**, overall survival [OS, hazard ratio (HR): 1.75, $P = 0.0013$], disease-specific survival (DSS, HR: 1.64, $P = 0.027$), progression-free interval (PFI, HR: 1.39, $P = 0.028$), and risk-free survival (RFS, HR: 1.34, $P = 0.095$) for LIHC patients with high-*NDRG1* expression were statistically worse than those patients with the low-*NDRG1* expression. In contrast, OS (HR: 0.43, $P = 2.9e{-}06$), DSS (HR: 0.59, $P = 0.00046$), PFI (HR: 0.63, $P = 0.0054$), and RFS (HR: 0.42, $P = 0.00014$) for high-*NDRG2* expression groups were all statistically better than those of the low-*NDRG2* expression group (**Figures 6F–I**).

Subsequently, we constructed a prognostic nomogram using multivariate Cox regression analysis and validated the efficiency of the nomogram by drawing a calibration curve. As shown in **Figures 7A–C**, tumor TNM stage and age, as well as the expression level of *NDRG1* or *NDRG2*, were included in the nomogram to predict OS (C-index: 0.676, **Figure 7A**), DSS (C-index: 0.741, **Figure 7B**) and PFI (C-index: 0.630, **Figure 7C**). The calibration curves showed the desired predictive performance of these nomograms of 1-, 3-, and 5-year clinical outcomes (**Figures 7D–F**).

Predictive Values of *NDRG1* or *NDRG2* For Clinicopathological Subgroups of LIHC

The LIHC patients were further divided into different clinicopathological subgroups according to sex, age, clinical TNM stage, and vascular invasion. Next, we also performed Cox

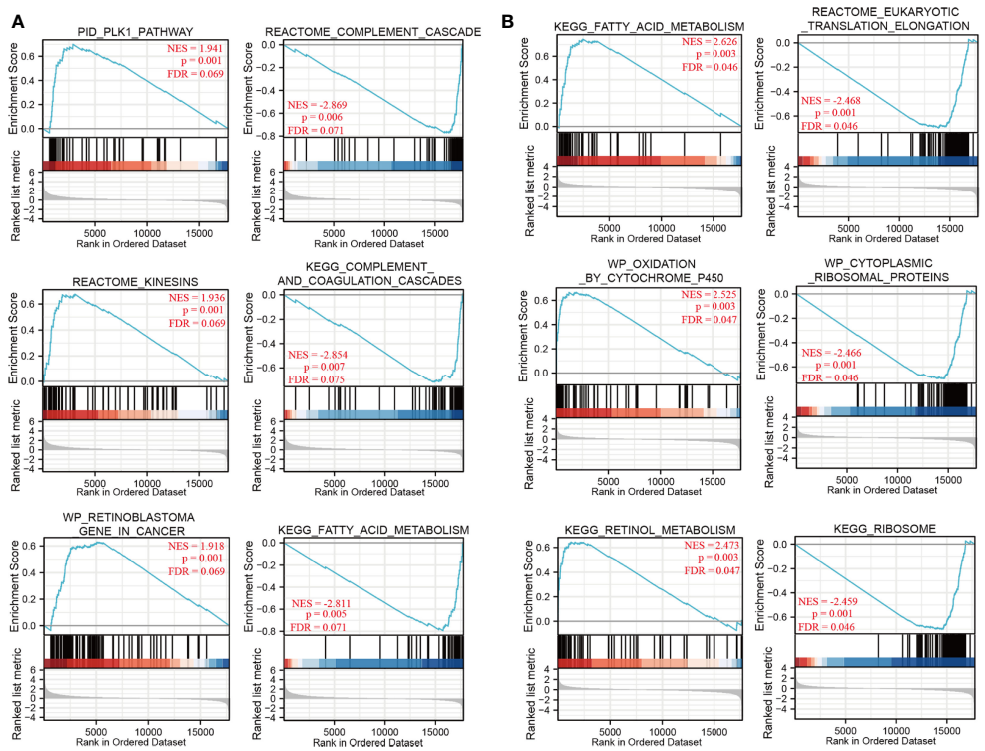

FIGURE 4 | The gene set enrichment analysis of *NDRG1* and *NDRG2*. **(A, B)** Representative enrichment plots from GSEA. Several pathways and biological processes were differentially enriched in *NDRG1 and NDRG2*-related hepatocellular carcinoma. NES, normalized enrichment score; p.adj, adjusted P-value; FDR, false discovery rate.

regression analyses on each subgroup to assess the prognostic performance of *NDRG1* (**Table 3**) or *NDRG2* (**Table 4**) expression on OS, DSS, and PFI. As shown in **Table 3**, *NDRG1* was a significant risk factor for OS in male patients (HR = 1.97, P = 0.003), patients aged above 60 (HR = 1.78, P = 0.014), patients at N0 stage (HR = 1.55, P = 0.048), patients at M0 stage (HR = 1.60, P = 0.034), patients with vascular invasion (HR = 2.19, P = 0.028), and patients with tumor (HR = 1.58, P = 0.048). *NDRG1* was also a significant risk factor for DSS in patients with tumors (HR = 1.58, P = 0.048), and for PFI in females (HR = 2.55, P = 0.008), patients at T stage I–II (HR = 1.48, P = 0.034), and patients at N1 stage (HR = 1.44, P = 0.044).

As shown in **Table 4**, *NDRG2* was a significant favorable factor for OS in male patients (HR = 0.62, P = 0.034), patients aged below 60 (HR = 0.45, P = 0.004), and patients at M0 stage (HR = 0.60, P = 0.020). Similar observations occurred for DSS in male patients (HR = 0.53, P = 0.031), patients aged below 60 (HR = 0.46, P = 0.019), patients at the N0 stage (HR = 0.53, P = 0.029), and patients at the M0 stage (HR = 0.56, P = 0.043). All the results demonstrated significantly better clinical outcomes in the low-*NDRG1* or high-*NDRG2* expression groups.

DISCUSSION

To date, clinical outcomes of LIHC are far from satisfactory owing to the lack of efficient indicators and effective treatment (26). Therefore, it is crucial to find potential biomarkers for predicting clinical prognosis and guiding individualized treatment. Many cancers have been reported to have the N-myc downstream-regulated gene (*NDRG1–4*) family. To our knowledge, the expression levels of *NDRG* family members and their potential prognostic values in LIHC have not been fully explored. Hence, we focused on the expression and prognostic values of *NDRG1* and *NDRG2* in LIHC by analyzing datasets from the TCGA and GEO.

Here, the data analysis from UCSC XENA indicated that the *NDRG1* expression had a significant increase in LIHC tumor tissues compared to normal tissues (P <0.001). The same result can be found in the GEO database (GSE14520, GSE25097, and GSE36376), the HPA database, and our experiment validation (qPCR). N*DRG1* is a member of the *NDRG* superfamily and has been found to be involved in embryonic development (7), cellular vesicle transportation (27), and membrane protein circulation (28). *NDRG1* is strongly upregulated under hypoxic conditions, and this condition is prevalent in solid tumors (29). Previous studies suggested that *NDRG1* could inhibit proliferation and induce apoptosis of cancer cells by regulating Bcl-2 and Ca^{2+}-associated proteins (30, 31) and epithelial–mesenchymal transition (EMT) (32). Another study indicated that the encoded protein of *NDRG1* is necessary for p53-mediated caspase activation and apoptosis (33). However, *NDRG1* protein is expressed at low levels in normal tissues

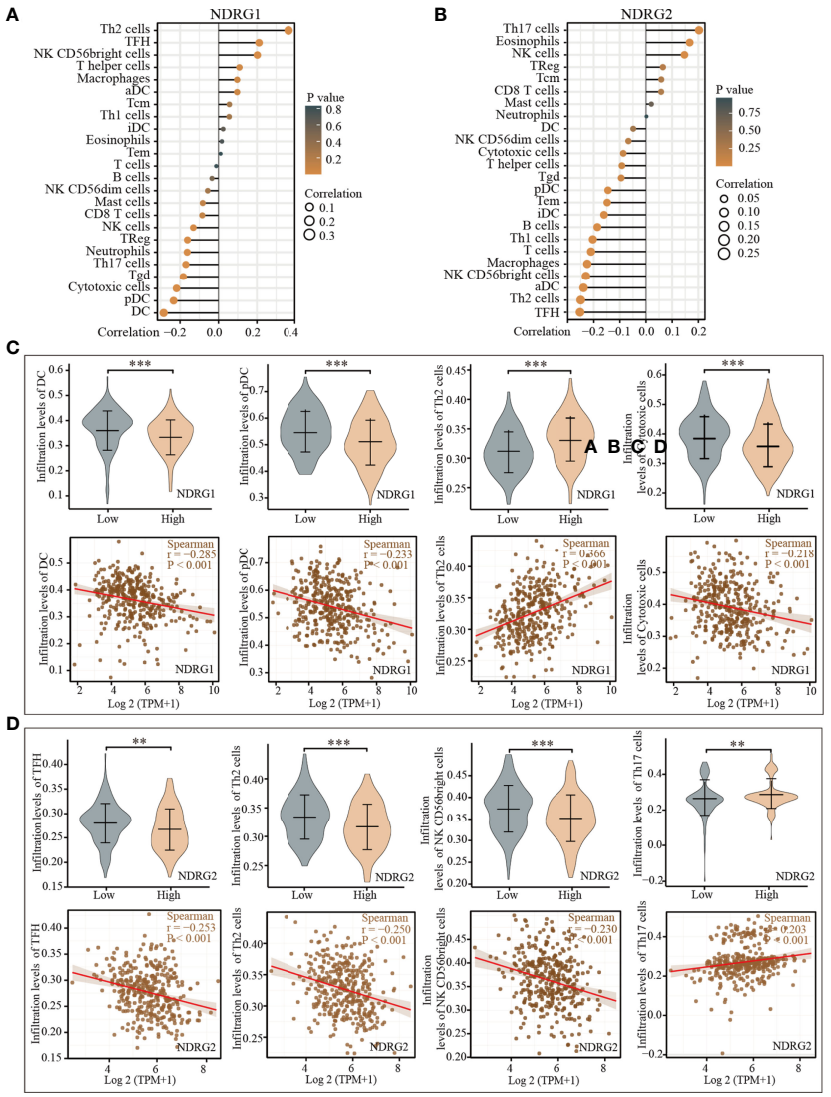

FIGURE 5 | Correlation of the expression of *NDRG1 or NDRG2* with immune infiltration. **(A, B)** The forest plots showed the correlations of *NDRG1 or NDRG2* expression with immune infiltration in 24 types of immune cells. The size of the dots shows the absolute values of Spearman's correlation coefficient. **(C, D)** Violin plots and scatter plots showing the difference and relevance of representative immune cells infiltration level. $^{**}P < 0.01$; $^{***}P < 0.001$.

while *NDRG1* mRNA is ubiquitously over-expressed in various human cancers. In other words, the regulation mechanism involved in *NDRG1* is somewhat complex, governed by hypoxia-inducible factor 1 alpha (HIF-1α)- and p53-dependent pathways (29), which makes the *NDRG1* gene potentially an important biomarker for tumor progression.

Furthermore, Kaplan–Meier analysis showed that high *NDRG1* expression correlates significantly with poor clinical outcomes in LIHC patients, which was consistent with previous research (34). Our results suggest that *NDRG1* is an independent risk factor for LIHC and could act as an oncogene to accelerate LIHC progression. However, previous studies revealed that the expression of *NDRG1* decreased in esophageal (16), colorectal (35), and breast cancers (10), and was correlated with poor clinical outcomes. This contradictory result may be tumor type-specific, further emphasizing that *NDRG1* is involved in complex biological processes. In contrast to *NDRG1*, *NDRG2* expression was reduced significantly in LIHC, and the downregulation of *NDRG2* was associated with poor prognosis, which was consistent with previous studies (9, 14). Past research has also shown that the *NDRG2* expression has a significant decrease in gastric (36), pancreatic (14), and breast cancers (15). Our results showed that *NDRG2* might act as an antioncogene to suppress the LIHC progression.

Different types of mutations can greatly increase the risk of developing certain cancers. Interestingly, we found that the *NDRG1* gene has a mutation frequency of up to 14% in LIHC patients, while the other *NDRG* family members have a mutation frequency of less than 2%. DNA methylation is a common epigenetic phenotype that exists in almost all types of human

TABLE 1 | Demographics and tumor characteristics based on the expression of *NDRG1* and *NDRG2*.

Characteristic	levels	*NDRG1*		*P*-values	*NDRG2*		*P*-values
		Low(n = 185)	High(n = 186)		Low (n = 185)	High (n = 186)	
Gender				0.530			0.083
	Female	57 (15.4%)	64 (17.3%)		52 (14%)	69 (18.6%)	
	Male	128 (34.5%)	122 (32.9%)		133 (35.8%)	117 (31.5%)	
Age				0.076			0.469
	≤60	79 (21.4%)	98 (26.5%)		92 (24.9%)	85 (23%)	
	>60	105 (28.4%)	88 (23.8%)		92 (24.9%)	101 (27.3%)	
BMI				**0.018**			0.882
	≤25	79 (23.6%)	98 (29.3%)		91 (27.2%)	86 (25.7%)	
	>25	92 (27.5%)	66 (19.7%)		79 (23.6%)	79 (23.6%)	
T stage				**0.031**			0.301
	T1	97 (26.4%)	84 (22.8%)		82 (22.3%)	99 (26.9%)	
	T2	51 (13.9%)	43 (11.7%)		53 (14.4%)	41 (11.1%)	
	T3	28 (7.6%)	52 (14.1%)		43 (11.7%)	37 (10.1%)	
	T4	6 (1.6%)	7 (1.9%)		6 (1.6%)	7 (1.9%)	
N stage				0.622			0.350
	N0	126 (49.2%)	126 (49.2%)		133 (52%)	119 (46.5%)	
	N1	1 (0.4%)	3 (1.2%)		1 (0.4%)	3 (1.2%)	
M stage				1.000			0.624
	M0	130 (48.1%)	136 (50.4%)		138 (51.1%)	128 (47.4%)	
	M1	2 (0.7%)	2 (0.7%)		3 (1.1%)	1 (0.4%)	
Pathologic stage				**0.016**			0.142
	Stage I	90 (25.9%)	81 (23.3%)		79 (22.8%)	92 (26.5%)	
	Stage II	49 (14.1%)	37 (10.7%)		51 (14.7%)	35 (10.1%)	
	Stage III	30 (8.6%)	55 (15.9%)		43 (12.4%)	42 (12.1%)	
	Stage IV	3 (0.9%)	2 (0.6%)		4 (1.2%)	1 (0.3%)	
Residual tumor				**0.008**			0.542
	R0	167 (48.8%)	157 (45.9%)		161 (47.1%)	163 (47.7%)	
	R1	3 (0.9%)	14 (4.1%)		7 (2%)	10 (2.9%)	
	R2	0 (0%)	1 (0.3%)		1 (0.3%)	0 (0%)	
Histologic grade				**0.027**			**0.005**
	G1	31 (8.5%)	24 (6.6%)		19 (5.2%)	36 (9.8%)	
	G2	98 (26.8%)	79 (21.6%)		83 (22.7%)	94 (25.7%)	
	G3	51 (13.9%)	71 (19.4%)		74 (20.2%)	48 (13.1%)	
	G4	3 (0.8%)	9 (2.5%)		8 (2.2%)	4 (1.1%)	

Bold indicates significant differences.

cancers (37), and its occurrence in the promoter region often results in gene silencing (38). In this study, the methylation of *NDRG1* and *NDRG2* was related to the clinical prognosis of LIHC patients, and patients with hypomethylated *NDRG1* or hypermethylated *NDRG2* had worse OS. Of note, their mRNA expression was consistent with DNA methylation levels for clinical prognosis. Therefore, the promoter methylation status and mRNA levels of *NDRG1* and *NDRG2* can be used as independent predictors of LIHC patients.

The tumor microenvironment (TME), composed of diverse cell populations in a complex matrix, plays a crucial role in the occurrence and progression of tumors. Tumor-associated

TABLE 2 | Correlation between *NDRG1* or *NDRG2* expression and clinicopathological characteristics in LIHC patients by logistic regression analysis.

Characteristics	Total(N)	*NDRG1*		*NDRG2*	
		Odds Ratio (OR)	*P*-values	Odds Ratio (OR)	*P*-values
Gender (Male vs. Female)	371	0.849 (0.549–1.311)	0.460	0.663 (0.427–1.025)	0.065
Age (>60 vs. ≤60)	370	0.676 (0.448–1.017)	0.061	1.188 (0.790–1.789)	0.408
BMI (>25 vs. ≤25)	335	0.578 (0.374–0.890)	**0.013**	1.058 (0.689–1.626)	0.796
T stage (T3 & T4 vs. T1 & T2)	368	2.022 (1.253–3.306)	**0.004**	0.866 (0.540–1.386)	0.549
N stage (N1 vs. N0)	256	3.000 (0.378–61.094)	0.344	3.353 (0.423–68.283)	0.298
M stage (M1 vs. M0)	270	0.956 (0.113–8.062)	0.964	0.359 (0.018–2.847)	0.378
Histologic grade (G3 & G4 vs. G1 & G2)	366	1.855 (1.208–2.867)	**0.005**	0.498 (0.321–0.765)	**0.002**
AFP (ng/ml) (>400 vs. ≤400)	278	4.090 (2.259–7.680)	**<0.001**	0.709 (0.402–1.237)	0.228
Vascular invasion (Yes vs. No)	315	1.409 (0.885–2.250)	0.149	0.660 (0.413–1.052)	0.082
Fibrosis ishak score (3/4&5/6 vs. 0&1/2)	212	1.131 (0.655–1.958)	0.659	1.253 (0.729–2.159)	0.416
Adjacent tissue inflammation (Mild & Severe vs. None)	234	1.584 (0.940–2.685)	0.085	0.499 (0.295–0.839)	**0.009**

Bold indicates significant differences.

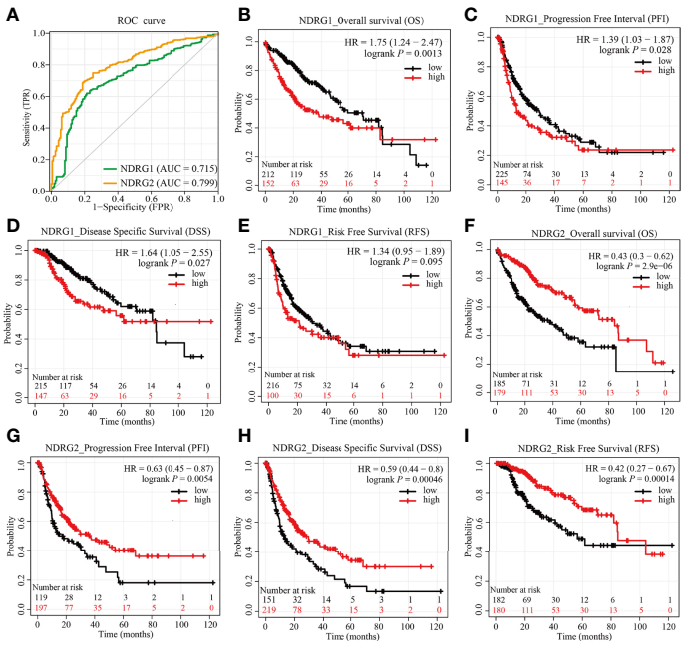

FIGURE 6 | Predictive values of *NDRG1* or *NDRG2* for diagnosis and prognosis in LIHC. **(A)** AUROC analysis evaluating the diagnosis performance of *NDRG1* or *NDRG2* for LIHC between tumor and normal tissue. **(B–E)** Kaplan–Meier (KM) survival curves comparing *NDRG1*-high and -low patients with hepatocellular carcinoma. **(F–I)** KM survival curves of OS, PFI, DSS, and RFS between high and low expression groups of *NDRG2* in LIHC.

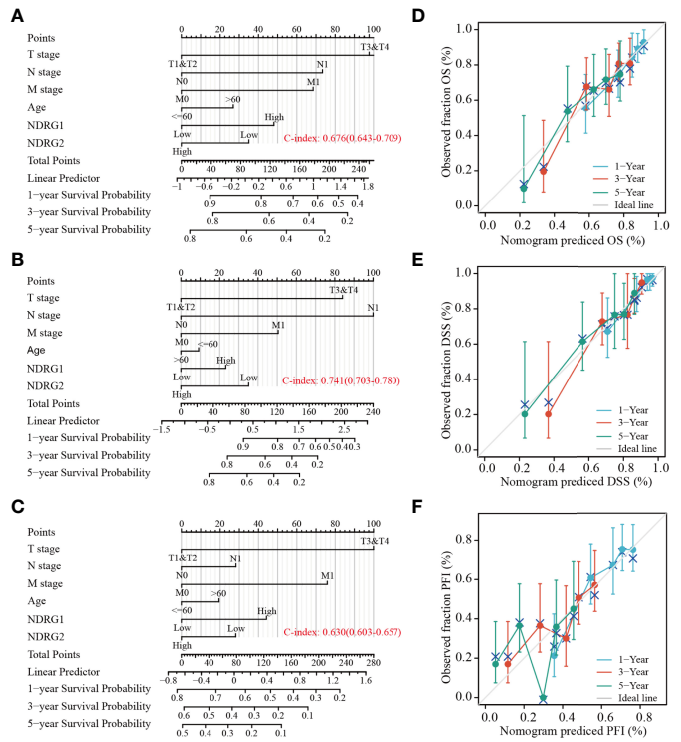

FIGURE 7 | Construction and calibration of nomograms based on *NDRG1 or NDRG2* expression. **(A–C)** Risk scoring models for 1-, 3-, and 5-year overall survival (OS), disease-specific survival (DSS), and progression-free interval (PFI). **(D–F)** Calibration diagrams validating the efficiency of nomograms for OS, DSS, and PFI.

TABLE 3 | Prognostic performance of *NDRG1* on clinical prognosis in various liver cancer patient subgroups by Cox regression analysis.

Characteristics	N (%)	HR for overall survival (95% CI)	*P*	HR for disease-specific survival (95% CI)	*P*	HR for progression-free interval (95% CI)	*P*
Sex							
Female	121 (32.6%)	1.18 (0.68–2.05)	0.557	1.44 (0.70–2.93)	0.319	2.05 (1.21–3.47)	**0.008**
Male	250 (67.4%)	1.97 (1.25–3.11)	**0.003**	1.62 (0.91–2.86)	0.100	1.15 (0.80–1.65)	0.442
Age							
≤60	177 (47.8%)	1.3 (0.76–2.20)	0.339	1.19 (0.64–2.21)	0.585	1.27 (0.84–1.92)	0.266
>60	193 (52.2%)	1.78 (1.12–2.84)	**0.014**	1.8 (0.95–3.41)	0.072	1.49 (0.98–2.25)	0.060
Clinical T stage							
Stage I–II	275 (74.7%)	1.4 (0.89–2.21)	0.146	1.41 (0.76–2.61)	0.278	1.48 (1.03–2.13)	**0.034**
Stage III–IV	93 (25.3%)	1.65 (0.96–2.86)	0.071	1.32 (0.69–2.53)	0.397	1.29 (0.77–2.16)	0.336
Clinical N stage							
N0	252 (98.4%)	1.55 (1.00–2.40)	**0.048**	1.58 (0.90–2.77)	0.113	1.44 (1.01–2.06)	**0.044**
N1	4 (1.6%)	N.A.		N.A.		N.A.	
Clinical M stage							
M0	266 (98.5%)	1.6 (1.04–2.47)	**0.034**	1.42 (0.82–2.49)	0.213	1.38 (0.97–1.96)	0.073
M1	4 (1.5%)	N.A.		N.A.		N.A.	
Vascular invasion							
No	206 (65.4%)	1.21 (0.73–2.01)	0.465	1.11 (0.55–2.23)	0.766	1.48 (0.95–2.32)	0.082
Yes	109 (34.6%)	2.19 (1.09–4.41)	**0.028**	1.31 (0.50–3.40)	0.580	1.26 (0.75–2.12)	0.382
Tumor status							
Tumor free	201 (57.1%)	1.7 (0.92–3.15)	0.088	1.15 (0.87–1.51)	0.333	1.76 (0.82–3.76)	0.144
With tumor	151 (42.9%)	1.58 (1.00–2.49)	**0.048**	1.58 (1.00–2.49)	**0.048**	1.31 (0.94–1.82)	0.108

HR, hazard ratio; CI, confidence interval; N.A, Not Available. Bold indicates significant differences.

fibroblasts in TME contribute to the progression of LIHC by secreting various growth factors and cytokines (39). Tumor-associated immune cells in TME could be divided into tumor-antagonizing and tumor-promoting immune cells (40). In this study, we observed that *NDRG1* and *NDRG2* expression were negatively associated with most of the immune infiltration cells in LIHC, namely, DCs, macrophages, and neutrophils. As is known to all, DCs are the most effective antigen-presenting cells, which can activate $CD8^+$ T cells and then initiate anti-tumor immunity (41). In the following immune response, neutrophils and macrophages work together against tumors (42). Therefore, the upregulation of *NDRG1* or downregulation of *NDRG2* seemed to suppress tumor immunity, assist cancer cells to escape from immune elimination, and finally promote tumorigenesis. Meanwhile, *NDRG1* mRNA level was positively associated with Th2 cell infiltration level, and *NDRG2* expression was positively correlated with Th17 and NK cell infiltration level. These results indicate that *NDRG1* and *NDRG2* may play vital roles in tumor infiltration immunity. Here, we observed the correlations between immune cell infiltration and the expression of *NDRG1* and *NDRG2*. However, there remains a gap to be filled between *NDRG1* and *NDRG2* in LIHC cancer and various types of immune cells.

The clinical significance of *NDRG1* and *NDRG2* is another concern. Our AUROC provided strong evidence that *NDRG1* or *NDRG2* could be biomarkers for LIHC diagnosis and prognosis. Further Cox regression analysis and nomograms further demonstrated that *NDRG1* or *NDRG2* had promising performance for evaluating clinical outcomes. Patients with higher *NDRG1* or lower *NDRG2* levels had worse OS, PFI, and DSS. In particular, the prognostic value of *NDRG1* or *NDRG2* was better when considering gender, age, and clinical TNM stages (**Figure 7**). As a result, *NDRG1* or *NDRG2* could be a promising biomarker for poor prognosis prediction. Our findings are consistent with previous reports that *NDRG1* plays a role in promoting tumorigenesis in liver, kidney, and esophageal cancers (43). In contrast, evidence has elucidated that *NDRG1* is associated with anti-oncogenic and anti-metastatic effects in breast, prostate, colorectum, and pancreatic cancers (44). The inconsistent results might be that *NDRG1* is potentially involved in many biological processes and the bi-directional crosstalk and may not play one single role. The pleiotropy of NDRG1 may reflect the heterogeneity of signal transduction in different tumor cell-types. Nowadays, the multi-omics approach (45) and the emerging single-cell studies (46) provide a new perspective on identifying biomarkers for clinical diagnosis and tumor typing.

TABLE 4 | Prognostic performance of *NDRG2* on clinical prognosis in various liver cancer patient subgroups by Cox regression analysis.

Characteristics	N (%)	HR for overall survival (95% CI)	*P*-values	HR for disease-specific survival (95% CI)	*P*-values	HR for progression-free interval (95% CI)	*P*-values
Sex							
Female	121 (32.6%)	0.87 (0.50–1.51)	0.611	1.10 (0.53–2.28)	0.796	0.99 (0.59–1.64)	0.959
Male	250 (67.4%)	0.62 (0.39–0.96)	**0.034**	0.53 (0.29–0.94)	**0.031**	0.79 (0.55–1.14)	0.209
Age							
≤60	177 (47.8%)	0.45 (0.26–0.78)	**0.004**	0.46 (0.24–0.88)	**0.019**	0.67 (0.44–1.01)	0.058
>60	193 (52.2%)	0.94 (0.59–1.47)	0.776	0.94 (0.50–1.76)	0.842	0.99 (0.650–1.49)	0.955
Clinical T stage							
Stage I–II	275 (74.7%)	0.68 (0.43–1.07)	0.095	0.73 (0.40–1.35)	0.320	0.88 (0.61–1.26)	0.493
Stage III–IV	93 (25.3%)	0.61 (0.35–1.06)	0.078	0.52 (0.27–1.01)	0.054	0.64 (0.38–1.08)	0.092
Clinical N stage							
N0	252 (98.4%)	0.65 (0.42–1.01)	0.054	0.53 (0.30–0.94)	**0.029**	0.81 (0.56–1.15)	0.236
N1	4 (1.6%)	N.A.		N.A.		N.A.	
Clinical M stage							
M0	266 (98.5%)	0.60 (0.39–0.92)	**0.020**	0.56 (0.32–0.98)	**0.043**	0.82 (0.58–1.17)	0.275
M1	4 (1.5%)	N.A.		N.A.		N.A.	
Vascular invasion							
No	206 (65.4%)	0.67 (0.40–1.13)	0.134	0.76 (0.37–1.54)	0.443	0.88 (0.56–1.36)	0.556
Yes	109 (34.6%)	0.96 (0.49–1.89)	0.911	0.85 (0.33–2.21)	0.745	1.02 (0.61–1.73)	0.931
Tumor status							
Tumor free	201 (57.1%)	0.71 (0.39–1.30)	0.261	0.79 (0.60–1.05)	0.101	1.09 (0.51–2.31)	0.825
With tumor	151 (42.9%)	0.72 (0.46–1.14)	0.161	0.72 (0.46–1.14)	0.161	0.93 (0.67–1.28)	0.108

HR, hazard ratio; CI, confidence interval; N.A, Not Available. Bold indicates significant differences.

In short, the mRNA expression and DNA methylation of NDRG superfamily members (*NDRG1* and *NDRG2*) show the potential for LIHC diagnosis and prognosis *via* integrative analysis from multiple cohorts. Considering the multiple mechanisms of the *NDRG* family, more experiments and a larger sample size will be needed to demonstrate and validate our bioinformatics results for future clinical application.

DATA AVAILABILITY STATEMENT

The original contributions presented in the study are included in the article/supplementary material. Further inquiries can be directed to the corresponding author.

ETHICS STATEMENT

The studies involving human participants were reviewed and approved by The hospital ethics committee, Zhongnan Hospital of Wuhan University. The patients/participants provided their written informed consent to participate in this study. Written informed consent was obtained from the individual(s) for the publication of any potentially identifiable images or data included in this article.

AUTHOR CONTRIBUTIONS

S-ML and SX conceived and designed the experiments. SX, YZho, YY, and RG analyzed data and drafted the original manuscript. YZha and RG performed the experiments. S-ML, CL and QL critically revised the manuscript. All authors listed have made a substantial, direct, and intellectual contribution to the work and approved it for publication.

FUNDING

This work was supported by the National Natural Science Foundation of China (81772276) and the Hubei Provincial Natural Science Fund for Creative Research Groups (2019CFA018).

REFERENCES

1. Bray F, Ferlay J, Soerjomataram I, Siegel RL, Torre LA, Jemal A. Global Cancer Statistics 2018: GLOBOCAN Estimates of Incidence and Mortality Worldwide for 36 Cancers in 185 Countries. *CA Cancer J Clin* (2018) 68 (6):394–424. doi: 10.3322/caac.21492
2. Yu LX, Schwabe RF. The Gut Microbiome and Liver Cancer: Mechanisms and Clinical Translation. *Nat Rev Gastroenterol Hepatol* (2017) 14(9):527–39. doi: 10.1038/nrgastro.2017.72
3. Njei B, Rotman Y, Ditah I, Lim JK. Emerging Trends in Hepatocellular Carcinoma Incidence and Mortality. *Hepatology* (2015) 61(1):191–9. doi: 10.1002/hep.27388
4. Mokdad AA, Hester CA, Singal AG, Yopp AC. Management of Hepatocellular in the United States. *Chin Clin Oncol* (2017) 6(2):21. doi: 10.21037/cco.2017.04.04
5. Boyault S, Rickman DS, de Reynies A, Balabaud C, Rebouissou S, Jeannot E, et al. Transcriptome Classification of HCC is Related to Gene Alterations and to New Therapeutic Targets. *Hepatology* (2007) 45(1):42–52. doi: 10.1002/hep.21467
6. El-Serag HB. Epidemiology of Viral Hepatitis and Hepatocellular Carcinoma. *Gastroenterology* (2012) 142(6):1264–73.e1. doi: 10.1053/j.gastro.2011.12.061
7. Melotte V, Qu X, Ongenaert M, van Criekinge W, de Bruine AP, Baldwin HS, et al. The N-Myc Downstream Regulated Gene (NDRG) Family: Diverse Functions, Multiple Applications. *FASEB J* (2010) 24(11):4153–66. doi: 10.1096/fj.09-151464
8. Sun J, Zhang D, Bae DH, Sahni S, Jansson P, Zheng Y, et al. Metastasis Suppressor, NDRG1, Mediates its Activity Through Signaling Pathways and Molecular Motors. *Carcinogenesis* (2013) 34(9):1943–54. doi: 10.1093/carcin/bgt163
9. Lee DC, Kang YK, Kim WH, Jang YJ, Kim DJ, Park IY, et al. Functional and Clinical Evidence for NDRG2 as a Candidate Suppressor of Liver Cancer Metastasis. *Cancer Res* (2008) 68(11):4210–20. doi: 10.1158/0008-5472
10. Kovacevic Z, Richardson DR. The Metastasis Suppressor, Ndrg-1: A New Ally in the Fight Against Cancer. *Carcinogenesis* (2006) 27(12):2355–66. doi: 10.1093/carcin/bgl146
11. Choi SC, Kim KD, Kim JT, Kim JW, Lee HG, Kim JM, et al. Expression of Human NDRG2 by Myeloid Dendritic Cells Inhibits Down-Regulation of Activated Leukocyte Cell Adhesion Molecule (ALCAM) and Contributes to Maintenance of T Cell Stimulatory Activity. *J Leukoc Biol* (2008) 83(1):89–98. doi: 10.1189/jlb.0507300
12. Park KC, Lee DC, Yeom YI. NDRG3-Mediated Lactate Signaling in Hypoxia. *BMB Rep* (2015) 48(6):301–2. doi: 10.5483/bmbrep.2015.48.6.080
13. Qu X, Jia H, Garrity DM, Tompkins K, Batts L, Appel B, et al. Ndrg4 is Required for Normal Myocyte Proliferation During Early Cardiac Development in Zebrafish. *Dev Biol* (2008) 317(2):486–96. doi: 10.1016/j.ydbio.2008.02.044
14. Hu XL, Liu XP, Lin SX, Deng YC, Liu N, Li X, et al. NDRG2 Expression and Mutation in Human Liver and Pancreatic Cancers. *World J Gastroenterol* (2004) 10(23):3518–21. doi: 10.3748/wjg.v10.i23.3518
15. Lorentzen A, Lewinsky RH, Bornholdt J, Vogel LK, Mitchelmore C. Expression Profile of the N-Myc Downstream Regulated Gene 2 (NDRG2) in Human Cancers With Focus on Breast Cancer. *BMC Cancer* (2011) 11:14. doi: 10.1186/1471-2407-11-14
16. Ando T, Ishiguro H, Kimura M, Mitsui A, Kurehara H, Sugito N, et al. Decreased Expression of NDRG1 is Correlated With Tumor Progression and Poor Prognosis in Patients With Esophageal Squamous Cell Carcinoma. *Dis Esophagus* (2006) 19(6):454–8. doi: 10.1111/j.1442-2050.2006.00618.x
17. Goldman MJ, Craft B, Hastie M, Repecka K, McDade F, Kamath A, et al. Visualizing and Interpreting Cancer Genomics Data *via* the Xena Platform. *Nat Biotechnol* (2020) 38(6):675–8. doi: 10.1038/s41587-020-0546-8
18. Vivian J, Rao AA, Nothaft FA, Ketchum C, Armstrong J, Novak A, et al. Toil Enables Reproducible, Open Source, Big Biomedical Data Analyses. *Nat Biotechnol* (2017) 35(4):314–6. doi: 10.1038/nbt.3772
19. Love MI, Huber W, Anders S. Moderated Estimation of Fold Change and Dispersion for RNA-Seq Data With Deseq2. *Genome Biol* (2014) 15(12):550. doi: 10.1186/s13059-014-0550-8
20. Yu G, Wang LG, Han Y, He QY. Clusterprofiler: An R Package for Comparing Biological Themes Among Gene Clusters. *OMICS* (2012) 16(5):284–7. doi: 10.1089/omi.2011.0118
21. Subramanian A, Tamayo P, Mootha VK, Mukherjee S, Ebert BL, Gillette MA, et al. Gene Set Enrichment Analysis: A Knowledge-Based Approach for Interpreting Genome-Wide Expression Profiles. *Proc Natl Acad Sci U S A* (2005) 102(43):15545–50. doi: 10.1073/pnas.0506580102
22. Hanzelmann S, Castelo R, Guinney J. GSVA: Gene Set Variation Analysis for Microarray and RNA-Seq Data. *BMC Bioinf* (2013) 14:7. doi: 10.1186/1471-2105-14-7
23. Bindea G, Mlecnik B, Tosolini M, Kirilovsky A, Waldner M, Obenauf AC, et al. Spatiotemporal Dynamics of Intratumoral Immune Cells Reveal the Immune Landscape in Human Cancer. *Immunity* (2013) 39(4):782–95. doi: 10.1016/j.immuni.2013.10.003
24. Gao J, Aksoy BA, Dogrusoz U, Dresdner G, Gross B, Sumer SO, et al. Integrative Analysis of Complex Cancer Genomics and Clinical Profiles Using the Cbioportal. *Sci Signal* (2013) 6(269):l1. doi: 10.1126/scisignal.2004088
25. Modhukur V, Iljasenko T, Metsalu T, Lokk K, Laisk-Podar T, Vilo J. MethSurv: A Web Tool to Perform Multivariable Survival Analysis Using DNA Methylation Data. *Epigenomics* (2018) 10(3):277–88. doi: 10.2217/epi-2017-0118
26. Yang JD, Hainaut P, Gores GJ, Amadou A, Plymoth A, Roberts LR. A Global View of Hepatocellular Carcinoma: Trends, Risk, Prevention and Management. *Nat Rev Gastroenterol Hepatol* (2019) 16(10):589–604. doi: 10.1038/s41575-019-0186-y
27. Askautrud HA, Gjernes E, Gunnes G, Sletten M, Ross DT, Borresen-Dale AL, et al. Global Gene Expression Analysis Reveals a Link Between NDRG1 and Vesicle Transport. *PLoS One* (2014) 9(1):e87268. doi: 10.1371/journal.pone.0087268
28. Pietiainen V, Vassilev B, Blom T, Wang W, Nelson J, Bittman R, et al. NDRG1 Functions in LDL Receptor Trafficking by Regulating Endosomal Recycling and Degradation. *J Cell Sci* (2013) 126(Pt 17):3961–71. doi: 10.1242/jcs.128132
29. Ellen TP, Ke Q, Zhang P, Costa M. NDRG1, a Growth and Cancer Related Gene: Regulation of Gene Expression and Function in Normal and Disease States. *Carcinogenesis* (2008) 29(1):2–8. doi: 10.1093/carcin/bgm200
30. Yang X, Zhu F, Yu C, Lu J, Zhang L, Lv Y, et al. N-Myc Downstream-Regulated Gene 1 Promotes Oxaliplatin-Triggered Apoptosis in Colorectal Cancer Cells *via* Enhancing the Ubiquitination of Bcl-2. *Oncotarget* (2017) 8 (29):47709–24. doi: 10.18632/oncotarget.17711
31. Kawahara A, Akiba J, Hattori S, Yamaguchi T, Abe H, Taira T, et al. Nuclear Expression of N-Myc Downstream Regulated Gene 1/Ca(2+)-Associated Protein 43 is Closely Correlated With Tumor Angiogenesis and Poor Survival in Patients With Gastric Cancer. *Exp Ther Med* (2011) 2(3):471–9. doi: 10.3892/etm.2011.222
32. Chen Z, Zhang D, Yue F, Zheng M, Kovacevic Z, Richardson DR. The Iron Chelators Dp44mT and DFO Inhibit TGF-Beta-Induced Epithelial-Mesenchymal Transition *via* Up-Regulation of N-Myc Downstream-Regulated Gene 1 (NDRG1). *J Biol Chem* (2012) 287(21):17016–28. doi: 10.1074/jbc.M112.350470
33. Stein S, Thomas EK, Herzog B, Westfall MD, Rocheleau JV, Jackson RS2nd, et al. NDRG1 is Necessary for P53-Dependent Apoptosis. *J Biol Chem* (2004) 279(47):48930–40. doi: 10.1074/jbc.M400386200
34. Cheng J, Xie HY, Xu X, Wu J, Wei X, Su R, et al. NDRG1 as a Biomarker for Metastasis, Recurrence and of Poor Prognosis in Hepatocellular Carcinoma. *Cancer Lett* (2011) 310(1):35–45. doi: 10.1016/j.canlet.2011.06.001
35. Mao Z, Sun J, Feng B, Ma J, Zang L, Dong F, et al. The Metastasis Suppressor, N-Myc Downregulated Gene 1 (NDRG1), is a Prognostic Biomarker for Human Colorectal Cancer. *PLoS One* (2013) 8(7):e68206. doi: 10.1371/journal.pone.0068206
36. Choi SC, Yoon SR, Park YP, Song EY, Kim JW, Kim WH, et al. Expression of NDRG2 is Related to Tumor Progression and Survival of Gastric Cancer Patients Through Fas-Mediated Cell Death. *Exp Mol Med* (2007) 39(6):705–14. doi: 10.1038/emm.2007.77
37. Klutstein M, Nejman D, Greenfield R, Cedar H. DNA Methylation in Cancer and Aging. *Cancer Res* (2016) 76(12):3446–50. doi: 10.1158/0008-5472.CAN-15-3278
38. Yamashita K, Hosoda K, Nishizawa N, Katoh H, Watanabe M. Epigenetic Biomarkers of Promoter DNA Methylation in the New Era of Cancer Treatment. *Cancer Sci* (2018) 109(12):3695–706. doi: 10.1111/cas.13812
39. Zhang J, Gu C, Song Q, Zhu M, Xu Y, Xiao M, et al. Identifying Cancer-Associated Fibroblasts as Emerging Targets for Hepatocellular Carcinoma. *Cell Biosci* (2020) 10(1):127. doi: 10.1186/s13578-020-00488-y

40. Lei X, Lei Y, Li JK, Du WX, Li RG, Yang J, et al. Immune Cells Within the Tumor Microenvironment: Biological Functions and Roles in Cancer Immunotherapy. *Cancer Lett* (2020) 470:126–33. doi: 10.1016/j.canlet.2019.11.009
41. Fu C, Jiang A. Dendritic Cells and CD8 T Cell Immunity in Tumor Microenvironment. *Front Immunol* (2018) 9:3059. doi: 10.3389/fimmu.2018.03059
42. Qu X, Tang Y, Hua S. Immunological Approaches Towards Cancer and Inflammation: A Cross Talk. *Front Immunol* (2018) 9:563. doi: 10.3389/fimmu.2018.00563
43. Fang BA, Kovacevic Z, Park KC, Kalinowski DS, Jansson PJ, Lane DJ, et al. Molecular Functions of the Iron-Regulated Metastasis Suppressor, NDRG1, and its Potential as a Molecular Target for Cancer Therapy. *Biochim Biophys Acta* (2014) 1845(1):1–19. doi: 10.1016/j.bbcan.2013.11.002
44. Bae DH, Jansson PJ, Huang ML, Kovacevic Z, Kalinowski D, Lee CS, et al. The Role of NDRG1 in the Pathology and Potential Treatment of Human Cancers. *J Clin Pathol* (2013) 66(11):911–7. doi: 10.1136/jclinpath-2013-201692
45. Su J, Song Q, Qasem S, O'Neill S, Lee J, Furdui CM, et al. Multi-Omics Analysis of Brain Metastasis Outcomes Following Craniotomy. *Front Oncol* (2020) 10:615472. doi: 10.3389/fonc.2020.615472
46. Song Q, Su J, Miller LD, Zhang W. scLM: Automatic Detection of Consensus Gene Clusters Across Multiple Single-Cell Datasets. *Genomics Proteomics Bioinf* (2021) 19(2):330–41. doi: 10.1016/j.gpb.2020.09.002

Conflict of Interest: The authors declare that the research was conducted in the absence of any commercial or financial relationships that could be construed as a potential conflict of interest.

Publisher's Note: All claims expressed in this article are solely those of the authors and do not necessarily represent those of their affiliated organizations, or those of the publisher, the editors and the reviewers. Any product that may be evaluated in this article, or claim that may be made by its manufacturer, is not guaranteed or endorsed by the publisher.

frontiers | Frontiers in Oncology

ORIGINAL RESEARCH
published: 24 June 2022
doi: 10.3389/fonc.2022.923009

Bioinformatics-Driven Identification of p62 as A Crucial Oncogene in Liver Cancer

Ling Wang[1,2]*, *Culton R. Hensley*[1], *Mary E. Howell*[1] and *Shunbin Ning*[1,2]

[1] Department of Internal Medicine, Quillen College of Medicine, East Tennessee State University, Johnson City, TN, United States, [2] Center of Excellence for Inflammation, Infectious Diseases and Immunity, Quillen College of Medicine, East Tennessee State University, Johnson City, TN, United States

OPEN ACCESS

Edited by:
Hua Tan,
National Human Genome Research Institute (NIH), United States

Reviewed by:
Zeguo Sun,
Icahn School of Medicine at Mount Sinai, United States
Hao Yan,
Stanford University, United States

***Correspondence:**
Ling Wang
wangl3@etsu.edu

Specialty section:
This article was submitted to Cancer Genetics, a section of the journal Frontiers in Oncology

Received: 18 April 2022
Accepted: 27 May 2022
Published: 24 June 2022

Citation:
Wang L, Hensley CR, Howell ME and Ning S (2022) Bioinformatics-Driven Identification of p62 as A Crucial Oncogene in Liver Cancer. Front. Oncol. 12:923009. doi: 10.3389/fonc.2022.923009

Liver hepatocellular carcinoma (LIHC) is the major form of liver cancer that is the fourth most common cause of cancer death worldwide. It has been reported that the multifunctional protein p62 (also known as SQSTM1) plays a cancer-promoting role in LIHC, but the detailed mechanisms underlying p62 interaction with LIHC remains unclear. To gain a comprehensive understanding of p62 interaction with LIHC in clinical settings, we performed bioinformatic analyses using various online algorithms derived from high throughput profiling. Our results indicate that p62 expression is significantly upregulated, partially due to its promoter demethylation, rather than p62 gene mutation, in LIHC. Mutation of TP53, CTNNB1, or ALB significantly correlates with, and mutation of AXIN1 reversely correlates with, the p62 expression level. Its upregulation occurs as early as liver cirrhosis, and go through all stages of the carcinogenesis. HCV infection makes a significant contribution to p62 upregulation in LIHC. We further identified p62-associated molecular signatures in LIHC, including many genes that are involved in antioxidant stress and metabolism, such as SRX1 and TXNRD1. Regarding to the clinical outcome, p62 expression level reversely correlates with the survival of LIHC patients ($p<0.01$). Importantly, we experimentally validated that p62 depletion in liver cancer cell lines downregulates the expression of SRX1 and TXNRD1 at both transcriptional and translational levels, and reduces cell proliferation. As the potential mechanisms underlying the tumor-promoting role of p62, we show that p62 upregulation is remarkably associated with reprogramming of pathways mediated by p53, Wnt/β-catenin, and Keap1-NRF2, which are crucial for oncogenesis in many contexts. Our findings provide a comprehensive insight into the interaction between p62 and LIHC, offering valuable information for understanding of LIHC pathogenesis.

Keywords: p62, LIHC, SRX1, TXNRD1, algorithm analysis

INTRODUCTION

Liver hepatocellular carcinoma (LIHC), or hepatocellular carcinoma (HCC), is the major form of liver cancer that is the fourth most common cause of cancer death worldwide, with a 5-year survival rate of about 18% (1). LIHC is causally associated with chronic tissue damage and inflammation, and stress and environmental carcinogen exposure (such as obesity and alcohol consumption), with chronic viral infections (HCV and HBV) playing the major role.

Nearly three thousand genetic mutations have been identified in LIHC patients, and the most frequently mutated loci include the TERT promoter and the genes coding for P53, β-Catenin, ALB, KEAP1, and NRF2 (2). Interestingly, both Keap1 and NRF2 are the components of the Keap1-NRF2 pathway that transactivate a pool of approximate 250 target genes, of which many are involved in antioxidant defense including p62 (as known as SQSTM1), Cox-2, iNOS, PRDX1, HIF1, NQO1, HMOX1, GSTs, and Keap1 and NRF2 themselves (3–6).

As a key transcriptional target of the transcription factor NRF2, p62 plays crucial roles in DNA damage response (DDR), cancer development, mTORC1-mediated nutrient sensing and metabolism, cell death, aging, inflammation and immunity, cell differentiation, osteoclastogenesis, neurotrophin properties and obesity, dependently or independenely of the autophagy machinery (2, 7–12).

The tumor-promoting properties of p62 are underscored by the facts that p62 is upregulated in different cancer contexts, including LIHC, and breast and prostate cancers (2, 13–17), and that p62 is induced by the oncoprotein Ras that accounts for more than 25% of human cancers (18). p62 overexpression in LIHC predicts poor prognosis (15). In mouse models with defective autophagy, p62 ablation decreases tumorigenesis (18).

To achieve a comprehensive understanding of the association of p62 with the development of LIHC, in this study, we have employed various online algorithms to conduct secondary analyses of available datasets. We show that p62 expression is significantly upregulated in LIHC, and identified p62-associated molecular signatures in this setting. We experimentally confirmed that p62 depletion in liver cancer cell lines downregulates the expression of SRX1 and TXNRD1 at both transcriptional and translational levels, and reduces cell proliferation. Moreover, these meta-analyses of clinical samples consolidate the claim that p62 can serve as a prognostic marker for LIHC patients.

METHODS

Algorithm Meta-Analysis

We employed different online algorithms for metadata analysis, including Oncomine (19), Genotype-Tissue Expression (GTEx), Gene Expression Atlas, ProteinAtlas, proteomicsDB, Tumor Immune Estimation Resource (TIMER v2) (20, 21), Gene Expression Profiling Interactive Analysis (GEPIA v2) (22), Tumor-Immune System Interactions Database (TISIDB) (23), UALCAN (24), COSMIC, Tumor Fusion Gene Data Portal (TumorFusions) (25), FusionGDB (26), ChimerDB v4 that integrates several different fusion portals such as STARFusion, TCGA-FAWG, and FusionScan (27), cBioportal (28, 29), DriverDBv3 (30), Kaplan Meier Plotter (KMPlot) (31), muTarget (32), and EMSEMBL, for mRNA and protein expression, correlation, gene mutation, fusion, tumor-immune interaction, and survival analyses. All portals include the Cancer Genome Atlas (TCGA) datasets, in addition to other unique datasets obtained from patients and cell lines. BioGRID (33, 34), GeneMANIA (35, 36), STRING, Uniprot, and KEGG portals were applied for post-translational modifications, signaling pathway, and protein-protein and functional interaction analyses.

All analyses were conducted using the default settings if not otherwise indicated, with the detailed dataset information and guidelines provided online by each portal. $p<0.05$ is considered statistically significant and >0.05 is non-significant (n.s.), and $p<0.01$ is considered statistically very significant.

Cell Lines

Two liver cancer epithelial cell lines, Huh7D12 and HepG2 were used to validate the target genes regulated by p62 at the transcriptional and translational levels. These cell lines were cultured at 37°C with DMEM media plus 5% FBS (the lower percentage was reported to reduce cell aggregation without affecting cell growth) and antibiotics (Life Technologies).

Lentiviral Transfection and CRISPR-Mediated Depletion

p62-specific CRISPR/Cas9 plasmids were generated by GenScript by cloning p62 sgRNAs into pLenti-CRISPRv2 eSpCas9 lentiviral vector (puro), and the targeting sequences are (both in cDNA): p62 sgRNA#1: 5'-GAAGATGTCATCCTTCACGT, and p62 sgRNA#2: 5'-TTCGGATTCTGGCATCTGTA. Lentivirus packing and transfection, and selection of stable polyclonal transfectants with puromycin were carried out as detailed in our previous publication (37).

Reagents, Antibodies and Immunoblotting

p62 (clone D-3) mouse monoclonal antibody was from Santa Cruz. Mouse TXNRD1 (clone 1B10C4) and rabbit SRX1 (polyclonal) antibodies were purchased from Proteintech. HRP-coupled secondary antibodies were from Cell Signaling Technologies.

Cell lysates were lysed with NP40 lysis buffer (150 mM NaCl, 1% NP-40, 50 mM Tris-pH 8.0, plus protease inhibitors), followed by immunoblotting (IB) with indicated antibodies, and signals were detected with the enhanced chemiluminescence (ECL) kit following the manufacturer's protocol (Amersham Pharmacia Biotech).

The broad-spectrum inhibitor of histone demethylases IOX1 was purchased from MedChemExpress.

Primers and Real-Time qPCR

Total RNA was isolated from the tested liver cancer cell lines with an RNeasy Mini kit (Qiagen). Reverse transcription was performed with an AMV-mediated RT kit (Promega). Quantitative real-time PCR (qPCR) was performed with the

use of SYBR Green (Applied Biosystems), on a CFX96™ Real-time PCR Detection System (Bio-Rad). All reactions were run in triplicates. Mean cycle threshold (C_t) values were normalized to 18s rRNA, yielding a normalized $C_t(\Delta C_t)$. $\Delta\Delta C_t$ value was calculated by subtracting respective control from the ΔC_t, and the expression level was then calculated by 2 raised to the power of respective $-\Delta\Delta C_t$ value. The averages of $2^{(-\Delta\Delta C_t)}$ in the control samples were set to 1 or 100%. Results are the average ± standard error (SE) of duplicates or triplicates for each sample. Primers for real-time qPCR are as follows: Txnrd1: F: 5'-GTTACTTGGGCATCCCTGGTGA-3'; R: 5'-CGCACTCCAAAGCGACATAGGA-3'. Srx1: 5'-GCAGAGCCTCGTGGACACGAT-3'; R: 5'-ATGGTCTCTCGCTGCAGTTGCT-3'; HTATIP2: F: 5'-GCCTGTTTTCCAAAGTCACGCTC-3'; R: 5'-CCTTGAAAGGCAGAGGCGTAGT-3'. TTC1: F: 5'-AACATGTCGGATGAAGAGAAACAG-3'; R: 5'- GGAAG CAGGATGGGCACATTTC-3'. p62: F: 5'-CAGGCGCA CTACCGCGATG-3', and R: 5'-ACACAAGTCGTAGTCTGG GCAGAC-3'. 18s rRNA: F: 5'-GGCCCTGTAATTGGAAT GAGTC-3', and R: 5'-CCAAGATCCAACTACGAGCTT-3'.

Proliferation Assay

MTT proliferation assay was carried out following the manufacturer's instructions (Promega). Cells were seeded $1X10^5$ per well in 6-well plates. The proliferation rates of the control sgRNA were set to 100%. Data are expressed as mean ± standard error (SE) of triplicate samples, and representative results from at least three independent repeats with similar results are shown.

RESULTS

Tissue- and Cell-Specific Expression of p62

To understand the role of p62 (also known as SQSTM1) in different contexts, we first evaluated its tissue- and cell-specific expression patterns in humans, in GTEx and ProteinAtlas portals, which include datasets obtained from human protein atlas (HPA), functional annotation of the mammalian genome (FANTOM v5), and GTEx projects. The p62-encoding gene *Sqstm1* produces sixteen alternatively spliced variants (**Figure 1A**). The ENSEMBL portal shows that nine of these sixteen splice variants encode proteins, with the size of 440 aa for the dominant transcript ENST00000389805. Analysis in GTEx portal indicates that five of the splice variants are widely expressed in various tissues and cell lines (**Figure 1B**), with the highest levels being culminated in skeletal muscle, adrenal gland, and cultured fibroblasts (**Figures 1B, C**).

Regarding cell-specific expression, analysis in ProteinAtlas portal shows that the transcript abundance of p62 is mainly enriched in epithelial cells from different tissues (**Figure 1D**).

p62 Is Upregulated in LIHC

We next analyzed p62 mRNA abundance in different human cancers, using Oncomine, TIMER2.0, GEPIA2, UALCAN, and DriverDBv3. Results from different portals show that *Sqstm1* transcript is significantly upregulated in LIHC, breast cancer (BRCA), colon adenocarcinoma (COAD), kidney cancers, and thyroid carcinoma (THCA), and downregulated in bladder urothelial carcinoma (BLCA) and prostate adenocarcinoma (PRAD), compared with the levels in corresponding normal (healthy) tissues. Results from the TCGA dataset in TIMER2 are shown in **Figure 2A**.

Analysis of the TCGA dataset in UALCAN shows that p62 mRNA level is 2.8-fold higher (p<1e-12) in primary LIHC (n=371) compared to normal liver tissues (n=50) (**Figure 2B**). Analysis of gene chip data from a combination of different datasets in TNMPlot, including the TCGA, GEO, GTEx, and TARGET datasets, indicates that p62 mRNA level is 2.40-fold higher in primary LIHC (n=806; p=5.72e-26), and is marginally higher (1.15-fold) in metastatic LIHC (n=24; p=5.13e-25), compared to the normal (n=379) (**Figure 2C**). Significant upregulation of p62 is consistently detected at other algorithm platforms with various datasets, including Mas liver cancer dataset and Roessler liver cancer 2 dataset in Oncomine (**Figures 2D, E**). Correspondingly, analysis of CPTAC samples indicates that p62 protein level is also significantly upregulated in LIHC (**Figure 2F**). Together, these analyses of various datasets reveal that SQSTM1/p62 is significantly upregulated at both transcriptional and translational levels in liver cancer patients.

Further analysis shows that p62 upregulation occurs at all stages of LIHC (**Figure 3A**), starting from as early as liver cirrhosis (**Figure 3B**). However, there are no significant differences between each two stages (**Figure 3A**), except a significant difference (p=1.86e-04) between liver cirrhosis (n=58) and liver cancer (n=38) (**Figure 3B**). Analysis of Wurmbach liver cancer dataset shows that HCV infection plays a significant role in p62 upregulation, with log2(FC)=2.36 and p=4.23e-08 comparing HCV-positive patients (n=96) to HCV-negative patients (n=19) (**Figure 3C**). Furthermore, p62 levels are significant different between tumor grades 1 and 2, and between grades 1 and 3 (**Figure 3D**). The difference between grade 4 and any other grade or normal is not significant, likely due to the small sample size (n=12) (**Figure 3D**). In addition, p62 levels are significant different in different races of liver cancer patients, with Caucasian patients (n=177) have the lowest p62 levels, compared to Africans and Asians (n=17, p= 3.91e-02, and n=157, p=2.74e-02, respectively).

In summary, p62 is accumulated during the cancer progress in LIHC, starting with a significant upregulation from liver cirrhosis, and HCV infection makes a significant contribution.

p62 Gene Undergoes a Low Rate of Mutations in LIHC

LIHC is very heterogeneous, with over 28,000 different somatic mutations of a large range of genes having been identified. Mutation analysis of TCGA dataset in TIMER, cBioportal, and DriverDBv3 portals shows that the *Sqstm1* gene undergoes near 8% of point mutation, followed by amplification and deep deletion, in various cancers (**Figure 4A**). However, contrast to the genes encoding Keap1 and NRF2 that among top genes

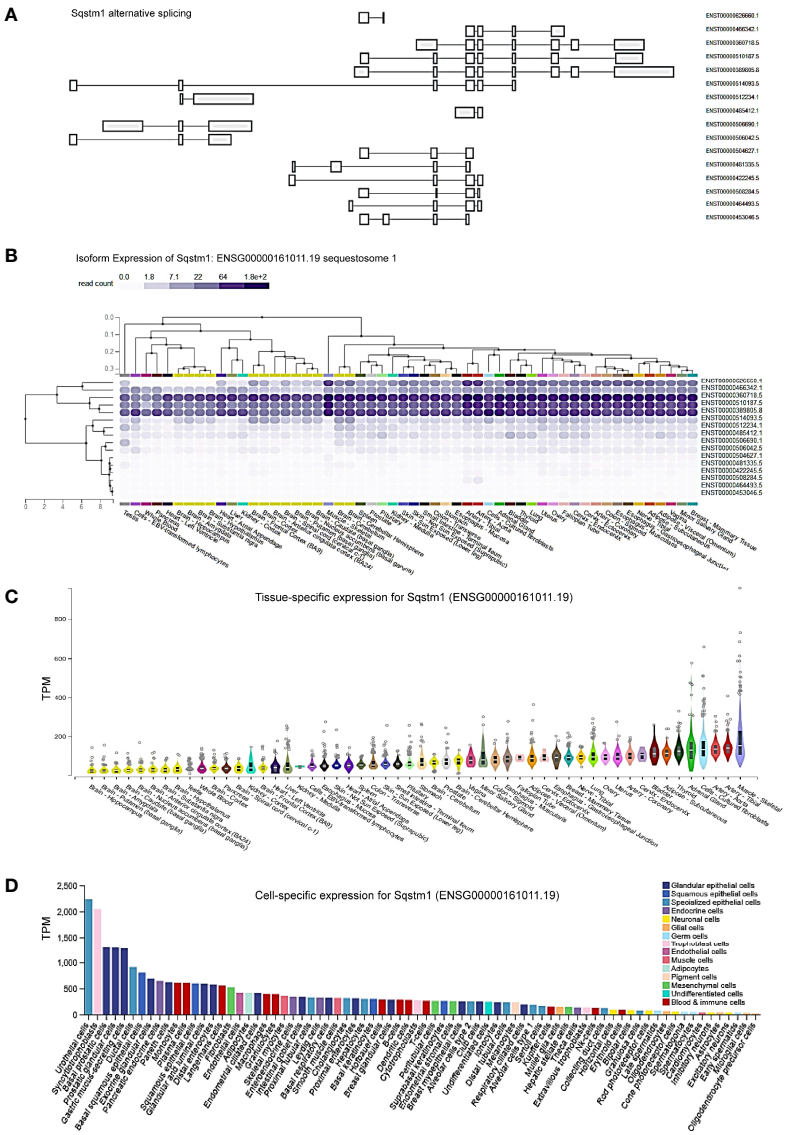

FIGURE 1 | Tissue- and cell-specific expression of Sqstm1. **(A)** Sixteen splicing variants of Sqstm1 primary transcript, nine of which encode proteins, with the dominant transcript ENST00000389805 encoding a protein of 440 aa in length. **(B, C)** Tissue- and cell-specific expression of *Sqstm1* splicing variants, respectively. Total transcript of *Sqstm1* gene (ENSG000000161011) is shown. **(D)** Cell-specific expression of Sqstm1 transcript. **(A–C)** are the results from GTEx portal, and **(D)** from ProteinAtlas portal. TPM, transcripts per million; NX, denoted normalized expression. Read counts and TPM values were generated with RNA-SeQC v1.1.9 (38).

undergo mutations in LIHC, *Sqstm1* only displays a low rate of mutations in LIHC (1/365), whereas undergoes higher mutation rates in UCEC (14/531), STAD (11/439), and PAAD (4/178) (**Figure 4B**). However, COSMIC portal shows that *Sqstm1* cDNA somatic mutations (substitutions and others) were detected in 24 out of 46 LIHC samples (52.17%) (**Figure 4C**).

FusionGDB analysis reveals 33 different *Sqstm1* fusion genes in various cancers and diseases (**Supplementary Table S1**). cBioportal analysis shows that *Sqstm1-Adgrv1* (not detected in FusionGDB) and *Sqstm1-Gria1* fusions occur in LUAD, *Sqstm1-Cpb1* fusion occurs in BRCA, and *Sqstm1-Ntrk2* occurs in LGG, with *Sqstm1-Adgrv1* fusion in LUAD associated with a remarkable decrease of Sqstm1 expression (**Figure 4D**). *Usp10-Sqstm1* fusion was found in a patient with combined hepatocellular and intrahepatic cholangiocarcinoma. Consistent results from different portals, including cBioportal and TIMER2, indicate that the overall *Sqstm1* mutation has significant effects on its expression in UCEC (increase, p=0.045) and STAD (decrease, p=0.03) (**Figure 4E**). Analysis was not performed for other types of cancer (including LIHC) in that the sample sizes with *Sqstm1* mutation of these cancers are not powerful enough (**Figure 4B**).

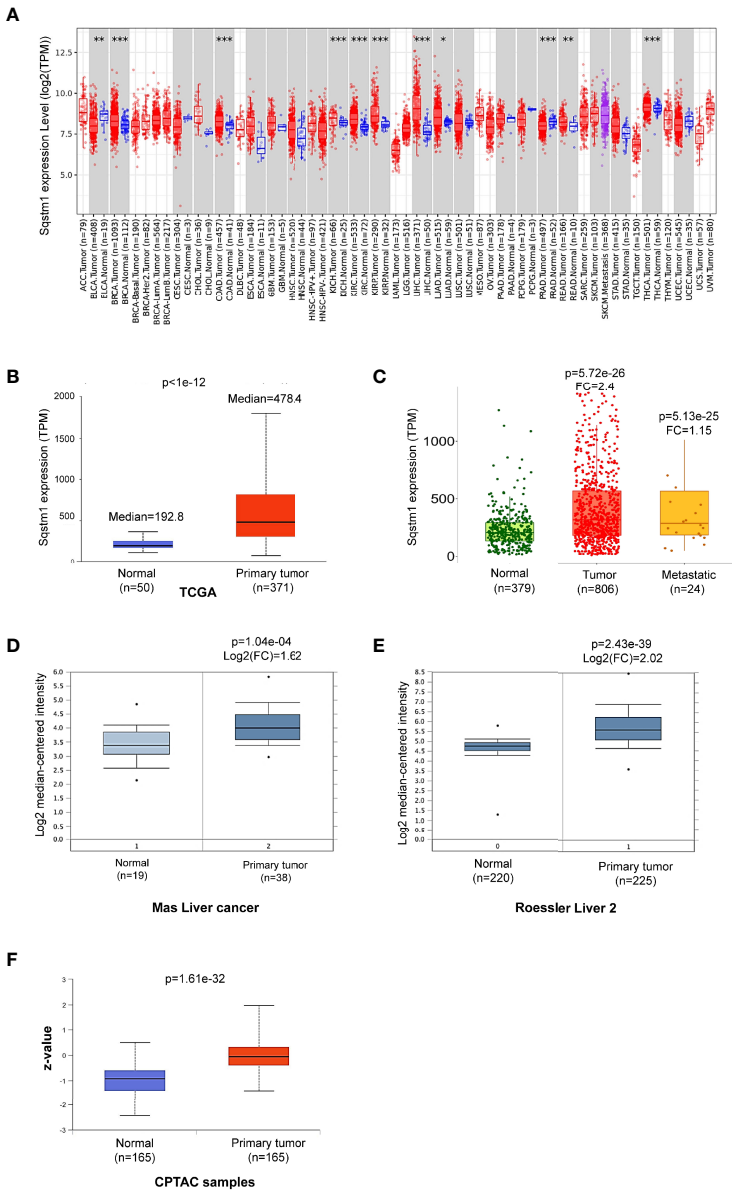

FIGURE 2 | Sqstm1 is upregulated in LIHC. **(A)** Deregulation of Sqstm1 at the transcriptional level in various cancers (*p < 0.05; **p < 0.01; ***p < 0.001). Methodology was described in detail in (20, 21). Blue: Normal tissues; Red: Tumor tissues. Pink: Tumor tissues without normal tissue controls; Purple: Metastasis tumor tissues. ACC, Adrenocortical carcinoma; BLCA, Bladder Urothelial Carcinoma; BRCA, Breast invasive carcinoma; CESC, Cervical squamous cell carcinoma and endocervical adenocarcinoma; CHOL, Cholangio carcinoma; COAD, Colon adenocarcinoma; DLBC, Diffuse large B-cell lymphoma; ESCA, Esophageal carcinoma; GBM, Glioblastoma multiforme; HNSC, Head and Neck squamous cell carcinoma; KICH, Kidney chromophobe; KIRC, Kidney renal clear cell carcinoma; KIRP, Kidney renal papillary cell carcinoma; LAML, Acute myeloid leukemia; LGG, Brain lower-grade glioma; LIHC, Liver hepatocellular carcinoma; LUAD, Lung adenocarcinoma; LUSC, Lung squamous cell carcinoma; MESO, Mesothelioma; OV, Ovarian serous cystadenocarcinoma; PAAD, Pancreatic adenocarcinoma; PCPG, Pheochromocytoma and paraganglioma; PRAD, Prostate adenocarcinoma; READ, Rectum adenocarcinoma; SARC, Sarcoma; SKCM, Skin cutaneous melanoma; STAD, Stomach adenocarcinoma; TGCT, Testicular germ cell tumors; THCA, Thyroid carcinoma; THYM, Thymoma; UCEC, Uterine corpus endometrial carcinoma; UCS, Uterine carcinosarcoma; UVM, Uveal melanoma. **(B–E)** Sqstm1 transcription is upregulated in LIHC. **(F)** Sqstm1 protein level is upregulated in LIHC. **(A)** is the results from TIMER2 portal, **(B, C)** from UALCAN, **(D, E)** from Oncomine, and **(F)** from UALCAN. Median Value = median(logData); Median-centered intensity= logData-Median Value. Z-values represent standard deviations from the median across LIHC samples.

Together, these findings support the claim that the deregulation of p62 expression in different cancers results from both epigenetic reprogramming and gene mutation. As one of these epigenetic mechanisms, *Sqstm1* gene transcription is transactivated by diverse transcription factors, including NRF2 that is activated in response to oxidative stress, NFκB, Ets/Pu.1, Myc, among many others (12). Importantly, we have collected solid evidence showing that p62 expression is induced by Epstein-Barr Virus (EBV) principal

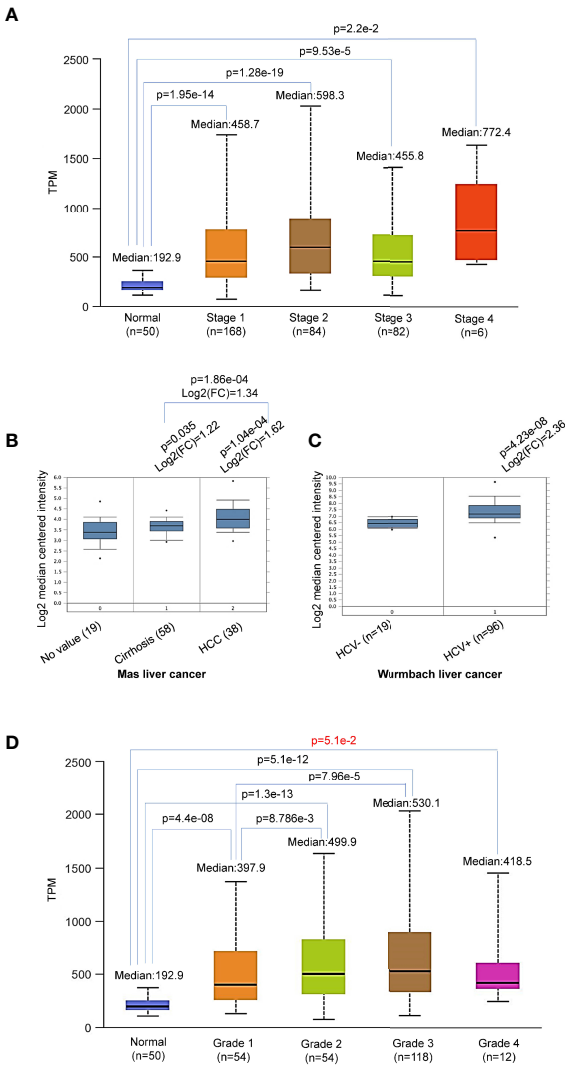

FIGURE 3 | Differential expression of Sqstm1 in liver cancer stages and grades. **(A, B)** Sqstm1 is upregulated as early as liver cirrhosis and through all stages. **(C)** HCV infection is significantly associated with Sqstm1 upregulation. **(D)** Differential upregulation of Sqstm1 in clinical stages of LIHC. p value in red is not significant. **(A)** is the results from UALCAN portal, **(B, C)** from Oncomine, and **(D)** from UALCAN. Median Value = median(logData); Median-centered intensity= logData-Median Value.

oncogenic product Latent Membrane Protein 1 (LMP1) in EBV latency, supporting a specific role for p62 in EBV-mediated cancers (39).

Mutation of Top Genes in Correlation With p62 Upregulation in LIHC

DriveDBv3 analysis shows that, in agreement with previous reports (40, 41), top genes mutated in liver cancer include TP53, CTNNB1, AXIN1, PIK3CA, JAK1, among many others (**Figure 5A**). The effects of mutation of top 30 genes on their own expression are shown in **Figure 5B**.

Among these mutated genes, TIMER2 analysis revealed that mutation of TP53, CTNNB1 (encoding β-catenin), or ALB (encoding serum albumin) significantly correlates with, and mutation of AXIN1 (a negative regulator of β-catenin stability) reversely correlates with, the p62 expression level ($p<0.05$) (**Figure 5C**). However, mutations of the genes encoding NRF2 (NFE2L2), Keap1, TTN, MUC4, PIK3CA, or JAK1, are not significantly correlated with p62 level (**Supplementary Figure 1**). Mutation of other genes on this list may be associated with p62 deregulation, but the sample sizes of their mutation are not powerful for statistical analysis.

In addition to these frequently mutated genes, we further analyzed whether mutations of any other genes are associated with p62 deregulation in LIHC in muTarget portal. 25 genes (including most of the above frequently mutated genes), such as DOCK2, TG, and DNAH10, whose mutations were found to be significantly correlated with p62 deregulation ($p<0.05$; fold change>1.44) (**Supplementary Table S2**).

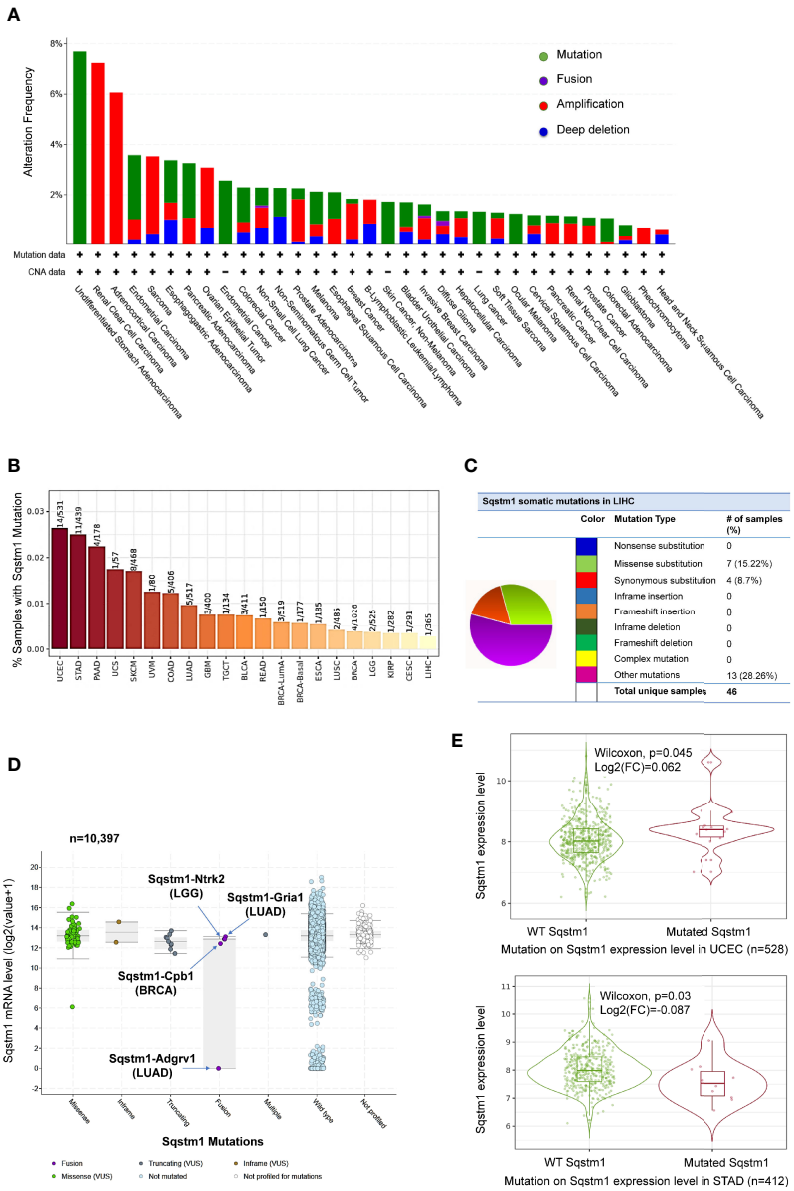

FIGURE 4 | Profile of *Sqstm1* gene mutation in cancers. **(A, B)** Frequencies of *Sqstm1* gene mutation in various cancers. **(C)** Frequencies of *Sqstm1* somatic mutations in LIHC. **(D)** *Sqstm1* gene fusion and its effect on Sqstm1 expression in various cancers. **(E)** Representative results from UCEC and STAT showing the association of *Sqstm1* mutation with its expression level. **(A)** is the results from cBioportal, **(B)** from TIMER2, **(C)** from COSMIC, **(D)** from cBioportal, and **(E)** from TIMER2. FC, Fold change (the differential expression levels between samples with WT and mutated *Sqstm1*).

p62 Promoter Methylation Is Downregulated in LIHC

Promoter methylation analysis of TCGA dataset in SMART portal indicates that the *Sqstm1* gene promoter is significantly demethylated (the chromosome 5 region spanning nucleotides 179805165~179837098) in LIHC (p=3.76e-12. **Figure 6A**), and more demethylation of the *Sqstm1* gene promoter was found in patients with p53 mutation (p=1.99e-4. **Figure 6B**). Interestingly, the downregulation of *Sqstm1* gene promoter methylation is progressed with the tumor grades (**Figure 6C**), and also with the stages (**Figure 6D**). Further analysis in DriverDBv3 shows that only 0.777% hypo methylation (beta value 0.25~0.3) and 0.223% hyper methylation (beta value 0.5~0.7) of the *Sqstm1* gene promoter methylation exist in LIHC and the methylation reversely correlates with its expression (Spearman correlation coefficient: -0.53, p=0) (**Figure 6E**). Analyses in cBioportal further confirm that the *Sqstm1* promoter methylation is reversely correlated with *Sqstm1* expression (**Figure 6F**). We further experimentally validated that treatment of liver cancer cell lines with the demethylase inhibitor

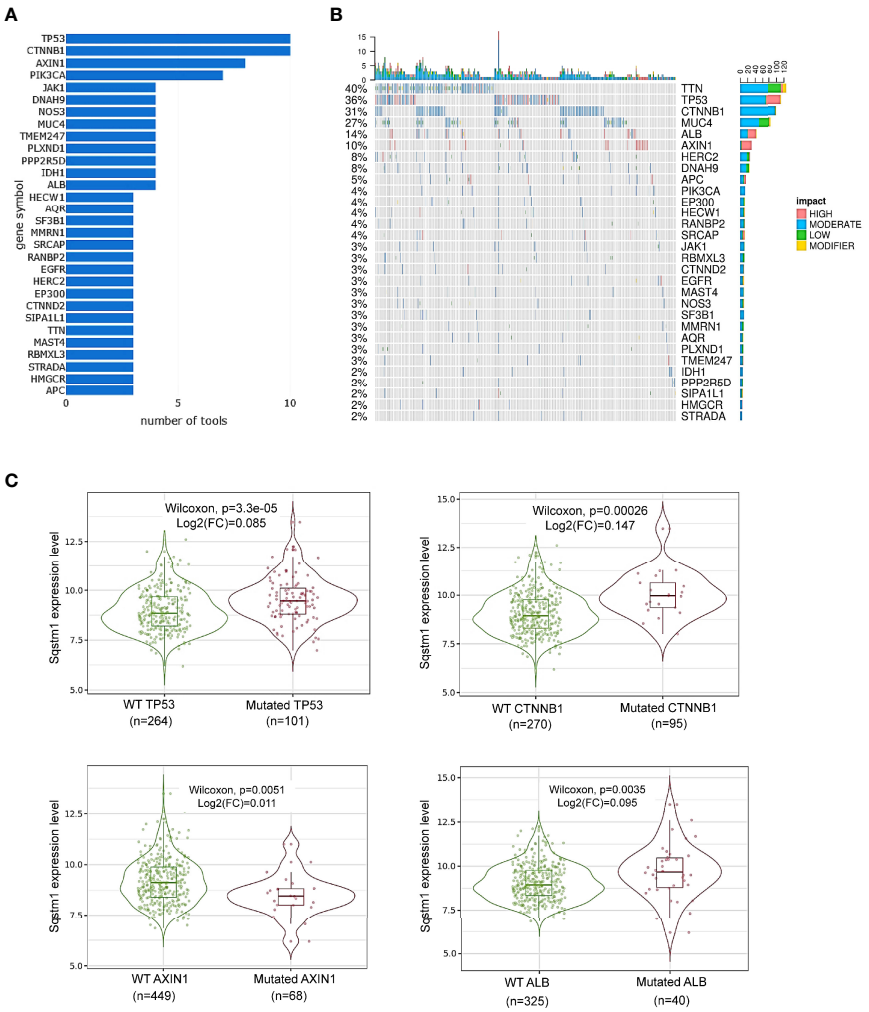

FIGURE 5 | Association of Sqstm1 expression level with gene mutation. **(A, B)** Top 30 genes that are mutated in LIHC. "number of tools" in **(A)** means the number of bioinformatic algorithms/tools were used to integrate multiomics to address the cancer driver events at distinct molecular levels (30). The percentage in **(B)** represents the total percentage of mutation in the samples for each mutated gene. The x-axis in **(B)** represents the samples from different LIHC patients. **(C)** Representative genes whose mutation is significantly associated with Sqstm1 expression in LIHC. **(A, B)** are the results from cBioportal, and **(C)** from TIMER2. FC, Fold change (the differential expression levels between samples with WT and mutated *Sqstm1*).

IOX1 downregulates the SQSTM1/p62 protein level (**Figure 6G**). These findings indicate that *Sqstm1* gene promoter demethylation significantly correlates with the upregulation of p62 expression in LIHC, suggesting that promoter demethylation plays an important role in upregulating p62 expression in LIHC.

p62 Genome-Wide Association Patterns in LIHC

Next, we performed genome-wide association studies (GWAS) to profile p62-associated molecular signatures in LIHC, in GEPIA2, Oncomine, TNMPlot, and UALCAN portals. Results have identified a pool of genes that correlate with p62 (PCC>0.5) at the mRNA level in LIHC, such as TXNRD1, SRXN1, NFE2L2, TTC1 (encoding TRP1), and TKT (**Supplementary Table S3**). Representative results from GEPIA2 portal are shown in **Figure 7A**. We validated the correlation of p62 with selected genes in both TCGA and GTEx lung cancer datasets, by one-to-one paired analysis in GEPIA2 and/or TIMER2 portals.

Representative results for the key regulators of oxidative stress and metabolism are shown in **Figure 7B**, including TXNRD1 (encoding the Thioredoxin reductase TrxR1), the reductase-encoding genes SRXN1 (encoding SRX1), HTATIP2 (encoding HIV1 TAT-Interactive Protein 2), AKR1b10 (encoding a member of the aldo/keto reductase superfamily), and TKT (encoding transketolase), as well as NFE2L2 (encoding the master antioxidant transcription factor NRF2) that governs the antioxidant stress in various cancers through the Keap1-NRF2-p62 pathway. SRX1 is known to contribute to oxidant stress resistance in various cancers by controlling the activity of a subgroup of PRDXs (42, 43). Consistent with our findings,

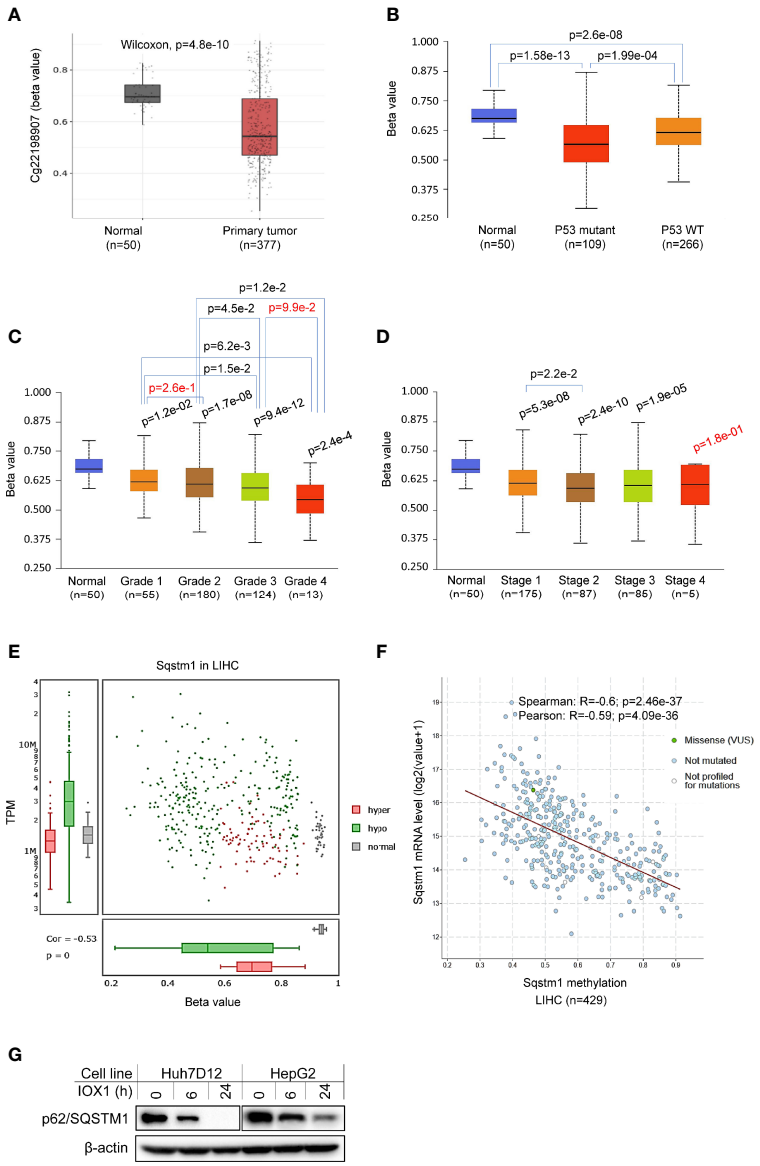

FIGURE 6 | Association of Sqstm1 expression level with its promoter methylation. **(A)** The *Sqstm1* gene promoter is significantly demethylated in LIHC. **(B)** p53 is association with *Sqstm1* gene promoter demethylation. **(C)** The *Sqstm1* gene promoter is significantly demethylated in all stages. **(D)** The *Sqstm1* gene promoter is gradually demethylated through the cancer progress. **(E)** Analysis of hyper- and hypo-methylation of the *Sqstm1* gene promoter. **(F)** The *Sqstm1* promoter methylation is reversely correlated with its expression. p values in red are not significant. **(A)** is the results from SAMRT portal, **(B–D)** from UALCAN, E from DriverDBv3, and F from cBioportal. **(G)** Experimental validation of demethylation in regulation of SQSTM1 expression. Huh7D12 and HepG2 cells were treated with 0.3 mM of the demethylase inhibitor IOX1 for indicated hours, followed by immunoblotting.

TXNRD1 was found to play a decisive role in hepatocellular carcinoma malignancy (44).

We further employed "loss-of-function" assays to assess which of four selected p62-correlated genes, including TXNRD1, SRXN1, HTATIP2, and TTC1, are deregulated by p62 in LIHC. To this end, we depleted p62 in in two liver epithelial cancer cell lines, Huh7D12 and HepG2, using CRISPR/Cas9-mediated approach with p62-specific sgRNA plasmids that were proven to be successful to downregulate p62 expression in our recent publication (39). qPCR and immunoblotting analyses revealed that SRX1 and TXNRD1, but not HTATIP2 or TTC1, are targeted by p62-mediated mechanisms at the transcriptional and translational levels (**Figures 7C, D**).

High p62 Levels Correlate With Severe Prognosis of LIHC Patients

Regarding the clinical outcomes of p62 deregulation in cancers, we first assessed the prognosis value of p62 deregulation across various

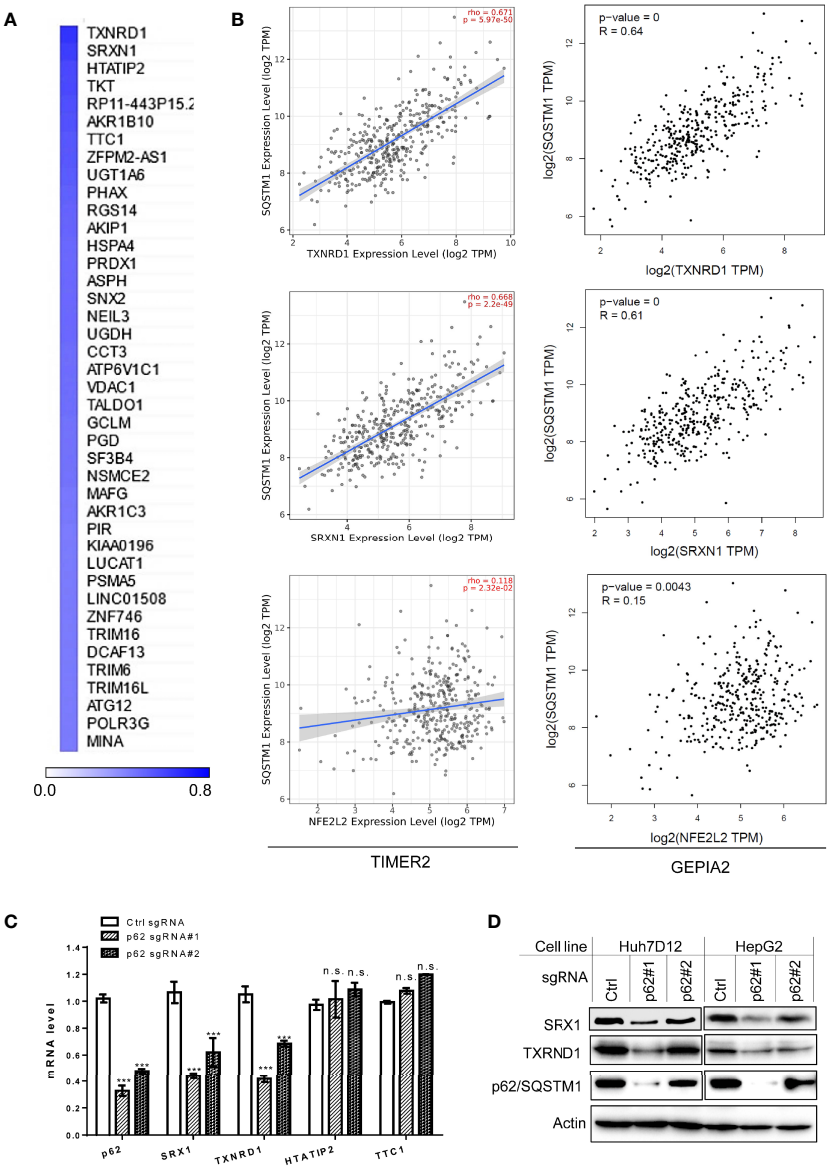

FIGURE 7 | Sqstm1-associated molecular signature in LIHC. **(A)** Top 40 genes correlated with Sqstm1 at the expression level in LIHC, with Pearson correlation coefficient values (PCC) >0.5. **(B)** Validation of individual genes in association with Sqstm1 at the transcriptional level. Results were obtained from TIMER2 (left) and GEPIA2 (right). **(C, D)** p62/Sqstm1 depletion downregulates SRX1 and TXNRD1 expression at both transcriptional and translational levels. In qPCR results, the mRNA level of each sample with control sgRNA was set to 1. ***p < 0.001. n.s., not significant.

cancers. The relation between p62 transcription levels and the overall survival (OS) rates of TCGA cancer patients was analyzed in TIMER2. Results show that the abundance of p62 reversely correlates with the OS of KIRP (z=4.31, p=0.00016), LIHC (z=4.03, p=0.00056), LGG (z=3.77, p=0.00016), amongst several other cancers (**Supplementary Table S4**), and positively correlates with the OS of ACC (z=-2.862, p=0.00421), SARC (z=-2.84, p=0.004473), and DLBC (z=-2.11, p=0.03448) (**Figure 8A**).

The reverse correlation of p62 upregulation with the OS of LIHC patients was further confirmed in TIMER2, GEPIA2, and DriverDBv3 portals with TCGA datasets, and in Kaplan Meier plotter (KMPlot) portal with TCGA, EGA, and GEO datasets (**Figure 8B**). Consistent with the results that HCV infection contributes to p62 upregulation (**Figure 3C**), the p62 level and the OS have a greater correlation in hepatitis virus-positive LIHC patients (p=0.0034) compared to hepatitis virus-negative patients (p=0.0073) (**Figure 8B**).

More importantly, we show that depletion of p62 in HepG2 liver cell line dramatically reduces cell proliferation (**Figure 8C**). Similar results were also obtained in the liver cell line Huh7D12 (not shown).

Together, these results indicate that p62 can serve as a promising prognostic biomarker for LIHC.

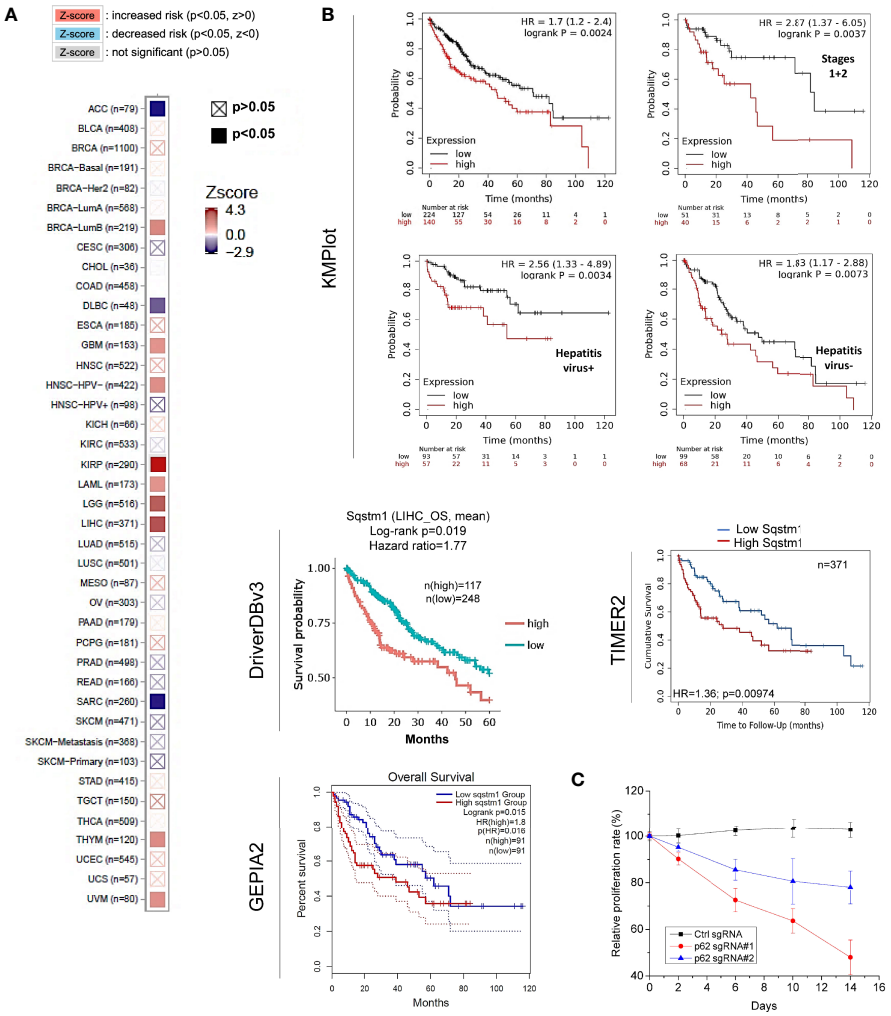

FIGURE 8 | Sqstm1 expression is associated with the overall survival of certain cancers. **(A)** Sqstm1 expression level is associated with the overall survival (OS) of certain cancer patients. **(B)** Sqstm1 expression level reversely correlates with the OS of LIHC patients. **(A)** is results from TIMER2, and **(B)** from different portals showing the consistency. For KMPlot, the settings were: JetSet best probe set, excluding outlier arrays, and univariate. **(C)** p62/Sqstm1 depletion reduces the proliferation of the liver cancer cell line Huh7D12. The proliferation rate of the cells with control sgRNA at each time point was set to 100%.

Possible Mechanism Underneath Tumor-Suppressing Function of p62 in LIHC

Accumulating evidence shows that p62 plays multifaceted roles in LIHC, including its ability to promote LIHC initiation by activating NRF2, mTORC1, and c-MYC pro-oncogenic pathways in hepatocytes (2).

To explore potential novel mechanisms responsible for p62-mediated tumor promoting function in LIHC, we analyzed genome-wide p62 interaction network in BioGRID, STRING, and GeneMANIA. Results show that a large pool of p62 interactors in both high and low throughput profiling assays (**Supplementary Table S5**), including many involved in the autophagy and ubiquitin systems such as UBC, LC3 (MAP1LC3A/B), ULK1, USPs, UBEs, AMFR (RNF45), and OTULIN and OTUB2; Keap1 and NRF2 that are components of the master antioxidative pathway; and GRIAs (Ionotropic glutamate receptors) that are involved in excitatory synaptic transmission in the central nervous system (**Figures 9A, B**).

Finally, we analyzed the possible pathways mediated by p62 in Pathcard, KEGG and Uniport, and those associated with p62 upregulation in LIHC in cBioportal. In agreement with its tumor-promoting role in LIHC, the p62 level in LIHC has a remarkable association with p53-mediated cell cycle regulation and cell survival/proliferation, WNT/β-Catenin-mediated cell proliferation, and Keap1-NRF2 antioxidative stress (**Figure 9C** and **Supplementary Figure 2**).

DISCUSSION

We show in this study that: 1) p62 is significantly upregulated in several malignancies, including LIHC (**Figure 2**); 2) the

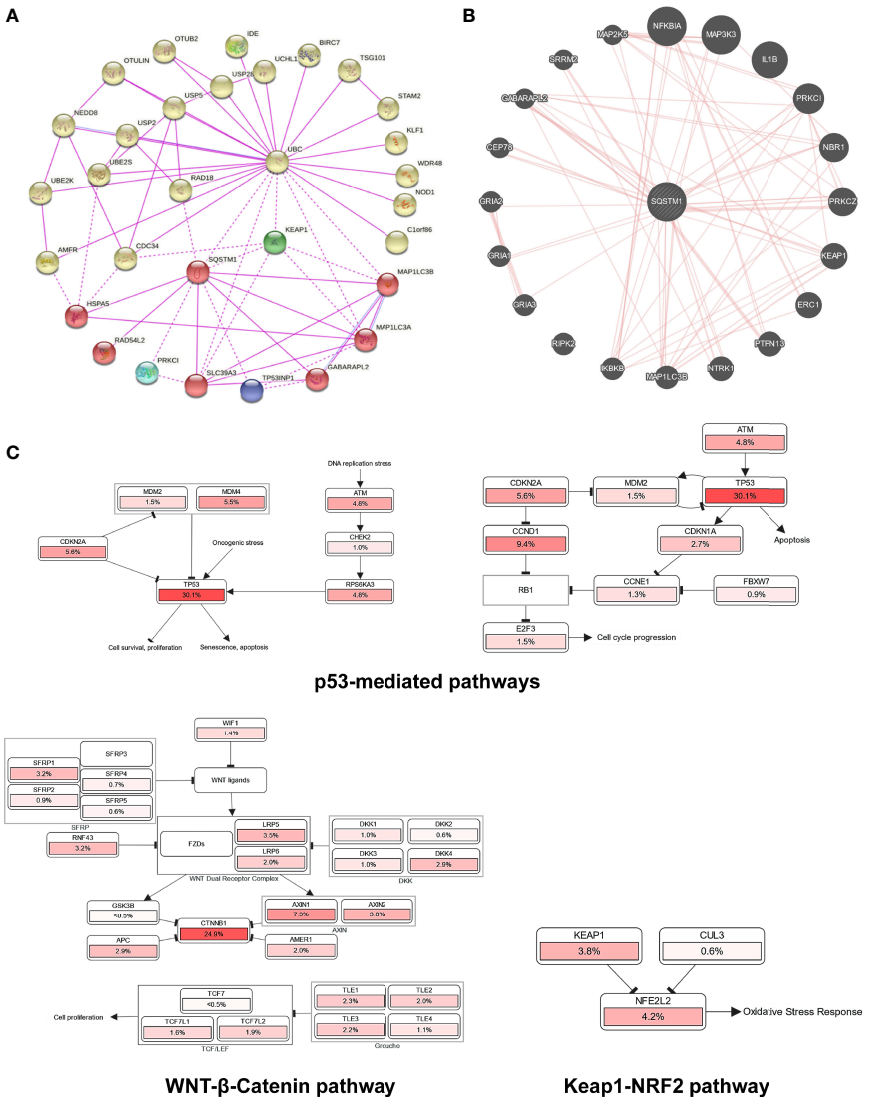

FIGURE 9 | Genome-wide interaction and pathway association of Sqstm1 in LIHC. **(A)** Known SQSTM1 protein physical interaction network, as analyzed in STRING databases. Co-expression, textmining, neighborhood, and gene fusion were excluded in the settings. **(B)** Physical interactors of SQSTM1 protein as identified in BioGRID with various databases from both high and low throughput assays. **(C)** The pathways that are deregulated in correlation with SQSTM1 in LIHC. The deregulation of individual genes is shown in red. The more frequently a given gene is deregulated, the deeper red is shown.

upregulation of p62 transcription starts as early as liver cirrhosis, and HCV infection makes a significant contribution to p62 upregulation (**Figure 3**); 3) the demethylation of p62-encoding gene (*Sqstm1*) promoter, but not its mutations that occur at low rates in LIHC, makes a significant contribution to its upregulation in LIHC (**Figure 6**); 4) genome-wide association analyses identified p62-associated molecular signature in LIHC, and SRX1 and TXNRD1 are further confirmed to be targeted by p62 at transcriptional and translational levels (**Figure 7**). 5) Higher p62 levels are significantly associated with worse prognosis of LIHC (**Figure 8**). 6) Mechanistically, p62 expression level reversely correlates with the deregulation of p53-mediated cell survival and cell cycle progress, and correlates with Keap1-NRF2-mediated antioxidative stress and Wnt/β-Catenin-mediated cell proliferation (**Figure 9**). Surprisingly, our analysis indicates that p62 expression level is poorly associated with the frequencies of tumor infiltrating lymphocytes (cutoff: R>0.3; p<0.05. **Supplementary Figure 3**), although it plays a crucial role in the tumor microenvironment in different cancer contexts (8, 45), and induces cancer-associated fibroblast activation in LIHC (46).

It is well known that the transcription factor NRF2, among many others (12), transactivates p62 gene expression in response to oxidative stress in various contexts (47). Importantly, our study implicates novel mechanisms for p62 upregulation in LIHC, including the demethylation of the *Sqstm1* gene

promoter, and the transcription factors p53 (loss-of-function mutation in LIHC) and β-Catenin/TCF. By analyzing the *Sqstm1* gene promoter, we identified multiple potential p53-binding sites (**Supplementary Figure 4**). In agreement with our findings, p62 was reported to be transcriptionally suppressed by the β-Catenin/TCF pathway (48), and in turn, autophagy negatively regulates the Wnt/β-Catenin/TCF pathway at least by targeting β-Catenin for degradation (49), in cancer cells. We will validate the transcriptional regulation of p62 by p53 and the Wnt/β-Catenin/TCF pathway in LIHC in separate projects.

p62 is a multifunctional protein that plays important roles in both cytoplasmic and nuclear compartments. In the cytoplasm, it is well known to act as a selective autophagy receptor, a ubiquitin sensor, and a signal transducing hub, which is involved in NRF2-mediated antioxidative defense, mTORC1-mediated nutrient sensing and metabolic reprogramming, cGAS-STING-mediated antitumor immunity, NFκB activation, inflammation, and apoptosis. In the nucleus, p62 regulates DNA damage response, proteasomal activity, and the assembly of PML bodies (2, 12, 50). Of note, our study has identified SRX1 and TXNRD1 as targets of p62 that are regulated by p62 at both mRNA and protein levels. The mechanism may involve p62-mediated activation of the transcription factors NFκB, NRF2, and STATs. In support of this possibility, SRX1 is a known NRF2 transcriptional target (51). TXNRD1 cooperates with Keap1 in sensing cellular stresses to modulate NRF2 activity, and plays a pivotal role in redox (reduction-oxidation) homeostasis related to the glutathione (GSH) and thioredoxin (Trx) systems that are mediated by NADPH-dependent disulfide reductases (52).

The protein p62 can be extensively modified at the post-translational level by site-specific phosphorylation, ubiquitination, acetylation, and others in different functional contexts (2, 12). For example, for human p62, S403 phosphorylation and K420 ubiquitination of p62 are involved in its autophagy function, S349 phosphorylation is required for its regulation of the Keap1-NRF2 pathway activity in a feedback loop, and T269/S272 phosphorylation is required for its cyto-nuclear shuttling. p62 itself is targeted by selective autophagy for degradation that requires its ubiquitination.

Our study supports the claim that p62 is a crucial cancer promoter that is significantly upregulated in LIHC, and could serve as a diagnostic and prognostic marker. Although p62 has previously implicated in LIHC, our comprehensive big data analyses disclose potential novel mechanisms underlying p62 regulation and its potential roles in this cancer context. Further experimental validation of these mechanisms is of importance for better understanding the interaction of p62 with LIHC.

Supplementary Tables S1-S5 and **Figures S1-S4** are available online.

DATA AVAILABILITY STATEMENT

The original contributions presented in the study are included in the article/**Supplementary Material**. Further inquiries can be directed to the corresponding author.

AUTHOR CONTRIBUTIONS

Conceptualization: LW and SN; Data analysis: SN, CH, and LW; Funding acquisition: LW and SN; Methodology: LW, MH, CH, and SN. Writing and editing: LW and SN. All authors have read and agreed to the published version of the manuscript.

FUNDING

This work was supported by NIH, CA252986 (LW), DE029621 (SN) and ASH (SN), and in part by the NIH grant C06RR0306551.

ACKNOWLEDGMENTS

This publication is the result of work supported with resources and the use of facilities at the James H. Quillen Veterans Affairs Medical Center. The contents in this publication do not represent the views of the Department of Veterans Affairs or the United States Government.

SUPPLEMENTARY MATERIAL

The Supplementary Material for this article can be found online at: https://www.frontiersin.org/articles/10.3389/fonc.2022.923009/full#supplementary-material

REFERENCES

1. Villanueva A. Hepatocellular Carcinoma. *N Engl J Med* (2019) 380:1450–62. doi: 10.1056/NEJMra1713263
2. Tan CT, Soh NJH, Chang HC, Yu VC. P62/SQSTM1 in Liver Diseases: The Usual Suspect With Multifarious Identities. *FEBS J* (2021). doi: 10.1111/febs.16317
3. Tonelli C, Chio IIC, Tuveson DA. Transcriptional Regulation by Nrf2. *Antioxidants Redox Signaling* (2018) 29:1727–45. doi: 10.1089/ars.2017.7342
4. Lee O-H, Jain AK, Papusha V, Jaiswal AK. An Auto-Regulatory Loop Between Stress Sensors INrf2 and Nrf2 Controls Their Cellular Abundance. *J Biol Chem* (2007) 282:36412–20. doi: 10.1074/jbc.M706517200
5. Ahmed SMU, Luo L, Namani A, Wang XJ, Tang X. Nrf2 Signaling Pathway: Pivotal Roles in Inflammation. *Biochim Biophys Acta (BBA) - Mol Basis Dis* (2017) 1863:585–97. doi: 10.1016/j.bbadis.2016.11.005
6. Kwak M-K, Itoh K, Yamamoto M, Kensler TW. Enhanced Expression of the Transcription Factor Nrf2 by Cancer Chemopreventive Agents: Role of Antioxidant Response Element-Like Sequences in the Nrf2 Promoter. *Mol Cell Biol* (2002) 22:2883–92. doi: 10.1128/MCB.22.9.2883-2892.2002
7. Wooten MW, Geetha T, Babu JR, Seibenhener ML, Peng J, Cox N, et al. Essential Role of Sequestosome 1/P62 in Regulating Accumulation of Lys63-Ubiquitinated Proteins. *J Biol Chem* (2008) 283:6783–9. doi: 10.1074/jbc.M709496200
8. Moscat J, Karin M, Diaz-Meco MT. P62 in Cancer: Signaling Adaptor Beyond Autophagy. *Cell* (2016) 167:606–9. doi: 10.1016/j.cell.2016.09.030

9. Moscat J, Diaz-Meco MT. P62: A Versatile Multitasker Takes on Cancer. *Trends Biochem Sci* (2012) 37:230–6. doi: 10.1016/j.tibs.2012.02.008
10. Nezis IP, Stenmark H. P62 at the Interface of Autophagy, Oxidative Stress Signaling, and Cancer. *Antioxidants Redox Signaling* (2011) 17:786–93. doi: 10.1089/ars.2011.4394
11. Bitto A, Lerner CA, Nacarelli T, Crowe E, Torres C, Sell C. P62/SQSTM1 at the Interface of Aging, Autophagy, and Disease. *AGE* (2014) 36:9626. doi: 10.1007/s11357-014-9626-3
12. Ning S, Wang L. The Multifunctional Protein P62 and Its Mechanistic Roles in Cancers. *Curr Cancer Drug Targets* (2019) 19:468–78. doi: 10.2174/1568009618666181016164920
13. Thompson HGR, Harris JW, Wold BJ, Lin F, Brody JP. P62 Overexpression in Breast Tumors and Regulation by Prostate-Derived Ets Factor in Breast Cancer Cells. *Oncogene* (2003) 22:2322–33. doi: 10.1038/sj.onc.1206325
14. Puissant A, Fenouille N, Auberger P. When Autophagy Meets Cancer Through P62/SQSTM1. *Am J Cancer Res* (2012) 2:397–413.
15. Umemura A, He F, Taniguchi K, Nakagawa H, Yamachika S, Font-Burgada J, et al. P62, Upregulated During Preneoplasia, Induces Hepatocellular Carcinogenesis by Maintaining Survival of Stressed HCC-Initiating Cells. *Cancer Cell* (2016) 29:935–48. doi: 10.1016/j.ccell.2016.04.006
16. Roodman GD, Hiruma Y, Kurihara N. P62: A Potential Target for Blocking Microenvironmental Support of Myeloma. *Clin Lymphoma Myeloma* (2009) 9:S25–6. doi: 10.3816/CLM.2009.s.004
17. Saito T, Ichimura Y, Taguchi K, Suzuki T, Mizushima T, Takagi K, et al. P62/Sqstm1 Promotes Malignancy of HCV-Positive Hepatocellular Carcinoma Through Nrf2-Dependent Metabolic Reprogramming. *Nat Commun* (2016) 7:12030. doi: 10.1038/ncomms12030
18. Duran A, Linares JF, Galvez AS, Wikenheiser K, Flores JM, Diaz-Meco MT, et al. The Signaling Adaptor P62 Is an Important NF-κb Mediator in Tumorigenesis. *Cancer Cell* (2008) 13:343–54. doi: 10.1016/j.ccr.2008.02.001
19. Rhodes DR, Kalyana-Sundaram S, Mahavisno V, Varambally R, Yu J, Briggs BB, et al. Oncomine 3.0: Genes, Pathways, and Networks in a Collection of 18,000 Cancer Gene Expression Profiles. *Neoplasia* (2007) 9:166–80. doi: 10.1593/neo.07112
20. Li T, Fan J, Wang B, Traugh N, Chen Q, Liu JS, et al. TIMER: A Web Server for Comprehensive Analysis of Tumor-Infiltrating Immune Cells. *Cancer Res* (2017) 77:e108–10. doi: 10.1158/0008-5472.CAN-17-0307
21. Li B, Severson E, Pignon JC, Zhao H, Li T, Novak J, et al. Comprehensive Analyses of Tumor Immunity: Implications for Cancer Immunotherapy. *Genome Biol* (2016) 17:174. doi: 10.1186/s13059-016-1028-7
22. Tang Z, Li C, Kang B, Gao G, Li C, Zhang Z. GEPIA: A Web Server for Cancer and Normal Gene Expression Profiling and Interactive Analyses. *Nucleic Acids Res* (2017) 45:W98–W102. doi: 10.1093/nar/gkx247
23. Ru B, Wong CN, Tong Y, Zhong JY, Zhong SSW, Wu WC, et al. TISIDB: An Integrated Repository Portal for Tumor–Immune System Interactions. *Bioinformatics* (2019) 35:4200–2. doi: 10.1093/bioinformatics/btz210
24. Chandrashekar DS, Bashel B, Balasubramanya SAH, Creighton CJ, Ponce-Rodriguez I, Chakravarthi BVSK, et al. UALCAN: A Portal for Facilitating Tumor Subgroup Gene Expression and Survival Analyses. *Neoplasia* (2017) 19:649–58. doi: 10.1016/j.neo.2017.05.002
25. Hu X, Wang Q, Tang M, Barthel F, Amin S, Yoshihara K, et al. TumorFusions: An Integrative Resource for Cancer-Associated Transcript Fusions. *Nucleic Acids Res* (2018) 46:D1144–9. doi: 10.1093/nar/gkx1018
26. Kim P, Zhou X. FusionGDB: Fusion Gene Annotation DataBase. *Nucleic Acids Res* (2019) 47:D994–d1004. doi: 10.1093/nar/gky1067
27. Jang YE, Jang I, Kim S, Cho S, Kim D, Kim K, et al. ChimerDB 4.0: An Updated and Expanded Database of Fusion Genes. *Nucleic Acids Res* (2019) 48:D817–24. doi: 10.1093/nar/gkz1013
28. Cerami E, Gao J, Dogrusoz U, Gross BE, Sumer SO, Aksoy BA, et al. The Cbio Cancer Genomics Portal: An Open Platform for Exploring Multidimensional Cancer Genomics Data. *Cancer Discovery* (2012) 2:401–4. doi: 10.1158/2159-8290.CD-12-0095
29. Gao J, Aksoy BA, Dogrusoz U, Dresdner G, Gross B , Sumer SO, et al. Integrative Analysis of Complex Cancer Genomics and Clinical Profiles Using the Cbioportal. *Sci Signal* (2013) 6l1:pl1. doi: 10.1126/scisignal.2004088
30. Liu S-H, Shen P-C, Chen C-Y, Hsu A-N, Cho Y-C, Lai Y-L, et al. DriverDBv3: A Multi-Omics Database for Cancer Driver Gene Research. *Nucleic Acids Res* (2019) 48:D863–70. doi: 10.1093/nar/gkz964
31. Győrffy B, Surowiak P, Budczies J, Lánczky A. Online Survival Analysis Software to Assess the Prognostic Value of Biomarkers Using Transcriptomic Data in non-Small-Cell Lung Cancer. *PLoS One* (2013) 8:e82241. doi: 10.1371/journal.pone.0082241
32. Nagy A, Gyorffy B. Mutarget: A Platform Linking Gene Expression Changes and Mutation Status in Solid Tumors. *Int J Cancer* (2021) 148:502–11. doi: 10.1002/ijc.33283
33. Stark C, Breitkreutz B-J, Reguly T, Boucher L, Breitkreutz A, Tyers M. BioGRID: A General Repository for Interaction Datasets. *Nucleic Acids Res* (2006) 34:D535–9. doi: 10.1093/nar/gkj109
34. Oughtred R, Stark C, Breitkreutz B-J, Rust J, Boucher L, Chang C, et al. The BioGRID Interaction Database: 2019 Update. *Nucleic Acids Res* (2018) 47:D529–41. doi: 10.1093/nar/gky1079
35. Mostafavi S, Ray D, Warde-Farley D, Grouios C, Morris Q. GeneMANIA: A Real-Time Multiple Association Network Integration Algorithm for Predicting Gene Function. *Genome Biol* (2008) 9:S4. doi: 10.1186/gb-2008-9-s1-s4
36. Warde-Farley D, Donaldson SL, Comes O, Zuberi K, Badrawi R, Chao P, et al. The GeneMANIA Prediction Server: Biological Network Integration for Gene Prioritization and Predicting Gene Function. *Nucleic Acids Res* (2010) 38:W214–20. doi: 10.1093/nar/gkq537
37. Wang L, Toomey NL, Diaz LA, Walker G, Ramos JC, Barber GN, et al. Oncogenic IRFs Provide a Survival Advantage for EBV- or HTLV1-Transformed Cells Through Induction of BIC Expression. *J Virol* (2011) 85:8328–37. doi: 10.1128/JVI.00570-11
38. DeLuca DS, Levin JZ, Sivachenko A, Fennell T, Nazaire M-D, Williams C, et al. RNA-SeQC: RNA-Seq Metrics for Quality Control and Process Optimization. *Bioinformatics* (2012) 28:1530–2. doi: 10.1093/bioinformatics/bts196
39. Wang L, Howell MEA, Sparks-Wallace A, Zhao J, Hensley CR, Nicksic CA, et al. The Ubiquitin Sensor and Adaptor Protein P62 Mediates Signal Transduction of a Viral Oncogenic Pathway. *mBio* (2021) 12:e0109721. doi: 10.1128/mBio.01097-21
40. Schulze K, Imbeaud S, Letouzé E, Alexandrov LB, Calderaro J, Rebouissou S, et al. Exome Sequencing of Hepatocellular Carcinomas Identifies New Mutational Signatures and Potential Therapeutic Targets. *Nat Genet* (2015) 47:505–11. doi: 10.1038/ng.3252
41. Cancer Genome Atlas Research Network. Comprehensive and Integrative Genomic Characterization of Hepatocellular Carcinoma. *Cell* (2017) 169(7):1327–41.e23. doi: e1323.10.1016/j.cell.2017.05.046
42. Nicolussi A, D'Inzeo S, Capalbo C, Giannini G, Coppa A. The Role of Peroxiredoxins in Cancer. *Mol Clin Oncol* (2017) 6:139–53. doi: 10.3892/mco.2017.1129
43. Mishra M, Jiang H, Wu L, Chawsheen HA, Wei Q. The Sulfiredoxin-Peroxiredoxin (Srx-Prx) Axis in Cell Signal Transduction and Cancer Development. *Cancer Lett* (2015) 366:150–9. doi: 10.1016/j.canlet.2015.07.002
44. McLoughlin MR, Orlicky DJ, Prigge JR, Krishna P, Talago EA, Cavigli IR, et al. TrxR1, Gsr, and Oxidative Stress Determine Hepatocellular Carcinoma Malignancy. *Proc Natl Acad Sci* (2019) 116:11408–17. doi: 10.1073/pnas.1903244116
45. Reina-Campos M, Shelton PM, Diaz-Meco MT, Moscat J. Metabolic Reprogramming of the Tumor Microenvironment by P62 and its Partners. *Biochim Biophys Acta (BBA) - Rev Cancer* (2018) 1870:88–95. doi: 10.1016/j.bbcan.2018.04.010
46. Kang JI, Kim DH, Sung KW, Shim SM, Cha-Molstad H, Soung NK, et al. P62-Induced Cancer-Associated Fibroblast Activation *via* the Nrf2-ATF6 Pathway Promotes Lung Tumorigenesis. *Cancers (Basel)* (2021) 13:864. doi: 10.3390/cancers13040864
47. Jain A, Lamark T, Sjøttem E, Bowitz Larsen K, Atesoh Awuh J, Øvervatn A, et al. P62/SQSTM1 Is a Target Gene for Transcription Factor NRF2 and Creates a Positive Feedback Loop by Inducing Antioxidant Response Element-Driven Gene Transcription. *J Biol Chem* (2010) 285:22576–91. doi: 10.1074/jbc.M110.118976
48. Petherick KJ, Williams AC, Lane JD, Ordóñez-Morán P, Huelsken J, Collard TJ, et al. Autolysosomal β-Catenin Degradation Regulates Wnt-Autophagy-P62 Crosstalk. *EMBO J* (2013) 32:1903–16. doi: 10.1038/emboj.2013.123
49. Lorzadeh S, Kohan L, Ghavami S, Azarpira N. Autophagy and the Wnt Signaling Pathway: A Focus on Wnt/β-Catenin Signaling. *Biochim Biophys Acta (BBA) - Mol Cell Res* (2021) 1868:118926. doi: 10.1016/j.bbamcr.2020.118926
50. Hewitt G, Carroll B, Sarallah R, Correia-Melo C, Ogrodnik M, Nelson G, et al. SQSTM1/p62 Mediates Crosstalk Between Autophagy and the UPS

in DNA Repair. *Autophagy* (2016) 12:1917–30. doi: 10.1080/15548627.2016.1210368
51. Singh A, Ling G, Suhasini AN, Zhang P, Yamamoto M, Navas-Acien A, et al. Nrf2-Dependent Sulfiredoxin-1 Expression Protects Against Cigarette Smoke-Induced Oxidative Stress in Lungs. *Free Radic Biol Med* (2009) 46:376–86. doi: 10.1016/j.freeradbiomed.2008.10.026
52. Cebula M, Schmidt EE, Arnér ESJ. TrxR1 as a Potent Regulator of the Nrf2-Keap1 Response System. *Antioxidants Redox Signaling* (2015) 23:823–53. doi: 10.1089/ars.2015.6378

Conflict of Interest: The authors declare that the research was conducted in the absence of any commercial or financial relationships that could be construed as a potential conflict of interest.

Publisher's Note: All claims expressed in this article are solely those of the authors and do not necessarily represent those of their affiliated organizations, or those of the publisher, the editors and the reviewers. Any product that may be evaluated in this article, or claim that may be made by its manufacturer, is not guaranteed or endorsed by the publisher.

frontiers | Frontiers in Oncology

ORIGINAL RESEARCH
published: 04 July 2022
doi: 10.3389/fonc.2022.911942

Comprehensive Analysis of the Brain-Expressed X-Link Protein Family in Glioblastoma Multiforme

Adilai Aisa[1,2†], *Yinuo Tan*[1,2†], *Xinyu Li*[1,2], *Ding Zhang*[1,2], *Yun Shi*[3] *and Ying Yuan*[1,2*]

[1] Department of Medical Oncology, Key Laboratory of Cancer Prevention and Intervention, Ministry of Education, The Second Affiliated Hospital, Zhejiang University School of Medicine, Hangzhou, China, [2] Cancer Center, Zhejiang University, Hangzhou, China, [3] Nursing Department, The Second Affiliated Hospital, Zhejiang University School of Medicine, Hangzhou, China

Glioblastoma multiforme (GBM) is the most common, malignant, and deadly primary brain tumor in adults. Brain-expressed X-link (BEX) protein family is involved in tumorigenesis. Here, we have explored the biological function and the prognostic value of the BEX family in GBM. Differentially expressed BEX genes between GBM and normal tissue were screened by using The Cancer Genome Atlas (TCGA) database. Univariate and multivariate Cox regression analyses identified the prognosis-related genes BEX1, BEX2, and BEX4, which were involved in the regulation of immune response. The results of correlation analysis and protein–protein interaction network (PPI network) showed that there was a significant correlation between the BEX family and TCEAL family in GBM. Furthermore, the expression of transcription elongation factor A (SII)-like (TCEAL) family is generally decreased in GBM and related to poor prognosis. With the use of the least absolute shrinkage and selection operator (LASSO) Cox regression, a prognostic model including the BEX family and TCEAL family was built to accurately predict the likelihood of overall survival (OS) in GBM patients. Therefore, we demonstrated that the BEX family and TCEAL family possessed great potential as therapeutic targets and prognostic biomarkers in GBM. Further investigations in large-scale, multicenter, and prospective clinical cohorts are needed to confirm the prognostic model developed in our study.

Keywords: glioblastoma, immunomodulation, prognosis, BEX family, TCEAL family

OPEN ACCESS

Edited by:
César López-Camarillo, Universidad Autónoma de la Ciudad de México, Mexico

Reviewed by:
Mehul S. Raval, Ahmedabad University, India
Wei-jiang Zhao, Jiangnan University, China
Wei-cheng Lu, The First Affiliated Hospital of China Medical University, China

***Correspondence:**
Ying Yuan
yuanying1999@zju.edu.cn

[†]*These authors have contributed equally to this work*

Specialty section:
This article was submitted to Cancer Genetics, a section of the journal Frontiers in Oncology

Received: *03 April 2022*
Accepted: *30 May 2022*
Published: *04 July 2022*

Citation:
Aisa A, Tan Y, Li X, Zhang D, Shi Y and Yuan Y (2022) Comprehensive Analysis of the Brain-Expressed X-Link Protein Family in Glioblastoma Multiforme. Front. Oncol. 12:911942. doi: 10.3389/fonc.2022.911942

INTRODUCTION

Glioblastoma multiforme (GBM) is a primary malignant glioma. It is one of the most common malignant brain tumors with high invasiveness and lethality (1). The general manifestations of GBM patients are headache, dizziness, nausea, convulsions, hemiplegia, memory disorders, or personality changes, of which convulsions are the most common clinical symptoms (2). CT is the main diagnostic method at present (3). The risk factors for GBM remain uncertain. Male gender, age group over 70, and Caucasian race seem to be independent prognostic factors for GBM (4). At present, the treatment of GBM includes tumor resection, radiotherapy, and temozolomide adjuvant chemotherapy (5). Recently, immunotherapy has also shown some efficacy in the treatment of GBM

(6). However, due to high drug resistance and close to 100% recurrence rate, the prognosis of GBM patients is poor, and the median survival time is only about 15 months (7). Therefore, in order to improve the efficacy of GBM, reduce drug resistance and recurrence rate, prolong the life of GBM patients, and improve their survival and treatment, further research on the mechanism of GBM occurrence and development is the main challenge at present.

The BEX family consists of five members, BEX1–5, located on the Xq22 chromosome. Members of the BEX family are widely expressed in several types of tissues and are closely associated with transcriptional regulation and signaling pathways, including neurodegeneration, cell cycle, apoptosis, autophagy, and tumor growth (8–10). The aforementioned studies highlighted an association between the BEX family members and GBM (11–13). However, there are few studies on the functional mechanism and therapeutic significance of the whole BEX family in GBM.

In this study, by comprehensively analyzing RNA-seq profiles and clinical information of GBM in The Cancer Genome Atlas (TCGA) database, we explored BEX family expression features and potential biological functions in GBM and firstly reported the correlation between the BEX family and TCEAL family in GBM. In addition, we built a prognostic model including the BEX family and TCEAL family to accurately predict the likelihood of overall survival (OS) in GBM patients.

MATERIAL AND METHODS

Data Retrieval and Processing for This Study

The RNA-seq profiles and clinical data of GBM patients from TCGA GBM cohort database (https://portal.gdc.cancer.gov/) were collected (14). The expression of the BEX family in GBM was analyzed and visualized on the online tool (http://gepia.cancer-pku.cn/). The data on WHO classification, IDH mutation status, and 1p/19q deletion are from the study of Ceccarelli et al. (15).

Correlation and Functional Enrichment Analysis of BEX Family Genes

The expression profiles (HTSeq-FPKM) between the high BEX expression group and the low BEX expression group were compared to identify differentially expressed genes (DEGs) using Wilcoxon rank-sum test in the R language-related software, stat package (3.6.3). Differences with a |log fold change (FC)| > 1.5 and an adjusted p-value <0.05 were considered as threshold values for identifying DEGs.

The Kyoto Encyclopedia of Genes and Genomes (KEGG) database was used to assign biological functions and utilities of target genes. R package Clusterprofiler and GOplot were applied to perform GOKEGG function enrichment analyses on the DEGs identified between the high and low BEX expression groups (16, 17). The default parameters in the tool were used, and enriched pathways were ranked according to their enrichment scores. A p-value of <0.05 was identified as enriched functions.

The Search Tool for the Retrieval of Interacting Genes (STRING; http://string-db.org; version 10.0) online database was used to predict the protein–protein interaction network of the BEX family co-expressed genes in GBM and to analyze the functional interactions among proteins. An interaction with a combined score >0.4 was considered statistically significant.

Gene Set Enrichment Analysis

Gene Set Enrichment Analysis (GSEA) is a computational method that determines whether a defined set of genes exhibits statistically significant concordant differences between two biological states (18). The gene set database used in this study is MSigDB Collections (https://www.gsea-msigdb.org/gsea/msigdb/index.jsp). The analysis and visualization of GSEA were performed with the R package ClusterProfiler (16) to elucidate the significant function and pathway differences between the high and low BEX expression groups. Each analysis procedure was repeated 1,000 times. A function or pathway term with an adjusted p-value <0.05 and a false discovery rate (FDR) <0.25 was considered to be statistically significant enrichment.

Immune Infiltrate Analysis

The correlation between BEX family genes and the abundance of immune infiltrates, including B cells, CD4+ T cells, CD8+ T cells, neutrophils, macrophages, and dendritic cells, were downloaded *via* tumor immune estimation resource (19) (TIMER; https://cistrome shinyapps.io/timer/). In addition, based on expression data, the immune score, stromal score, and ESTIMATE score of each GBM patient were analyzed by R packages "GSVA packages" to access the infiltration level of immune cells and the level of stromal cells in tumor tissues (20). Subsequently, Pearson's correlation coefficient was calculated to evaluate the associations between the expression of prognosis-related genes and the above three scores.

Construction and Evaluation of the Nomogram and Prognostic Model

To individualize the predicted survival probability for l, 3, and 5 years, a nomogram was constructed based on the results of the multivariate analysis. The RMS R package was used to generate a nomogram including clinical characteristics significantly associated with the BEX family and calibration plots. Calibration and discrimination are the most used methods for evaluating the performance of models (21). In this study, the calibration curves were graphically assessed by mapping the nomogram-predicted probabilities against the observed rates, and the 45° line represented the best predictive values. The concordance index (C-index) was used to determine the discrimination of the nomogram, which was calculated by a bootstrap approach with 1,000 resamples. In addition, using the least absolute shrinkage and selection operator (LASSO) Cox regression, a prognostic model including the BEX family and TCEAL family was built to accurately predict the likelihood of l,

3, and 5 years OS in GBM patients. All statistical tests were two-tailed with the statistical significance level set at 0.05.

Statistical Analysis

All statistical analyses and plots were conducted using R (version 3.6.3). Wilcoxon rank-sum test was used to analyze the expression of the BEX family in non-paired samples. The Kruskal–Wallis test, Dunn's test, Wilcoxon rank-sum test, and logistic regression evaluated relationships between clinical-pathologic features and BEX family expression. Furthermore, receiver operating characteristic (ROC) analysis and the frequently used method for binary assessment were performed using the pROC package to assess the effectiveness of expression to GBM from normal samples. The computed area under the curve (AUC) value ranging from 0.5 to 0.1 indicates the discriminative potential from 50% to 100%. The prognostic data were obtained from *Cell* (22). In this study, it was assumed that the hazard rates of any two individuals were proportional, and based on this assumption, Cox's regression model was used. The Kaplan–Meier method was used to evaluate prognostic factors; in all tests, a p-value <0.05 was considered statistically significant.

RESULTS

Expression Level of BEX Family in Glioblastoma Multiforme

According to the matched analysis of 163 GBM cases in TCGA database and 207 normal tissues in Genotype-Tissue Expression (GTEx) and TCGA normal database, the expression of mRNA of BEX family members was significantly downregulated in GBM, except BEX3. The results of the Mann–Whitney U test (Wilcoxon rank-sum test) showed that the difference between tumor and normal groups was statistically significant ($p < 0.05$) (**Figure 1**).

The Relationship Between BEX Family Expression and Clinical Indicators in Glioblastoma Multiforme Patients

We next compared BEX family expression among groups of patients through TCGA database, according to different clinical indicators. According to their malignancy, gliomas have been classified in four grades by WHO, and the higher grade was more malignant and related to a worse prognosis than the lower grade

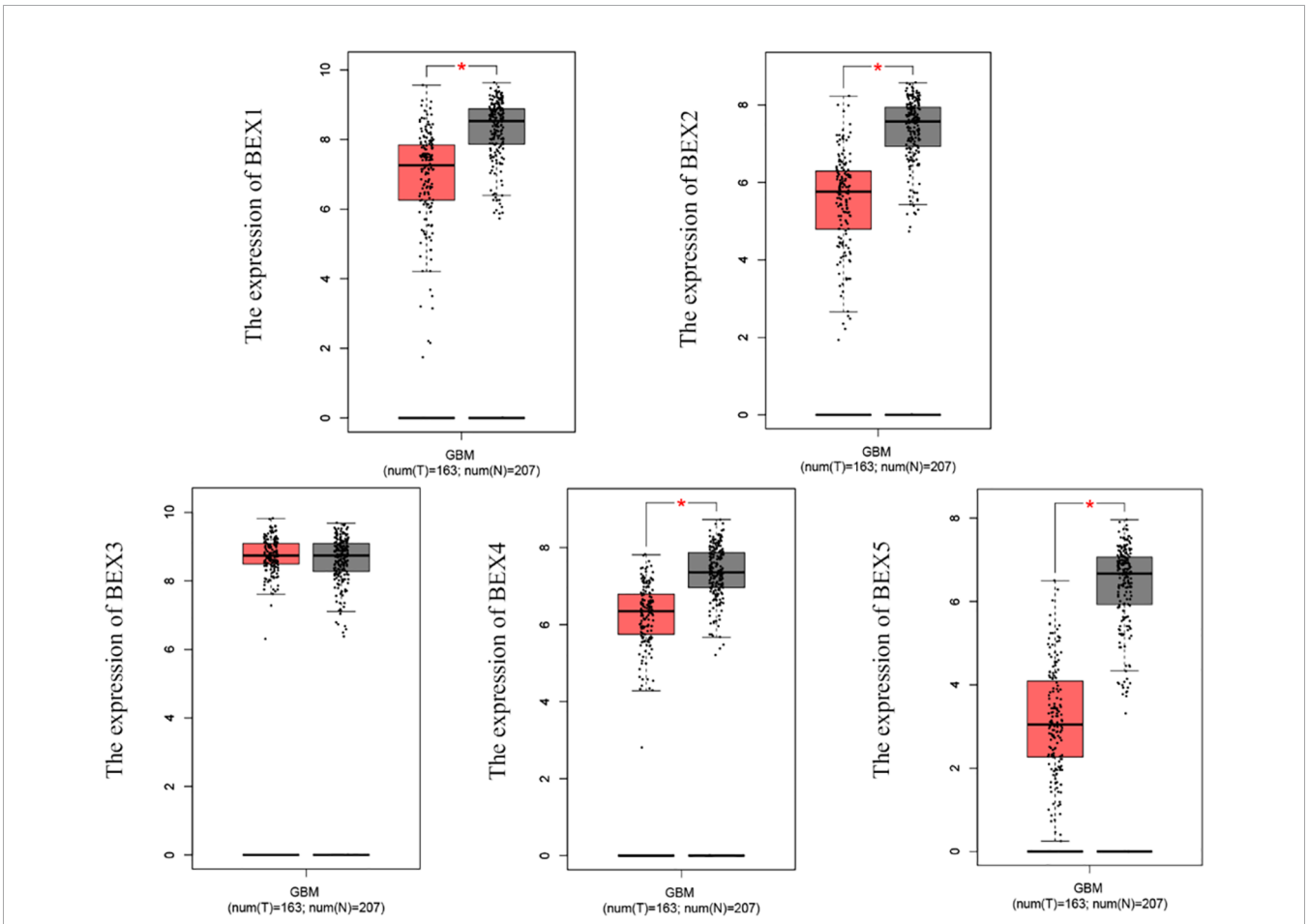

FIGURE 1 | The mRNA expression of BEX family in GBM based on TCGA database and GTEx database. GBM, glioblastoma multiforme; TCGA, The Cancer Genome Atlas; GTEx, Genotype-Tissue Expression ns, p≥0.05; *p< 0.05; **p<0.01; ***p<0.001.

(23). Regarding the WHO grade of GBM, the expression of the BEX family was significantly higher in the grade II (G2) group than in G3 and G4 groups (G2>G3>G4) (**Supplementary Figure 1A** and **Supplementary Table 1**). IDH status is another new classification of GBM and divides it into three subgroups based on isocitrate dehydrogenase (IDH) mutations: IDH wild type, IDH mutant, and not otherwise specified (NOS). According to the previous reports, the prognosis of GBM patients with IDH mutant is better than that of wild type (5). Our study revealed that BEX family gene expression of GBM tended to be downregulated in the IDH wild-type group than in the IDH mutant group (except BEX5) (**Supplementary Figure 1B** and **Supplementary Table 1**). Based on the new WHO integrated diagnosis, 1p/19q codeletion status reflects the genetic profile of GBM, and there is evidence that the presence of 1p/19q codeletion is not only a positive prognostic indicator but also a strong predictor of chemosensitivity (24). In this study, we found that 1p/19q codeletion status was associated with higher expression of the BEX family (**Supplementary Figure 1C** and **Supplementary Table 1**). GBM patients with different histological types also showed a different level of BEX family expression (**Supplementary Figure 1D** and **Supplementary Table 1**). We found that BEXs were obviously decreased in the glioblastoma subtype with respect to other subtypes.

Identification of Prognosis-Related BEXs in Glioblastoma Multiforme Samples

After univariate Cox regression analysis, we found that BEX1~4 had a significant correlation with GBM (**Table 1**). In addition, the Kaplan–Meier survival curve based on the median expression value showed that the high expression group of BEX1, BEX2, BEX3, and BEX4 had a better prognosis than the low expression group in the OS aspects (log-rank p-score <0.001), while bex5 had no significant prognostic value (**Figure 2**). Subsequently, multivariate Cox regression analysis indicated that BEX1 (hazard ratio [HR]: 0.5; $p < 0.001$), BEX2 (HR: 1.38; $p = 0.029$), and BEX4 (HR: 0.2; $p < 0.001$) exhibited an independent prognostic value for GBM (**Table 1**).

Correlation Between BEX Family Expression and Immune Infiltration

Immune infiltration analysis showed that BEX family expression was negatively correlated with the infiltration of Th cell, T cells, Tregs, B cells, mast cells, macrophage, neutrophils, cytotoxic cells, Th cells, Th17 cells, Tem, DCs, eosinophils, NK CD56dim, CD8 T cells, and iDCs and was positively correlated with the abundance of NK CD56bright cells and Tgd, Treg, Tfh, and pDC (**Supplementary Figure 2**).

Functional Enrichment Analysis of BEX Family Genes and Their Differentially Expressed Genes in Glioblastoma Multiforme

Identification of Differentially Expressed Genes Between the High and Low BEX Expression Groups

The data from TCGA were analyzed using the DSEeq2 package in R (|log FC| > 1.5, adjusted p-value <0.05), and 100 DEGs (protein-coding genes) were identified between the groups with high and low BEX family expression groups (20 top DEGs for each BEX family member) (shown in **Supplementary Table 2**).

Functional Annotation and Enrichment Analysis

To better understand the functional implication of BEX family members in GBM from the top 100 DEGs identified between the high and low expression groups, GO term analysis and KEGG pathway enrichment analysis were performed. The results suggested that BEX family genes and their DEGs were mainly involved in the humoral immune response, B cell-mediated immunity, lymphocyte-mediated immunity, lymphocyte-mediated immunity, immunoglobulin complex related terms, and immunoglobulin receptor binding process, which are immune response-related biological processes and pathways (**Supplementary Figure 3**).

TABLE 1 | Univariate and multivariate Cox regression analyses of BEX family in GBM.

Characteristics	Total (N)	Univariate analysis		Multivariate analysis	
		Hazard ratio (95% CI)	p-Value	Hazard ratio (95% CI)	P-value
BEX2	695				
Low	347	Reference			
High	348	0.596 (0.467–0.761)	**<0.001**	1.380 (1.034–1.842)	**0.029**
BEX3	695				
Low	347	Reference			
High	348	0.513 (0.401–0.657)	**<0.001**	1.243 (0.912–1.693)	0.168
BEX4	695				
Low	348	Reference			
High	347	0.262 (0.199–0.344)	**<0.001**	0.271 (0.192–0.381)	**<0.001**
BEX5	695				
Low	348	Reference			
High	347	0.993 (0.783–1.260)	0.956		
BEX1	695				
Low	348	Reference			
High	347	0.363 (0.281–0.470)	**<0.001**	0.530 (0.384–0.732)	**<0.001**

GBM, glioblastoma multiforme.
The bold values were considered statistically significant.

We screened the top 20 genes with the strongest correlation with each BEX family member through stat package Pearson analysis and established a protein interaction network using the string database. The results showed that there was a close and complex correlation between BEX family genes and TCEAL family genes (**Supplementary Figure 4**). Single-gene correlation analysis, once again, verified that there was a significant correlation between the expression levels of BEX family genes and TCEAL family genes in GBM (**Table 2** and **Figure 3**).

Expression Difference of TCEAL Family in Glioblastoma Multiforme and Its Correlation With Prognosis

According to the correlation analysis of TCGA database, compared with normal tissues, the mRNA expression of TCEAL1, 3, 4, 8, and 9 in GBM was significantly upregulated, and the mRNA expression of TCEAL2, 5, 6, and 7 was significantly downregulated. In addition, Kaplan–Meier survival curves based on median expression values showed that high expression of TCEAL1~5 and TCEAL7 and 9 had better prognosis in OS (log-rank p-score <0.001), while TCEAL6 and TCEAL8 had no significant prognostic value (**Figure 4**). After univariate Cox regression analysis, we found that TCEAL1~5 and TCEAL7 and 9 had a significant prognostic correlation with OS. Multivariate Cox regression analysis showed that TCEAL2 (HR: 0.322; $p < 0.001$), TCEAL4 (HR: 0.690; $p = 0.029$), TCEAL7 (HR: 1.873; $p < 0.001$), and TCEAL9 (HR: 1.913; $p < 0.001$) had an independent prognostic value for GBM (**Supplementary Table 3**).

DISCUSSION

Aberrant Expression of BEX Family Genes in Glioblastoma Multiforme Samples

Many studies have reported that the abnormal expression of BEX family genes was related to the development and prognosis of tumors, such as GBM, gastric cancer, colorectal cancer, hepatocellular carcinoma, lung cancer, and breast cancer (11, 25–28). Here, through the analysis of GBM samples in TCGA database, we once again verify that, except for BEX3, BEX family genes were significantly downregulated in GBM. We also found that there were significant differences in the expression level of BEX family genes among different WHO-G stages, pathological types, and IDH status (except BEX5), and the expression of BEX was lower in the group with higher malignancy and worse prognosis. We also searched for some information about immunohistochemical staining of the BEX family in GBM patients in THE HUMAN PROTEIN ATLAS database (https://www.proteinatlas.org/) and found that the immunohistochemical staining of the BEX family genes performed significantly differently between normal brain tissues and GBM tissues of different grades (**Supplementary Figure 7**). This supported our results that BEX family genes did express differently in GBM patients compared with normal tissues and have some heterogeneity between different grades. Low-grade GBM is generally stained lower than high-grade GBM (except for BEX3). Therefore, we speculate that BEX family genes play a tumor-suppressive role in GBM as a whole facture.

However, previous studies have suggested the oncogenic or tumor-suppressive roles of BEXs, with much controversy. Foltz et al. reported that BEX1 and BEX2 were silenced in GBM and may play an important role in a novel signaling pathway regulating apoptosis as tumor suppressor genes (13). Yan and his colleagues found that BEX1 expression was decreased in GBM (24). Tan et al. reported that BEX2 negatively modulates the hedgehog signaling pathway by retaining Zic2 in the cytoplasm in colorectal cancer cells, thereby inhibiting migration and metastasis of colorectal cancer cells (26). Another study found that the expression of BEX1 and BEX4 was upregulated in radiotherapy-resistant GBM cells and enhanced the tumor formation, growth, and radioresistance of GBM cells by activating the YAP/TAZ signaling pathway (11). Zhou et al. reported that Bex2 was upregulated in GBM and regulated cell proliferation and apoptosis *via* the c-Jun NH2-terminal kinase pathway (12). These different research conclusions illustrated that further relevant studies are needed to explore the specific mechanism of BEX family genes in the occurrence and development of GBM.

Identification of Prognosis-Related BEXs in Glioblastoma Multiforme Samples

Members of the BEX family have also reported a prognostic correlation in other tumors, such as gastric cancer and liver cancer (27, 29). In our study, it can also be found that the

TABLE 2 | There was a significant correlation between the expression levels of BEX family genes and TCEAL family genes in GBM (Pearson's analysis).

BEX family	TCEAL family	Cor_ Pearson
BEX2	TCEAL5	0.701584
BEX2	TCEAL6	0.59547
BEX2	TCEAL2	0.595103
BEX3	TCEAL4	0.562
BEX3	TCEAL3	0.532
BEX3	TCEAL5	0.489
BEX3	TCEAL2	0.483
BEX3	TCEAL1	0.48
BEX4	TCEAL2	0.785
BEX5	TCEAL6	0.782218

GBM, glioblastoma multiforme.

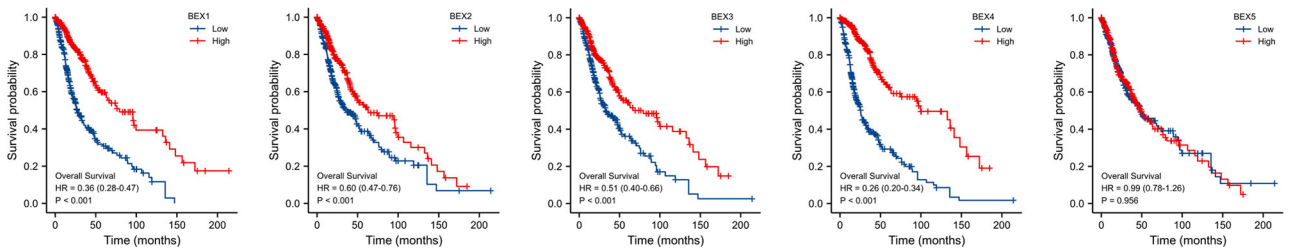

FIGURE 2 | The OS of BEX family for GBM patients. The prognostic value of BEX family mRNA expression for OS in GBM patients by Kaplan–Meier analysis. The Cox regression analysis was performed to evaluate survival differences with the best cutoff value. OS, overall survival; GBM, glioblastoma multiforme.

downregulation of the BEX genes was correlated with the worse prognosis (except for BEX5). Multivariate Cox regression analysis showed that BEX1, BEX2, and BEX4 were independent risk factors for the prognosis of GBM. However, the specific mechanism of how they affect the prognosis of GBM patients is unknown, and further studies are needed.

Associations of BEX Family With Immune Infiltration

In our study, the immune infiltration analysis showed that the expression of BEX family genes in GBM was negatively correlated with the infiltration of most of the immune cells. The enrichment analysis of the BEX family and their neighbor DEGs suggested that the BEX family and their DEGs were mainly involved in the immune response-related biological processes and pathways including humoral immune response and lymphocyte-mediated immunity, especially B cell-mediated immunity. To further investigate the functions of the BEX family in GBM, we performed GSEA using TCGA data (**Supplementary Figure 4**). GSEA showed that PD-1 signaling, CTLA4 pathway, DNA methylation, P53 signaling pathway, etc. were differentially enriched in the BEX low expression group. Therefore, it can be reasonably speculated that the abnormal expression of BEX family genes may affect the immune cell infiltration of GBM patients, change the normal immune microenvironment, and promote the occurrence and development of GBM by affecting the signal pathway related to immune response.

Correlation Between BEX Family and TCEAL Family

The single-gene correlation analysis and PPI network show that there is a close and complex correlation between BEX family genes and TCEAL family genes. The correlation between the two gene families has been reported in previous studies that BEX family proteins and BEX domains are also found in TCEAL proteins (30, 31), and the function of this domain is involved in the control of cellular growth (32–34).

Our study also showed that compared with the normal tissues, the expression of TCEAL1, 3, 4, 8, and 9 was significantly upregulated in GBM, and the expression of TCEAL2, 5, 6, and 7 was significantly downregulated in GBM. In addition, survival analysis and univariate Cox regression analysis showed that patients with high expression of TCEAL1~5 and TCEAL7 and 9 had longer OS. Multivariate

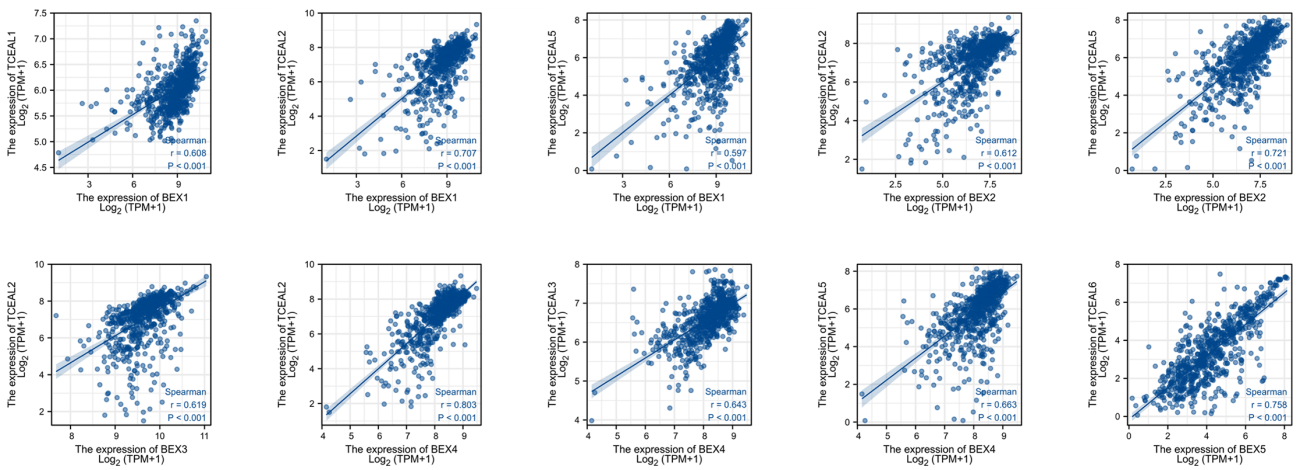

FIGURE 3 | Single-gene correlation analysis showed that BEX family was highly correlated with TCEAL family.

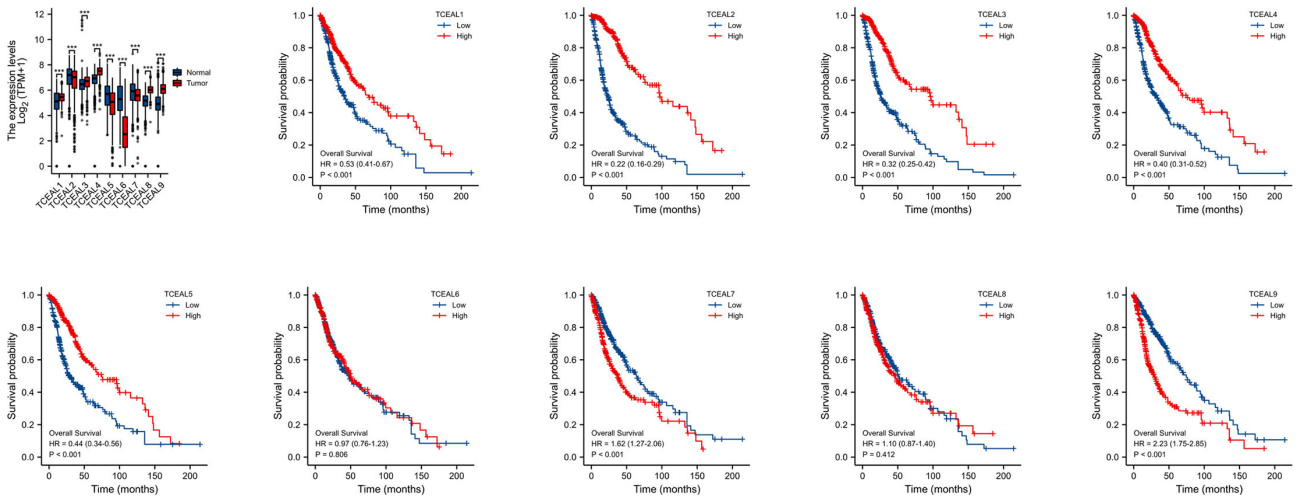

FIGURE 4 | mRNA expression of TCEAL family in GBM and the prognostic value of TCEAL family mRNA expression for OS in GBM patients by Kaplan–Meier analysis. GBM, glioblastoma multiforme; OS, overall survival ns, p≥0.05; *p< 0.05; **p<0.01; ***p<0.001.

Cox regression analysis showed that TCEAL2, TCEAL4, TCEAL7, and TCEAL9 had independent predictive values for the prognosis of GBM. The previous results suggest that BEX1, BEX2, and BEX4 also have an independent prognostic value for GBM. Therefore, we use the above seven genes to establish a preliminary multivariate prognostic model.

Construction of a Prognostic Scoring Model Based on BEX1, BEX2, BEX4, TCEAL2, TCEAL4, TCEAL7, and TCEAL9 Expression

To provide clinicians with a quantitative approach for predicting the prognosis of GBM patients, a nomogram was constructed that integrated the clinical characteristics as well as BEX and TCEAL members determined to be independently associated with survival *via* multivariate analysis (WHO-G grade, IDH status, and 1p/19q codeletion). Within the nomogram (**Supplementary Figure 5A**), WHO-G grade was found to contribute the most extreme data points (ranging from 0 to 100) as compared with the other clinical variables, which was consistent with the results of multivariate Cox regression. The C-index of the nomogram (**Supplementary Figure 5B**) was 0.836 (95% CI: 0.824–0.849). The bias-corrected line in the calibration plot was close to the ideal curve, indicating a good agreement between the predicted and observed values. Overall, the nomogram was found to be a superior model for predicting long-term survival in GBM patients than individual prognostic factors.

In order to construct a risk score model for predicting OS of GBM, the LASSO Cox regression model was used to build a prognostic classifier, which included BEX1, BEX2, BEX4, sf5TCEAL2, TCEAL4, TCEAL7, and TCEAL9 (**Figures 5A,B**). Using the LASSO Cox regression models, we calculated a risk score for each patient: risk score = (BEX4 * −0.3762202) + (TCEAL2 * −0.1629317) + (TCEAL4 * −0.2063245) + (TCEAL7 * 0.25805615) + (TCEAL9 * 0.26348946). Survival analysis revealed that the survival time of GBM patients in the high-risk group was significantly shorter than that of patients in the low-risk group (**Figure 5C**). Then, the model reliability was verified through the ROC curves analysis. In the time-dependent ROC curve, the AUC values of 1-, 3- and 5-year OS were 0.858, 0.890 and 0.814, respectively (**Figure 5D**), and the AUC value of the diagnostic ROC curve was 0.836 (**Figure 5E**). The above results indicated that the BEX and TCEAL risk assessment models had a predictive value for the prognosis of GBM patients.

In the present study, there still exist some limitations. First, we acknowledge that, in this study, we did not rigorously test whether the proportional hazards assumption holds. To furtherly confirm the assumption of proportional hazards, time-dependent covariate analysis could be suggested, and if the premise of proportional hazards does not hold, it is generally recommended to use the limited mean survival time instead of the median survival time for the description and comparison of survival analysis. Second, our present study is limited to the existing information in TCGA database, and more in-depth studies are necessary to verify the results with an expanded sample size in the future. What is more, the mechanisms of the BEX family involved in the initiation and progression of GBM, especially in the immune regulation processes, require further investigation.

Taken together, by assessing the global gene expression profile, we demonstrated that except for BEX3, the expression of the other four members of BEX family genes was downregulated in GBM, related to a worse prognosis of GBM, and involved in the initiation and progression of GBM, especially in the immune regulation processes. Among them, BEX1, 2, and 4 were independently correlated with the prognosis of GBM. In addition, there is a significant correlation between BEX family genes and TCEAL family genes, which also had an abnormal expression in GBM, and were significantly related to the

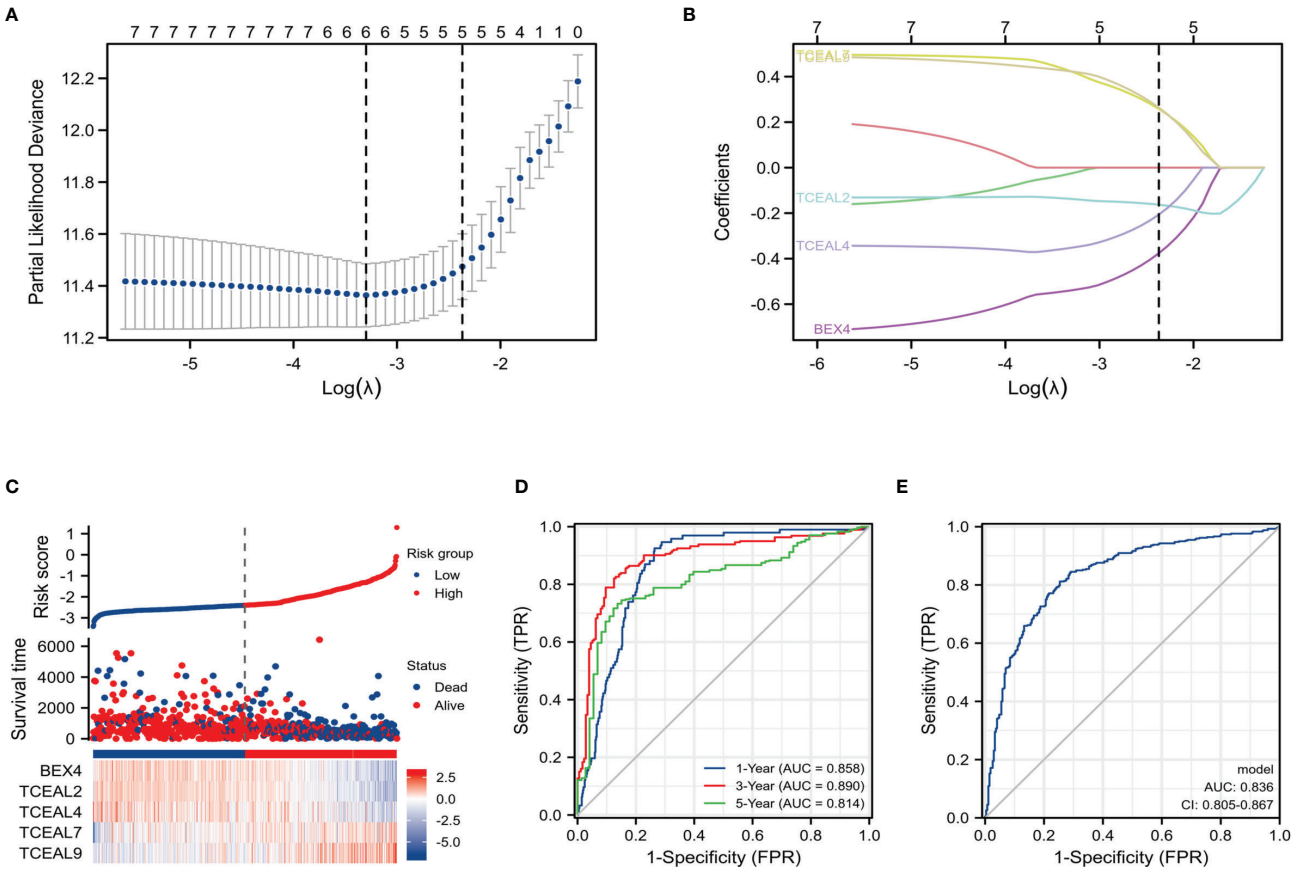

FIGURE 5 | LASSO Cox regression model of GBM and ROC curves analysis of LASSO Cox regression model. **(A)** Partial likelihood deviance of OS for the LASSO coefficient profiles. **(B)** LASSO coefficient profiles of the BEX4 and TCEAL2, TCEAL4, TCEAL7, and TCEAL9 expression for OS. **(C)** The survival time of GBM patients in the high-risk group was significantly shorter than that of patients in the low-risk group. **(D)** The time-dependent ROC curve; the AUC values of 1-, 3-, and 5-year OS were 0.858, 0.890, and 0.814, respectively. **(E)** The AUC value of the diagnostic ROC curve was 0.836. LASSO, least absolute shrinkage and selection operator; GBM, glioblastoma multiforme; ROC, receiver operating characteristic; OS, overall survival; AUC, area under the curve.

prognosis of GBM patients. Based on the above conclusions, we established an accurate and practical prognosis prediction model with the two gene families and clinical characteristics independently related to the prognosis of GBM.

DATA AVAILABILITY STATEMENT

The datasets presented in this study can be found in online repositories. The names of the repository/repositories and accession number(s) can be found in the article/**Supplementary Material**.

AUTHOR CONTRIBUTIONS

AA, YT, YS, and YY: conceptualization. AA: methodology. AA, DZ, and XL: software. AA and YT: validation. AA and XL: formal analysis. DZ and XL: data curation. AA, DZ, and XL: writing—original draft preparation. YT, YS, and YY: writing—review and editing. All authors contributed to the article and approved the submitted version.

FUNDING

This research was supported by the National Natural Science Foundation of China (82102708 to YT), the Zhejiang Provincial Natural Science Foundation of China under Grant (LQ21H160024 to YT), the Zhejiang Provincial Medicine and Technology Projects Grant (2020RC063 to YT), the Zhejiang Provincial Key R&D Program (2021C03125 to YY), and the Health Commission of Zhejiang Province (grant number: 2019KY082).

SUPPLEMENTARY MATERIAL

The Supplementary Material for this article can be found online at: https://www.frontiersin.org/articles/10.3389/fonc.2022.911942/full#supplementary-material

Supplementary Figure 1 | Relationship between BEX family expression and clinical indicators in GBM patients. **(A)** Correlation between gene expression level of BEX family and WHO-G stage in glioma patients. **(B)** Correlation between gene expression level of BEX family and IDH status in glioma patients. **(C)** Correlation between gene expression

level of BEX family and 1p19q codeletion in glioma patients. **(D)** Correlation between gene expression level of BEX family and histological type in glioma patients.

Supplementary Figure 2 | Immune infiltration analysis of BEX family in GBM. Immune cells. aDC [activated DC]; B cells; CD8 T cells; Cytotoxic cells; DC; Eosinophils; iDC [immature DC]; Macrophages; Mast cells; Neutrophils; NK CD56bright cells; NK CD56dim cells; NK cells; pDC [Plasmacytoid DC]; T cells; T helper cells; Tcm [T central memory]; Tem [T effector memory]; Tfh [T follicular helper]; Tgd [T gamma delta]; Th1 cells; Th17 cells; Th2 cells; Treg.

Supplementary Figure 3 | GO term analysis and KEGG pathway enrichment analysis of BEX family in GBM.

Supplementary Figure 4 | PPI network of BEX family and TCEAL family: there was a significant correlation between the expression levels of BEX family genes and TCEAL family genes in GBM.

Supplementary Figure 5 | Enrichment plots from gene set enrichment analysis (GSEA). PD-1signaling, CTLA4 pathway, DNA methylation and P53 signaling pathway et al. were enriched in low BEXs expression phenotypes and might be closely correlated with prognosis of GBM.

Supplementary Figure 6 | Relationship between 7 Independent prognostic value genes and other clinical factors with overall survival (OS). **(A)** Nomogram for predicting the probability of 1-, 3-, and 5-year OS for GBM patients. **(B)** Calibration plot of the nomogram for predicting the OS likelihood. (Concordance, C-index: 0.836; 95% confidence interval:0.824-0.849).

Supplementary Figure 7 | The immunohistochemical staining of the BEX family genes in normal brain tissues and GBM tissues of different grades: BEX family genes generally stained medium to high in brain tissues, especially in neuronal cells, when they stained medium to low in high grade GBM and stained low or not detected in low grade GBM. (except for BEX3,which stained high in low grade GBM).

REFERENCES

1. Ghosh M, Shubham S, Mandal K, Trivedi V, Chauhan R, Naseera S. Survival and Prognostic Factors for Glioblastoma Multiforme: Retrospective Single-Institutional Study. *Indian J Cancer* (2017) 54(1):362–7. doi: 10.4103/ijc.IJC_157_17
2. Rolim GB, Dantas Lima AJP, Dos Santos Cardoso VI, de Fátima Machado Soares É, Nunes DN, Barros HCS, et al. Can Inflammasomes Promote the Pathophysiology of Glioblastoma Multiforme? A View About the Potential of the Anti-Inflammasome Therapy as Pharmacological Target. *Crit Rev Oncol Hematol* (2022) p:103641. doi: 10.1016/j.critrevonc.2022.103641
3. Simińska D, Korbecki J, Kojder K, Kapczuk P, Fabiańska M, Gutowska I, et al. Epidemiology of Anthropometric Factors in Glioblastoma Multiforme-Literature Review. *Brain Sci* (2021) 11(1):116. doi: 10.3390/brainsci11010116
4. Korja M, Raj R, Seppä K, Luostarinen T, Malila N, Seppälä M, et al. Glioblastoma Survival is Improving Despite Increasing Incidence Rates: A Nationwide Study Between 2000 and 2013 in Finland. *Neuro Oncol* (2019) 21 (3):370–9. doi: 10.1093/neuonc/noy164
5. Delgado-Martín B, Medina M. Advances in the Knowledge of the Molecular Biology of Glioblastoma and Its Impact in Patient Diagnosis, Stratification, and Treatment. *Adv Sci (Weinh)* (2020) 7(9):1902971. doi: 10.1002/advs.201902971
6. Guan X, et al. CTLA4-Mediated Immunosuppression in Glioblastoma is Associated With the Infiltration of Macrophages in the Tumor Microenvironment. *J Inflammation Res* (2021) 14:7315–29. doi: 10.2147/JIR.S341981
7. Filley AC, Henriquez M, Dey M. Recurrent Glioma Clinical Trial, CheckMate-143: The Game is Not Over Yet. *Oncotarget* (2017) 8 (53):91779–94. doi: 10.18632/oncotarget.21586
8. Fernandez EM, Díaz-Ceso MD, Vilar M. Brain Expressed and X-Linked (Bex) Proteins are Intrinsically Disordered Proteins (IDPs) and Form New Signaling Hubs. *PLoS One* (2015) 10(1):e0117206. doi: 10.1371/journal.pone.0117206
9. Hu Z, Wang Y, Huang F, Chen R, Li C, Wang F, et al. Brain-Expressed X-Linked 2 Is Pivotal for Hyperactive Mechanistic Target of Rapamycin (mTOR)-Mediated Tumorigenesis. *J Biol Chem* (2015) 290(42):25756–65. doi: 10.1074/jbc.M115.665208
10. Kazi JU, Kabir NN, Rönnstrand L. Brain-Expressed X-Linked (BEX) Proteins in Human Cancers. *Biochim Biophys Acta* (2015) 1856(2):226–33. doi: 10.1016/j.bbcan.2015.09.001
11. Lee S, Kang H, Shin E, Jeon J, Youn H, Youn B. BEX1 and BEX4 Induce GBM Progression Through Regulation of Actin Polymerization and Activation of YAP/TAZ Signaling. *Int J Mol Sci* (2021) 22(18). doi: 10.3390/ijms22189845
12. Zhou X, Meng Q, Xu X, Zhi T, Shi Q, Wang Y, et al. Bex2 Regulates Cell Proliferation and Apoptosis in Malignant Glioma Cells via the C-Jun NH2-Terminal Kinase Pathway. *Biochem Biophys Res Commun* (2012) 427(3):574–80. doi: 10.1016/j.bbrc.2012.09.100
13. Foltz G, et al. Genome-Wide Analysis of Epigenetic Silencing Identifies BEX1 and BEX2 as Candidate Tumor Suppressor Genes in Malignant Glioma. *Cancer Res* (2006) 66(13):6665–74. doi: 10.1158/0008-5472.CAN-05-4453
14. Blum A, Wang P, Zenklusen JC. SnapShot: TCGA-Analyzed Tumors. *Cell* (2018) 173(2):530. doi: 10.1016/j.cell.2018.03.059
15. Vivian J, Rao AA, Nothaft FA, Ketchum C, Armstrong J, Novak A, et al. Toil Enables Reproducible, Open Source, Big Biomedical Data Analyses. *Nat Biotechnol* (2017) 35(4):314–6. doi: 10.1038/nbt.3772
16. Yu G, Foltz G, Ryu GY, Yoon JG, Nelson T, Fahey J, et al. Clusterprofiler: An R Package for Comparing Biological Themes Among Gene Clusters. *Omics* (2012) 16(5):284–7. doi: 10.1089/omi.2011.0118
17. Walter W, Sánchez-Cabo F, Ricote M. GOplot: An R Package for Visually Combining Expression Data With Functional Analysis. *Bioinformatics* (2015) 31(17):2912–4. doi: 10.1093/bioinformatics/btv300
18. Subramanian A, Kuehn H, Gould J, Tamayo P, Mesirov JP. GSEA-P: A Desktop Application for Gene Set Enrichment Analysis. *Bioinformatics* (2007) 23(23):3251–3. doi: 10.1093/bioinformatics/btm369
19. Li T, Fan J, Wang B, Traugh N, Chen Q, Liu JS, et al. TIMER: A Web Server for Comprehensive Analysis of Tumor-Infiltrating Immune Cells. *Cancer Res* (2017) 77(21):e108–10. doi: 10.1158/0008-5472.CAN-17-0307
20. Hänzelmann S, Castelo R, Guinney J. GSVA: Gene Set Variation Analysis for Microarray and RNA-Seq Data. *BMC Bioinf* (2013) 14:7. doi: 10.1186/1471-2105-14-7
21. Liu J, Lichtenberg T, Hoadley KA, Poisson LM, Lazar AJ, Cherniack AD, et al. An Integrated TCGA Pan-Cancer Clinical Data Resource to Drive High-Quality Survival Outcome Analytics. *Cell* (2018) 173(2):400–16.e11. doi: 10.1016/j.cell.2015.12.028
22. Ceccarelli M, Barthel FP, Malta TM, Sabedot TS, Salama SR, Murray BA, et al. Molecular Profiling Reveals Biologically Discrete Subsets and Pathways of Progression in Diffuse Glioma. *Cell* (2016) 164(3):550–63. doi: 10.1016/j.cell.2015.12.028
23. Louis DN, Perry A, Reifenberger G, von Deimling A, Figarella-Branger D, Cavenee WK, et al. The 2016 World Health Organization Classification of Tumors of the Central Nervous System: A Summary. *Acta Neuropathol* (2016) 131(6):803–20. doi: 10.1007/s00401-016-1545-1
24. Massaad E, Tabbarah A, Barmada M, Rbeiz J, Nasser S, Farra C, et al. FISH Analyses for 1p and 19q Status on Gliomas: Reporting an 8 Years' Experience From a Tertiary Care Center in the Middle East. *Ann Diagn Pathol* (2022) 57:151899. doi: 10.1016/j.anndiagpath.2022.151899
25. Naderi A, Liu J, Hughes-Davies L. BEX2 has a Functional Interplay With C-Jun/JNK and P65/RelA in Breast Cancer. *Mol Cancer* (2010) 9:111. doi: 10.1186/1476-4598-9-111
26. Tan Y, Hu Y, Xiao Q, Tang Y, Chen H, He J, et al. Silencing of Brain-Expressed X-Linked 2 (BEX2) Promotes Colorectal Cancer Metastasis Through the Hedgehog Signaling Pathway. *Int J Biol Sci* (2020) 16(2):228–38. doi: 10.7150/ijbs.38431
27. Zhu C, Xiao D. Aberrant Brain-Expressed X-Linked 4 (BEX4) Expression is a Novel Prognostic Biomarker in Gastric Cancer. *Med (Baltimore)* (2020) 99 (47):e23133. doi: 10.1097/MD.0000000000023133

28. Zhao Z, Li J, Tan F, Gao S, He J. mTOR Up-Regulation of BEX4 Promotes Lung Adenocarcinoma Cell Proliferation by Potentiating OCT4. *Biochem Biophys Res Commun* (2018) 500(2):302–9. doi: 10.1016/j.bbrc.2018.04.064
29. Wang Q, Liang N, Yang T, Li Y, Li J, Huang Q, et al. DNMT1-Mediated Methylation of BEX1 Regulates Stemness and Tumorigenicity in Liver Cancer. *J Hepatol* (2021) 75(5):1142–53. doi: 10.1016/j.jhep.2021.06.025
30. Chien J, Staub J, Avula R, Zhang H, Liu W, Hartmann LC, et al. Epigenetic Silencing of TCEAL7 (Bex4) in Ovarian Cancer. *Oncogene* (2005) 24 (32):5089–100. doi: 10.1038/sj.onc.1208700
31. Akaishi J, Onda M, Okamoto J, Miyamoto S, Nagahama M, Ito K, et al. Down-Regulation of Transcription Elogation Factor A (SII) Like 4 (TCEAL4) in Anaplastic Thyroid Cancer. *BMC Cancer* (2006) 6:260. doi: 10.1186/1471-2407-6-260
32. Chien J, Narita K, Rattan R, Giri S, Shridhar R, Staub J, et al. A Role for Candidate Tumor-Suppressor Gene TCEAL7 in the Regulation of C-Myc Activity, Cyclin D1 Levels and Cellular Transformation. *Oncogene* (2008) 27 (58):7223–34. doi: 10.1038/onc.2008.360
33. Rattan R, Narita K, Chien J, Maguire JL, Shridhar R, Giri S, et al. TCEAL7, a Putative Tumor Suppressor Gene, Negatively Regulates NF-kappaB Pathway. *Oncogene* (2010) 29(9):1362–73. doi: 10.1038/onc.2009.431
34. Lindblad O, Li T, Su X, Sun J, Kabir NN, Levander F, et al. BEX1 Acts as a Tumor Suppressor in Acute Myeloid Leukemia. *Oncotarget* (2015) 6 (25):21395–405. doi: 10.18632/oncotarget.4095

Conflict of Interest: The authors declare that the research was conducted in the absence of any commercial or financial relationships that could be construed as a potential conflict of interest.

Publisher's Note: All claims expressed in this article are solely those of the authors and do not necessarily represent those of their affiliated organizations, or those of the publisher, the editors and the reviewers. Any product that may be evaluated in this article, or claim that may be made by its manufacturer, is not guaranteed or endorsed by the publisher.

Advantages of publishing in Frontiers

OPEN ACCESS
Articles are free to read for greatest visibility and readership

FAST PUBLICATION
Around 90 days from submission to decision

HIGH QUALITY PEER-REVIEW
Rigorous, collaborative, and constructive peer-review

TRANSPARENT PEER-REVIEW
Editors and reviewers acknowledged by name on published articles

Frontiers
Avenue du Tribunal-Fédéral 34
1005 Lausanne | Switzerland

Visit us: www.frontiersin.org
Contact us: frontiersin.org/about/contact

REPRODUCIBILITY OF RESEARCH
Support open data and methods to enhance research reproducibility

DIGITAL PUBLISHING
Articles designed for optimal readership across devices

FOLLOW US
@frontiersin

IMPACT METRICS
Advanced article metrics track visibility across digital media

EXTENSIVE PROMOTION
Marketing and promotion of impactful research

LOOP RESEARCH NETWORK
Our network increases your article's readership